

FUNCTIONALIZED NANOCARRIERS FOR EFFECTIVE TREATMENT OF LIVER FIBROSIS

A Dissertation submitted to
The Maharaja Sayajirao University of Baroda,
in partial fulfillment of the requirements for the award of degree of

Doctor of Philosophy
In
Pharmacy

GUIDED BY

Dr. Ambikanandan Misra
(PROFESSOR OF PHARMACEUTICS)

SUBMITTED BY

Gaurang G. Patel



**PHARMACY DEPARTMENT
FACULTY OF TECHNOLOGY AND ENGINEERING
THE M.S. UNIVERSITY OF BARODA
VADODARA– 390001, GUJARAT
2010-2011**

CERTIFICATE

This is to certify that, this dissertation entitled,

FUNCTIONALIZED NANOCARRIERS FOR EFFECTIVE TREATMENT OF LIVER FIBROSIS

Submitted by

Mr. Gaurang G. Patel

in partial fulfillment for the award of degree of

Doctor of Philosophy

In

Pharmacy

At Pharmacy Department, The Maharaja Sayajirao University of Baroda, Vadodara has been carried out under my supervision and guidance. The matter compiled in this thesis the original research work carried out by him under my guidance and supervision and has not been submitted earlier for the award of any other degree or fellowship.

GUIDE

PROF. AMBIKANANDAN MISRA
PHARMACY DEPARTMENT,
FACULTY OF TECHNOLOGY & ENGINEERING,
THE M.S. UNIVERSITY OF BARODA,
VADODARA-390001

HEAD

PHARMACY DEPARTMENT,
FACULTY OF TECHNOLOGY & ENGINEERING,
THE M.S. UNIVERSITY OF BARODA,
VADODARA-390001

DEAN

FACULTY OF TECHNOLOGY & ENGINEERING,
THE M.S. UNIVERSITY OF BARODA,
VADODARA-390001

PLACE:-

DATE :-

DECLARATION

I hereby declare that the topic entitled “**Functionalized Nanocarriers for Effective Treatment of Liver Fibrosis**” which is submitted herewith to The Maharaja Sayajirao University of Baroda, Vadodara for the partial fulfillment for the award of degree of **Doctor of Philosophy In Pharmacy** is the result of work done by me in Pharmacy Department, Faculty of Technology and Engineering, The M. S. University of Baroda, under the guidance of **Dr. Ambikanandan Misra**, Professor of Pharmaceutics, Pharmacy Department, Faculty of Technology and Engineering, The M. S. University of Baroda, Vadodara.

I further declare that the result of this work have not been previously been submitted for any degree or fellowship.

BARODA:

DATE:

GAURANG G PATEL

Certified by and forwarded through the research guide,

Guide,
Prof. Ambikanandan Misra,
Professor in Pharmaceutics,
Pharmacy Department,
Faculty of Tech. & Engg.,
The Maharaja Sayajirao University of Baroda,
Vadodara-390001

**DEDICATED
TO
MY
BELOVED FAMILY
&
MAA AMBE**



ACKNOWLEDGEMENT

Research is an endless process for acquisition of knowledge, which never achieves milestones merely by an individual effort. The nest of good research is always woven with endless endeavors put by scientists together. The value of information provided by such self-driven peoples is always of high importance. At present occasion, when I am ready to accept the challenges in the field of pharmaceutical research, I sense that the present exercise for investigation would not have touched objectives without blessing and guidance from dedicated researchers and well wishers. I am indebted to all, who have contributed, directly or indirectly, in completion of my work.

With a deep sense of respect and gratitude, I express my indebtedness to my guide, Dr. Ambikanandan Misra, Prof. of Pharmaceutics, Pharmacy department, Faculty of tech and Engineering, the M.S.University of Baroda, for his invaluable guidance, boundless enthusiasm and constant inspiration through out the course of the study.

I am thankful to Dr. M.R.Yadav, Prof. of Drug design and development and Head of pharmacy department, Dr. R.S.R. Murthy and Dr. Krutika Sawant, Pharmacy department for their helpful suggestion throughout the study. I am grateful to Dr. R.Balaraman, Prof. of pharmacology; Dr. S.H.Mishra, Prof. of Herbal drug technology for their guidance and valuable suggestion during this course of investigation.

I am enormously thankful to Indian Council of Medical Research (ICMR), New Delhi, India for providing me the financial support. I am also thankful to The M.S.University of Baroda for the financial support in the initial phase of the work and also for providing the facility to accomplish my endeavor. I am immensely thankful to Zydus Research Center, Ahmedabad, India and Alembic Research Center, Vadodara for providing drug samples. Special thanks also to Mr. Yogesh raichandani, Kiruba Florence, Sachin Naik, and Prudhvi Raju for their valuable

suggestion, constructing criticism and the unending inspiration that have given a shape to this work.

I acknowledge the support of my colleagues and my friends Bhavik, Jigar, Nirav, Manisha, Kaustubh, Deepa, Gitanjali, Mohan, Mukesh ukawala, Himanshu, Vaibhav, Kiran, Mukesh kumar, Sandip, Kailash, Chenna, Ram, BHAGIRATH, all my seniors and juniors for their wonderful company and support during the whole year.

I would like to bid special thanks to Hasumati madam, Vaishali madam and other non teaching staff who have indirectly contributed to this work.

Finally I would like to appreciate endless love, care, patience, and faith shown on me by my wife and my parents who have stood behind me in every endeavor and have provide constant encouragement what ever be the situation.

I am thankful to all those who have helped me in what so ever manner during this work whom I might have missed inadvertently.

Gaurang G Patel

LIST OF TABLES

Table No.	Title	Page No.
Table 2.1	Typical Advantages and Limitations of Liver Biopsy in Comparison to Noninvasive Biomarkers	39
Table 2.2	Fibrosis markers	45
Table 2.3	Diagnostic accuracy of direct and indirect laboratory markers in distinguishing between low stages of 'insignificant' fibrosis (F0–F1 by METAVIR) and 'significant' fibrosis (F2–F4 by METAVIR)	55
Table 2.4	Anti-fibrogenic agents and strategies	65
Table 2.5	Major modes of liposomal action and related applications	80
Table 2.6	Denotation of various levels of two factors	95
Table 3.1	Calibration plot of RGZ in methanol for the estimation of RGZ in liposomes	148
Table 3.2	Optical characteristics of RGZ in methanol	148
Table 3.3	Accuracy and precision of RGZ estimation by UV- spectroscopic method in methanol	149
Table 3.4	Calibration plot of RGZ in diffusion medium (50 mM HPBCD, 20 mM HEPES, pH 7.4) for the estimation of RGZ during diffusion	150
Table 3.5	Optical characteristics of RGZ in diffusion medium (50 mM HPBCD, 20 mM HEPES, pH 7.4)	151
Table 3.6	Accuracy and precision of RGZ estimation by UV method in diffusion medium	151
Table 3.7	Calibration Plot of CDS in methanol for the estimation of CDS in liposomes	152
Table 3.8	Optical characteristics of CDS in methanol	153
Table 3.9	Accuracy and precision of CDS estimation by UV- spectroscopic method in methanol	153
Table 3.10	Calibration plot of CDS in diffusion medium (100 mM HPBCD, 20 mM HEPES, pH 7.4) for the estimation of CDS during diffusion	154
Table 3.11	Optical characteristics of CDS in diffusion medium (100 mM HPBCD, 20 mM HEPES, pH 7.4)	155
Table 3.12	Accuracy and precision of CDS estimation by UV- spectroscopic method in diffusion medium	155
Table 3.13	Calibration plot of RGZ in plasma by HPLC method	157
Table 3.14	Chromatographic conditions	158
Table 3.15	Accuracy and precision of RGZ estimation by HPLC method	158
Table 3.16	Calibration plot of CDS in plasma by HPLC method	160
Table 3.17	Chromatographic conditions	161

Table 3.18	Accuracy and precision of CDS estimation by HPLC method	161
Table 3.19	Calibration plot of D-Mannose	162
Table 3.20	Optical characteristics	162
Table 3.21	Accuracy and precision of D-Mannose estimation by Colorimetric method	163
Table 3.22	Calibration plot of Phosphorus	165
Table 3.23	Optical characteristics	165
Table 3.24	Accuracy and precision of Phosphorus by spectroscopic method	166
Table 3.25	Procedure for determination of total protein	166
Table 3.26	Basic parameters for determination of Albumin in serum	167
Table 3.27	Procedure for determination of Albumin in serum	167
Table 3.28	Procedure for determination of AST	169
Table 3.29	Procedure for determination of ALT	170
Table 3.30	Calibration plot of Hydroxyproline	173
Table 3.31	Calibration parameters	174
Table 3.32	Accuracy and precision of Hydroxyproline by spectroscopic method	174
Table 3.33	Calibration plot of Hyaluronic acid by ELISA method	177
Table 3.34	ELISA parameters	177
Table 3.35	Accuracy and precision of Hyaluronic acid estimation by ELISA assay	178
Table 4.1	Coded Values of the formulation parameters	191
Table 4.2	Coded Values of the formulation parameters	194
Table 4.3	Selection of process parameters by TFH method for RGZ and CDS liposomes	201
Table 4.4	3 ³ Full factorial design outline with results for PDE and PR	202
Table 4.5	Analysis of Variance (ANOVA) of full and reduced models	203
Table 4.6	Checkpoint Analysis	212
Table 4.7	Derivation of optimized formulation	213
Table 4.8	3 ³ Full factorial design outline with results for PDE and PR	214
Table 4.9	Analysis of Variance (ANOVA) of full and reduced models	215
Table 4.10	Checkpoint Analysis	224
Table 4.11	Derivation of optimized formulation	225
Table 4.12	Size and Zeta Potential of RGZ and CDS Liposomal Formulations	230
Table 4.13	Lyophilization of RGZ liposomes	234
Table 4.14	Lyophilization of CDS liposomes	234
Table 5.1	Comparative <i>in-vitro</i> drug diffusion of plain RGZ and RGZ liposomal formulations	248
Table 5.2	Comparative <i>in-vitro</i> drug diffusion of plain CDS and CDS liposomal formulations	250

Table 5.3	Drug diffusion model, Regression coefficient (r^2) and mean steady state flux of different formulations	251
Table 6.1	Stability testing data of RGZ liposomal formulation	257
Table 6.2	Stability testing data of CDS liposomal formulation	258
Table 7.1	The effect of various treatments on body weight, liver weight, liver coefficient and fibrosis grade	274
Table 7.2	The effect of various treatments on serum AST, ALT, A/G ratio, total bilirubin, hyaluronic acid, glucose and liver hydroxyproline content	275
Table 7.3	The pharmacokinetic parameters for different formulations in fibrotic rats after single intravenous bolus injection	278

LIST OF FIGURES

Figure No.	Title	Page No.
Figure 2.1	Sub-endothelial changes during stellate cell activation accompanying liver injury	20
Figure 2.2	Pathways of stellate cell activation and resolution during liver injury	22
Figure 2.3	Biological actions of hepatic stellate cells (HSCs) during liver fibrogenesis and potential sites for therapeutic intervention	23
Figure 2.4	The renin-angiotensin-aldosterone and endothelin pathways and potential sites for therapy of liver fibrosis	70
Figure 2.5	Schematic representation of M6P-HSA conjugated carrier	72
Figure 2.6	The structure of multilamellar vesicles showing the organization of phospholipid bilayers and the encapsulation of lipophilic and hydrophilic compounds	74
Figure 2.7	Seven-step ladder for optimizing drug delivery systems	85
Figure 2.8	System with controllable input variables (X), uncontrollable input variables (U), transfer function (T), and output variables (Y)	89
Figure 2.9	Diagrammatic depiction of interaction. Unparallel lines in (b) describe the phenomenon of interaction between the levels of drug and polymer amount affecting drug dissolution	91
Figure 2.10	Quantitative factors and factor space	96
Figure 2.11	Diagrammatic representation of (a) 2^2 factorial design; (b) 2^3 factorial design	99
Figure 2.12	Diagrammatic representation of 2^3 factorial design with added center point	100
Figure 2.13	Different types of responses as functions of factor settings; (a) linear; (b) quadratic; (c) cubic	104
Figure 2.14	(a) A typical response surface plotted between a response variable, release exponent, and two factors, HPMC and sodium CMC, in case of mucoadhesive compressed matrices; (b) the corresponding contour plot	106
Figure 3.1	Calibration plot of RGZ in methanol	148
Figure 3.2	Calibration plot of RGZ in diffusion medium (50 mM HPBCD, 20 mM HEPES, pH 7.4)	150
Figure 3.3	Calibration plot of CDS in methanol	152
Figure 3.4	Calibration plot of CDS in diffusion medium (100 mM HPBCD, 20 mM HEPES, pH 7.4)	154
Figure 3.5	Calibration plot of RGZ in plasma by HPLC Method	157
Figure 3.6	Calibration plot of CDS in plasma by HPLC	160

Figure 3.7	Calibration plot of D-Mannose	162
Figure 3.8	Calibration plot of Phosphorus	165
Figure 3.9	Calibration plot of Hydroxyproline	174
Figure 3.10	Calibration plot of Hyaluronic acid by ELISA method	177
Figure 4.1	Response surface plot and corresponding contour plot showing the influence of Drug:Lipid and Lipid:Chol ratio on PDE (a & b) and PR (c & d) for RGZ	205
Figure 4.2	Response surface plot and corresponding contour plot showing the influence of Drug:Lipid and Total solid:Hydration medium ratio on PDE (a & b) and PR (c & d) for RGZ	207
Figure 4.3	Response surface plot and corresponding contour plot showing the influence of Lipid:Chol and Total solid:Hydration medium ratio on PDE (a & b) and PR (c & d) for RGZ	209
Figure 4.4	Cube plots for PDE (a) and PR (b) representing the effects of three factors at a time for RGZ	210
Figure 4.5	Linear correlation plots of the experimental response values versus the predicted response values for PDE (a) and PR (b) for RGZ	212
Figure 4.6	Response surface plot and corresponding contour plot showing the influence of Drug: Lipid and Lipid: Chol ratio on PDE (a & b) and PR (c & d) for CDS	217
Figure 4.7	Response surface plot and corresponding contour plot showing the influence of Drug: Lipid and Total solid: Hydration medium ratio on PDE (a & b) and PR (c & d) for CDS	219
Figure 4.8	Response surface plot and corresponding contour plot showing the influence of Lipid: Chol and Total solid: Hydration medium ratio on PDE (a & b) and PR (c & d) for CDS	221
Figure 4.9	Cube plots for PDE (a) and PR (b) representing the effects of three factors at a time for CDS	222
Figure 4.10	Linear correlation plots of the experimental response values versus the predicted response values for PDE (a) and PR (b) for CDS	224
Figure 4.11	IR spectra of p-nitrophenyl-a-D-mannopyranoside	225
Figure 4.12	IR spectra of p-nitrophenyl-6-phospo-a-D-mannopyranoside	226
Figure 4.13	IR spectra of p-aminophenyl-6-phospo-a-D-mannopyranoside	226
Figure 4.14	IR spectra of HSA	227
Figure 4.15	IR spectra of M6P-HSA	227
Figure 4.16	IR spectra of Sebacic acid	228

Figure 4.17	IR spectra of Sebacic anhydride	228
Figure 4.18	IR spectra of DSPE	229
Figure 4.19	IR spectra of DSPE-Sebacic acid conjugate	229
Figure 4.20	Particle size and Zeta potential of unconjugated RGZ liposomes	230
Figure 4.21	Particle size and Zeta potential of M6P-HSA conjugated RGZ liposomes	230
Figure 4.22	Particle size and Zeta potential of unconjugated CDS liposomes	231
Figure 4.23	Particle size and Zeta potential of M6P-HSA conjugated CDS liposomes	231
Figure 4.24	TEM images of RGZ unconjugated (A) and RGZ M6P-HSA conjugated (B) liposomes	232
Figure 4.25	TEM images of CDS unconjugated (A) and CDS M6P-HSA conjugated (B) liposomes	232
Figure 4.26	DSC curve of RGZ plain drug (A) RGZ liposomes (B)	235
Figure 4.27	DSC curve of CDS plain drug (A) CDS liposomes (B)	235
Figure 4.28	X-ray diffractograms of RGZ plain drug and liposomal formulation	236
Figure 4.29	X-ray diffractograms of CDS plain drug and liposomal formulation	236
Scheme 4.1	TFH process stages in the preparation of RGZ liposomes	190
Scheme 4.2	TFH process stages in the preparation of CDS liposomes	193
Scheme 4.3	Synthesis of M6P-HSA	196
Scheme 4.4	M6P-HSA Conjugation to Liposomes	197
Figure 5.1	Comparative <i>in-vitro</i> drug diffusion profiles of plain RGZ and RGZ liposomal formulations	249
Figure 5.2	Comparative <i>in-vitro</i> drug diffusion profiles of plain CDS and CDS liposomal formulations	251
Figure 7.1	Representative histopathological images of liver tissues	273
Figure 7.2	Pharmacokinetic profiles of RGZ (different formulations) after single intravenous bolus injection in fibrotic rats	277
Figure 7.3	Pharmacokinetic profiles of CDS (different formulations) after single intravenous bolus injection in fibrotic rats	277
Figure 7.4	Complete tissue distribution of RGZ formulations after single intravenous bolus injection	280
Figure 7.5	Complete tissue distribution of CDS formulations after single intravenous bolus injection	280

CHAPTER 1

INTRODUCTION



Introduction

1.1 INTRODUCTION

1.2 RESEARCH ENVISAGED

1.3 PROPOSED PLAN OF WORK

1.4 REFERENCES

1.1 INTRODUCTION

Hepatic fibrosis is a reversible wound healing response characterized by accumulation of extracellular matrix (ECM) or "scar" tissues that follows chronic but not self-limited liver disease. The ECM components in fibrotic liver are similar regardless of the underlying cause. Hepatic fibrosis has evolved in the past 20 years from a pure laboratory discipline to an area of great bedside relevance to practicing hepatologists. This evolution reflects growing awareness not only of the molecular underpinnings of fibrosis, but also of its natural history and methods of detection in chronic liver disease. These advances have culminated in clear evidence that cirrhosis can be reversible, and in realistic expectations that effective antifibrotic therapy will significantly alter the management and prognosis of patients with liver disease.

In view of this remarkable progress, clinicians must now view liver fibrosis in a new light as a clinical problem in its own right amenable to specific diagnostic tests and therapies that are independent of the etiology. In that spirit, it is necessary to integrate current knowledge about the nature and prognosis of fibrosis in different forms of chronic liver disease with recent advances in elucidating its pathophysiology. These advances form the basis for rational treatment of hepatic fibrosis (Friedman, 2001; Gressner et al., 2002; Mann and Smart, 2002).

Cirrhosis can be defined as the end stage consequence of fibrosis of the hepatic parenchyma resulting in nodule formation and altered hepatic function. A notable omission from this contemporary definition is that cirrhosis is irreversible, since ample evidence now demonstrates that reversal of cirrhosis is often possible. Fibrosis and cirrhosis represent the consequences of a sustained wound healing response to chronic liver injury from a variety of causes including viral, autoimmune, drug induced, cholestatic and metabolic diseases. The clinical manifestations of cirrhosis vary widely, from no symptoms at all, to liver failure, and are determined by both the nature and severity of the underlying liver disease as well as the extent of hepatic fibrosis. Up to 40% of patients with cirrhosis are asymptomatic and may remain so for more than a decade, but progressive deterioration is inevitable once complications develop including ascites, variceal hemorrhage or encephalopathy. In such patients there is 50% 5-year mortality, with approximately 70% of these deaths directly attributable to liver disease (Fattovich et al., 1997). In asymptomatic individuals, cirrhosis may be first suggested during routine examination or diagnosed at autopsy,

although biopsy is still required to establish the diagnosis antemortem. The overall prevalence of cirrhosis in the United States is estimated at 360 per 100,000 population, or 900,000 total patients, the large majority of whom have chronic viral hepatitis or alcoholic liver disease.

Cirrhosis affects hundreds of millions of patients worldwide. In the US, it is the most common non-neoplastic cause of death among hepatobiliary and digestive diseases, accounting for approximately 30,000 deaths per year. In addition 10,000 deaths occur due to liver cancer, the majority of which arise in cirrhotic livers, with the mortality rate steadily rising (El-Serag and Mason, 2000; Befeler and Di Bisceglie, 2002).

The molecular composition of the scar tissue in cirrhosis is similar regardless of etiology and consists of the extracellular matrix constituents, collagen types I and III (i.e. 'fibrillar' collagens), sulfated proteoglycans, and glycoproteins (Schuppan et al., 2001). These scar constituents accumulate from a net increase in their deposition in liver and not simply collapse of existing stroma. Although the cirrhotic bands surrounding nodules are the most easily seen form of scarring, it is actually the early deposition of matrix molecules in the subendothelial space of Disse so called 'capillarization' of the sinusoid – that more directly correlates with diminished liver function.

In normal liver, hepatic stellate cells (HSCs) are nonparenchymal, quiescent cells whose main functions are to store vitamin A and probably to maintain the normal basement membrane-type matrix. However, numerous *in vivo* and *in vitro* studies indicate that in response to liver injury, HSCs undergo an "activation" process in which they lose vitamin A, become highly proliferative, and synthesize "fibrotic" matrix rich in type I collagen. This understanding has helped to identify underlying mechanisms, and will likely lead to new therapies for fibrotic diseases of many organs, including liver (Van Waes and Lieber, 1977).

Stellate cell "activation" is a key event in liver injury, and refers to the transition from a quiescent vitamin A-rich cell to a highly fibrogenic cell. Cells with features of both quiescent and activated states are often called "transitional cells." Proliferation of stellate cells occurs in regions of greatest injury, and is typically preceded by an influx of inflammatory cells and associated with subsequent ECM accumulation.

The rate of progression of fibrosis in an individual patient with chronic liver disease cannot be predicted with certainty. Accurate assessment of the extent of fibrosis is

essential in guiding management and predicting prognosis in patients with chronic liver injury. Histologic assessment of a liver biopsy specimen remains the gold standard for quantifying fibrosis, with increasing interest in the use of noninvasive markers to allow more frequent sampling and avoid the risks of percutaneous biopsy.

In reason of their role in hepatic fibrogenesis and of the several pro-fibrogenic mechanisms identified, HSC represents a major focus of anti-fibrotic research. Indeed, the well-described pathway of HSC activation, subsequent fibrogenesis, with the potential for apoptosis and reversibility, provides a logical framework to define sites of intervention. Consequently the search for effective antifibrogenic strategies is based on the knowledge gained in the area of HSC biology, including the biology of the factors (growth factors, cytokines, etc.) conditioning their profibrogenic attitude [10,80]. Although this major progress in understanding is fairly recent and, hence, still difficult to be translated into practical strategies, more and more articles published in top specialized journals report on the potent anti-fibrogenic action of old and new drugs, including single agents or mixtures derived from traditional herbal medicine. As any treatment aimed at curing the chronic disease, any potential anti-fibrotic agent should fulfill several criteria: (1) the treatment should be well tolerated, in view of a long duration and of multiple administrations; and (2) the active moiety of the drug should reach a sufficient concentration within the liver, possibly with some cell specific targeting (e.g. HSC, and other ECM-producing cells). The liver is an advantageous destination for orally administered drugs and those with efficient first pass metabolism will have inherent liver targeting. However, while this statement is true for a healthy liver, several limitations apply when liver tissue is affected by progressive scarring and initial or advanced derangement of the normal angio-architecture, as often happens when the patient reaches clinical attention.

Obviously, the best anti-fibrogenic treatment would be represented by any strategy able to eliminate the primary cause of parenchymal damage, metabolic overload or excessive oxidative stress. Once this primary requirement is fulfilled, the association with an anti-fibrogenic drug would be relevant for stabilizing the cure and favor optimal remodeling. Since the fibrogenic process is in its essence a compensatory phenomenon aimed at maintaining sufficient tissue continuity and cohesion in the presence of continuous microscopic parenchymal collapse, it would be erroneous to

attempt to cure fibrogenic chronic liver diseases (CLDs) only with anti-fibrogenic drugs once some effective compounds will become available for clinical use.

Along with the elucidation of the cellular and molecular mechanisms responsible for hepatic fibrogenesis, an impressive amount of experimental data proposing the anti-fibrogenic effect of several compounds has been accumulating. In general, all reports suggest that the compound under investigation is able to reduce or abolish the pro-fibrogenic potential of HSC in culture, and/or prevent and even reverse the fibrogenic evolution in animal models. These positive results need, however, to be subjected to some objective criticism before being translated into clinical applications for human CLDs. In vitro studies performed on activated HSC in their myofibroblast like phenotype provide thoughtful insights on the biology of this cell type, on the intracellular mechanisms regulating their pro-fibrogenic role, and on the effects of a drug added to the cell culture.

So far no effective treatment has been established other than removal of primary cause of the disease and liver transplantation for severe fibrosis. Therefore, research is being carried out on therapeutic agents who inhibit activation and proliferation of HSC, reduce ECM production by HSC, neutralize HSC contractile responses or stimulate HSC apoptosis (Wu and Zern, 2000; Lee et al., 2008; Bataller and Brenner, 2001; Adrian et al., 2007).

The peroxisome proliferator-activated receptors (PPARs) belong to the superfamily of nuclear receptors (Green and Wahli, 1994). PPAR forms heterodimers with the retinoid X receptor and binds to specific response elements to induce transcription in response to a variety of endogenous and exogenous ligands, including fatty acids, arachidonic acid metabolites, and synthetic drugs (Forman et al., 1996). Of the PPAR isoforms, PPAR- γ is the most widely studied (Auwerx, 1999). Previous studies indicated that expression of PPAR- γ inhibited PDGF-induced proliferation and migration of vascular smooth muscle cells (Fu et al., 2001). Three recent studies independently demonstrated that the level of PPAR- γ and its trans-activating activity were diminished during HSC activation in vitro, whereas NF- κ B and activator protein- 1 (AP-1) activities were increased (Galli et al., 2000; Marra et al., 2000). PPAR- γ ligands inhibited cell proliferation and collagen- α 1(I) expression in primary HSC (3–4 days) (Miyahara et al., 2000). The dramatic reduction in the abundance of PPAR- γ results in a significant decline in response to exogenous PPAR- γ ligands in

activated HSC. These findings implied a potential therapeutic value of PPAR- γ ligands in treatment of liver fibrosis if the expression of PPAR- γ can be induced in activated HSC.

Angiotensin II (Ang II) plays a central role in the regulation of systemic blood pressure and fluid homeostasis. The action of Ang II is mediated by mainly two subtypes of receptors, angiotensin II type 1 (AT1) receptors and type 2 (AT2) receptors, which are distributed in many kinds of organs and tissues. Recently, several lines of evidence have suggested that the rennin-angiotensin system (RAS) plays an important role in the pathogenesis of organ fibrosis (Brilla, 2000; Sun et al., 2000). In mesangial cells and other cell types, Ang II has been shown to promote the proliferation and collagen synthesis (Ray et al., 1991; Wolf et al., 1992; Kagami et al., 1994; Weber et al., 1994; Tharaux et al., 2000). Moreover, the expression of transforming growth factor- β (TGF- β), the key cytokine in the development of cardiac and renal fibrosis, is increased by Ang II (Weber, 1997). Blockade of the RAS by angiotensin converting enzyme (ACE) inhibitors or by AT1 antagonists has been shown to improve the progression of organ fibrosis (Ishidoya et al., 1995; Kim et al., 1995; Molteni et al., 2000). In the liver, Ang II is considered to play a role in the regulation of intrahepatic circulation (Schneider et al., 1999). Recently, it has been reported that Ang II induces proliferation and contraction of human HSCs, and TGF- β expression in rat HSCs, which are mainly mediated by AT1 receptors (Bataller et al., 1999; Yoshiji et al., 2001), and that ACE inhibitors or AT1 antagonists attenuate the progression of liver fibrosis in vivo (Ramos et al., 1994; Jonsson et al., 2001; Ohishi et al., 2001; Paizis et al., 2001; Yoshiji et al., 2002). These reports suggest that Ang II and RAS might play an important role in the pathogenesis of liver fibrosis.

Liposomes are vesicles composed of a phospholipid bilayer in which pharmaceutical agents can be contained. Liposomal drug delivery allows controlled release, target specificity, prolonged half life of drugs with its unique membrane properties, and resemblance of the membrane structure to cell membranes makes liposomes non-immunogenic and diversifies intake methods. Liposomes have tremendous potential as a carrier because they are nontoxic, non-immunogenic, and biodegradable and have a high loading capacity for a variety of therapeutic agents and have been investigated for long period of time. Particulate carriers such as liposomes have many attractive features, one of the perceived benefits of liposomes as a drug carrier is based on their

ability to alter favorably the pharmacokinetic profile of the encapsulated species and thus provide selective and prolonged pharmacological effects at the site of administration. However, effectiveness of these conventional liposomes is often limited due to the lack of the target specificity. Liposomes can be surface modified in many ways by conjugating cell specific ligands to target wide variety of cells. In liver, galactosylated (Managi et al., 2005; Hattori et al., 2000; Sliedregt et al., 1999) or asialofetuin (Dasi et al., 2001) coated liposomes target hepatocytes, aconitylated human serum albumin coated (Kamps et al., 1997) liposomes recognize endothelial cells and mannosylated liposomes (Opanasopit et al., 2002; Kawakami et al., 2000) identify kupffer cells as their targets (Adrian et al., 2007).

Mannose 6-phosphate/ insulin like growth factor II (M6P/IGF II) receptor are over expressed on the surface of HSCs during liver fibrosis. Mannose 6-phosphate modified human serum albumin (M6P-HSA) is selective to M6P/IGF II receptor and thus accumulates in activated HSCs of fibrotic liver. M6P-HSA as such has been investigated as a carrier for a number of drugs, including pentoxifyline, mycophenolic acid, doxorubicine and gliotoxin. M6P-HSA conjugated liposomes can be used as HSCs selective carrier of antifibrotic drugs to improve the efficacy of drugs at the same time to reduce their adverse effects. Liposomes with bioactive lipid dilinoleoylphosphatidylcholine (DLPC) into the membrane as a major constituent act as a bioactive drug carrier which can deliver drugs and simultaneously have beneficial antifibrotic effects (Beljaars et al., 1999; Beljaars et al., 2001; De Bleser et al., 1996; De Bleser et al., 1995; Adrian et al., 2006; Cao et al., 2002).

An attempt was made to develop liposomal formulation by thin film hydration method and optimized for drug: total lipid ratio, Phospholipid: cholesterol ratio and total solid: hydration medium ratio to maximize the percentage drug entrapment (PDE) and to minimize percentage reduction (PR) in PDE after 10 days by 3³ full factorial design. M6P-HSA was synthesized, characterized and conjugated to optimized liposomal formulations to provide targeting ability. *In vitro* drug diffusion studies were ascertained to identify release kinetics of developed formulations. *In-vivo* pharmacokinetic and pharmacodynamic properties of prepared formulation were evaluated in carbon tetrachloride (CCL₄) induced rat liver fibrosis model for exploitation of the findings of the studies in developing relevant product for effective treatment of liver fibrosis.

1.2 RESEARCH ENVISAGED

The research project focuses on the different aspects of pharmaceutical development and optimization of liposomal formulations of selected drugs [PPAR- γ ligand (Rosiglitazone) and AT1 receptor antagonist (Candesartan)]; surface conjugation with M6P-HSA to provide targeting potential; characterization, evaluation of prepared formulation for *in vitro* drug diffusion studies and for *in vivo* pharmacokinetic and pharmacodynamic properties.

1.3 PROPOSED PLAN OF WORK

- I. Literature reviews covering various aspects of liver fibrosis, treatment options for liver fibrosis, liposomes as drug delivery carrier, targeting liposomes to hepatic stellate cells, liposomes surface conjugation technologies, *in vitro* and *in vivo* evaluation techniques and profiles of selected drugs like Rosiglitazone and Candesartan cilexetil.
- II. Preparation of liposomes using thin film hydration method using lipids such as dilinoleoyl phosphatidylcholine, hydrogenated soya phosphotidylcholine, distearoyl phosphoethanolamine and cholesterol. Optimization of liposomal formulations for drug: total lipid ration, phospholipid: cholesterol ration and total solid: hydration medium to maximize the percentage drug entrapment (PDE) and to minimize percentage reduction (PR) in PDE after 10 days employing 3³ full factorial design. Characterization of optimized liposomes with respect to: particle size and size distribution, zeta potential etc.
- III. Lyophilization of optimized liposomal formulations using appropriate cryoprotectants and anti adherents to stabilize the formulations.
- IV. Preparation and characterization of M6P-HSA.
- V. Conjugation of M6P-HSA to optimized liposomes.
- VI. *In-vitro* drug diffusion studies.
- VII. Stability studies of potential formulations with respect to percentage drug retention, particle size, zeta potential and physical changes like caking and discoloration.
- VIII. Comparative evaluation of the developed formulations for *In vivo* pharmacokinetic and pharmacodynamic properties in carbon tetrachloride (CCL₄) induced rat liver fibrosis model.

1.4 REFERENCES

Adrian JE, Kamps JA, Scherphof GL, Meijer DK, van Loenen-Weemaes AM, Reker-Smit C, Terpstra P, Poelstra K. A novel lipid-based drug carrier targeted to the non-parenchymal cells, including hepatic stellate cells, in the fibrotic livers of bile duct ligated rats. *Biochim Biophys Acta*. 2007 Jun;1768(6):1430-9.

Adrian JE, Poelstra K, Scherphof GL, Molema G, Meijer DK, Reker-Smit C, Morselt HW, Kamps JA. Interaction of targeted liposomes with primary cultured hepatic stellate cells: Involvement of multiple receptor systems. *J Hepatol*. 2006 Mar;44(3):560-7.

Auwerx J. PPARgamma, the ultimate thrifty gene. *Diabetologia*. 1999 Sep;42(9):1033-49.

Bataller R, Brenner DA. Hepatic stellate cells as a target for the treatment of liver fibrosis. *Semin Liver Dis*. 2001 Aug;21(3):437-51.

Bataller R, Gines P, Nicolas JM, Gorbig MN, Garcia-Ramallo E, Gasull X, Bosch J, Arroyo V, Rodes J. Angiotensin II induces contraction and proliferation of human hepatic stellate cells. *Gastroenterology*. 2000 Jun;118(6):1149-56. (Bataller et al., 1999)

Befeler AS, Di Bisceglie AM. Hepatocellular carcinoma: diagnosis and treatment. *Gastroenterology*. 2002 May;122(6):1609-19.

Beljaars L, Molema G, Weert B, Bonnema H, Olinga P, Groothuis GM, Meijer DK, Poelstra K. Albumin modified with mannose 6-phosphate: A potential carrier for selective delivery of antifibrotic drugs to rat and human hepatic stellate cells. *Hepatology*. 1999 May;29(5):1486-93.

Beljaars L, Olinga P, Molema G, de Bleser P, Geerts A, Groothuis GM, Meijer DK, Poelstra K. Characteristics of the hepatic stellate cell-selective carrier mannose 6-phosphate modified albumin (M6P(28)-HSA). *Liver*. 2001 Oct;21(5):320-8.

Brilla CG. Renin-angiotensin-aldosterone system and myocardial fibrosis. *Cardiovasc Res*. 2000 Jul;47(1):1-3.

Cao Q, Mak KM, Lieber CS. Dilinoleoylphosphatidylcholine prevents transforming growth factor-beta1-mediated collagen accumulation in cultured rat hepatic stellate cells. *J Lab Clin Med*. 2002 Apr;139(4):202-10.

Dasi F, Benet M, Crespo J, Crespo A, Aliño SF. Asialofetuin liposome-mediated human alpha1-antitrypsin gene transfer in vivo results in stationary long-term gene expression. *J Mol Med (Berl)*. 2001 May;79(4):205-12.

De Bleser PJ, Jannes P, van Buul-Offers SC, Hoogerbrugge CM, van Schravendijk CF, Niki T, Rogiers V, van den Brande JL, Wisse E, Geerts A. Insulinlike growth factor-II/mannose 6-phosphate receptor is expressed on CCl4-exposed rat fat-storing cells and facilitates activation of latent transforming growth factor-beta in cocultures with sinusoidal endothelial cells. *Hepatology*. 1995 May;21(5):1429-37.

De Bleser PJ, Scott CD, Niki T, Xu G, Wisse E, Geerts A. Insulin-like growth factor II/mannose 6-phosphate-receptor expression in liver and serum during acute CCl₄ intoxication in the rat. *Hepatology*. 1996 Jun;23(6):1530-7.

El-Serag HB, Mason AC. Risk factors for the rising rates of primary liver cancer in the United States. *Arch Intern Med*. 2000 Nov 27;160(21):3227-30.

Fattovich G, Giustina G, Degos F, Tremolada F, Diodati G, Almasio P, Nevens F, Solinas A, Mura D, Brouwer JT, Thomas H, Njapoum C, Casarin C, Bonetti P, Fuschi P, Basho J, Tocco A, Bhalla A, Galassini R, Noventa F, Schalm SW, Realdi G. Morbidity and mortality in compensated cirrhosis type C: a retrospective follow-up study of 384 patients. *Gastroenterology*. 1997 Feb;112(2):463-72.

Forman BM, Chen J, Evans RM. The peroxisome proliferator-activated receptors: ligands and activators. *Ann N Y Acad Sci*. 1996 Dec 27;804:266-75.

Friedman SL, editor. The hepatic stellate cell. P.D. Berk, series editor. *Semin Liver Dis*. New York, Vol 21. New York, NY: Thieme, 2001. pp. 307-452.

Fu M, Zhu X, Wang Q, Zhang J, Song Q, Zheng H, Ogawa W, Du J, Chen YE. Platelet-derived growth factor promotes the expression of peroxisome proliferator-activated receptor gamma in vascular smooth muscle cells by a phosphatidylinositol 3-kinase/Akt signaling pathway. *Circ Res*. 2001 Nov 23;89(11):1058-64.

Galli A, Crabb D, Price D, Ceni E, Salzano R, Surrenti C, Casini A. Peroxisome proliferator-activated receptor gamma transcriptional regulation is involved in platelet-derived growth factor-induced proliferation of human hepatic stellate cells. *Hepatology*. 2000 Jan;31(1):101-8.

Green S, Wahli W. Peroxisome proliferator-activated receptors: finding the orphan a home. *Mol Cell Endocrinol*. 1994 Apr;100(1-2):149-53.

Gressner AM, Weiskirchen R, Breitkopf K, Dooley S. Roles of TGF-beta in hepatic fibrosis. *Front Biosci*. 2002 Apr 1;7:d793-807.

Hattori Y, Kawakami S, Yamashita F, Hashida M. Hattori Y, Kawakami S, Yamashita F, Hashida M. *J Control Release*. 2000 Dec 3;69(3):369-77.

Ishidoya S, Morrissey J, McCracken R, Reyes A, Klahr S. Angiotensin II receptor antagonist ameliorates renal tubulointerstitial fibrosis caused by unilateral ureteral obstruction. *Kidney Int*. 1995 May;47(5):1285-94.

Jonsson JR, Clouston AD, Ando Y, Kelemen LI, Horn MJ, Adamson MD, Purdie DM, Powell EE. Angiotensin-converting enzyme inhibition attenuates the progression of rat hepatic fibrosis. *Gastroenterology*. 2001 Jul;121(1):148-55.

Kagami S, Border WA, Miller DE, Noble NA. Angiotensin II stimulates extracellular matrix protein synthesis through induction of transforming growth factor-beta expression in rat glomerular mesangial cells. *J Clin Invest*. 1994 Jun;93(6):2431-7.

Kamps JA, Morselt HW, Swart PJ, Meijer DK, Scherphof GL. Massive targeting of liposomes, surface-modified with anionized albumins, to hepatic endothelial cells. *Proc Natl Acad Sci U S A*. 1997 Oct 14;94(21):11681-5.

Kawakami S, Sato A, Nishikawa M, Yamashita F, Hashida M. Mannose receptor-mediated gene transfer into macrophages using novel mannosylated cationic liposomes. *Gene Ther.* 2000 Feb;7(4):292-9.

Kim S, Ohta K, Hamaguchi A, Omura T, Yukimura T, Miura K, Inada Y, Ishimura Y, Chatani F, Iwao H. Angiotensin II type I receptor antagonist inhibits the gene expression of transforming growth factor-beta 1 and extracellular matrix in cardiac and vascular tissues of hypertensive rats. *J Pharmacol Exp Ther.* 1995 Apr;273(1):509-15.

Lee MK, Ha NR, Yang H, Sung SH, Kim GH, Kim YC. Antiproliferative activity of triterpenoids from *Eclipta prostrata* on hepatic stellate cells. *Phytomedicine.* 2008 Sep;15(9):775-80.

Managit C, Kawakami S, Yamashita F, Hashida M. Effect of galactose density on asialoglycoprotein receptor-mediated uptake of galactosylated liposomes. *J Pharm Sci.* 2005 Oct;94(10):2266-75.

Mann DA, Smart DE. Transcriptional regulation of hepatic stellate cell activation. *Gut.* 2002 Jun;50(6):891-6.

Marra F, Efsen E, Romanelli RG, Caligiuri A, Pastacaldi S, Batignani G, Bonacchi A, Caporale R, Laffi G, Pinzani M, Gentilini P. Ligands of peroxisome proliferator-activated receptor gamma modulate profibrogenic and proinflammatory actions in hepatic stellate cells. *Gastroenterology.* 2000 Aug;119(2):466-78.

Miyahara T, Schrum L, Rippe R, Xiong S, Yee HF Jr, Motomura K, Anania FA, Willson TM, Tsukamoto H. Peroxisome proliferator-activated receptors and hepatic stellate cell activation. *J Biol Chem.* 2000 Nov 17;275(46):35715-22.

Molteni A, Moulder JE, Cohen EF, Ward WF, Fish BL, Taylor JM, Wolfe LF, Brizio-Molteni L, Veno P. Control of radiation-induced pneumopathy and lung fibrosis by angiotensin-converting enzyme inhibitors and an angiotensin II type 1 receptor blocker. *Int J Radiat Biol.* 2000 Apr;76(4):523-32.

Ohishi T, Saito H, Tsusaka K, Toda K, Inagaki H, Hamada Y, Kumagai N, Atsukawa K, Ishii H. Anti-fibrogenic effect of an angiotensin converting enzyme inhibitor on chronic carbon tetrachloride-induced hepatic fibrosis in rats. *Hepatol Res.* 2001 Oct;21(2):147-158.

Opanasopit P, Sakai M, Nishikawa M, Kawakami S, Yamashita F, Hashida M. Inhibition of liver metastasis by targeting of immunomodulators using mannosylated liposome carriers. *J Control Release.* 2002 Apr 23;80(1-3):283-94.

Paizis G, Gilbert RE, Cooper ME, Murthi P, Schembri JM, Wu LL, Rumble JR, Kelly DJ, Tikellis C, Cox A, Smallwood RA, Angus PW. Effect of angiotensin II type 1 receptor blockade on experimental hepatic fibrogenesis. *J Hepatol.* 2001 Sep;35(3):376-85.

Ramos SG, Montenegro AP, Goissis G, Rossi MA. Captopril reduces collagen and mast cell and eosinophil accumulation in pig serum-induced rat liver fibrosis. *Pathol Int.* 1994 Sep;44(9):655-61.

Ray PE, Aguilera G, Kopp JB, Horikoshi S, Klotman PE. Angiotensin II receptor-mediated proliferation of cultured human fetal mesangial cells. *Kidney Int.* 1991 Oct;40(4):764-71.

Schneider AW, Kalk JF, Klein CP. Effect of losartan, an angiotensin II receptor antagonist, on portal pressure in cirrhosis. *Hepatology.* 1999 Feb;29(2):334-9.

Schuppan D, Ruehl M, Somasundaram R, Hahn EG. Matrix as modulator of stellate cell and hepatic fibrogenesis. *Semin Liver Dis.* 2001;21:351-72.

Sliedregt LA, Rensen PC, Rump ET, van Santbrink PJ, Bijsterbosch MK, Valentijn AR, van der Marel GA, van Boom JH, van Berkel TJ, Biessen EA. Design and synthesis of novel amphiphilic dendritic galactosides for selective targeting of liposomes to the hepatic asialoglycoprotein receptor. *J Med Chem.* 1999 Feb 25;42(4):609-18.

Sun Y, Zhang J, Zhang JQ, Ramires FJ. Local angiotensin II and transforming growth factor-beta1 in renal fibrosis of rats. *Hypertension.* 2000 May;35(5):1078-84.

Tharaux PL, Chatziantoniou C, Fakhouri F, Dussaule JC. Angiotensin II activates collagen I gene through a mechanism involving the MAP/ER kinase pathway. *Hypertension.* 2000 Sep;36(3):330-6.

Van Waes L, Lieber CS. Early perivenular sclerosis in alcoholic fatty liver: an index of progressive liver injury. *Gastroenterology.* 1977 Oct;73(4 Pt 1):646-50.

Weber H, Taylor DS, Molloy CJ. Angiotensin II induces delayed mitogenesis and cellular proliferation in rat aortic smooth muscle cells. Correlation with the expression of specific endogenous growth factors and reversal by suramin. *J Clin Invest.* 1994 Feb;93(2):788-98.

Weber KT. Fibrosis, a common pathway to organ failure: angiotensin II and tissue repair. *Semin Nephrol.* 1997 Sep;17(5):467-91.

Wolf G, Haberstroh U, Neilson EG. Angiotensin II stimulates the proliferation and biosynthesis of type I collagen in cultured murine mesangial cells. *Am J Pathol.* 1992 Jan;140(1):95-107.

Wu J, Zern MA. Hepatic stellate cells: a target for the treatment of liver fibrosis. *J Gastroenterol.* 2000;35(9):665-72.

Yoshiji H, Kuriyama S, Yoshii J, Ikenaka Y, Noguchi R, Nakatani T, Tsujinoue H, Fukui H. Angiotensin-II type 1 receptor interaction is a major regulator for liver fibrosis development in rats. *Hepatology.* 2001 Oct;34(4 Pt 1):745-50.

Yoshiji H, Yoshii J, Ikenaka Y, Noguchi R, Tsujinoue H, Nakatani T, Imazu H, Yanase K, Kuriyama S, Fukui H. Inhibition of renin-angiotensin system attenuates liver enzyme-altered preneoplastic lesions and fibrosis development in rats. *J Hepatol.* 2002 Jul;37(1):22-30.

CHAPTER 2

LITERATURE REVIEW



Literature Review

2.1 MAJOR COMPONENTS OF THE LIVER

- 2.1.1 The Hepatocytes
- 2.1.2 Liver Sinusoidal Cells
- 2.1.3 Liver Endothelial Cells
- 2.1.4 Kupffer Cells
- 2.1.5 Hepatic Stellate Cells

2.2 LIVER FIBROSIS

- 2.2.1 The Cellular Basis of Hepatic Fibrosis
- 2.2.2 General Mechanisms Regulating Hepatic Fibrosis
 - 2.2.2.1 Stellate Cell Activation
 - 2.2.2.2 Necrosis
 - 2.2.2.3 Apoptosis
 - 2.2.2.4 Lymphocytes
 - 2.2.2.5 Soluble Growth Factors
- 2.2.3 Disease-Specific Mechanisms Regulating Hepatic Fibrosis
 - 2.2.3.1 Hepatitis C
 - 2.2.3.2 Non-Alcoholic Steatohepatitis
- 2.2.4 Transcription Factors and Signaling Pathways
- 2.2.5 Different Types of Liver Fibrosis
 - 2.2.5.1 Hepatitis B Virus-Induced Fibrosis
 - 2.2.5.2 Hepatitis C Virus-Induced Fibrosis
 - 2.2.5.3 Liver Fibrosis Due to Genetically Inheritable Factors
 - 2.2.5.4 Autoimmune-Mediated Liver Disease
 - 2.2.5.5 Drug-Induced Liver Disease, Alcoholic and Non-Alcoholic Steatohepatitis
- 2.2.6 Determinants of Fibrosis Progression
 - 2.2.6.1 Liver Biopsy
 - 2.2.6.2 Non-Invasive Biochemical Markers of Liver Fibrosis
 - 2.2.6.3 Imaging Methods
- 2.2.7 Reversibility of Fibrosis and Cirrhosis
- 2.2.8 Clinical Trials

2.2.9 Emerging Treatments for Hepatic Fibrosis

2.2.9.1 Reducing Injury and Inflammation

2.2.9.2 Attenuating Stellate-Cell Activation

2.2.9.3 Inhibiting Properties of Activated Stellate Cells

2.2.9.4 Promoting Specific Apoptosis of Hepatic Stellate Cells

2.2.9.5 Degrading Scar Matrix

2.3 PPAR γ LIGANDS AND LIVER FIBROSIS

2.4 ANGIOTENSIN II RECEPTOR ANTAGONIST AND LIVER FIBROSIS

2.5 DRUG TARGETING TO HSC

2.6 LIPOSOMES

2.6.1 Composition of Liposomes

2.6.1.1 Phospholipids

2.6.1.2 Sterols

2.6.2 Types of Liposomes

2.6.3 Methods of Preparation of Liposomes

2.6.4 Characterization of Liposomes (New, 1990)

2.6.4.1 Size and Size Distribution

2.6.4.2 Lamellarity

2.6.4.3 Determination of Percentage Capture

2.6.5 Stability of Liposomes

2.6.6 Liposomes as Drug Delivery Systems

2.6.7 Liposomes in Drug Delivery to Liver Cells

2.6.7.1 Liposomes Targeted to Hepatocytes

2.6.7.2 Liposomes and Kupffer Cells

2.6.7.3 Targeting Liposomes to Liver Endothelial Cells

2.7 FORMULATION OPTIMIZATION

2.7.1 Variables

2.7.2 Effect, Interaction, and Confounding

2.7.2.1 Screening Designs

2.7.2.2 Factor Influence Study

2.7.3 Coding

2.7.4 Experimental Domain

2.7.5 Experimental Design

2.7.5.1 Factorial Designs

- 2.7.5.2 2k Factorial Designs
- 2.7.5.3 Higher Level Factorial Designs
- 2.7.5.4 Blocking in Experimental Designs
- 2.7.5.5 Resolution of Experimental Designs
- 2.7.5.6 Design Augmentation

2.7.6 Response Surfaces

2.7.7 Mathematical Models

2.8 DRUG PROFILE

2.8.1 Rosiglitazone (RGZ)

- 2.8.1.1 Chemical Structure
- 2.8.1.2 Physical Properties
- 2.8.1.3 Mechanism of Action
- 2.8.1.4 Pharmacokinetics
- 2.8.1.5 Side Effects
- 2.8.1.6 Interaction
- 2.8.1.7 Contraindication
- 2.8.1.8 Methods for Estimation

2.8.2 Candesartan (CDS)

- 2.8.2.1 Structure
- 2.8.2.2 Physical Properties
- 2.8.2.3 Mechanism of Action
- 2.8.2.4 Pharmacokinetics
- 2.8.2.5 Side Effects
- 2.8.2.6 Interaction
- 2.8.2.7 Contraindication
- 2.8.2.8 Methods for Estimation

2.9 REFERENCES

Considerable progress has been made, over the last 20 years, in understanding of the molecular pathophysiology of liver fibrosis. Liver fibrosis represents a wound healing response to a variety of chronic hepatic injuries including alcohol, autoimmune disease, viral hepatitis and toxic injury (Friedman, 2000). Common to wound healing in other tissues, the liver response to hepatocellular damage includes inflammation and tissue remodeling. Associated with this are changes in the quantity and quality of the extracellular matrix. There is accumulation of fibrillar collagen (mainly types I and III) in the space of Disse between the sinusoidal endothelial cells and the plates of hepatocytes. With chronic injury, the excess ECM in the liver causes architectural distortion and disruption of the normal pattern of blood flow through the liver. This eventually results in deterioration of hepatic performance with hepatic insufficiency and increased intrahepatic resistance to blood flow with portal hypertension.

Research into the pathogenesis of liver fibrosis has been facilitated by the observation that HSCs are the major mediators of the fibrotic process. Moreover, *in vitro* culture of extracted HSC and animal models has provided invaluable insights into hepatic fibrogenesis. Animal models include the carbon tetrachloride (CCl₄) model of liver fibrosis (Iredale et al., 1998) and the bile duct ligation model in the rat (Issa et al., 2002). In both models liver fibrosis may be induced in a reproducible manner. Furthermore, resolution of fibrosis may be observed to occur when the liver injury is stopped (cessation of injection or biliary jejunal anastomosis). These models have allowed identification of the activated HSCs as the key cell type responsible for production of the extracellular matrix (ECM) in chronic liver disease. Furthermore, they have highlighted that the stellate cell interacts with many other cell types within the liver, including hepatocytes, sinusoidal endothelial cells, lymphocytes, neutrophils and Kupffer cells (KCs) (liver macrophages). Many of these interactions play an important role in stellate cell biology and have been exploited to design and evaluate novel strategies and potential antifibrotic therapies.

2.1 MAJOR COMPONENTS OF THE LIVER

The liver is localized in the abdominal cavity between the digestive tract and the spleen. Functionally, it is in a strategic position between the gastro-intestinal tract and the general blood circulation. The organ has a double blood supply; most of the total blood influx is provided by the portal vein bringing nutrient-rich blood from the

digestive tract while the hepatic artery delivers blood supplemented with oxygen. Within the liver, the blood passes through a network of micro-vessels, called sinusoids, after which it is collected in the hepatic central veins and finally drained by the inferior vena cava.

The liver plays a central role in the metabolism of carbohydrates, proteins and fats, among other substances, and is thereby important for the maintenance of homeostasis in the body. The liver synthesizes most of the plasma proteins, such as albumin and globulins. Another function of the liver is detoxification, namely the biotransformation of xenobiotic compounds, pollutants and drugs into water-soluble compounds which then can be excreted either in bile or in urine. Importantly, the liver also eliminates particulate substances such as bacteria and viruses and different kinds of macromolecules from the blood stream.

At the microscopical level the liver is anatomically organised in functional units called lobules, built up from the three major liver cell types, the parenchymal cells or hepatocytes, the sinusoidal endothelial cells lining the sinusoids and a resident macrophage population, called KCs. The lobules have a hexagonal shape with the terminal hepatic vein in the centre and the portal triads at the corners of the hexagon. Each portal triad consists of a portal vein, a hepatic artery and a common hepatic bile duct. The parenchymal cells are structured in cords that are symmetrically distributed around the central vein and separated by liver sinusoids in which blood flows from portal triads towards the central vein.

The metabolic functions of the liver are maintained mainly by the parenchymal cells, which represent the major population of cells in the liver. In the narrow space between the endothelial cells and the hepatocytes, called the space of Disse, a fourth population of cells is localised, the HSCs. This population of non-parenchymal cells normally stores vitamin A and is involved in the production of ECM proteins. Other non-parenchymal cells that can be found in the liver are lymphocytes; including natural killer cells also known as pit cells, and biliary epithelial cells that line the bile ducts.

In the healthy liver, ECM constituents account for 0.5 % of the liver weight. In spite of its relatively small volume, the composition of the ECM in the space of Disse is of

great importance for the functioning of the liver cells. Hepatocytes, endothelial cells and HSCs require a proper ECM composition to express their phenotypes.

2.1.1 The Hepatocytes

Hepatocytes represent about 65 % of all liver cells in number and more than 90 % of liver volume and are the main functional unit of this organ. Although they have a polyhedral shape, functionally two major domains can be distinguished with regard to the outer plasma membranes of these cells. The bile canalicular (i.e. apical) surface is specialized in transport of bile salts, bilirubin, cholesterol, phospholipids as well as xenobiotics into the bile. The contact of hepatocytes with the blood occurs at the basolateral domain, bordering the space of Disse. Numerous microvilli on this membrane domain allow for a substantial increase in exchange surface. In addition, the plasma membrane of the basolateral domain contains many transmembrane transport proteins and also has endocytotic properties. Thus, this domain is rich in receptors such as the asialoglycoprotein receptor, the transferrin receptor and several lipoprotein receptors.

Hepatocytes are crucial for the glucose homeostasis in the body and can store as well as release glucose. Thus, their cytoplasm contains the storage form of glucose, the glycogen granules. Beside, hepatocytes harbour specific metabolic pathways such as the urea cycle, regulating the blood levels of amino acids and ammonia derived from the intestine, and the specific lipogenic and lipolytic enzyme systems involved in the synthesis and metabolism of a variety of serum and intestinal lipoproteins. Also the formation of bilirubin from heme and the excretion of cholesterol and its conversion into bile acids are specific hepatocytic processes.

2.1.2 Liver Sinusoidal Cells

KCs, endothelial cells and HSCs are major cells of hepatic sinusoid (Figure 2.1). Each of these cell populations has its own specific characteristics and functionality. Although these cells form a minority of the total liver cell population, they are essential for the proper functioning of the organ.

2.1.3 Liver Endothelial Cells

Liver endothelial cells (LEC) comprise approximately one fifth of all liver cells and represent about half of the non-parenchymal cells in number. They form the

endothelial lining of the hepatic sinusoids and as such possess unique features allowing them to provide a selective barrier between the blood stream on the one hand and the hepatocytes and HSCs on the other. LEC distinguish themselves from other vascular endothelial cells because they contain pores or fenestrations varying in diameter from 150–175 nm that are grouped in clusters (Wisse et al., 1985). Furthermore, a basal lamina underneath the all other endothelial cells in the body is lacking in the sinusoids of the liver. This architecture of the sinusoidal capillaries allows substances smaller than the diameter of the fenestrations to freely exchange between the blood and the space of Disse.

LEC also play an important functional role in a variety of liver-associated processes. High endocytotic activity of these cells enables them to clear the blood from different macromolecular waste products. Moreover, LEC are known to secrete cytokines, such as tumor necrosis factor - α (TNF- α) (Nagano et al., 1992) and interleukin (IL)-6 (Knolle et al., 1997) and express adhesion molecules such as intercellular adhesion molecule - 1 (ICAM-1) and vascular cell adhesion molecule - 1 (VCAM-1) (van Oosten et al., 1995) which are crucial in the interaction with leukocytes and neutrophils. In addition LEC express several scavenger receptors, which bind and take up negatively charged proteins and lipoproteins from the blood and are involved in the regulation of lipoprotein metabolism as well as in antigen presentation.

In the healthy liver, LEC play a role in the turn-over of ECM. They secrete collagen type IV and laminin (Maher and McGuire, 1990) and clear hyaluronan (McGary et al., 1993), (pro)collagen and fibronectin (Smedsrod et al., 1994), degradation products of ECM.

2.1.4 Kupffer Cells

KCs account for 15 % of the total liver cell population. Together with macrophages of the spleen they are a major part of the so-called mononuclear phagocyte system. KCs are predominantly located in the sinusoids, where they are directly exposed to the blood stream while being anchored to the endothelial cells. In addition to their strategic location, KCs are characterised by their high phagocytic activity and they are responsible for the removal of circulating microorganisms, immune complexes, dead cells and other debris from the blood stream as well as the detoxification of bacterial endotoxins. In addition to performing these phagocytic processes, KCs take up

different substances from the circulation via receptor mediated endocytosis. There are several receptors which facilitate this process, for example: mannose receptors, fucose receptors, Fc receptors, CD14 receptors (Smedsrod et al., 1994) and scavenger receptors class A I, A II and B I (Van Berkel et al., 2000).

As part of the innate immune system, KCs play a central role in the regulation of inflammatory processes and other immunological reactions in the liver. In response to stimuli, for example by bacterial endotoxin, KCs produce various cytokines, such as TNF- α , IL-1, IL-6 (Luster et al., 1994) eicosanoids and reactive oxygen species (ROS), which promote chemotaxis, phagocytosis and ROS production by other inflammatory cells, as well as stimulating different reactions of other liver cells. On the other hand, KCs are also capable to release factors which have an anti-inflammatory action, like IL-10 (Knolle et al., 1997).

2.1.5 Hepatic Stellate Cells

Hepatic stellate cells (HSC) represent 5 to 8 % of all liver cells in the healthy organ. A characteristic feature of these cells is the expression of two different phenotypes; quiescent in the normal liver, and activated in the diseased. As a consequence of this ability of transformation, HSCs also change their functions.

Quiescent HSC have a star-like shape and their cytoplasm contains vitamin A droplets, for which they were formerly also known as fat-storing cells (other former names are Ito cells, lipocytes). Storage and controlled release of retinoids is a major function of HSCs in the healthy liver. In the digestive tract esterified retinol is incorporated into chylomicrons which enter the blood stream after being secreted into the lymphatic system. After having been depleted from part of their triglyceride-load in the peripheral vasculature, the resulting chylomicron remnants are taken up from the blood by the hepatocytes and from there the retinol is transported to HSC with the help of retinol binding proteins (RBP), where it is stored as retinyl ester. From HSC, retinol bound to RBP can be secreted into the circulation or transported back to the hepatocytes.

The crucial process of ECM turnover in the space of Disse is also controlled by HSC. They secrete limited amounts of ECM proteins such as collagen type III, collagen type IV and laminin (Maher and McGuire, 1990). Furthermore, HSC express several matrix metalloproteinases (MMP), such as MMP-2, MMP-3, MMP-10, MMP-13 and

MMP-14, as well as their inhibitors (tissue inhibitors of matrix metalloproteinase -1 (TIMP-1) and TIMP-2) to control the matrix degradation processes (Knittel et al., 1999).

Because of their anatomical position, it is likely that quiescent HSCs also are involved in controlling the blood flow through the hepatic sinusoids. In fact, HSCs encircle the sinusoid with their long cellular processes in a cylindrical manner and can produce vasoactive proteins, including substance P, neuropeptide Y and somatostatin (Geerts, 2001).

Quiescent HSC are producers of hepatocyte growth factor (HGF) (Ramadori et al., 1992), which stimulates hepatocyte proliferation, and vascular endothelial growth factor (VEGF) (Ishikawa et al., 1999), a stimulus for growth of sinusoidal and vascular endothelial cells. In addition, molecules such as endothelin (ET)-1 (Shao et al., 1999), transforming growth factor- β (TGF- β) (De Bleser et al., 1997), neutrophins and erythropoietin (Maxwell et al., 1994) are secreted by HSC in the normal liver. All these mediators tightly control homeostasis within sinusoids and pathological processes within the liver.

2.2 LIVER FIBROSIS

Hepatic fibrosis, or scarring of the liver, is emerging as a treatable complication of advanced liver disease, following significant progress in understanding its underlying mechanisms. Efforts have focused on the HSCs, as these cells can undergo 'activation' into proliferative and fibrogenic myofibroblast-like cells during liver injury. Stimuli driving stellate cell activation include hepatocellular necrosis due to oxidant stress, apoptosis, and soluble growth factors. Specific lymphocyte subsets can also stimulate fibrogenesis. A cascade of signaling and transcriptional events in stellate cells underlies the fibrogenic response to liver injury, with each step in the cascade being a potential target for antifibrotic therapy. Disease specific fibrogenic mechanisms have also been uncovered: in hepatitis C, this may include direct stimulation of stellate cell activation by viral infection; in nonalcoholic steatohepatitis, elevated levels of leptin and increased leptin signaling by stellate cells increase fibrogenesis. Determinants of fibrosis progression include both environmental and genetic factors, with ongoing efforts to define specific polymorphisms correlating with fibrosis progression rates. Human studies now indicate that fibrosis and even cirrhosis could be reversible,

especially if the underlying disease is eradicated. A key challenge is to establish noninvasive means of assessing fibrosis stage and progression using either serum tests and/or imaging. In addition, endpoints of antifibrotic clinical trials need to be established so that reliable evidence of benefit can be identified. We are on the cusp of a new era in which antifibrotic therapies could become important in treating chronic fibrosing liver disease (Friedman, 2003; Friedman, 2008; Bataller and Brenner, 2005).

Hepatic fibrosis refers to the accumulation of interstitial or 'scar' ECM after either acute or chronic liver injury. Cirrhosis, the end-stage of progressive fibrosis, is characterized by septum formation and rings of scar that surround nodules of hepatocytes. The composition of ECM molecules in the fibrotic liver is similar to those of other fibrosing parenchyma, including lung and kidney, and is also similar among different etiologies of liver disease. Typically fibrosis requires years or decades to become clinically apparent, but notable exceptions in which cirrhosis develops over months may include pediatric liver disease (e.g. biliary atresia), drug-induced liver disease, and viral hepatitis associated with immunosuppression after liver transplantation.

Rapid progress in understanding the mechanisms of hepatic fibrosis exemplifies how basic research has begun to yield meaningful prospects for translation into new diagnostics and treatments for patients with liver disease. These advances include the isolation and characterization of fibrogenic cell types in liver, the clarification of general and disease-specific pathogenic mechanisms, and the broader appreciation of the natural history and reversibility of hepatic fibrosis. Recent reviews highlighting molecular mechanisms and historical aspects are recommended to the reader for more detail (Friedman, 2000; Schuppan et al., 2001; Geerts, 2001; Pinzani and Marra, 2001; Rocky, 2003).

2.2.1 The Cellular Basis of Hepatic Fibrosis

The HSC, a resident perisinusoidal cell that stores vitamin A, has been the focus of efforts to identify the source of extracellular matrix, because it can undergo 'activation' when the liver is injured. This activation is characterized by the acquisition of a proliferative, contractile, migratory, fibrogenic and inflammatory phenotype (Friedman, 2000) (Figure 2.1 and 2.2). Indeed, the model of sequential stellate cell

activation towards myfibroblasts has provided a robust conceptual framework, allowing new advances to be placed in a clear biological context. Recent studies have underscored the heterogeneity of mesenchymal populations in liver ranging from classic stellate cells to portal fibroblasts (Kinnman et al., 2003), with the variable expression of neural (Cassiman et al., 2002), angiogenic (Corpechot et al., 2002), contractile (Rocky, 2003) and even bone-marrow-derived (Forbes et al., 2004) markers. Moreover, experimental genetic 'marking' of stellate cells, by expressing fluorescent proteins downstream of either fibrogenic or contractile gene promoters, illustrates the plasticity of fibrogenic cell populations in vivo (Magness et al., 2004). In view of this capacity for 'transdifferentiation' between different mesenchymal cell lineages and possibly even epithelial cells (Kalluri and Neilson, 2003), the key issue is not necessarily where fibrogenic cells arise from, but rather whether they express target molecules such as receptors or cytokines (Figure 2.1) in sufficient concentrations in vivo to merit their targeting by diagnostic agents or antifibrotic compounds.

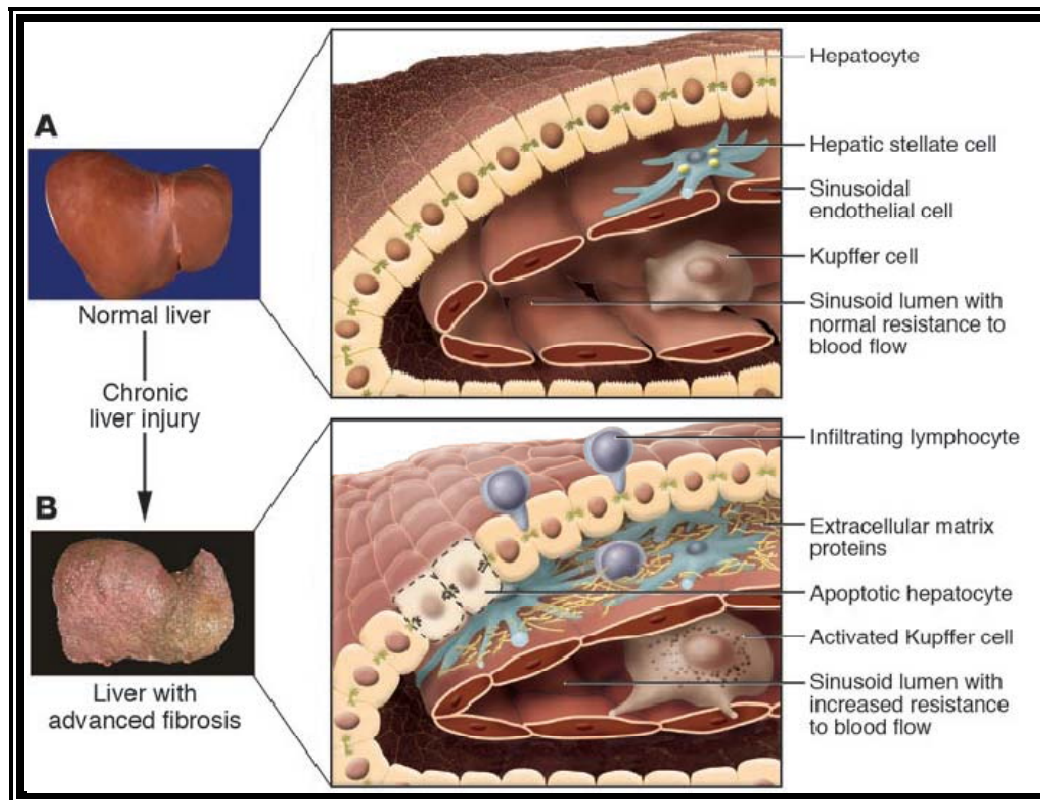


Figure 2.1 Sub-endothelial changes during stellate cell activation accompanying liver injury (Bataller and Brenner, 2005)

2.2.2 General Mechanisms Regulating Hepatic Fibrosis

More importantly, HSCs and sinusoidal endothelial cells have emerged as inflammatory effectors. Sinusoidal endothelial cells, which are normally fenestrated to allow rapid bidirectional transport of solutes between sinusoidal blood and parenchymal cells, may rapidly lose their fenestrations on injury and express pro-inflammatory molecules including ICAM-1, Vascular Endothelial Cell Growth Factor (VEGF) and adhesion molecules (LeCouter et al., 2003; Olaso et al., 2003). Together with stellate cells, they activate angiogenic pathways in response to the hypoxia associated with local injury or malignancy (Olaso et al., 2003; Marra, 2002; Yoshiji et al., 2003; Ankoma-Sey et al., 2000).

HSCs are a nexus for converging inflammatory pathways leading to fibrosis. On activation, they release chemokines (Marra, 2002; Schwabe et al., 2003) and other leukocyte chemoattractants, and upregulate the expression of key inflammatory receptors including ICAM-1 (Bataller et al., 2004), chemokine receptors (Efsen et al., 2002), as well as those mediating lipopolysaccharides signaling, including Toll-like receptor 4 (Paik et al., 2003). Stellate cells might also contribute to the intrahepatic apoptosis of T lymphocytes (Kobayashi et al., 2003).

2.2.2.1 Stellate Cell Activation

Stellate cell activation is the central event in hepatic fibrosis. Activation consists of 2 major phases: (1) initiation (also called preinflammatory stage) and (2) perpetuation (Figure 2.2) (Friedman, 2000). Initiation refers to early paracrine-mediated changes in gene expression and phenotype that render the cells responsive to other cytokines and stimuli. Perpetuation then results from the effects of these stimuli on maintaining the activated phenotype and generating fibrosis.

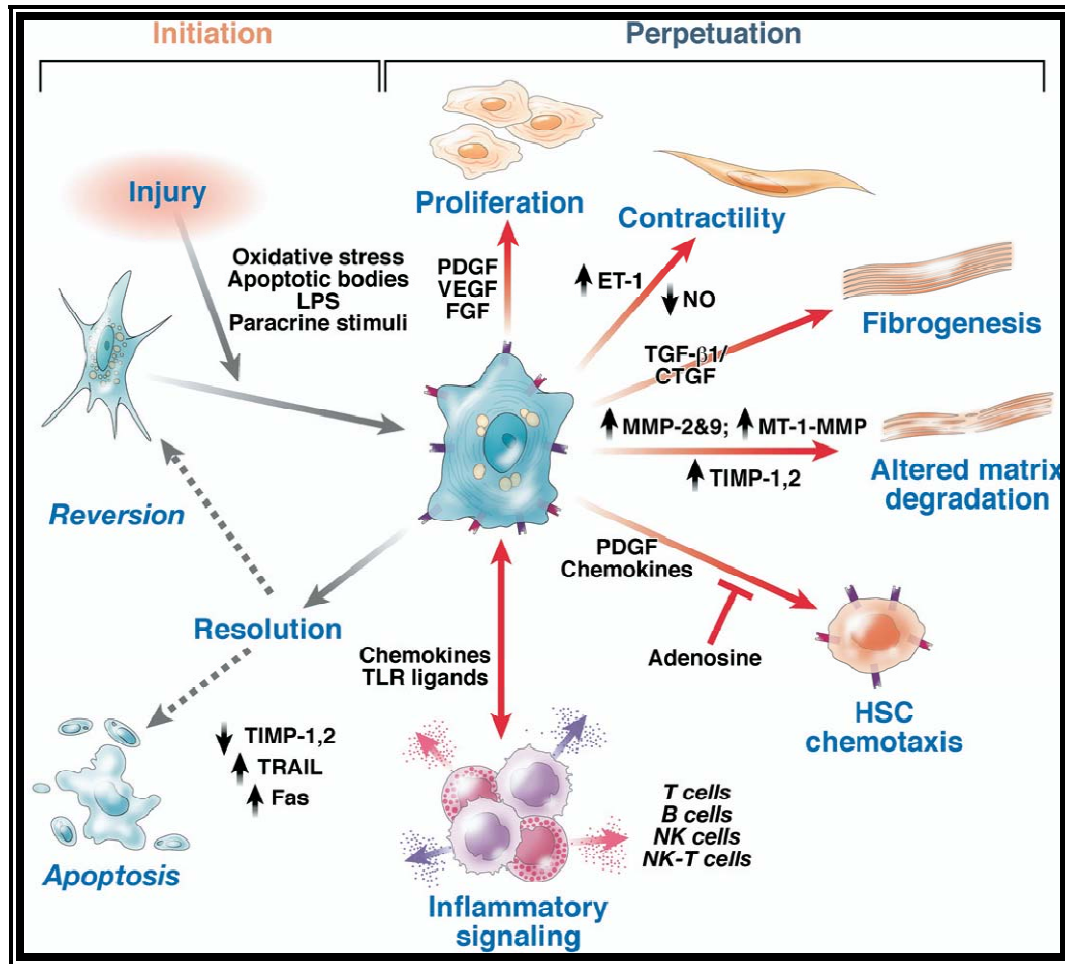


Figure 2.2 Pathways of stellate cell activation and resolution during liver injury
(Friedman, 2008)

2.2.2.1.1 Initiation of Stellate Cell Activation

The earliest changes in stellate cells are likely to result from paracrine stimulation by all neighboring cell types, including sinusoidal endothelium, KCs, hepatocytes, platelets, and leukocytes. Endothelial cells are also likely to participate in activation, both by production of cellular fibronectin and via conversion of TGF- β from the latent to active, profibrogenic form (Figure 2.3) (Bataller and Brenner, 2001).

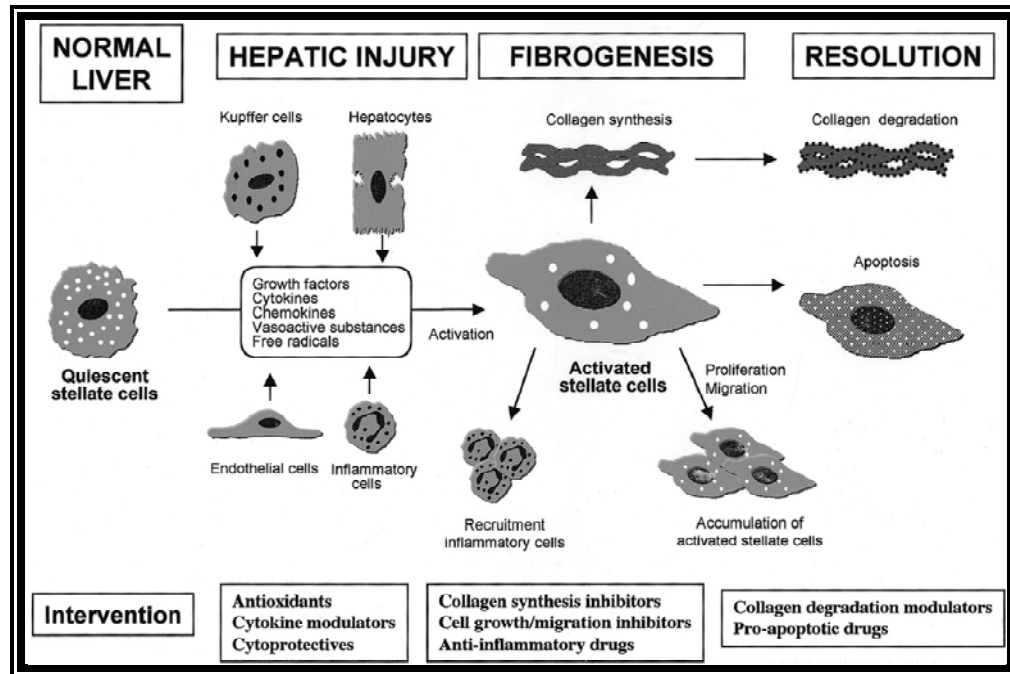


Figure 2.3 Biological actions of hepatic stellate cells (HSCs) during liver fibrogenesis and potential sites for therapeutic intervention (Bataller and Brenner, 2001)

Kupffer cell infiltration and activation also play a prominent role in the process. The influx of KCs coincides with the appearance of stellate cell activation markers. KCs can stimulate matrix synthesis, cell proliferation, and release of retinoids by stellate cells through the actions of cytokines (especially, TGF- β_1) and reactive oxygen intermediates/lipid peroxides. Proliferation has been attributed to Kupffer cell-derived TGF- α (Gressner, 1995; Friedman and Arthur, 1989). TGF- β derived from KCs markedly stimulates stellate cell ECM synthesis (Gressner, 1995; Gressner et al., 1993). KCs produce anti-inflammatory as well as proinflammatory cytokines, including IL-10 (Nieto et al., 2000). Of interest, IL-10 downregulates fibrogenesis in cultured stellate cells by decreasing collagen synthesis and increasing production of collagenase (Wang et al., 1998(b)).

Another means by which KCs can influence stellate cells is through secretion of MMP-9 (gelatinase B) (Winwood et al., 1995). MMP-9 can activate latent TGF- β , which in turn can stimulate stellate cell collagen synthesis (Yu and Stamenkovic, 2000). Lastly, KCs are an important source of ROS in the liver. ROS, whether produced internally within stellate cells (Nieto et al., 1999; Svegliati-Baroni et al.,

2001) or released into the extracellular environment (Lee et al., 1995), are capable of enhancing stellate cell activation and collagen synthesis. KCs also produce nitric oxide (NO), which can counterbalance the stimulatory effects of ROS by reducing stellate cell proliferation and contractility. Hepatocytes, as the most abundant cell type in liver, are a potent source of fibrogenic lipid peroxides in inflammatory liver diseases.

Platelets are a potent source of growth factors, and are present in the injured liver (Bachem et al., 1989). Potentially important platelet mediators include platelet derived growth factor (PDGF), TGF- β_1 , and epidermal growth factor.

Leukocytes that are recruited to the liver during injury join with KCs in producing compounds that modulate stellate cell behavior. Neutrophils are an important source of ROS, which have a direct stimulatory effect on stellate cell collagen synthesis. The specific role of neutrophils as a stimulus to stellate cells was demonstrated in a coculture experiment in which cells activated by N-formyl-methionyl-leucyl-phenylalanine were plated in direct contact with stellate cells (Casini et al., 1997). Activated neutrophils increased stellate cell collagen synthesis 3-fold over control levels. Superoxide was identified as the principal mediator of the neutrophil effect. Activated neutrophils also produced NO, which dampened the effect of superoxide on collagen expression but did not abrogate it completely. Lymphocytes, including CD4+ T-helper (Th) cells, reside in the liver (Winnock et al., 1995; Tiegs et al., 1992) and represent a further potential source of cytokines. Th lymphocytes help orchestrate the host-response via cytokine production and can differentiate into Th1 and Th2 subsets, a classification that is based on the pattern of cytokines produced. In general, Th1 cells produce cytokines that promote cell-mediated immunity and include interferon (IFN)- γ , TNF, and IL-2. Th2 cells produce IL-4, IL-5, IL-6, and IL-13, and promote humoral immunity. Th1 cytokines inhibit the development of Th2 cells and Th2 cytokines inhibit the development of Th1 cells. Thus, the host response to infection or injury frequently polarizes to either a Th1 or Th2 response, but not both.

Several experimental models offer evidence implicating Th cell-derived cytokines in determining the immune response. The polarization of the immune response is enhanced when chronic exposure to an agent occurs, such as with persistent infections or exposure to environmental toxins. Furthermore, polarization of the immune

response to Th1 or Th2 cytokines is under genetic control, as demonstrated by divergent responses of different inbred strains of mice to experimental murine leishmaniasis (Guler et al., 1996). Genetically resistant mice - such as C57BL/6 mice - exhibit an expansion of IFN- γ -producing Th1 cells and control the infection, whereas susceptible strains (BALB/c mice) develop an IL-4-mediated Th2 response (Heinzel et al., 1989; Wang et al., 1994).

More intriguing data have been obtained from studies comparing the effects of T lymphocytes on liver fibrosis. Overall, data suggest that Th2 lymphocytes favor fibrogenesis in liver injury over Th1 lymphocytes. The effects of CCl₄ have been examined in mice with several different lymphocyte profiles, including T-cell depletion (severe combined immunodeficiency, SCID), Th1 predominance (C57/BL6), and Th2 predominance (BALB/c) (Shi et al., 1997). SCID mice from both C57/BL6 and BALB/c backgrounds develop liver fibrosis after treatment with CCl₄ for 4 weeks. The degree of fibrosis is modified significantly, however, in immunocompetent mice from both strains. Immunocompetent C57/BL6 mice, whose lymphocyte cytokine profile includes IFN- γ , actually exhibit less fibrosis than SCID mice from the same background. Indeed, when C57/BL6 mice with targeted disruption of IFN- γ are treated with CCl₄, fibrosis returns to the level seen in C57/BL6 SCID mice. However, immunocompetent BALB/c mice, whose lymphocyte cytokine profile includes the fibrogenic compounds IL-4 and TGF- β , exhibit more fibrosis than BALB/c SCID mice. Among all of the studies examining immunoregulation of fibrosis, those demonstrating modulation by T-lymphocytes appear the most convincing.

2.2.2.1.2 Perpetuation of Stellate Cell Activation

Perpetuation of stellate cell activation involves several discrete changes in cell behavior, as discussed below.

2.2.2.1.2.1 Proliferation

PDGF is the most potent stellate cell mitogen identified. Induction of PDGF receptors early in stellate cell activation increases responsiveness to this potent mitogen (Wong et al., 1996). Downstream pathways of PDGF signaling have been carefully characterized in stellate cells.

2.2.2.1.2.2 Chemotaxis

Stellate cells can migrate towards cytokine chemoattractants (Maher, 2001; Marra et al., 1999), an action that is characteristic of woundinfiltrating mesenchymal cells in other tissues as well. Chemotaxis of stellate cells explains in part why stellate cells align within inflammatory septa in vivo.

2.2.2.1.2.3 Fibrogenesis

Increased matrix production is the most direct way that stellate cell activation generates hepatic fibrosis. The most potent stimulus to collagen I production is TGF- β , which is derived from both paracrine and autocrine sources.

Lipid peroxidation products are emerging as important stimuli to ECM production; their effects may be amplified by loss of antioxidant capacity of stellate cells as they activate (Whalen et al., 1999). These important insights have provoked efforts to use antioxidants as therapy for hepatic fibrosis.

2.2.2.1.2.4 Contractility

Contractility of stellate cells may be a major determinant of early and late increases in portal resistance during liver fibrosis. Activated stellate cells impede portal blood flow by both constricting individual sinusoids and contracting the cirrhotic liver, because the collagenous bands typical of end-stage cirrhosis contain large numbers of activated stellate cells (Rocky, 2001). The major contractile stimulus towards stellate cells is ET-1. Receptors for the latter are expressed on both quiescent and activated stellate cells, but its subunit composition may vary (Housset et al., 1993). Contractility of stellate cells in response to ET-1 has also been observed in vivo (Zhang et al., 1994). Other, less potent contractile stimuli have also been identified (Rocky, 2001). For example, KCs produce eicosanoids, including prostaglandin D2 (PGD2), prostaglandin E2 (PGE2), and thromboxanes (Peters et al., 1990; Kawada et al., 1992(b)). Eicosanoids modulate stellate cell contractility, with thromboxanes typically promoting contraction and PGE2 mediating relaxation (Kawada et al., 1992(a)).

Locally produced vasodilator substances may counteract the constrictive effects of ET-1 (Rocky, 2001). NO, which is also produced by stellate cells, is a well-characterized endogenous antagonist to ET.

2.2.2.1.2.5 Matrix Degradation

Quantitative and qualitative changes in matrix protease activity play an important role in ECM remodeling accompanying fibrosing liver injury. Stellate cells express virtually all of the key components required for pathologic matrix degradation and therefore play a key role not only in matrix production, but also in matrix degradation. An enlarging family of matrix-metalloproteinases has been identified that are calcium-dependent enzymes which specifically degrade collagens and noncollagenous substrates (Benyon and Arthur, 2001). Broadly, these enzymes fall into 5 categories based on substrate specificity: (1) interstitial collagenases (MMP-1, -8, -13); (2) gelatinases (MMP-2,-9) and fibroblast activation protein (Levy et al., 1999); (3) stromelysins (MMP-3, -7, -10, 11); (4) membrane-type (MMP-14, 15, -16, -17, -24, -25); and (5) a metalloelastase (MMP-12). Inactive metalloproteinases can be activated through proteolytic cleavage by either membrane-type matrix metalloproteinase 1 (MTMMP-1) or plasmin, and inhibited by binding to specific inhibitors known as TIMPs. Thus, net collagenase activity reflects the relative amounts of activated metalloproteinases and their inhibitors, especially TIMPs.

In liver, "pathologic" matrix degradation refers to the early disruption of the normal subendothelial matrix that occurs through the actions of at least 4 enzymes: MMP2 and MMP-9 degrade type IV collagen; MTMMP-1 or -2 activates latent MMP-2; and stromelysin-1 degrades proteoglycans and glycoproteins, and also activates latent collagenases. Stellate cells are a key source of MMP-2 (Arthur et al., 1992; Milani et al., 1994) as well as increases in the specific MMP inhibitor molecules, TIMP-1 (Murawaki et al., 1997; Iredale et al., 1998) and TIMP-2, (Herbst et al., 1997) leading to a net decrease in protease activity, and therefore, more unopposed matrix accumulation. Moreover, an emerging role for TIMPs in regulating apoptosis suggests that their influence on liver homeostasis extends beyond that of direct effects on ECM turnover.

2.2.2.1.2.6 Retinoid Loss

As stellate cells activate, they lose their characteristic perinuclear retinoid (vitamin A) droplets and acquire a more fibroblastic appearance. In culture, retinoid is stored as retinyl esters, whereas as stellate cells activate, the retinoid released outside the cell is retinol, suggesting that there is intracellular hydrolysis of esters prior to export

(Friedman, 1996). However, it is generally unknown whether retinoid loss is required for stellate cells to activate and which retinoids may accelerate or prevent activation *in vivo*. Recently, peroxisome proliferator-activated receptors (PPAR), in particular PPAR γ , have also been identified in stellate cells, and their expression increases with activation (Miyahara et al., 2000; Marra et al., 2000). Ligands for this newly identified nuclear receptor family downregulate stellate cell activation (Marra et al., 2000).

2.2.2.1.2.7 WBC Chemoattractant and Cytokine Release

Increased production and/or activity of cytokines may be critical for both autocrine and paracrine perpetuation of stellate cell activation. Direct effects on stellate cell matrix production and contractility have been attributed to autocrine TGF- β and ET-1, respectively. Stellate cells can amplify the inflammatory response by inducing infiltration of mono- and polymorphonuclear leukocytes.

2.2.2.2 Necrosis

Hepatic injury, whether subclinical or overt, indicates that there is a perturbation of normal liver homeostasis, with the extracellular release of either free radicals (i.e. 'oxidant stress'), intracellular constituents, and/or cytokines and signaling molecules. Sources of these mediators may be circulating (i.e. endocrine), transferred between cells (i.e. paracrine) or act within the same cell (i.e. autocrine). In particular, oxidant-stress-mediated necrosis leading to stellate cell activation may underlie various liver diseases, including hemochromatosis, alcoholic liver disease, viral hepatitis and nonalcoholic steatohepatitis (NASH) (Tsukamoto, 2002; Bataller et al., 2003(b); Tuma, 2002). Liver injury is typically associated with the infiltration of inflammatory cells, but even in their absence the liver contains sufficient resident macrophages (KCs) and natural killer cells (pit cells) to initiate local inflammation before the arrival of extrahepatic cells.

2.2.2.3 Apoptosis

Although necrosis is considered a classical inflammatory and fibrogenic stimulus, recent findings also implicate apoptosis, or programmed cell death, in the fibrogenic response. Apoptotic fragments released from hepatocytes are fibrogenic for cultured stellate cells (Canbay et al., 2003), and FAS((TNF receptor superfamily, member 6)) -

mediated hepatocyte apoptosis *in vivo* in experimental animals is also fibrogenic (Canbay et al., 2002).

2.2.2.4 Lymphocytes

Remarkably, little attention has focused on the contribution of different lymphocyte subsets to hepatic fibrogenesis even though lymphocyte infiltration is a major feature of many forms of chronic liver disease. Interest has increased recently, in part because of the observation that patients infected with hepatitis C virus (HCV) who are co-infected with Human immunodeficiency virus (HIV), as well as those who are immunosuppressed after liver transplantation, have accelerated fibrosis rates, which implicates the immune system as a determinant of fibrogenesis. These observations are supported by animal studies demonstrating that the immune phenotype regulates fibrogenesis by means other than simply increasing the extent of hepatocyte injury (Shi et al., 1997). These findings led in turn to efforts to map the genetic loci accounting for these differences (Hillebrandt et al., 2002). Most recently, CD8+ lymphocytes have emerged as potential profibrogenic cells based on their ability to induce early fibrogenesis after adoptive transfer from animals with liver injury to naive SCID mice (Safadi et al., 2004).

2.2.2.5 Soluble Growth Factors

The range of soluble growth factors regulating stellate cell activation continues to broaden, although the key proliferative, fibrogenic, and contractile stimuli that were identified previously (Friedman, 2000) (including PDGF, TGF- β , and ET-1, respectively) remain the dominant stimuli in current models of hepatic fibrosis. In addition, CCN2 (previously known as connective tissue growth factor, or CTGF), is a downstream target of TGF- β 1 that has been recognized as an additional fibrogenic signal (Rachfal and Brigstock, 2003). Pathways regulating the synthesis, secretion and activation of cytokines during fibrosis are well characterized, and offer many potential therapeutic targets. In addition, the proteolytic release by activated stellate cells of bound growth factors from ECM reservoirs may regulate local fibrogenic activity within the pericellular milieu (Schuppan et al., 2001).

2.2.3 Disease-Specific Mechanisms Regulating Hepatic Fibrosis

In addition to generic mechanisms of fibrogenesis that are common to all experimental and human liver disease, there has been progress in elucidating disease-specific mechanisms, in particular in hepatitis C and NASH.

2.2.3.1 Hepatitis C

A recent study has raised the possibility that stellate cells could be infected by HCV, by identifying the expression of putative HCV receptors in activated stellate cells, including CD80, Low-density lipoprotein (LDL) receptor and C1q. Moreover, adenoviral transduction of HCV nonstructural and core proteins induces stellate cell proliferation and the release of inflammatory signals (Bataller et al., 2004). In HCV infected liver, chemokines and their receptors are upregulated, stimulating lymphocyte recruitment (Bonacchi et al., 2003). HCV proteins could also interact directly with sinusoidal endothelium (Pohlmann et al., 2003).

2.2.3.2 Non-Alcoholic Steatohepatitis

The rising prevalence of obesity in the US and Western Europe is associated with an alarming increase in NASH (Angulo, 2002) leading to advanced fibrosis and cirrhosis. Leptin, a circulating adipogenic hormone whose serum levels are proportionate to adipose mass in circulating blood, has been clearly tied to stellate cell fibrogenesis (Ikejima et al., 2002; Leclercq et al., 2002; Saxena et al., 2003). Sources are likely to be both endocrine and autocrine, and its activity is amplified because of enhanced signaling through the leptin receptor, the expression of which is upregulated during stellate cell activation (Ikejima et al., 2002). Concurrently, downregulation of adiponectin in obesity, a counter-regulatory hormone, might amplify the fibrogenic activity of leptin. This possibility is supported by findings in mice lacking adiponectin, which have enhanced fibrosis after toxic liver injury (Kamada et al., 2003).

2.2.4 Transcription Factors and Signaling Pathways

There have been too many advances in dissecting the pathways of membrane and intracellular signaling and transcriptional gene regulation in activated HSCs to detail here (Mann and Smart, 2002). A growing number of transcription factors could regulate stellate cell behavior, including PPAR- β (Hellemans et al., 2003; Marra et al.,

2000; Miyahara et al., 2000) and retinoid receptors (Hellemans et al., 2004), nuclear factor B (NFB) (Paik et al., 2003), Jun D (Mann and Smart, 2002), Kruppel like factor 6, Foxf1 (Kalinichenko et al., 2003), among others. Similarly, both general and cell-type-specific membrane receptors and signaling pathways have also been thoroughly characterized, including Receptor Tyrosine Kinases (Pinzani and Marra, 2001), chemokine receptors (Marra, 2002), and Integrins (Yang et al., 2003(a)).

2.2.5 Different Types of Liver Fibrosis

To date, therapies that interfere with the underlying cause of the disease represent the best pharmacological treatment options for liver fibrosis. The following paragraphs will therefore give a brief outline of the generally applied pharmacological interventions in patients with this disease. Pharmacological treatment strategies are discussed in relation to the different injurious events leading to liver scarring.

2.2.5.1 Hepatitis B Virus-Induced Fibrosis

Viral hepatitis is an important cause of chronic liver disease and fibrosis. World wide, approximately 350 million people are chronically infected with hepatitis B virus (HBV), and it is estimated that approximately 25% of these patients will develop liver cirrhosis. The virus infects hepatocytes by binding to certain cell surface receptors, subsequently followed by uncoating of the virus particle and translocation of the HBV genome to the nucleus. Viral deoxyribonucleic acid (DNA) resides in hepatocytes very persistently and its clearance appears to be dependent on the clearance of infected hepatocytes by CD8⁺ T-lymphocytes. This immune response is mainly responsible for the liver injury that follows from HBV infection, although also direct cytopathic effects of HBV have been described in patients with very high viral loads (Pinzani et al., 2005; Colombo and Sangiovanni, 2003; Fung and Lok, 2005; Lok, 2000).

Until recently, only (pegylated) IFN- α was available for the treatment of patients with chronic hepatitis B infection. IFN- α is an immunomodulating drug that improves the cytotoxic T-lymphocyte response against infected hepatocytes. Unfortunately, its use is contra-indicated in patients with clinical cirrhosis. Because IFN- α acts by increasing the clearance of HBV infected hepatocytes, in cirrhotic patients with decompensated liver function, this can result in the loss of a relative large fraction of

the remaining functional liver parenchyma and thus in an acute deterioration of liver function. Moreover, an increased incidence of bacterial infections has been associated with the use of IFN- α in cirrhotic patients, which is related to myelosuppressive effects of the drug (Fung and Lok, 2005; Lok, 2000).

However, with the advent of the HBV DNA polymerase inhibitors lamivudine and adefovir, also the treatment of HBV-infected patients with clinical cirrhosis has become an option. In contrast to IFN- α , lamivudine and adefovir have an excellent tolerability and side effect profile. Lamivudine is metabolized intracellularly to its active triphosphate, which acts as a nucleoside analog that inhibits HBV DNA polymerase and causes DNA chain termination. Adefovir is a nucleotide analog to adenosine monophosphate and acts via a similar mechanism (Hardman et al., 2001). Long term monotherapy with either drug has been shown to exert beneficial effects on fibrosis and inflammation. In HBV-infected patients with cirrhosis and decompensated liver function, treatment with lamivudine extended the time to liver transplantation (Hadziyannis et al., 2003; Marcellin et al., 2003; Dienstag et al., 2003; Lau et al., 2005; Lai et al., 1998).

For all anti-HBV drugs it is necessary to maintain viral suppression for long periods of time, because these drugs only inhibit active viral replication and leave the intracellular reservoir of viral DNA in hepatocytes largely intact. Indeed, relapse occurs in a large percentage of treated patients after cessation of therapy. Furthermore, development of lamivudine-resistant mutants presents a serious problem. Resistance occurs in 28% of treated patients after 1 year of treatment and increases to 68% after 4 years (Leung et al., 2001; Liaw et al., 2000). Interestingly, no viral resistance has been reported in response to adefovir therapy yet, and therefore adefovir is usually added to lamivudine monotherapy at the first signs of development of drug-resistant mutants (Fung and Lok, 2005). New anti-HBV drugs, such as entecavir, clevudine and emtricitabine, are expected to find their way to the clinic soon and it is very well possible that a combination therapy with mechanistically different acting drugs can improve the response rate to therapy in the near future (Hardman et al., 2001).

2.2.5.2 Hepatitis C Virus-Induced Fibrosis

Worldwide, approximately 150 million people are infected with HCV. After HCV infection approximately 85% of patients will develop a chronic hepatitis. Similar to HBV, HCV itself is not directly cytotoxic to hepatocytes, but by continuous stimulation of the immune system, cytotoxic T lymphocyte-mediated clearance of infected hepatocytes forms the main mechanism of hepatic injury. After the initial infection, it may take up to 20 years for these patients to develop advanced fibrosis/cirrhosis and approximately 25-30 years for the development of hepatocellular carcinoma (Boyer and Marcellin, 2000). This long asymptomatic period of time often prevents an early onset of therapy.

The number of drugs available for the pharmacological treatment of chronic HCV infection is even smaller than that for HBV-infected patients. Combination therapy of pegylated IFN- α with ribavirin has been proven to be effective in suppressing HCV activity (Torriani et al., 2004). Similar to HBV-infected patients, the treatment aims at reducing viral replication to induce seroconversion and reduce the risk of hepatocellular carcinoma and progression of fibrosis and cirrhosis into end-stage liver disease. Ribavirin is a purine nucleoside analog that inhibits the replication of a wide variety of ribonucleic acid (RNA) and DNA viruses (Hardman et al., 2001). Dose-limiting side effects of the drug are anemia and leucopenia, whereas IFN- α therapy is associated with depression, flu-like symptoms, fever and myelosuppression. Especially in cirrhotic patients a dose reduction is required to avoid drug related morbidity, which generally results in low sustained viral response rates in those patients. Although adjuvant therapy with erythropoietin and granulocyte colony stimulating factor has been proposed in order to reduce anemia and leucopenia in cirrhotic patients, limited clinical evidence for its efficacy is available and treatment of patients with advanced HCV-induced cirrhosis therefore remains very difficult (Boyer and Marcellin, 2000; Everson, 2005).

The overall response rate to IFN- α /ribavirin in HCV-infected patients is approximately 50%, and as pointed out in the above paragraphs, for nonresponders there is no alternative treatment available. Particularly difficult to treat are the HCV/HIV co-infected and patients with an HCV re-infection of the liver after liver

transplantation. These patients often develop fulminant fibrosis, which progresses to end stage liver disease within 5 years (Pinzani et al., 2005).

2.2.5.3 Liver Fibrosis Due to Genetically Inheritable Factors

Wilson's disease and hemochromatosis are genetically inheritable disorders that can lead to liver fibrosis. Wilson's disease, or copper overload disease, is a result of a mutation in the ATP7B gene which codes for a protein that is essential for copper excretion into the bile. The resulting decrease in copper excretion into the bile leads to its accumulation in the body, which is primarily deposited within the liver, and in a later stage of the disease, also in the brain (Brewer and Askari, 2005). Hemochromatosis, or iron overload disease, is the result of an increased iron uptake from the small intestine due to a mutation in the HFE (High Iron Fe) gene. It is believed that the increased levels of metal ions in hepatocytes induce necrosis via facilitation of the generation of reactive oxygen intermediates within hepatocytes, which leads to hepatocellular injury and, ultimately, hepatic fibrosis (Pietrangelo, 2004; Bacon et al., 2003).

The treatment of cirrhotic patients with Wilson's disease is mainly based on procedures aimed at the reduction of tissue copper levels. A well known anticopper agent is penicillamine, which acts as a reductive chelator that mobilizes intracellular copper deposits in the liver and brain, and facilitates its urinary excretion. However, the use of penicillamine has become obsolete with the arrival of much safer alternatives. One option is treatment with zinc, which inhibits the copper uptake from the small intestine via the induction of metallothionein in the intestinal wall. Another possibility is treatment with tetrathiomolybdate, which complexes copper in the intestine and in the circulation, thus preventing cellular uptake and favoring its urinary excretion either via faeces or urine. Treatment of patients with decompensated cirrhosis with these drugs has been shown to improve liver function, often successfully postponing a liver transplantation (Brewer and Askari, 2005). In analogy to the treatment strategy in Wilson's disease, pharmacological intervention in hemochromatosis also aims at reducing the amount of metal ions in the body. Currently, medical phlebotomy is considered a safe and effective treatment for hemochromatosis (Pietrangelo, 2004).

2.2.5.4 Autoimmune-Mediated Liver Disease

Autoimmune-mediated liver disease can be divided into autoimmune hepatitis (AIH), primary biliary cirrhosis (PBC) and primary sclerosing cholangitis (PSC). Whereas AIH and PBC mostly occur in women, 70% of the patients with PSC are men. Autoimmune diseases in general are the consequence of a breakdown of tolerance to self-antigens. For instance in AIH type II, high circulating levels of anti-CYP2D6 immunoglobulins can be detected, predominantly affecting hepatocytes. In type I and III, other cellular structures are targeted by antibodies, but it is not yet exactly clear which types of immunoglobulins are responsible. In PBC and PSC the small and medium-sized intrahepatic bile ducts are attacked, whereas in PSC especially the large extrahepatic ducts are affected. In all three forms of immune-mediated liver injury liver fibrosis develops, mainly of the periportal type (Bacon et al., 2003).

Although AIH, PSC and PBC are all autoimmune diseases, only AIH responds well to immunosuppressive therapy with corticosteroids and azathioprine. Conversely, for the treatment of PBC, corticosteroid therapy is explicitly not recommended because a worsening of osteoporosis can be expected, of which a higher incidence is associated with the disease already. Especially in PBC patients that are diagnosed in an early stage of hepatic injury, treatment with ursodeoxycholic acid (UDCA) inhibits histopathological progression significantly. However, when hepatic injury has already progressed further, most studies show no beneficial effect of treatment anymore. The mechanism of action of UDCA is probably related to the reduction of toxic effects of hydrophobic bile acids by a choleric effect and/or a direct inhibitory effect on bile acid-induced apoptosis of hepatocytes (Schoemaker et al., 2004).

Even less pharmacotherapeutical options exist for PSC. UDCA appears ineffective and to date no drugs have been identified that show significant therapeutic effects in PSC, except those drugs that provide symptomatic relief of the mainly cholestasis-associated symptoms (Czaja et al., 2005; Beuers, 2005; Kaplan and Gershwin, 2005; Cullen and Chapman, 2005).

2.2.5.5 Drug-Induced Liver Disease, Alcoholic and Non-Alcoholic Steatohepatitis

Although the use of certain drugs has been associated with the development of liver fibrosis, most hepatic drug reactions are followed by recovery upon withdrawal of the

injurious stimulus, without the occurrence of significant fibrosis. Examples of drugs which have been associated with drug-induced fibrosis are methotrexate, isoniazid, and valproic acid (Bacon et al., 2003; Kaplowitz, 2000; Larrey, 2000).

Clearly, best known are the detrimental effects of chronic alcohol abuse on the liver. In fact, this drug-induced form of liver fibrosis is the most common cause of cirrhosis in the western world. Chronic exposure to alcohol leads to benign macrovesicular steatosis of the liver in over 90% of alcohol abusers, and generally steatosis will spontaneously resolve upon alcohol abstinence. Nevertheless, in 20- 40% of the cases a more severe liver pathology develops as a result of chronic oxidative stress via alcohol metabolites (Sougioultzis et al., 2005). The resulting perivenous infiltration of neutrophils into the fatty liver, typically in combination with ballooning of hepatocytes and the formation of Mallory bodies, is termed alcoholic steatohepatitis (ASH). This is very often accompanied by pericellular fibrosis. Besides alcohol-induced oxidative stress, which results in a cytokine-mediated initiation and perpetuation of the inflammatory and fibrotic process, also antibodies against the ethanol metabolite acetaldehyde, as well as auto-antibodies against alcohol dehydrogenase and CYP2E1 have been implicated in the pathophysiology (Bacon et al., 2003; Tilg and Diehl, 2000). Patients with an acute exacerbation of ASH present with decompensated liver function, encephalopathy and gastrointestinal bleeding. The one-month survival rate of these patients is only 50% and the survivors of such an exacerbation will generally develop end stage liver cirrhosis within 5 years, despite withdrawal from alcohol use (Tilg and Diehl, 2000).

NASH is considered to be the hepatic manifestation of the “metabolic syndrome”. The metabolic syndrome is characterized by obesity, insulin resistance and hyperlipidemia and can be considered a typical welfare disease which is the consequence of an unhealthy diet and limited physical activity. The hepatic pathology of NASH is in many ways similar to that of ASH and typical features are ballooning of hepatocytes and lobular inflammation leading to pericellular fibrosis. It is estimated that 10-15% of the patients with NASH will progress to advanced fibrosis and cirrhosis. In the future, NASH may become a more important cause of liver fibrosis because its prevalence is expected to parallel the increase in patients suffering from the metabolic syndrome (Bacon et al., 2003; Wright and Rockey, 2004).

Currently, weight loss or withdrawals of alcohol or drugs are the main treatments available for patients suffering from NASH, ASH and drug-induced liver fibrosis. If this does not sort any effect and fibrosis still progresses, only symptomatic treatments can be initiated to ensure that the patient survives until a liver transplantation can be performed (Sougioultzis et al., 2005; Wright and Rockey, 2004).

2.2.6 Determinants of Fibrosis Progression

Fibrosis progression can vary tremendously between different liver diseases and even among patients with the same disease. Risk factors for disease progression can be acquired or genetic and are best characterized for hepatitis C, for which acquired factors include alcohol intake, adiposity, male gender, age at onset, duration of infection, concurrent liver diseases and immunosuppression. Animal studies (described above) have identified some genetic determinants of fibrosis progression, and these have now been complemented by large-scale studies in humans, which are intended to identify gene polymorphisms that predict progression rates in both hepatitis C and NASH (Bataller et al., 2003(a)). Accurate stratification of fibrosis progression risk will be vital for the identification of those patients meriting earlier or more aggressive therapies, and to optimize the design of clinical trials, enabling smaller enrollment and shorter study intervals.

The foremost challenge is to find the optimal method of diagnosing fibrosis. Although liver biopsy combined with connective tissue stains has been a mainstay of diagnosis, it is prone to sampling error and inter-observer variability. This may account for a one-stage difference in up to a third of patients when using conventional five- or six-point scoring scales (e.g. METAVIR, ISHAK). A potentially more quantitative and feasible application of liver biopsy might include the measurement of key fibrogenic mRNAs by Real-Time polymerase chain reaction (PCR). For example, changes in the expression of fibrogenic genes, including those correlating with stellate cell activation (e.g. the gene encoding PDGFB receptor) may reveal early evidence of regression even before the matrix content has changed. Efforts to make this application a reality are currently under development.

There has been significant progress in the development of noninvasive markers, which will be essential to obtain early biomarkers of efficacy for clinical trials and to guide clinical usage. Current clinical trials of antifibrotic drugs anticipate that at least

6-12 months will be required to demonstrate efficacy by biopsy, based on observed rates of regression in patients cured of their underlying liver disease (e.g. those infected with HBV or HCV); however, lengthy trials are costly and may discourage drug development.

The ideal noninvasive fibrosis marker must be reproducible and linear, reflecting fibrosis in all types of chronic liver disease, and correlating with matrix content and clinical outcome (Albanis and Friedman, 2002). It must also be sensitive enough in individual patients to discriminate between different stages of fibrosis, and reflect the response to antifibrotic therapy over time. There are several approaches currently being developed. First is the serum measurement of one or more circulating matrix proteins and/or serum biochemistries in combination. Second are serum proteomics or glycomics, which assess patterns of protein peaks or glycoprotein branching, respectively. A recent study combined glycomics with a serum marker panel (Callewaert et al., 2004). It achieved a high level of discrimination in diagnosing compensated and decompensated cirrhosis, however, these patients are also readily diagnosed by standard clinical means. Third are imaging methods [Computed tomography (CT), Magnetic resonance imaging (MRI), Positron emission tomography (PET), elastography, radionuclide receptor scanning], which can assess either intrahepatic blood flow patterns, organ texture, or the mass of activated stellate cells using cell-specific reagents to bind membrane receptors.

Currently, several of these approaches are already successful in distinguishing patients with little or no fibrosis, and those with advanced disease. However, they are less reliable at discriminating intermediate stages over time. Nonetheless, evidence of either minimal or advanced fibrosis can be extremely important in making treatment decisions, especially in patients infected with HCV, for which current antiviral therapies are often poorly tolerated or ineffective in a substantial fraction of patients.

Given the apparent importance of fibrosis in predicting prognosis and, moreover, data indicating that it is important to stage fibrosis prior to therapy (and to judge the effect of therapy), histologic assessment of the liver has taken on a major role in the management of patients with liver disease.

While liver histology remains an important part of the clinical assessment of hepatic injury and indeed is considered the current gold standard, a number of questions have

arisen as to the accuracy of liver biopsy in correctly staging disease. Thus, in recent years it has been recognized that noninvasive markers of hepatic fibrogenesis may be appropriate as alternatives to liver biopsy (NIH Consensus Statement on Management of Hepatitis C, 2002; ANAES, 2002). Although the concept of using radiological, clinical, and laboratory parameters of inflammation and fibrosis as alternatives to liver biopsy has been around for some time, the importance of accurate staging of fibrosis for guiding antiviral therapy and following disease progression in patients with chronic hepatitis C (and other types of chronic liver disease) has resulted in the development of newer algorithms employing noninvasive markers. A number of biochemical marker panels have been developed by cross-sectional study design and validated mostly in patients with chronic hepatitis C. Given the common downstream pathways of hepatic fibrosis, some of these panels also appear useful for disease staging in non-virally mediated hepatic injury. Promising newer approaches being developed for assessment of fibrosis in chronic hepatitis C patients include the use of transient elastography as well as emerging technologies such as proteomics and metabolomics.

2.2.6.1 Liver Biopsy

Liver biopsy provides useful information to the clinician for determining prognosis and the urgency of therapy, predicting response to treatment, and investigating the etiology of liver injury, as well as for providing a baseline to allow comparisons of future histologic outcomes (Table 2.1) (Bravo et al., 2001).

Table 2.1 Typical Advantages and Limitations of Liver Biopsy in Comparison to Noninvasive Biomarkers

	Liver Biopsy	Biomarkers
Diagnosis	Fibrosis stage, necro-inflammation and activity, steatosis, iron content, hepatotoxicity, and other chronic liver diseases	Fibrosis stage, activity
Prognosis and guide to therapy	Established role	Exclusion of significant disease in chronic viral hepatitis. To be determined in other liver disease
Posttransplant	Established role	None at this time

False results	Subcapsular biopsy, nonliver sampling	Common causes include acute hepatitis or other inflammation, hemolysis, cholestasis
Assessment	Semiquantitative and qualitative	Semiquantitative or quantitative
Adverse events	Mortality 3/10,000 Morbidity 3/1,000 Localized pain 3/10	None
Sampling error	33% for fibrosis stage	None known
Observer error	20% for fibrosis stage 40% for activity (METAVIR)	None
Sample requirements	Interpretation limited by quality of biopsy size and staining	Standardized assays and analyzers
Hospital stay	Usually 4–6 hours	None
Contraindications	Inability to cooperate Severe comorbid disease Coagulopathy Obesity	None
Cost	Very expensive (uncomplicated biopsy)	Inexpensive to moderately expensive

However, percutaneous liver biopsy is an invasive procedure and may be associated with significant complications in 3% of recipients, with a mortality rate of 0.03% (Perrault et al., 1978; Perrillo, 1997; Poynard et al., 2000). A study evaluating complication rates from 2,084 liver biopsies performed in France noted severe complications in 0.57% of patients and no deaths (Cadranet et al., 2000). Risk factors such as age and cirrhosis increase the likelihood of adverse events from liver biopsy. Furthermore, liver biopsy is costly: the direct costs of an uncomplicated liver biopsy in the United States are estimated at \$1,500–\$2,000, and do not account for lost productivity and time off work (Wong et al., 2000). For these reasons many patients are reluctant to undergo liver biopsies, further limiting the ability to assess and follow disease progression or determine efficacy of treatment.

An additional concern with liver biopsy is that it samples only 1/50,000 of the liver and thus is subject to sampling error, particularly in non-homogenously distributed chronic liver disease. Several studies have highlighted the inaccuracy of liver biopsy for staging of advanced liver disease. Single biopsies may misclassify cirrhosis in 10–30% of cases (Pagliaro et al., 1983; Poniachik et al., 1996). The number of biopsies performed also appears important. One study that obtained liver biopsies immediately

prior to autopsy demonstrated that the diagnostic accuracy of cirrhosis increased from 80% for a single biopsy to 100% with three samples (Abdi et al., 1979). Additionally, in patients with cirrhosis, even when three consecutive biopsies obtained through a single entry site were performed, the rate of concurrent findings about the histologic presence of cirrhosis was only 50% (Maharaj et al., 1986). Varying the site of biopsy also appears to result in significant discordance.

A recent study evaluated laparoscopic biopsies obtained from the right and left lobes in 124 patients with chronic hepatitis C. There was a discordance of at least one stage in one third of patients, and in 14% of cases cirrhosis was present in one lobe, and a diagnosis of bridging fibrosis only in the other lobe (Ragev et al., 2002). Most liver biopsies in clinical practice, however, are not obtained using laparoscopy. Further, the type and size of needle used may also be important. Compared to the Menghini needle, cutting-type instruments may increase the likelihood of making a correct diagnosis of cirrhosis (Vargas-Tank et al., 1985; Colombo et al., 1988).

Another important limitation of liver biopsy is inter- and intraobserver variation among pathologists (The French METAVIR Cooperative Study Group, 1994; Westin et al., 1999; Gronbaek et al., 2002). In chronic hepatitis C, the use of standardized grading systems such as Knodell, METAVIR, or Ishak (among others) results in good concordance rates between pathologists about fibrosis (there is concordance in 70–80% of samples), but there is generally less agreement about inflammation scores (Poynard et al., 2004(b)). Specimen size appears to be very important for the pathologist, with smaller samples leading to an underestimation of disease severity (Colloredo et al., 2003). A study from France that created digitized virtual image biopsy specimens of varying lengths from large picosirius-stained liver tissue sections noted that 75% of 25-mm biopsy specimens were correctly classified using the METAVIR system, compared to only 65% of biopsies 15 mm in length (Bedossa et al., 2003). In clinical practice most needle biopsies are likely to be less than 25 mm; however, a recent study noted that the experience of the pathologist may have more influence than specimen length on interobserver agreement (Rousselet et al., 2005).

Given the limitations of liver biopsy, alternative methods for quantifying liver tissue in histologic specimens have been utilized with variable success. Computer-aided image analysis can provide an objective measurement of the proportion of liver with

fibrous tissue (O'Brien et al., 2000). However, the coefficient of variation for image analysis remains unacceptably high at approximately 45%, even for 25-mm biopsies, precluding its routine clinical use for assessing fibrosis (Bedossa et al., 2003). Nonetheless, there may be a potential role for image analysis in evaluating paired biopsies, or as a research tool in the development of noninvasive markers when quantitation of total matrix deposition is required. By comparison, histologic staging takes into account additional, subjective factors such as architectural distortion or nodule formation, although such morphologic assessment is clearly dependent upon the inherent bias of the individual pathologist.

Immunohistochemical analysis of ECM components on liver biopsy may provide useful information regarding disease progression (Afdhal and Nunes, 2004). For example, matrix glycoproteins such as tenascin are deposited early in the fibrogenesis cascade into relatively immature matrix tissue that has the potential for reversibility (Koukoulis et al., 1999). Conversely, vitronectin is a marker of mature fibrous tissue that is unlikely to have significant potential for reversal (Koukoulis et al., 2001). Alternatively, assessment of stellate cell activation may be an attractive approach to evaluating fibrogenesis. Both assessment of ECM and stellate cell activation could potentially be correlated with serologic markers, thus providing a reflection of the dynamic state of fibrogenesis, as opposed to the standard static histologic measurements of disease stage. ECM and stellate cell activation could be useful in assessing treatment response and monitoring the disease process.

Limitations in liver biopsy have important implications for the development and validation of newer, noninvasive measures of fibrosis. Both the quality of the biopsy and the skill of the pathologist have to be taken into account. Furthermore, the semiquantitative grading systems developed for histopathologic analysis do not reflect linearity of fibrosis deposition or actual matrix content. For example, the Ishak system stages fibrosis on an ordinal scale where scores of 1 and 2 indicate portal fibrosis, 3 and 4 bridging fibrosis, and 5 and 6 incomplete and established cirrhosis, respectively (Ishak et al., 1995). Likewise, the METAVIR classification scores fibrosis on a 5-point scale from F0 to F4, with F1 and F2 indicating portal fibrosis with and without portal septae, respectively, F3 bridging fibrosis, and F4 cirrhosis (Bedossa and Poynard, 1996). However, stage F2 does not imply twice as much fibrous tissue as F1.

These noncontinuous scales were developed to standardize and improve observer variability, and provide some assessment of the severity of chronic liver injury that could be used to determine thresholds for therapy in chronic hepatitis C in particular. Although certain ECM-specific serum markers are intuitively expected to reflect matrix deposition, their main limitation is that they are correlated with a semiquantitative morphologic assessment of fibrosis that is itself imperfect. Despite the obvious drawbacks of validating Noninvasive markers against a liver biopsy for staging of fibrosis, alternative measures of fibrosis that achieve predictive area under receiver operating characteristics (AUROC) curve values above 0.85 should be acceptable as being equivalent to a liver biopsy (Afdhal and Nunes, 2004).

2.2.6.1.1 Grading and Staging of Liver Fibrosis

There are a variety of ways to interpret a liver biopsy. The most common scoring methods include Metavir and histologic activity index (HAI) also called the Knodell. It is important to remember that the length of the liver specimen and the knowledge of the professional reading the biopsy can influence the interpretation of the report.

2.2.6.1.1.1 METAVIR

The Metavir scoring system was specially designed for patients with hepatitis C. The scoring consists of using a grading and a staging system. The grade gives an indication of the activity or amount of inflammation and the stage represents the amount of fibrosis or scarring (Brunt, 2000).

The grade is assigned a number based on the degree of inflammation, which is usually scored from 0-4 with 0 being no activity and 3 or 4 considered severe activity. The amount of inflammation is important because it is considered a precursor to fibrosis.

The fibrosis score is also assigned a number from 0-4:

- 0 = no scarring
- 1 = minimal scarring
- 2 = scarring has occurred and extends outside the areas in the liver that contains blood vessels
- 3=bridging fibrosis is spreading and connecting to other areas that contain fibrosis
- 4=cirrhosis or advanced scarring of the liver

2.2.6.1.1.1 KNODELL

The Knodell score or HAI is also commonly used to stage liver disease. It is a somewhat more complex process, but some experts believe that it is a better tool for defining the extent of liver inflammation and damage (Brunt, 2000). It is composed of four individually assigned numbers that make up a single score. The first component (periportal and/or bridging necrosis) is scored 0-10. The next two components (intralobular degeneration and portal inflammation) are scored 0-4. The combination of these three markers indicates the amount of inflammation in the liver:

- 0 = no inflammation
- 1-4 = minimal inflammation
- 5-8 = mild inflammation
- 9-12 = moderate inflammation
- 13-18 = marked inflammation

2.2.6.2 Non-Invasive Biochemical Markers of Liver Fibrosis

Laboratory markers of liver fibrosis should be the ideal diagnostic tool to assess the grade of fibrosis. They are supposed to provide accurate and reliable results in a simple, fast and cost-effective manner. Indeed, much effort has been dedicated in the past years to investigate non-invasive markers, which discriminate between low fibrotic stages such as Metavir <F2 and higher fibrotic stages F2–F4, in order to identify patients who are at risk of clinically relevant fibrosis progression. However a panel of routine laboratory markers, which are widely used in clinical practice and novel direct and indirect biochemical markers of hepatic fibrosis have been evaluated, but none of the tests met the expectations, and their superiority to standard clinical evaluation is still questionable.

2.2.6.2.1 Direct Serological Markers of Liver Fibrosis

These markers are supposed to be directly involved in the deposition and removal of ECM, i.e. in fibrogenesis and fibrolysis. They include markers of matrix metabolism as well as cytokines. Fibrosis markers can be classified according to their molecular structure (Table 2.2).

Table 2.2 Fibrosis markers

Type	Name
Collagens	Procollagen I C peptide (PICP)
	Procollagen III N peptide (PIIINP)
	Type IV collagen and its fragments (NC1 and PIVNP)
Glycoproteins and polysaccharides	Hyaluronic acid (HA)
	Laminin
	Tenascin
	YKL-40
Collagenases and their inhibitors	Metalloproteinases (MMPs)
	Tissue inhibitors of metalloproteinases (TIMPs)
Cytokines	TGF- β 1
	PDGF

It is very difficult to make a clear delimitation between markers of ECM deposition and degradation. Serum levels of direct markers reflect simultaneously both processes as well as the total mass of ECM undergoing remodeling (Afdhal and Nunes, 2004).

There are strong arguments for this supposition:

- the levels of direct markers are elevated in disease with rapidly progressing fibrosis severe alcoholic hepatitis or active hepatitis;
- the levels of these markers have a decreasing tendency in response to treatment of the disease, before reduction in the stage of fibrosis;
- there is an independent correlation between serum direct markers and the stage of fibrosis in chronic liver diseases (Ramadori et al., 1991; Pares et al., 1996; Camps et al., 1994; Guechot et al., 1995(a); McHutchison et al., 2000).

Also, there is a good correlation between different direct fibrosis markers, suggesting that they investigate a similar process.

The proposal to assess simultaneously markers of matrix deposition and degradation by using a different combination of these markers in an attempt to evaluate the whole process of matrix remodelling has added little diagnostic accuracy (Afdhal and Nunes, 2004).

The assessment of direct markers could be useful for:

- staging liver disease and for
- assessing the effect of treatment and predicting disease progression (Afdhal and Nunes, 2004).

2.2.6.2.1.1 Direct Individual Markers in Staging Liver Disease

2.2.6.2.1.1.1 Markers Associated With Matrix Deposition

Several studies have investigated the value of procollagen peptides. During synthesis of collagen, procollagen suffers an enzymatic cleavage at both the carboxy - and aminoterminal ends by two different enzymes: procollagen-C-proteinase and procollagen-N-proteinase. The peptides released into the serum: procollagen type I carboxy - terminal peptide and procollagen type III amino-terminal peptide can be used as a measure of matrix deposition (Schuppan et al., 1991; Schuppan et al., 1995).

Procollagen type I carboxy terminal peptide (PICP)

PICP has little value in the diagnosis of chronic hepatitis and is elevated in cirrhosis, quantifying disease severity or indicating the alcoholic etiology (Fabris et al., 1997).

Procollagen type III amino-terminal peptide (PIIINP)

Serum levels of P III NP were extensively studied alone or in combination with different other markers and the results showed the correlation between their levels and histological stage of hepatic fibrosis in alcoholic liver disease, viral hepatitis and primary biliary cirrhosis (Schuppan et al., 1995; Fabris et al., 1997; Bentsen et al., 1987; Babbs et al., 1988).

When refining the methods of assessment by using two assays methods of PIIINP (for col 1-3 : collagen synthesis and for col 1: collagen degradation), some authors found a significant correlation between serum PIIINP (col 1-3 and col-1) and histological changes: fibrosis, periportal necrosis and histological activity index (Walsh et al., 1999(a)).

Serum type IV collagen

Type IV collagen is an important component of ECM. Unlike type I and III collagens, which are processed by proteolysis, type IV collagen is deposited intact in the matrix and the serum component of type IV collagen reflects matrixdegradation (Murawaki et al., 1995). The assay of fragments of type IV collagen in serum (carboxyterminal cross-linking domain - NC1 and aminoterminal 7S domain of procollagen type IV – PIVNP) are used most frequently in practice (Shahin et al., 1992; Hirayama et al., 1996; Hayasaka et al., 1990). Irrespective of the methods used for determination,

serum levels of type IV collagen had a positive correlation with the degree of hepatic fibrosis in patients with chronic viral hepatitis, alcoholic liver disease and were sensitive indicators of the presence of cirrhosis in haemochromatosis (Fontana and Lok, 2002; Afdhal and Nunes, 2004).

In hepatitis C, a cut-off value was established for diagnosing stages greater than F2 (110 ng/ml) and for predicting stage F3 (130 ng/ml) (Murawaki et al., 2001(b)).

Laminin

A major non-collagenous glycoprotein synthesized by HSC, laminin is deposited in the basement membrane of the liver and increases during fibrosis around the vessels, in the perisinusoidal spaces and the portal tract.

Serum laminin levels and pepsin-resistant fragment of laminin (laminin P1) are elevated in chronic liver diseases irrespective of etiology: viral or alcoholic and reflect an increase in perisinusoidal fibrosis (Kropf et al., 1988; Walsh et al., 2000).

Some studies suggest that the serum levels of laminin correlate with the severity of fibrosis and liver inflammation in chronic hepatitis C, and are superior to serum ALT in reflecting liver injury (Walsh et al., 2000), particularly in cirrhosis (Afdhal and Nunes, 2004). Also, these studies showed a good correlation of serum laminin with Child-Pugh's score, complications of liver cirrhosis, portal pressure and hepatic vein portal gradient (Korner et al., 1996).

Hyaluronic acid

Hyaluronic acid (HA) is a glycosaminoglycan, component of the ECM, synthesized by HSC. In normal circumstances the endothelial cells of the liver sinusoid are the site of HA uptake and degradation (Eriksson et al., 1983). Increased levels of HA are due to decreased hepatic removal, increased production or both.

High levels of serum HA have been detected in patients with liver diseases of different etiologies and particularly in those with cirrhosis (Engstrom-Laurent et al., 1985; Guechot et al., 1996(b)).

Serum levels of HA have been shown to be related not only to the stage of fibrosis (Guechot et al., 1996(b)) but also to the degree of necroinflammation (Murawaki et al., 1995).

The assessment of both laminin and HA concentration has a good prognostic value for complications of liver cirrhosis: hepatic encephalopathy stage III and IV, refractory ascites, portal vein thrombosis (Korner et al., 1996).

Serum HA at a level of < 60 mg/l excludes vein significant fibrosis or cirrhosis with a positive predictive value (PPV) of 93% and 99% respectively and has an important role in identification of early fibrosis, thus reducing the need for biopsy in this subgroup of patients (McHutchison et al., 2000).

At the cut-off value of 85 mg/l serum HA had a sensibility of 64.5% and specificity of 91.2% for discriminating patients with extensive liver fibrosis from those with no or mild fibrosis. At the cut-off value of 110mg/l the sensitivity was 79.2% and specificity 89.4% for discriminating patients with from those without liver cirrhosis (Guechot et al., 1996).

It appears that as an isolated marker, HA is the most useful diagnostic tool for both staging and grading in patients with chronic C virus infection (Murawaki et al., 1995).

YKL-40 (human cartilage glycoprotein)

YKL-40 is a mammalian member of a chitinase family (18- glycosylhydrolases). YKL-40 is produced in a wide variety of cell types and especially in cells located in tissues with increased remodelling/degradation or inflammation of the ECM. The cellular source in the liver is supposed to be activated HSC (Johansen et al., 2000). Its physiological function is unknown, but YKL-40 may contribute to tissue remodelling, acts as a growth factor for fibroblasts, acts synergistically with insulin-like growth factor, as a chemoattractant for endothelial cells and has a role in angiogenesis (Johansen et al., 2000; Malinda et al., 1999). In liver diseases, serum levels of YKL-40 were closely related to the degree of fibrosis histologically documented, the highest values being found in severe fibrosis (Johansen et al., 2000).

In chronic HCV infection, serum levels greater than 284.8 ng/ml predict cirrhosis with a sensitivity of 80% and specificity of 71% and have a negative predictive value (NPV) of 78% (Saitou et al., 2005). Unlike PIIINP and HA, serum YKL-40 is significantly elevated in the subset of alcoholic cirrhotic patients who have also alcoholic hepatitis and is the best of these serological markers in discriminating

between patients with mild fibrosis and those with no fibrosis (Johansen et al., 2000; Tran et al., 2000).

2.2.6.2.1.1.2 Markers Associated With Matrix Degradation

Products of matrix degradation result from the activity of a family of enzymes: matrix metalloproteinases (MMPs).

Synthesized intracellularly and secreted as pro-enzymes, MMPs are activated by a proteolytic cleavage by membranetype matrix metalloproteinase 1 (MT1-MMP) or plasmin and inhibited by binding to specific tissue inhibitors of metalloproteinase (TIMPs).

Considering their substrate specificity there are five categories of MMPs: interstitial collagenases (MMP-1, -8, -13), gellatinases (MMP-2, - 9 and fibroblast activation protein), stromelysins (MMP-3, -7, -10, -11), membrane type (MMP-14, - 15, - 16, - 17, -24, - 25) and metalloelastase (MMP-12) (Arthur, 1998; Friedman, 1999; Aparicio and Lehy, 1999). The MMPs and their inhibitors are involved in the control of matrix degradation (Friedman, 1999).

In chronic liver disease, the investigations have centered on MMP2 (gellatinase or 72 kDA type IV collagenase), membrane-type metalloproteinase-1 or – 2 which activate latent MMP2 and TIMP-1 and TIMP-2.

MMP-1 shows a substrate specificity for interstitial collagen type I and III, while MMP-2 has as substrate collagen type IV, V, VII, X elastin and fibronectin.

TIMPs can irreversibly bind the proenzyme or active forms of MMPs and inactivate them. Excess production of TIMPs relative to MMPs may be an important factor for progression of liver fibrosis (Iredale et al., 1992).

HSC are the principal source of MMP-2 in the human liver and activation of MMP-2 require interaction withhepatocytes. TIMP-1 is produced by HSC and hepatocytes (Arthur, 1998; Friedman, 1999; Iredale et al., 1992).

Regarding the diagnostic value of MMP-2 and TIMP-1, one study reported that MMP-2 levels were elevated only when cirrhosis had developed, while TIMP-1 had a diagnostic value in detecting earlier stage of fibrosis (Boeker et al., 2002). Also, this study revealed that TIMP-1 levels had a strong correlation with histological

inflammatory scores and that MMP-2 levels had no relationship to the stage of fibrosis in the noncirrhotic liver.

Other studies established that serum levels of MMP-1 had a declining tendency with the severity of liver fibrosis and inflammation and abnormal serum MMP-1 did not appear until the patients were in the advanced stages of fibrosis (Zhang et al., 2003(a)).

However, older studies which investigated the role of TIMP-1 in patients with various liver disease, comparing TIMP-1 with PIIINP, type IV collagen, laminin P1 and the histological aspect, suggested that the serum levels of TIMP1 may be useful to estimate hepatic fibrogenesis associated with active inflammatory activity (Ueno et al., 1996).

Also, the serum levels of TIMP-1 were shown to correlate positively with the degree of fibrosis and a striking increase in serum TIMP-1 levels was observed in the late stage of fibrosis, but not in the mild stage (Walsh et al., 1999(b)).

The ratio of TMP-1/MMP-1 could be useful in the diagnosis of hepatic fibrosis (Zhang et al., 2003(a)).

2.2.6.2.1.1.2 Cytokines and Chemokines Associated With Hepatic Fibrosis

TGF- β 1

Transforming growth factor- β 1 (TGF- β 1) is a homodimeric polypeptide that is secreted in an inactive form which requires activation. It has pleiotropic effects through membrane receptors on a wide variety of cells. In hepatic pathology, TGF- β 1 is the most important stimulus for the production of ECM by HSC (Sasaki et al., 1992) and it is also an inhibitor of hepatocyte growth and proliferation (Nakamura et al., 1985).

In the liver biopsy from patients with chronic liver disease, TGF- β 1, mRNA levels correlate with type I collagen mRNA (Breitkopf et al., 2001).

The value of serum TGF- β 1 levels has some limitations related to the contamination of the sample by TGF - β from platelets, the interference with plasmin activity in the plasma that increases the amount of TGF- β 1 through opening LAP/TGF- β complex, the binding of TGF- β at the sites of injury to ECM and to vascular endothelium, the

sequestration by soluble proteins and the complicated clearance of TGF- β 1. These factors explain why plasma levels of TGF β 1 are unlikely to be of diagnostic value (Zhang et al., 2003(a); Breitkopf et al., 2001).

However, some studies showed a good correlation between serum levels of total TGF - β , and Knodell scores (Nelson et al., 1997) and also a correlation with the rate of fibrosis progression (Kanzler et al., 2001).

Moreover, some authors established cut-off values with prognostic significance for patients with no progression of fibrosis and those with progressive disease. A TGF- β 1 level below 75 ng/ml was predictive for stable disease (Kanzler et al., 2001).

PDGF

Platelet derived growth factor (PDGF) is the main stimulus of HSC proliferation and migration and is upregulated following liver injury. PDGF-BB is the main subunit with the most important role for the signalling pathway in HSC (Gressner, 1998; Pinzani and Marra, 2001).

The serum level of PDGF-BB was found to have the highest value for assessment of hepatic fibrosis, when compared to other eight markers (Zhang et al., 2003(a)).

2.2.6.2.1.2 Combination of Direct Markers

The combination of direct markers to generate an algorithm capable of evaluating the existence of fibrosis and its stage is an alternative approach. There are several studies which made use of this approach.

Oberti et al. (1997) studied four specific markers of fibrosis: hyaluronic acid, PIII NP, laminin and TGF-b, together with other nonspecific markers: prothrombin index, GGT, apolipoprotein-A1 (PGA score) and α 2-macroglobulin in a prospective study. The best diagnostic accuracy was found for HA (86%), followed by laminin (81%), P III NP (74%) and TGF-b1 (67%).

Taken together, the results of the Oberti's study did not show any diagnostic advantage of the specific over nonspecific markers of fibrosis.

In another investigation, the serum markers of fibrosis: C-terminal peptide of procollagen I, PIIINP, collagen IV and serum prolylhydroxylase were studied in cirrhotic and noncirrhotic patients (Fabris et al., 1997). By stepwise logistic regression

analysis and ROC curves the authors established that collagen IV and PIIINP were independently associated with cirrhosis.

One study investigated the diagnostic value of PIIINP, PIVNP, HA, MMP-1, MMP-2 and TIMP -1 in order to assess by ROC the usefulness of serum direct markers for fibrosis staging and necroinflammatory grading in chronic hepatitis C (Murawaki et al., 2001(a)). The authors concluded that HA and MMP-2 were most useful in that order for diagnosing stages greater than F2, while serum HA and PIVNP for diagnosing moderate grade. Because of the great overlap among stages and grades they did not consider that the above mentioned investigated markers can replace liver biopsy for the assessment of liver histology, but have a value for the global clinical status judgement and for prognosis.

The European Liver Fibrosis Study, conceived as an international, multicenter, cross-sectional cohort study, compared the diagnostic performance of three direct serum markers: HA, PIIINP and TIMP-1 with liver biopsy to generate a diagnostic algorithm for estimating the severity of liver fibrosis. By adopting as thresholds sensitivity greater than 90% and specificity greater than 90%, this algorithm was found to exclude significant fibrosis. Also, this algorithm can detect cirrhosis with a sensitivity greater than 90% (Rosenberg et al., 2004).

Recently, another study investigated the diagnostic value of a combination of three markers: HA, TIMP-1 and α 2-macroglobulin, with the aim of generating an algorithm able to discriminate between significant and non-significant fibrosis. Establishing cut-off values for these markers, they may reliably differentiate chronic hepatitis C patients with moderate / severe fibrosis (F2 to F4 Metavir) from those with no or mild fibrosis (F0 to F1 Metavir) (Patel et al., 2004).

In an attempt to find a better combination of markers, serum levels of PDGF-BB, TGF- β 1, MMP-1, TIMP-1, HA, PC III, collagen IV, laminin and mRNA-TIMP-1 and mRNA-MMP-1 in peripheral blood mononuclear cells (PBMCs) were investigated in patients with chronic viral B infection. Serum levels of PDGF-BB, TIMP-1 mRNA, the ratio TIMP-1 mRNA/MMP-1 mRNA in PBMCs and serum levels of TIMP-1 and TIMP-1/MMP-1 ratio were valuable markers for fibrosis assessment. The combination of serum PDG-BB, TIMP-1 mRNA and MMP-1 mRNA in PBMCs was the best test in screening of liver fibrosis (Zhang et al., 2003(a)).

2.2.6.2.1.3 The Role of Fibrosis Markers in Assessing Treatment Efficacy and Predicting Disease Progression

The dynamic assessment of direct markers of liver fibrosis: HA, PIIINP, YKL-60 and TIMP-1 showed decreased levels in patients who achieved a sustained biochemical or virological response and a good correlation with histological findings (Fabris et al., 1999; Yagura et al., 2000; Leroy et al., 2001; Nojgaard et al., 2003(b)).

The fall of the TGF- β levels after antiviral therapy suggests that interferon has also a direct antifibrotic effect through a direct inhibition of TGF- β expression (Castilla et al., 1991).

Noninvasive markers have also a prognostic value, by predicting clinical evolution and fibrosis progression. Serum HA levels have a great predictive value and correlate with Child–Pugh’s score in patients with viral C cirrhosis.

HA and PIIINP were independently predictive of disease progression in primary biliary cirrhosis (Forns et al., 2002), serum laminin levels correlate with Child-Pugh’s score of liver cirrhosis irrespective of etiology (Korner et al., 1996) and elevated levels of PIIINP and YKL-40 are predictive of shorter survival in alcoholic cirrhosis (Nojgaard et al., 2003(a)).

High basal levels of TGF β 1 allow for the identification of a subset of patients with chronic hepatitis C who will have progressive liver fibrosis (Kanzler et al., 2001), a statement that has been documented by serial evaluations of serum TGF- β 1. Patients with progressive hepatic fibrosis had a parallel increase in TGF- β 1 levels.

2.2.6.2.1.4 Limitations of the Serum Direct Markers of Liver Fibrosis

Using either a single marker or a combination of tests, direct markers have some limitations:

- they reflect the rate of matrix turnover, not only deposition, and have the tendency to be more elevated when there is an associated high inflammatory activity. As a consequence, extensive matrix deposition might not be detected in the presence of minimal inflammation;
- they are not liver–specific and their serum levels may be elevated in the presence of concomitant sites of inflammation;

- serum levels of markers depend on clearance rates, which are influenced by dysfunction of endothelial cells, impaired biliary excretion or renal function.

2.2.6.2.2 Indirect Markers of Liver Fibrosis

Liver fibrosis may be predicted by using a single routine laboratory test that reflects alteration in hepatic function, or a combination of such tests.

2.2.6.2.2.1 Individual Serum Indirect Markers of Fibrosis

Serum ALT levels

Although serum ALT levels generally reflect liver injury, the correlation between ALT levels and necroinflammatory and fibrosis score is poor, especially in chronic viral C infection. However, an extensive study established that ALT levels had a good sensitivity and specificity for the prediction of histologic substrate (Pradat et al., 2002).

ROC analysis showed that the best theoretical ALT threshold with the best histologic predictive value is 2.25 times the upper limit of normal, but it implies the overlooking of 28% of patients with a histologic score greater than A1F1 Metavir. At the same time, among patients with persistently normal ALT levels, about 26% have a histologic score greater than A1F1, and a liver biopsy must be taken into consideration (Pradat et al., 2002).

AST / ALT ratio

Assay of AST levels had a stronger correlation than ALT with hepatic fibrosis (Gordon et al., 2000). The increase in ALT levels is related to mitochondrial dysfunction and to reduced clearance of AST by hepatic sinusoidal cells. Reversal of the AST / ALT ratio was reported in patients who progress from chronic hepatitis to liver cirrhosis and the AST/ALT ratio of more than 1 had a good predictive value for advanced fibrosis or cirrhosis (Giannini et al., 2003). A good correlation with Child-Pugh's score, MELD score and monoethylglycinexylidide (MEGX) was found.

The AST/ALT ratio had also a predictive value. An AST/ALT ratio greater than 1.16 had 81.3% sensitivity and 55.3% specificity in identifying cirrhotic patients who died within 1 year of follow-up (Giannini et al., 2003).

Platelet count (PLT)

Trombocytopenia is a valuable marker of advanced liver disease, but it may be related to many mechanisms: hypersplenism, myelosuppression by HCV, decreased thrombopoietin production, autoimmune process (Peck-Radosavljevic, 2001). Combined assessment of the AST/ALT ratio and PLT had a high diagnostic value for cirrhosis (Giannini et al., 2003).

Prothrombin index

Prothrombin time as an index that reflects the synthesis capacity of the liver is one of the earliest indicators of liver cirrhosis (Croquet et al., 2002). In the HALT-C study, a multivariate logistic regression model that comprised prothrombin time, PLT, AST/ALT ratio and alkaline phosphatase was predictive of cirrhosis. In another study, prolonged prothrombin time correlated with the presence and size of esophageal varices (Pilette et al., 1999). Prothrombin time is also a part of different composite indexes.

2.2.6.2.2 Multicomponent Indirect Fibrosis Tests

In order to improve the diagnostic value of different laboratory tests, several combinations of indirect tests have been developed (Table 2.3).

Table 2.3 Diagnostic accuracy of direct and indirect laboratory markers in distinguishing between low stages of ‘insignificant’ fibrosis (F0–F1 by METAVIR) and ‘significant’ fibrosis (F2–F4 by METAVIR)

Laboratory marker	Disease	Sensitivity	Specificity	AUC	References
Direct laboratory markers of liver fibrosis					
Hyaluronic acid	HCV	75–79	80-100	0.82–0.92	(McHutchison et al., 2000) (Murawaki et al., 2001(a)) (Guechot et al., 1996) (Walsh et al., 2000)
	AFLD	87	93	0.79–0.91	(Pares et al., 1996) (Naveau et al., 2005)
	NAFLD	66-85	68-91	0.78–0.87	(Suzuki et al., 2005) (Santos et al., 2005)
YKL-40	AFLD	88.5	50.8	m.d.	(Tran et al., 2000)
	HCV	78	81	0.81	(Saitou et al., 2005)
Laminin	HCV	80	83	0.82	(Walsh et al., 2000)
	NAFLD	82	89	m.d.	(Santos et al., 2005)
Type IV collagen	HCV	73-80	81-85	0.83	(Walsh et al., 2000) (Murawaki et al., 2001(b))
Type IV collagen-7S	HCV	74-83	75-88	m.d.	(Murawaki et al., 2001(b))
	NAFLD	70	81	0.83	(Sakugawa et al., 2005)

Procollagen III	HCV	60-78	75	0.69	(Guechot et al., 1996) (Saitou et al., 2005)
MMP-2	HCV	7-75	70-100	0.59	(Murawaki et al., 2001(b)) (Boeker et al., 2002)
TIMP-1	HCV	67	68	0.71	(Boeker et al., 2002)
Indirect laboratory markers of liver fibrosis					
PGA	HCV	91	81	m.d.	(Teare et al., 1993)
Fibrotest	HCV	65-87	59-81	0.74–0.87	(Imbert-Bismut et al., 2001) (Sebastiani et al., 2006) (Rossi et al., 2003) (Poynard et al., 2004(a))
	HCV/HIV	90	60	0.85	(Myers et al., 2003(a))
	AFLD	88	60	0.84	(Naveau et al., 1994)
APRI	HCV	41-91	47-95	0.69-0.88	(Sebastiani et al., 2006) (Wai et al., 2003)
Forns' Index	HCV	80-94	95-98	0.78-0.86	(Sebastiani et al., 2006) (Forns et al., 2002) (Patel et al., 2003) (Thabut et al., 2003)
	HCV/HIV	43	96	0.77	(Macias et al., 2006)

Two other studies are reported. Fortunato et al (2001) combined the determination of pseudocholesterase, fibronectin, prothrombin, ALT, N-acetyl-b-glucosaminidase, manganese superoxide dismutase and obtained a correct classification of cirrhosis in 81% of cases.

With the aim of limiting the need for liver biopsy in patients with chronic hepatitis C, the MULTIVIRC group developed a panel of biochemical markers that combines six markers: α 2-macroglobulin, haptoglobin, GGT, total bilirubin, apolipoprotein A1 and ALT with the patient's age and gender to generate a measure of fibrosis stage (FibroTest) and of necroinflammatory grade (ActiTest) of the liver (Imbert-Bismut et al., 2001).

The choice of these markers was justified by their significance in liver disease. α 2-macroglobulin is an acute phase protein, that is a feature of HSC activation and as a consequence is related to hepatic fibrosis (Tiggelman et al., 1997). It is also a proteinase inhibitor that can inhibit catabolism of matrix proteins, enhancing fibrotic process. Haptoglobin is negatively associated with fibrosis (Bacq et al., 1993). The complex role of hepatocyte growth factor and TGF- β 1 on the synthesis of these two markers explains the different behaviour of these proteins (101). GGT is associated with fibrosis and early cholestasis and an increase of epidermal growth factor may be the cause of increased GGT levels, parallel with the stage of fibrosis (Edwards, 1987). Apolipoprotein A1 is trapped in ECM and decreases in liver fibrosis (Paradis et al., 1996).

Activated HSCs express α -smooth muscle actin (α -SMA) and produce an excess of collagen and other ECM components. As a result, liver fibrosis is developed.

In conclusion, a number of laboratory tests have been developed, but their utility in clinical practice is still a matter of debate. While the current body of literature allows the use of laboratory parameters and test panels in advanced fibrosis/cirrhosis, these tests are adopted slowly in clinical routine. The following reasons may be responsible for the restricted use of laboratory tests in assessing fibrosis.

Mild and moderate stages of fibrosis cannot be detected by any of the test systems. However, the early detection of patients at risk of fibrosis progression, e.g. in viral hepatitis or autoimmune liver disease, has an impact on the necessity and intensity of therapy.

The precision of tracking intra-individual changes, e.g. in therapy, has not been sufficiently investigated.

The superiority of any direct laboratory marker to routine laboratory parameters has still to be demonstrated. This is also with respect to the cost of medical diagnostics an important factor.

2.2.6.2.1 Ideal Features for a Marker of Liver Fibrosis

- Liver-specific
- Inexpensive and easy to perform
- Measures:
 - Stage of fibrosis (or mass of extracellular matrix)
 - Activity of matrix deposition
 - Activity of matrix removal
 - Levels not altered by changes in liver, renal, or reticuloendothelial function
 - Reproducible performance characteristics
 - Follows dynamic changes in fibrogenesis

2.2.6.3 Imaging Methods

2.2.6.3.1 Ultrasound, CT and MRI

Ultrasound, CT and MRI are inadequate to diagnose and differentiate early stages of fibrosis. Even diagnosis of cirrhosis is often based only on signs of advanced liver

cirrhosis e.g. signs of portal hypertension, reduction of the right liver lobe with enlargement of the left liver lobe or caudate lobe resulting in a high specificity but lower sensitivity of the methods (Honda et al., 1990). Ultrasound studies (Aube et al., 1999) combining up to 11 ultrasound parameters and Doppler measurements achieved accuracies for the diagnosis of cirrhosis up to a maximum of 88%.

In recent years special MRI and ultrasound techniques have been developed for non invasive detection and quantification of liver fibrosis.

2.2.6.3.1 Magnetic Resonance Elastography

Diffusion-weighted MR imaging technique is based on the measurement of the apparent diffusion coefficient (ADC), which is influenced by the hydration and metabolic status of the liver. Studies showed a reduction of the ADC values in fibrotic liver tissue, but the differences were relatively small (Aube et al., 2004; Boulanger et al., 2003).

Another approach evaluating liver elasticity uses an external probe at the back of the patient sending low frequency vibrations (60 Hz) through the liver and measuring the MRI spin-echo sequence. With this technique shear elasticity and viscosity maps are obtained. A study comparing MR elastography of 30 healthy volunteers and 50 patients with chronic liver disease with liver histology showed a sensitivity of 86% and a specificity of 85% for discrimination between patients with moderate and severe fibrosis (Metavir F2–F4) and those with mild fibrosis (Yin et al., 2007). Up to now there is only a small number of studies dealing with MRI detection and quantification of liver fibrosis, and one has to wait for further studies for assessing the diagnostic potential of the method more precisely.

2.2.6.3.1 Transient Elastography (Fibroscan)

Transient elastography (Fibroscan, EchoSens) evaluates liver fibrosis based on measuring the elasticity of the liver using ultrasound (Sandrin et al., 2002). The system consists of an ultrasound transducer combined with a vibration probe, which is positioned intercostally and transmits a low frequency vibration wave with mild amplitude (50 Hz) into the right liver lobe. The vibration induces an elastic shear wave that propagates through the liver tissue. Pulse-echo ultrasound waves then measure the velocity of the shear wave in the liver tissue at a distance of 2.5–6.5 cm

under the skin level. This corresponds to a measured distance of 4 cm in the liver tissue. The velocity correlates with liver tissue stiffness and therefore the degree of fibrosis. The stiffer the tissue, the faster the shear wave propagates. The values are recorded in kilopascal (kPa). The mean value is established from ten valid measurements. The learning curve is steep with a low inter- and intra-observer variability after at least 50 prior fibroscan examinations (Kettaneh et al., 2007). Technical limitations of the method are the presence of ascites and obesity. Currently a new elastography probe, which can penetrate chest wall fat, is being evaluated in obese patients to overcome this.

The method has been widely evaluated in studies on patients with chronic liver disease in comparison to histological fibrosis staging. In most studies the liver tissue samples were obtained by percutaneous liver biopsy.

The main focus of the initial tests was the evaluation of liver fibrosis in chronic hepatitis C. A prospective study of 327 patients with chronic hepatitis C (Ziol et al., 2005) compared transient elastography with liver histology for detection of relevant fibrosis or cirrhosis. The AUCs were 0.79 for >F2; 0.91 for <F3 and 0.97 for histological Metavir score F4. The optimum cut-off value as the highest product of sums for sensitivity and specificity for F4 was 14.6 kPa. For this value a sensitivity of 86%, specificity of 96%, a positive predictive value of 0.78 and a negative predictive value of 0.97 were achieved. After showing high diagnostic accuracy in chronic hepatitis C the method has also been used for determination of graft fibrosis after liver transplantation due to recurrent hepatitis C, with comparable high diagnostic accuracy for the diagnosis of severe fibrosis or cirrhosis (AUC 0.90 for Metavir score ≥ 4) (Harada et al., 2008). First results of transient elastography in post-liver transplant follow up in a small number of patients (Rigamonti et al., 2008) showed promising concordance of stiffness changes with histological staging and grading over a time interval of 6 months. This indicates a possible role of the method in the follow-up of liver fibrosis in chronic liver diseases.

Recently a meta-analysis (Friedrich-Rust et al., 2008) screened and weighted published studies from 2002 to 2007 comparing transient elastography with liver histology in chronic liver diseases. Fifty studies fulfilled quality requirements and were included in the analysis. The mean AUC for the diagnosis of significant fibrosis

($F \leq 1$ vs. $F \geq 2$), severe fibrosis ($F \leq 2$ vs. $F \geq 3$) and cirrhosis ($F \leq 3$ vs. $F = 4$) were 0.84 (CI 0.82–0.86); 0.89 (CI 0.88–0.91) and 0.94 (CI 0.93–0.95) in a recent meta-analysis (Friedrich-Rust et al., 2008). Transient elastography performed excellently at the differentiation of cirrhosis vs. no cirrhosis with an optimal cut-off value of 13.01 kPa. For the diagnosis of cirrhosis no significant difference in AUC was found between the different underlying liver diseases. These results support transient elastography to be able to diagnose cirrhosis with a high diagnostic accuracy independent from the underlying liver disease eventually replacing liver biopsy.

The diagnostic accuracy of the method decreases in the presence of low degrees of fibrosis (Metavir score F1 and F2), as the ascertained values often overlap. In the meta-analysis (Friedrich-Rust et al., 2008) the AUC for $F \geq 2$ (diagnosis of significant fibrosis) varied between the different studies with a range of 68–100%, a mean AUC of 0.84 and an adjusted AUC of 0.91. Here a significant reduction of heterogeneity was achieved by differentiating between the underlying liver diseases. The optimal cut-off value suggested from the SROC was 7.65 kPa. Probably, focusing to the underlying liver disease with certain AUC and cut-off values may reduce this heterogeneity but one has to interpret the results in this range with caution.

Further studies evaluated the correlation of liver stiffness with complications of liver cirrhosis in patients with HCV. The reported AUC for the prediction of portal hypertension (Vizzutti et al., 2007) correlated with a HVPG ≥ 10 mmHg and ≥ 12 mmHg were 0.99 and 0.92, respectively. However prediction of oesophageal varices regardless of grading them resulted in a rather low sensitivity (90%) and specificity (43%) at the chosen cut-off value of 17.6 kPa. Other data (Foucher et al., 2006) ascertained the occurrence of complications in liver cirrhosis at a 90% negative predictive value with high cut-off values of 27.5 kPa, indicating already an advanced stage of cirrhosis for the presence of oesophageal varices and 53.7 kPa for the presence of hepatocellular carcinoma. Assuming that liver stiffness reflects an increase in portal pressure, it does not record all the complex hemodynamic changes occurring in the development of portal hypertension. Liver stiffness measurement may therefore be able to indicate a portal hypertension, e.g. with correlation to a HVPG of 10 mmHg, but is limited in gradation between further complications of portal hypertension.

Acute inflammation (Arena et al., 2008) (Sagir et al., 2008) and extrahepatic cholestasis (Millonig et al., 2008) have been shown to increase liver stiffness values. During the acute phase of liver damage in toxic hepatitis (Arena et al., 2008) and acute viral hepatitis (Sagir et al., 2008), liver stiffness values exceeded the cut-off values for prediction of significant fibrosis or cirrhosis. In the follow-up examinations liver stiffness values returned to baseline with the decline of aminotransferases and bilirubin. For reliable estimation of transient elastography biochemical activity of chronic liver disease has to be taken in account; liver stiffness values in acute hepatitis with acute liver damage lead to an overestimation of liver fibrosis.

Summarising the imaging data, transient elastography allows diagnosis of liver cirrhosis and significant fibrosis with a high degree of diagnostic accuracy, while it has to be remarked that percutaneous liver biopsy as the reference method, used as gold standard, can also coincide with an underestimation of the degree of fibrosis (Denzer et al., 2007).

The diagnostic accuracy of transient elastography decreases in the presence of acute liver inflammation or extrahepatic cholestasis and in the presence of low degrees of fibrosis (Metavir score F1 and F2), as the ascertained values often overlap. Probably, the combination of transient elastography and serum markers of fibrosis may differentiate milder degrees of fibrosis more accurately in the future.

Nevertheless, due to the uncomplicated and rapid procedure and the non-invasive character, transient elastography appears to be an attractive alternative for liver biopsy, if the aetiology of liver disease is clear, e.g. in chronic hepatitis C. The method seems also suitable for monitoring the course of chronic liver disease, as it is widely accepted by patients.

- Ultrasound, CT and MRI are inadequate to diagnose and differentiate early stages of fibrosis. Even diagnosis of cirrhosis is often based on signs of advanced liver cirrhosis, e.g. signs of portal hypertension resulting in a high specificity but lower sensitivity of the methods.
- Diffusion-weighted MR imaging technique and MR elastography need to be evaluated by further studies for assessment of the diagnostic potential of the methods more precisely.

- Transient elastography allows the diagnosis of liver cirrhosis and significant fibrosis. Diagnostic accuracy decreases in the presence of low degrees of fibrosis (Metavir score F1 and F2). Referring to the reported data, the technique may be of practical relevance in the diagnosis of significant fibrosis and in the follow-up of chronic liver diseases.

2.2.7 Reversibility of Fibrosis and Cirrhosis

The demonstration that hepatic fibrosis and even cirrhosis may regress (Bonis et al., 2001; Desmet and Roskams, 2004) has overturned a longstanding dogma, and has accelerated enthusiasm for developing antifibrotic therapies. Regression has been documented in patients with hepatitis B, hepatitis C (Poynard et al., 2002), delta hepatitis, metabolic diseases and cholestasis, among others, although so far improvement has only been seen when the underlying disease has been eradicated. A key determinant of fibrosis reversion is clearance of activated HSCs through apoptosis, which requires downregulation of tissue inhibitor of metalloproteinase-1 (TIMP-1) (Murphy et al., 2002).

Although the point at which human cirrhosis becomes truly irreversible is unknown, animal and human studies suggest that more prolonged injury leads to increasingly thickened fibrotic septae with enhanced crosslinking that is mediated by tissue transglutaminase (Wanless et al., 2000; Issa et al., 2004). These septae become insoluble and may be more resistant to proteolysis by metalloproteinases, which limits complete regression. Interstitial collagen within these septae might provide an important survival signal to activated stellate cells, preventing their clearance through apoptosis. Moreover, it is uncertain whether complete or partial matrix regression will restore normal portal blood flow, because the distorted vascularity and shunting characteristic of advanced liver disease may not be reversible.

2.2.8 Clinical Trials

The choice of patients and endpoints for clinical trials of antifibrotic drugs presents a conundrum. Current efforts focus mainly on patients with hepatitis C and advanced fibrosis or cirrhosis who have failed antiviral therapies, in part because of the large number of such patients and their well characterized natural history. On the one hand, antifibrotics are more urgently needed in patients with HCV cirrhosis and are more likely, if successful, to yield improved survival and reduced morbidity. On the other

hand, cirrhosis is probably less reversible than earlier fibrosis stages and will require longer treatment, and these patients will be less able to tolerate any idiosyncratic hepatotoxicity from an investigational agent. They are also at higher risk for hepatocellular cancer. Thus, initial trials should be aimed at demonstrating the capacity for matrix resorption without insisting that complete reversal of fibrosis or improved morbidity and mortality be documented; findings from such studies will support the rationale for longer, larger trials with 'hard' clinical endpoints including survival and decreased complications. Other potential target populations include either children with neonatal fibrosis, or patients with hepatitis C post-liver transplantation, because fibrosis is accelerated in these groups, or those with cholestatic liver disease or NASH.

2.2.9 Emerging Treatments for Hepatic Fibrosis

The clarification of the mechanisms of fibrosis has led to a surge in enthusiasm for treating hepatic fibrosis, and animal models strongly support the rationale of this approach. In fact, much like the paradigm of cancer treatment, success in animal models has been far easier to achieve than in human trials, possibly because the duration of injury and the extent of matrix deposition and crosslinking are greater in humans. Key obstacles remain to be overcome before antifibrotic therapies can reach widespread clinical use.

2.2.9.1 Reducing Injury and Inflammation

- 1.1 Antiviral therapy for viral hepatitis
- 1.2 Antihelminthic therapy for schistosomiasis
- 1.3 Chelation/venesection, treatment of copper/iron overload disease
- 1.4 AT1 receptor antagonists, ACE inhibitors
- 1.5 Hepatoprotectants:
 - 1.5.1 Caspase inhibitors
 - 1.5.2 HGF/HGF mimetics

2.2.9.2 Attenuating Stellate-Cell Activation

- 2.1 Alpha interferon

2.2 Antioxidants:

2.2.1 Vitamin E, PDTC

2.2.2 AT1 receptor antagonists

2.3 Cytokine-directed therapy:

2.3.1 TGF- β antagonists

2.3.2 Endothelin receptor antagonists

2.3.3 HGF/HGF mimetics

2.4 PPAR agonists

2.5 FXR agonists

2.6 Aldosterone antagonists

2.7 Pentoxifylline

2.2.9.3 Inhibiting Properties of Activated Stellate Cells

3.1 Antiproliferative:

3.1.1 PDGF receptor antagonists

3.1.2 Sodium exchange inhibitors

3.1.3 HMG CoA reductase inhibitors

3.1.4 Plasmin/thrombin receptor antagonists

3.2 Anticontractile:

3.2.1 Endothelin/endothelin receptor antagonists

3.2.2 Nitric oxide donors

3.3 Antifibrogenic:

3.3.1 Collagen synthesis inhibitors

3.3.2 TGF- β inhibitors (including soluble receptors and neutralizing antibodies)

3.3.3 HGF/HGF mimetics

3.3.4 AT1 receptor antagonists

3.3.5 ACE inhibitors/Integrin antagonists

3.3.6 CTGF/CCN antagonists

3.3.7 SMAD7 agonists

2.2.9.4 Promoting Specific Apoptosis of Hepatic Stellate Cells

4.1 Gliotoxin

4.2 NGF agonists

4.3 TIMP antagonists

2.2.9.5 Degrading Scar Matrix

5.1 Direct collagenase administration

5.2 Inhibitors of transglutaminase or collagen crosslinking

5.3 TIMP antagonists

 5.4 TGF- β inhibitors

Table 2.4 describes the classification of a number of pharmacological agents or strategies whose therapeutic potential has been demonstrated in carefully and/or originally conducted studies (Pinzani et al., 2005).

Table 2.4 Anti-fibrogenic agents and strategies

Agent or strategy	Mode of action	Ref.
Direct anti-fibrogenic effect		
Colchicine	Inhibition of pro-collagen secretion and conversion to collagen synthesis. Suppression α -SMA and TGF β ₁ expression in activated HSC	(Lee et al., 2004; Poupon et al., 1996)
Prostaglandins	Inhibition of both basal and TGF β ₁ -mediated induction of collagen synthesis by HSC	(Hui et al., 2004)
OPC-13013: a cyclic nucleotide phosphodiesterase type III, inhibitor	Augmentation of forskolin-induced increase in intracellular cyclic AMP level (inhibitory effect on HSC activation)	(Shimizu et al., 1999)
6-Ethyl chenodeoxycholic acid (6-ECDCA): a FXR ligand	Induction of SHP expression, down-regulation of α 1(I) collagen and TGF β ₁ mRNA steady state level in HSC	(Fiorucci et al., 2004)
Pentoxifylline	Down-regulation of pro-collagen type I, TGF β ₁ and CTGF expression in HSC	(Romanelli et al., 1997; Raetsch et al., 2002)
HDAC inhibitors: trichostatin A and sodium butyrate	Inhibition of mRNA and de novo protein synthesis of pro-collagens type I, III and α -SMA	(Niki et al., 1999)

All trans retinoic acid	Inhibition of steady state mRNA and de novo protein synthesis of pro-collagen type I, III, IV and fibronectin and laminin	(Hellemans et al., 1999)
Lovastatin, simvastatin: HMG-Co reductase inhibitors	Inhibition of protein synthesis of pro-collagens type I, III and IV	(Rombouts et al., 2003)
Canrenone	Inhibition of TGF β ₁ -induced de novo protein synthesis of pro-collagens type I and IV and fibronectin. Indirectly: inhibition of PDGF-induced proliferation and migration of HSC	(Caligiuri et al., 2003)
Tetrandrine	Reduction of HSC activation and collagen accumulation in liver fibrosis induced by biliary obstruction. Indirectly: promotion of HSC apoptosis	(Zhao et al., 2004)
Butein	Down-regulation of α -SMA and collagen type-I protein expression. Reduction of α 1(I) collagen and TIMP-1 mRNA expression and induction of MMP-13 mRNA expression	(Woo et al., 2003)
Hepatocyte growth factor (HGF)	Reduction of TGF β ₁ levels in the liver	(Ikeda et al., 1998; Ueki et al., 1999)
Halofuginone	Reduction of total collagen content, α 1(I) collagen gene expression, TIMP-2 content, α -SMA expression and inhibition of the proliferation of other cell types of the fibrotic liver in vivo	(Bruck et al., 2001)
IL-10	Upregulation of mRNA steady state expression of interstitial collagenase and inversely down-regulation of α 1(I) collagen	(Zhang et al., 2004; Wang et al., 1998(b))
Dilinoleoylphosphatidylcholine (DLPC)	Down-regulation of collagen accumulation induced by TGF β ₁ in cultured HSC	(Cao et al., 2002)
Relaxin	Reduction of the levels of total collagen by inhibition of new collagen synthesis. Downregulation of α -SMA expression and up-regulation of expression and secretion of MMP-13, TIMP-1 and TIMP-2	(Bennett et al., 2003)
Camostat mesilate, a serine protease inhibitor	Down-regulation of the activity of TGF β , which blocked in vitro activation of HSC. Markedly attenuation of plasmin and TGF β levels, HSC activation and hepatic fibrosis in an in vivo model	(Okuno et al., 2001)
HOE 077 and S4682: prolyl 4-hydroxylase inhibitors	Reduction of the stability of the collagen triple helix by inhibiting prolyl-4 hydroxylase. Inhibition of collagen synthesis in HSC	(Aoyagi et al., 2002; Bickel et al., 1998)
Malotilate	Down-regulation of collagen synthesis in CCl ₄ -induced hepatic fibrogenesis	(Nojgaard et al., 2003(a))
LU 135252: a non-peptide ET-A receptor antagonist	Reduction of α 1(I) collagen and TIMP-1 mRNA steady state levels	(Cho et al., 2000)
S-Farnesylthiosalicylic acid (FTS)	Augmentation in MMP-2 and MMP-9-induced collagenolytic activity and up-regulation of TIMP-2 expression	(Reif et al., 2004)
PPAR γ ligands: 15dPGJ(2) and troglitazone	Reduction in α 1(I) pro-collagen, α -SMA and MCP-1 mRNA levels and up-regulation of MMP-3 and CD36. Inhibition of α 1(I) pro-collagen promoter activity. Modulation of pro-fibrogenic and proinflammatory actions in	(Miyahara et al., 2000; Marra et al., 2000)

HSC		
TTNPB: an RAR agonist, AGN194204: an RXR agonist	Inhibition of collagen and fibronectin synthesis	(Hellemans et al., 2004)
Indirect anti-fibrogenic effect		
NS-398: a COX-2 inhibitor	Inhibition of α -SMA protein and PCNA expression. Reduction in cell growth: Downregulation of the generation of PGE ₂ , IL-8, IL-6 and hyaluronan in HSC	(Cheng et al., 2002)
Non-specific COX inhibitors: indomethacin and ibuprofen	Inhibition MCP-1 gene and protein expression in HSC	(Efsen et al., 2001)
Gliotoxin	Induction of apoptosis in HSC through a thiol redox-dependent interaction with adenine nucleotide transporter (ANT)	(Orr et al., 2004)
Ethylisopropylamiloride	Inhibition of the activity of Na ⁽⁺⁾ H ⁽⁺⁾ exchanger 1 and reduction in PDGF-BB induced proliferation of HSC	(Yang et al., 2003(a); Benedetti et al., 2001) (Di Sario et al., 2003)
Cariporide	Inhibition of the activity of Na ⁽⁺⁾ H ⁽⁺⁾ exchanger 1 and reduction in PDGF-BB induced proliferation of HSC	(Baik et al., 2003)
Losartan: an angiotensin II receptor inhibitor	Reduction in the contraction and growth of HSC	(Yoshiji et al., 2002)
Perindopril, an ACE inhibitor	Suppression of activated HSC proliferation and TIMP-1 expression	(Okuyama et al., 2001)
N-acetyl-L-cysteine (NAC)	Induction of extracellular proteolysis of PDGF receptor- β and down regulation of type II TGF- β receptor	(Iwamoto et al., 1999(b))
Arg-Gly-As peptides	Induction of apoptosis in HSC through integrin antagonism and stimulation of collagenase expression by HSC	(Iwamoto et al., 1999(a); Gutierrez-Ruiz et al., 2001)
Anti-oxidants		
Metadoxine	Inhibition of acetaldehyde-induced increase in collagen and attenuation of TNF- α secretion	(Lee et al., 2001)
α -Tocopherol	Down-regulation of collagen type I, α -SMA and PCNA expression. Protection against CCl ₄ -induced chronic liver damage and cirrhosis	(Parola et al., 1992)
Quercetin: a flavonoid	Reduction of collagen content, iNOS expression and lipid peroxidation in total liver. Augmentation of total peroxy radical- trapping anti-oxidant capacity of liver. Antioxidant and free radical-scavenging activities	(Pavanato et al., 2003)
Epigallocatechin-3-gallate	Inhibition of the TGF β signal transduction pathway and inhibition of the expression of α 1(I) collagen, fibronectin and α -SMA genes	(Chen et al., 2002)
Trans-resveratrol	Inhibition of type I collagen mRNA. Inhibition of proliferation and down- regulation of α -SMA expression. Reduction of the secretion of MMP-2	(Godichaud et al., 2000)
Herbes		
Da Ding Feng Zhu	Down-regulation of serum indexes of liver fibrosis	(Li et al., 2003(c))
Trichilia roka root	Hepatoprotective agent preventing a preferential deposition of collagen around the sinusoidal cell layer	(Germano et al., 2001)

Sylimarin	Down-regulation of pro-collagen $\alpha 1(I)$, TIMP-1 and TGF β_1 mRNA levels	(Jia et al., 2001)
Sho-saiko-to	Suppression of pro-collagen type I and III mRNA expression and III and cell cycle	(Kayano et al., 1998)
Herbal Compound 861	Inhibition of the cell cycle and activation of HSC by reduction of the expression levels of α -SMA mRNA in HSC	(Wang et al., 2004)
Salvionolic acid-A (SA-A): active compound of <i>Salvia miltiorrhiza</i>	Inhibition of cell proliferation and collagen production in HSC	(Liu et al., 2000(a))
Monomer IH764-3: active compound of <i>Salvia miltiorrhiza</i>	Inhibition of HSC proliferation and induction of HSC apoptosis	(Zhang et al., 2002)
Qinggan Huoxue recipe (QGHR)	Reduction of the levels of liver fibrosis markers and cytokines, alleviation of the antilipid superoxidation damage in liver, and markedly improvement in the degree of fatty liver	(Ji et al., 2004)
Hujin pill	Down-regulation of the retardation of liver fibrosis	(Huang et al., 2000)
Dahuang Zhechong pill	Inhibition of HSC proliferation and secretion of TGF β_1 - Reduction in collagen synthesis	(Li et al., 2003(b))
HanDanGanLe	Up-regulation of collagenase activity in immune hepatic fibrosis	(Lu et al., 2000; Zhang et al., 2003(b))
Inchin-ko-to (TJ-135)	Regulation of PDGF-BB-dependent signaling pathways of HSC. Down-regulation of collagen and fibronectin synthesis	(Imanishi et al., 2004)
Maotai liquor	Inhibition of proliferation of HSC and reduction in collagen gene and protein expression	(Cheng et al., 2004)
Aloe emodin	Inhibition of type I collagen production and α -SMA expression	(Woo et al., 2002)
Curcumin	Reduction in cell proliferation, induction of apoptosis and suppression of ECM gene expression through PPAR γ activity in activated HSC	(Zheng and Chen, 2004)
Glycyrrhizin	Reduction of serum ALT and AST values, inhibition of the NF-kappaB binding activity in CCl $_4$ and ethanol-induced chronic liver injury	(Park et al., 1997; Wang et al., 1998(a))
Biotechnologies		
Soluble decoy receptors for TGF β_1	Reduction of collagen type I expression during hepatic fibrosis	(Muriel and Castro, 1998)
Anti-sense oligonucleotides phosphothioate (AdCATb-TR), adenovirus-mediated local expression of a dominant-negative type II TGF- β receptor	Inhibition of TIMP-1 gene expression	(Muriel et al., 1994)
(Ad5-CMV-asPDGF), an adenoviral vector serotype 5 (Ad5) expressing an anti-sense mRNA of the PDGF B-chain	Reduction of liver fibrosis and hydroxyproline content, serum levels of HA and transaminases	(George et al., 1999)
(Ad5-CMV-asPDGF), an adenoviral vector serotype 5 (Ad5) expressing an anti-sense mRNA of the PDGF B-chain	Regulation of endogenous PDGF B-chain and PDGFR β mRNA in culture-activated HSC and rat livers. Attenuation of experimental liver fibrogenesis by reduction of α -SMA and collagen type I expression	(Nie et al., 2001)

Anti-sense oligonucleotides against TGF- β 1	Inhibition of HSC activation, secretion of TGF β ₁ , and downregulation of collagen synthesis	(Qi et al., 1999)
Anti-sense TIMP-1 recombinant plasmid	Inhibition of collagens type I and III synthesis	(Borkham-Kamphorst E et al., 2004)
Peptide-modified albumin (pPB-HSA)	Reduction of PDGF-BB-induced fibroblast proliferation	(Liu et al., 2000(b))
Anti-sense T beta R I and T beta R II recombinant plasmids	Blocks mRNA and protein expression of T beta R I and T beta R II and decreases collagen types I and III	(Liu et al., 2003)
Miscellaneous		
NCX-1000	Inhibition of HSC contraction. Metabolization of NCX-1000 and secretion of and release nitrite/nitrate in cell supernatants	(Beljaars et al., 2003)
Nitroglycerin (NTG): an NO-donor	Inhibition of proliferation, motility, and contractility of HSC and reduction of fibrillar ECM accumulation	(Jiang et al., 2004)
S-Adenosyl-L-methionine (SAME)	Hepatoprotective agent by restoring transmethylation loss in liver fibrosis	(Fiorucci et al., 2001; Failli et al., 2000)

2.3 PPAR γ LIGANDS AND LIVER FIBROSIS

The PPARs belong to the superfamily of of ligand-dependent transcription factors that is predominantly expressed in adipose tissue, where it has been shown to have a key role in adipogenesis (Kliwer et al., 1994; Tontonoz et al., 1995; Green and Wahli, 1994). PPAR forms heterodimers with the retinoid X receptor and binds to specific response elements to induce transcription in response to a variety of endogenous and exogenous ligands, including fatty acids, arachidonic acid metabolites, and synthetic drugs (Forman et al., 1996). Of the PPAR isoforms, PPAR- γ is the most widely studied (Auwerx, 1999). Previous studies indicated that expression of PPAR- γ inhibited PDGF-induced proliferation and migration of vascular smooth muscle cells (Fu et al., 2001). Recently, additional functions such as regulation of inflammation; control of cell cycle and apoptosis were attributed to PPAR γ , suggesting a more pleiotropic role in multiple fundamental pathways with wide-ranging biomedical implications (Rocchi and Auwerx, 1999; Everett, 2000). Three recent studies independently demonstrated that the level of PPAR- γ and its trans-activating activity were diminished during HSC activation in vitro, whereas NF- κ B and activator protein- 1 (AP-1) activities were increased (Galli et al., 2000; Marra et al., 2000; Miyahara et al., 2000). PPAR- γ ligands inhibited cell proliferation and collagen- α_1 (I) expression in primary HSC (3–4 days) (Miyahara et al., 2000). The dramatic reduction in the abundance of PPAR- γ results in a significant decline in response to exogenous PPAR- γ ligands in activated HSC (Galli et al., 2000; Marra et al., 2000;

Miyahara et al., 2000). These findings implied a potential therapeutic value of PPAR- γ ligands in treatment of liver fibrosis if the expression of PPAR- γ can be induced in activated HSC.

2.4 ANGIOTENSIN II RECEPTOR ANTAGONIST AND LIVER FIBROSIS

Drugs modulating the action of vasoactive substances are currently used in the treatment of different types of human fibrosis. These vasoactive substances include vasoconstrictors (angiotensin-II, aldosterone, and ET-1) and vasodilators (prostaglandins and nitric oxide). Among these factors, angiotensin-II appears to play an important role. Drugs interfering with angiotensin-II synthesis (i.e., angiotensin-converting enzyme inhibitors or Angiotensin-I antagonists) reduce the progression of cardiac and renal fibrosis in patients with severe arterial hypertension. Angiotensin-II induces contraction and is a mild mitogen toward HSCs. Moreover, in a preliminary study, an Angiotensin-I antagonist inhibited liver fibrosis in bile duct–ligated rats (Figure 2.4) (Bataller et al., 2000; Jonsson et al., 2001).

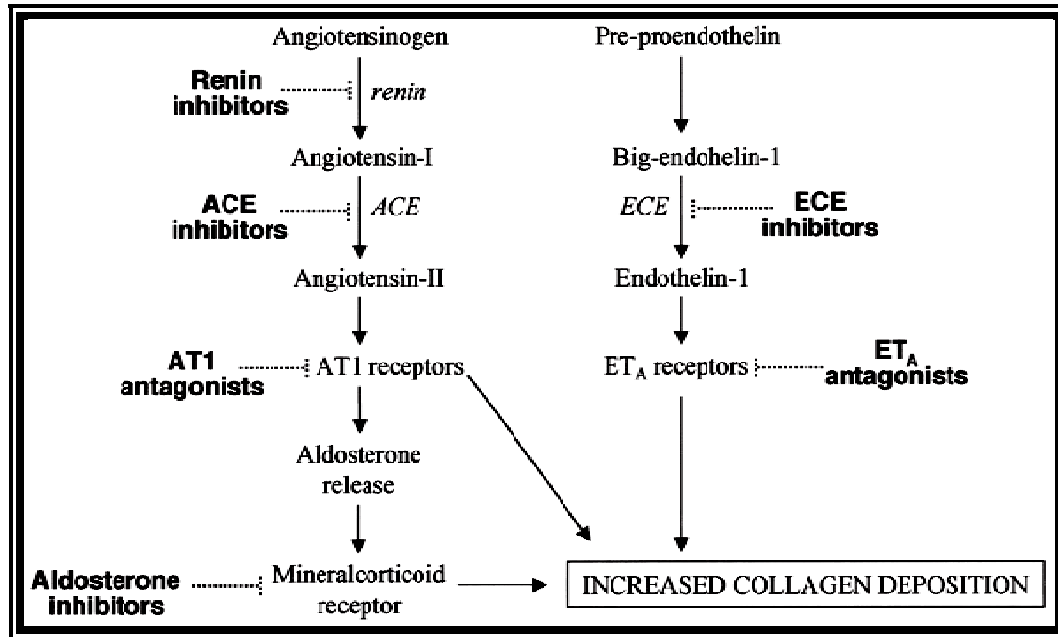


Figure 2.4 The renin-angiotensin-aldosterone and endothelin pathways and potential sites for therapy of liver fibrosis (ACE = angiotensin-converting enzyme; ECE = endothelin-converting enzyme)

2.5 DRUG TARGETING TO HSC

A large number of currently tested antifibrotic drugs aim, either direct or indirect, at activated HSC. In vivo, however, effectiveness of these compounds is often limited due to the lack of the specificity for HSC. Selective delivery of compounds to the HSC in the fibrotic liver by means of specific drug carriers is an alternative for traditional treatments.

Due to selective accumulation in the HSC, high drug concentrations can be achieved, while at the same time adverse effects will be avoided in other tissues and cells. In order to target HSC, protein based carriers were developed using chemically modified human serum albumin (HSA) with specific groups that are recognised by receptors expressed on the cell membrane of activated HSC. The introduction of mannose 6-phosphate (M6P-HSA) groups (Beljaars et al., 1999; Beljaars et al., 2001) into the albumin molecule yielded a carrier which was recognized by the mannose 6-phosphate/insulin like growth factor II receptor that is abundantly expressed on activated HSC. The best homing properties of this carrier were achieved when around 30 M6P groups were attached per albumin molecule. In two other carriers, specific sequences of cyclic peptides, that mimic the binding-sites of natural ligands such as PDGF (Beljaars et al., 2003) and collagen type VI (Beljaars et al., 2000) to their receptors, were attached to HSA. Both PDGF receptor and collagen type VI receptor are up-regulated on activated HSA and the association of these carriers with activated HSC was demonstrated. In vivo, it was shown that all these carriers accumulate in HSC in the fibrotic livers of bile duct ligated rats.

Modified HSA can function as a drug carrier, as was recently proved by coupling several drugs, including pentoxifyline (Gonzalo et al., 2006), mycophenolic acid (Greupink et al., 2005), doxorubicine (Greupink et al., 2006) and gliotoxin (Hagens et al., 2006) to M6P-HSA. These drug-carrier constructs retained their antifibrotic properties, as was demonstrated in cultured HSC, and were also delivered to HSC in the fibrotic liver. Another application of modified HSA would be to serve as a homing ligand for other of drug carrier systems such as liposomes, cationic lipoplexes or polymers (Figure 2.5).

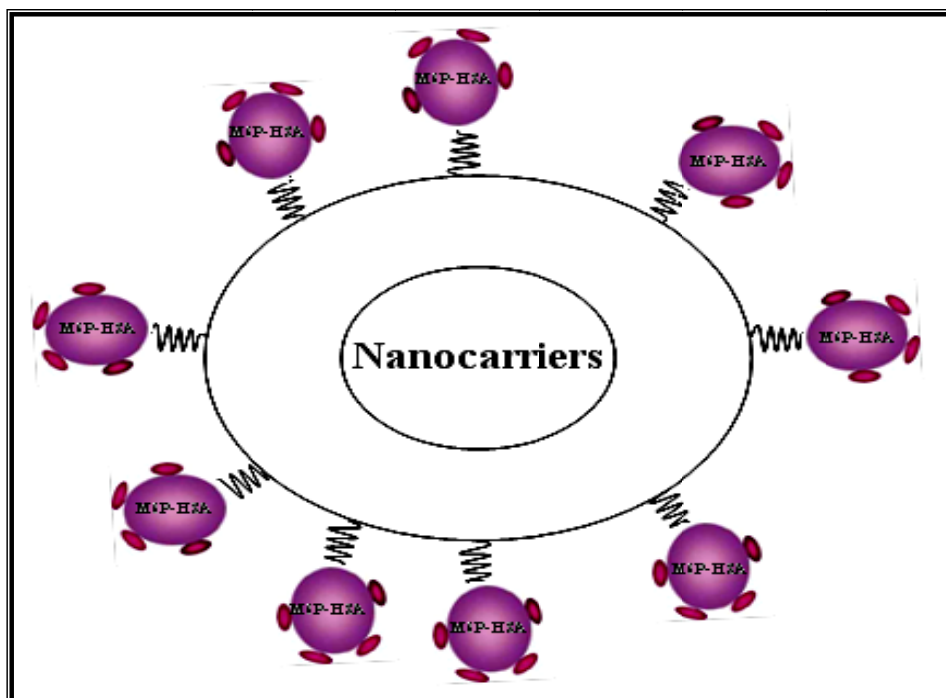


Figure 2.5 Schematic representation of M6P-HSA conjugated carrier

2.6 LIPOSOMES

Liposomes are synthetic, single or multi-compartmental vesicles having lipid membranes enclosing aqueous chambers. Liposomes are vesicles composed of phospholipids bilayers surrounding aqueous compartments as described by Bangham et al (1965) (Bangham et al., 1965). They consist of one or more bilayers. The driving force for bilayer assembly is the amphiphilic nature of phospholipid molecules. Liposomes are composed of phospholipid/s or lipids or and glycerides with or without sterols. Phospholipid typically consists of a hydrophilic head group attached to two hydrophobic fatty acid chains. When suspended in an excess of aqueous solution, phospholipid molecules orient themselves in ordered bilayers so that the polar heads are hydrated and hydrophobic tails are excluded from the aqueous environment (Figure 2.6). Although suspended phospholipids may also assume other geometric(s) such as micelles and tubular aggregates in hexagonal phases, this can be controlled by several factors including lipid composition and method of preparation. Entrapment of compounds is highly influenced by their physicochemical properties. Generally hydrophobic molecules are incorporated into the lipid bilayers whereas hydrophilic compounds are entrapped in the internal aqueous volume (Stamp and Juliano, 1979).

2.6.1 Composition of Liposomes

2.6.1.1 Phospholipids

Glycerol containing phospholipids are by far, the most commonly used component of liposome formulations and represent more than 50% of the weight of lipid present in biological membranes (Riaz et al., 1988). As examples of potentially useful lipids can be mentioned natural lipids such as egg lecithin, soya lecithin, and synthetic lipids such as phosphoglycerolipids, sphingolipids, and digalactosylglycerolipids. Amongst natural lipids may be mentioned sphingolipids such as sphingomyelin, ceramide and cerebroside; galactosylglycerolipids such as digalactosyldiacylglycerol; phosphoglycerolipids such as egg-yolk phosphatidylcholine and soya-bean phosphatidylcholine; and lecithins such as egg-yolk lecithin and soya-bean lecithin. Amongst synthetic lipids may be mentioned dimyristoyl phosphatidylcholine, dipalmitoyl phosphatidylcholine (DPPC), distearoyl phosphatidylcholine, dilauryl phosphatidylcholine, 1-myristoyl-2-palmitoyl phosphatidylcholine, 1-palmitoyl-2-myristoyl phosphatidylcholine, dioleoyl phosphatidylcholine, hydrogenated soyaphosphatidylcholines (HSPC), and the like. Some naturally occurring phospholipids include phosphatidylcholine (PC), phosphatidylinositol (PI) and phosphatidylglycerol (PG) while dipalmitoyl phosphatidylcholine (DPPC), dipalmitoyl phosphatidylserine (DPPS), dipalmitoyl phosphatidylethanolamine (DPPE), dipalmitoyl phosphatidic acid (DPPA), dipalmitoyl phosphatidylglycerol (DPPG), dioleoyl phosphatidylcholine (DOPC) and dioleoyl phosphatidylglycerol (DOPG) are some synthetic phospholipids.

2.6.1.2 Sterols

Sterols such as cholesterol, ergosterol, lanosterol, or its derivatives are often included as components of liposomal membrane. Cholesterol has been called the “mortar” of bilayer because by virtue of its molecular shape and solubility properties, it fills in empty spaces among the phospholipid molecules, anchoring them more strongly into the structure. Its inclusion in liposomal membranes has 3 effects (i) increasing the fluidity or microviscosity of the bilayer (ii) reducing the permeability of the membrane to water-soluble molecules and (iii) solubilizing the membrane in the presence of biological fluids such as plasma.

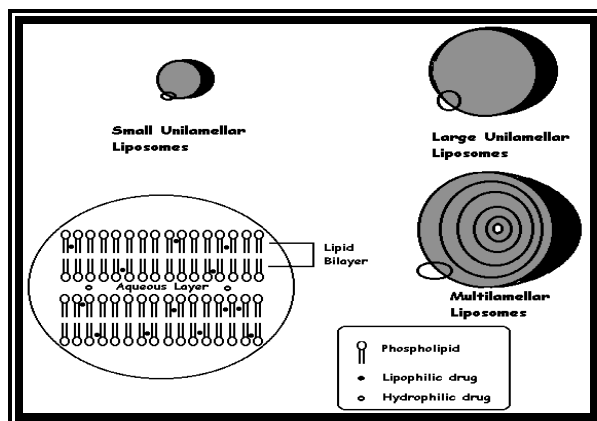


Figure 2.6 The structure of multilamellar vesicles showing the organization of phospholipid bilayers and the encapsulation of lipophilic and hydrophilic compounds

2.6.1.3 Other Non-Structural Components

Charge inducer materials which provides a negative charge, for example phosphatidic acid, dicetyl phosphate or beef brain ganglioside etc, or one which provides a positive charge for example stearylamine acetate or cetylpyridinium chloride etc. have been incorporated into liposomes so as to impart either a negative or a positive surface charge to these structures. Many single chain surfactants of number of single and double chain lipids having fluorocarbon chains and also compounds like quaternary ammonium salts and dialkyl phosphates (Ringdorf et al., 1988) can also be used to form liposomes.

2.6.2 Types of Liposomes

Different types of liposomes can be prepared and are classified by the size and structure. Different types of liposomes are small unilamellar vesicles (SUV), large unilamellar vesicles (LUV), oligolamellar vesicles (OLV), and multi-lamellar vesicles (MLVs). MLVs consist of numerous concentric bilayers separated by aqueous spaces and range up to 15 μm in diameter. Vesicles consisting of a single bilayer encompassing a central aqueous compartment are referred to as small unilamellar vesicles (SUVs), which range upto 100 nm in diameter and large unilamellar vesicles (LUVs) ranging from 100 to 500 nm in diameter (Figure 2.6).

2.6.3 Methods of Preparation of Liposomes

Numerous procedures have been developed to prepare liposomes. There are at least fourteen Major published methods for making liposomes (Ostro, 1988; Martin, 1990). The seven, most commonly employed methods are, Lipid film hydration method (Bangham et al., 1965), Ethanol injection method (Batzri and Korn, 1973), Ether infusion method (Deamer and Bangham, 1976), Detergent dialysis method (Kagawa and Racker, 1971), French press method (Barenholz et al., 1979), Rehydration-dehydration techniques (Shew and Deamer, 1985) and Reverse phase evaporation method (Cortesi et al., 1999).

2.6.4 Characterization of Liposomes (New, 1990)

The behavior of liposomes in both physical and biological systems is determined to a large extent by factors such as physical size, chemical composition, quantity of entrapped solutes etc. Hence, liposomes are characterized with respect to the following parameters:

2.6.4.1 Size and Size Distribution

There are number of methods reported in the literature to determine size and its distribution of the vesicles (Bangham et al., 1974; Meeren et al., 1992). The most commonly used ones are light microscopy preferably using electron microscope, laser light scattering or cryoelectron microscopy.

2.6.4.2 Lamellarity

The lamellarity, the average number of bilayers present in liposomes, can be determined either by ^{31}P -NMR spectroscopy or freeze fracture electron microscopy.

2.6.4.3 Determination of Percentage Capture

The quantity of material entrapped inside liposomes can be determined more commonly by mini-column centrifugation method, protamine aggregation method, dialysis technique or by gel chromatography.

2.6.5 Stability of Liposomes

A prerequisite for the successful introduction of liposomes in therapy is the long-term stability of the formulation. The stability of drug-laden liposome dispersions preferably should meet the standards of conventional pharmaceutical product. A 1-

year shelf life is considered to be an absolute minimum. Both chemical and physical determines the shelf life of a product.

In the literature, on the physical stability of liposomes, attention has been focused on two processes affecting the quality and therefore acceptability of liposomes (Talsma and Cormmelin, 1993). First, the encapsulated drug can leak from the vesicles into the extra-liposomal compartment (reduced retention). Second, liposomes can aggregate and/or fuse, forming larger particles. Both these processes change the disposition of the drug in vivo and thereby presumably affect the therapeutic index of the drug involved. Besides, other physical parameters may also change during storage. For instance, hydrolysis of phospholipids causes the formation of fatty acids and lysophospholipids. These compounds considerably affect the physical properties of the bilayer (Talsma and Cormmelin, 1993). Apart from this, chemical degradation process may influence the safety of liposomes. Solid experimental data on the safety of partially hydrolyzed liposomes are not yet available; lysophospholipids alone have been reported to be toxic.

Several approaches have been developed to ensure the physical stability of liposomes on storage.

1. For storage of aqueous dispersions, the lipid composition of the bilayer and the aqueous solvent can be adjusted to induce optimum stability by reducing permeability/leakage. Phospholipids with long and saturated alkyl chains (distearoyl phosphatidyl choline and dipalmitoyl phosphatidyl choline or saturated hydrogenated soyabean or egg phosphatidyl choline) provide rigid bilayers with low permeabilities for small, non-bilayer-interacting compounds (Talsma and Cormmelin, 1993). The incorporation of the bovine serum albumin in the liposomal membrane and treatment with glutaraldehyde has been reported to prevent leakage of the entrapped contents (Law et al., 1994). Crommelin has reported the effect of bilayer composition on permeability of carboxyfluoresce in (Crommelin and Van Bommel, 1984).

To formulate drugs in liposomes it is necessary to reduce the leakage of an entrapped drug. The rate of leakage of a molecule from liposomes is governed by the physio-chemical properties of a molecule. Liposomes are freely permeable to water, but cations are released at a slower rate than anions (Bangham et al., 1965), whereas

aqueous hydrogen bonding may determine the leakage rate of non-electrolytes (Cohen, 1975).

Phospholipids in the liquid-crystalline state are more permeable to entrapped material than when they are in the gel state. Thus, loss of entrapped material is temperature dependent, generally being greatest around the phospholipid phase transition temperature (T_c) (Papahadjopoulos et al., 1973). The stability of liposomes in terms of retention of dideoxyinosine triphosphate (ddITP) was measured by Betageri (Betageri, 1993) at 4°, 25°, and 37°C. He observed that retention of ddITP in liposomes was maximum when stored at 4°C followed by 25°C and 37°C.

Another way to control stability is to incorporate cholesterol into the lipid structure, since it is known to reduce leakage of various solutes through the lipid bilayer when the membrane is in a fluid-like state (Gregoriadis and Davis, 1979; Scherphof et al., 1984), or by polymerization of phospholipid molecules (Johnston and Chapman, 1984; Scherphof et al., 1981). The introduction of cholesterol in liposomes of 5,6-carboxyfluorescein (CF) has been reported to reduce the rate of leakage during storage (Hernandez-Caselles et al., 1990). He also observed that CF retention was greater in liposomes stored at 4°C in the presence of O_2 than those of room temperature, although liposomes stored at room temperature but in O_2 -free atmosphere were more stable than those stored at room temperature in the presence of O_2 .

2. Freezing the liposome dispersion is also an approach to achieve prolonged liposome shelf-life (Talsma et al, 1992(b)). Lyophilization and rehydration, which include a freezing and thawing cycle, represent another method, used by many laboratories for better stability of liposomal formulations (Venkataram et al., 1990). Several groups have published reports on freezing, drying (Hauser and Strauss, 1987) or freeze-drying of liposomes. Cryoprotectants play an important role in the physical stabilization of liposomes during freezing, drying or freeze-drying. The 100% CF retention could be found (Talsma and Cormmelin, 1993) using cryoprotectant after a full freezing-thawing cycle. Studies made on the stability of liposomes with time, when they were either freeze-dried or in solution have been reported (Crommelin and Van Bommel, 1984).

3. In addition, two other techniques can solve the problem of drug leakage during storage, proliposomes and remote loading (Talsma and Cormmelin, 1993) that permit liposome dispersion preparation in situ. Several reports have been published in this context. Chemical analysis mainly concerns hydrolysis of the ester bonds in phospholipids and oxidation of their unsaturated acyl chains if present. Hydrolysis of phospholipid to free fatty acid and lysophospholipids can disturb the phospholipid bilayer structure and may disrupt it, leading to leakage of encapsulated products. Oxidation of unsaturated phospholipids and cholesterol may be initiated by the action of light and heavy metals (New, 1990). According to Hernandez-caselles (Hernandez-Caselles et al., 1990), the presence of A-tocopherol decreased the breakdown of phosphatidyl choline to lysophosphatidyl choline and also reduced the level of peroxidation. Although the mechanism of the action of α -tocopherol is not clear, it is suggested that this may happen through specific binding to the phospholipid molecule (Villalain et al., 1986). α -tocopherol acetate was found to be much less effective than α -tocopherol in preventing lipid peroxidation (Fukuzawa et al., 1981). Further information about chemical stability can be found in reviews of hydrolytic and oxidation reactions in phospholipids (Talsma and Cormmelin, 1993).

2.6.6 Liposomes as Drug Delivery Systems

In the recent past, controlled release concept and technology have received increasing attention in the face of growing awareness to toxicity and ineffectiveness of drugs when administered or applied by conventional methods. Liposomes as drug delivery systems are among research topics that are being vigorously investigated in both academic and industrial laboratories, with different outlooks and common goals and end products. The scientific literature is rich with comprehensive review of liposomes as drug delivery systems (Gulati et al., 1998; Perugini and Pavanetto, 1998).

Over the last twenty years, the liposome has changed its status from being a novel plaything for the laboratory worker to a powerful tool for an industrialist with the gap between the ideal desired characteristics of liposomes and what is technically feasible becoming narrower all the time. Vastly improved technology in terms of drug capture, vesicle stability on storage, scale-up production and the design of formulations for special tasks has facilitated the application of a wide range of drugs in the treatment and prevention of diseases in experimental animals and clinically.

Liposomes may prove to be efficient carrier for targeting the drug to the site of action because of the following properties: Amphiphilic nature, flexibility in structural characteristics, localized drug effect, controllability of drug release rate, stability in vivo, direct cell liposome interaction, sterilizability, ability to protect drug and body from each other, non-toxicity, non immunogenicity, biocompatibility and biodegradability and accommodation of molecules with wide range of solubility and molecular weight. At the same time, there are certain problems associated with liposome as drug delivery systems (Deasy, 1984) such as difficulty in procuring pure phospholipids, difficulty in scale-up, poor stability over a long shelf-life, expensive, batch to batch variation in performance, low drug loading, difficulty in avoiding the reticulo-endothelial system and possibility of unwanted vascular obstruction caused by large liposomes. However, research into the use of liposomes in drug delivery has led to vastly improved technology in terms of drug capture, vesicle stability, storage, scaled up production and the design of formulations for specialized tasks. Table 2.5 shows the liposome application according to their mode of action.

Due to their high degree of biocompatibility, liposomes were initially considered as delivery systems for intravenous administration. The first parenterally applied formulation Ambisome (Vestar Inc., San Dimas, CA), a liposomal amphotericin formulation for the treatment of disseminated fungal infections that frequently occur in immunosuppressed patients, was launched in Ireland in 1990 that showed both high therapeutic activity and reduced toxicity (Talsma and Cormmelin, 1992(a)) as compared to the original product. More recently in 1995, a sterically stabilized liposomal formulation containing the anticancer drug, doxorubicin (Lasic, 1993) has been launched in United States.

It has since become apparent that liposomes can also serve as an effective tool for other delivery systems that include oral (Sveinsson and Holbrook, 1993), ophthalmic (Velpandian et al., 1999), aerosol (Conley et al., 1997), dermal/transdermal (Fresta and Puglisi, 1997; Trafny et al., 1999) applications, as immunological adjuvants, as carriers of antigens, leishmaniasis, lysosomal storage diseases, cell biological application etc. The recent research is concentrated on the use of liposomes to deliver hemoglobin and act as red blood cell substitutes. The scientists are also engaged in designing of liposomal prodrug using principle of specific enzyme cleavage and

facilitated spontaneous hydrolysis. Another field of liposomal research in producing sterically stabilized liposomes for prolonged circulation in blood stream. Liposomes are currently being studied as drug carriers for a variety of drugs that include recombinant proteins (Sugarman and Perez-Soler, 1992), gene transfer and immuno diagnostic applications (Tolstoshev, 1993). Of these, non-invasive route of administration continuously demands significant efforts in designing the liposomes that will no doubt continue to contribute significantly to more efficient use of "old drugs" with better and established therapeutic index vis-a-vis minimum side effects.

Table 2.5 Major modes of liposomal action and related applications

Mode of action	Application
Intracellular uptake (lysosomes, endosomes/cytoplasm)	Microbial disease, Metal storage disease, Gene manipulation, uptake by some tumour, cells, macrophage activation to a tumoricidal/microcidal state, efficient antigen presentation by antigen presenting cells (vaccines).
Slow release of drugs near the target area	Tumors near fixed macrophages.
Avoidance of tissue, sensitive to drugs	Cardio toxicity of doxorubicin
Circulating reservoirs	Blood surrogates
Facilitation of drug uptake by certain routes	Drug delivery to skin, lungs, eyes, mucosal tissues.

2.6.7 Liposomes in Drug Delivery to Liver Cells

Liposomes are formed through hydration of amphiphilic lipids. In these microscopic vesicles, an aqueous lumen is surrounded by one or more lipid bilayers. Most preparations of liposomes for drug delivery purposes are made from neutral or anionic phospholipids with addition of cholesterol to stabilise the liposomal membrane. This liposomal composition resembles the naturally occurring cell membrane, and thus liposomes are considered to be biocompatible, i.e. they are biodegradable, non-immunogenic and nontoxic. Because the liposomal structure comprises an aqueous phase and a lipid phase, it can accommodate both water- and lipid-soluble substances. Water-soluble compounds can be encapsulated in the aqueous inner part of the vesicle while lipophilic drugs can be accommodated in the lipid bilayer. Additionally, molecules such as antibodies, proteins and sugar groups can be coupled relatively easily to the surface of the liposomes to target them to specific tissues and cells. Polymers such as polyethyleneglycol (PEG) attached to the liposomal membrane prolong the circulation time of these particles in the blood. In principle, liposomes

change the pharmacokinetic properties and the biodistribution of the encapsulated drugs; they often prolong the circulation time in the blood and may enhance the deposition and internalisation at the target site. In addition, liposomes protect the carried drug from degradation in the blood stream while they safeguard the rest of the body from the encapsulated potentially toxic drugs.

Intravenously injected liposomes smaller than 1 μm readily accumulate in the liver, where they end up predominantly in KCs. However, depending on their size and lipid composition as well as on surface modification, they can be re-targeted to other types of liver cells, including hepatocytes and LEC. Therefore, in liver diseases such as fibrosis, showing a pathology that involves all major population of liver cells, delivery of drugs to particular types of the cells, using specifically targeted liposomes, provide the possibility to interfere simultaneously with different processes that occur during disease development.

2.6.7.1 Liposomes Targeted to Hepatocytes

To reach hepatocytes from the blood stream, liposomes have to pass the fenestrations in the endothelial cells. This limits the size of the liposomes that can be taken up by hepatocytes to about 150 nm. Indeed, small unilamellar vesicles with diameters around 50 nm and composed of neutral lipids, accumulate predominantly in hepatocytes (Spanjer et al., 1986). The interaction of liposomes with hepatocytes might be mediated by the apolipoprotein E (ApoE) remnant receptor, leading to the endocytosis of liposomes, and the scavenger receptor B-1 (also known as the HDL receptor) resulting in selective transfer of lipids (Scherphof et al., 2001; Yan et al., 2004; Yan et al., 2005(a)).

Interestingly, liposomes with a relatively large size of 200 – 400 nm, containing the negative lipid phosphatidylserine (PS), accumulated in large amounts in hepatocytes (Daemen et al., 1997). This phenomenon was not observed when PS was replaced by another negatively charged lipid, phosphatidylglycerol (PG). The uptake mechanism of large PS-containing liposomes by hepatocytes is not fully understood, but it is possible that either PS exerts a pharmacological effect on the dimensions of the endothelial fenestrations or that PS-containing liposomes, due to their weak interaction with endothelial cells are squeezed through the fenestrations by the blood cells (Romero et al., 1999).

The active targeting of liposomes to hepatocytes can be achieved by modifying the liposomal surface with ligands of the asialoglycoprotein receptor (ASGPr), such as galactose and N-acetylgalactosamine (Hattori et al., 2000; Rensen et al., 2001; Sliedregt et al., 1999). ASGPr on the surface of hepatocytes mediates the clearance process of desialylated proteins from the blood. The efficiency of the uptake of galactosylated liposomes by hepatocytes depends on the density of galactose groups attached to liposomes. In addition, the size of liposomes modified with galactose moieties seems to be critical for the interaction with hepatocytes through ASGPr. Galactosylated liposomes smaller than 70 nm are taken up by hepatocytes, larger ones do accumulate in KCs (Rensen et al., 2001). In the optimal interaction with ASGPr, parameters like the clustering of galactose moieties (tetraantennary or monoantennary) and an appropriate spacing of the sugar residues play a role as well (Sliedregt et al., 1999).

Recently, targeting of liposomes to hepatocytes was demonstrated using a peptide sequence originating from a surface protein of *Plasmodium*, a protozoan causing infections in humans (Longmuir et al., 2006). The 19-amino acid peptide from the circumsporozoite protein contained a heparan sulphate proteoglycan binding sequence which is recognised by the highly sulphated heparan sulphate proteoglycans located on the basolateral side of hepatocytes. Systemically injected liposomes modified with this peptide mainly accumulated in hepatocytes.

2.6.7.2 Liposomes and Kupffer Cells

KCs are specialised cells that clear the blood from foreign particles, microorganisms, and senescent blood cells. Also, most of the liposomal preparations injected intravenously are readily taken up by these cells. As a result, researchers tend to make an effort to develop strategies which allow liposomes to escape from Kupffer cell accumulation, rather than actively target liposomes to these cells. Reduction of liposome sizes from 800 nm to around 100 nm decreases Kupffer cell uptake but it does not eliminate accumulation in these cells. The mechanism underlying the fast blood elimination of liposomes by KCs is called opsonization. Once liposomes enter the blood circulation, they absorb a broad spectrum of plasma proteins. The amount and type of adhered proteins is determined by the physicochemical properties of the liposomes, including the size, lipid composition and surface charge. The adsorbed

plasma proteins that mediate the specific interaction of liposomes with receptors on the macrophage are called opsonins. In principle, opsonins adsorbed on the surface of liposomes mark them for fast recognition and enhanced uptake by KCs. Liposomal opsonins are classified in two groups: immune opsonins and non-immune opsonins (Yan et al., 2005(b)). The immune opsonins mainly include complement proteins and immunoglobulins (antibodies), which identify liposomes as foreign particles and mark them for uptake by the MPS. The second class of opsonins are proteins such as fibronectin, α 2-macroglobulin and apolipoproteins which are ligands that direct liposomes to specific receptors on the macrophage cell membrane.

In order to prevent rapid blood elimination and accumulation in KCs, liposomes can be surface-grafted with a hydrophilic polymer, polyethylene glycol (PEG). The flexibility of PEG allows a relatively small number of surface-grafted polymer molecules to create a protective layer. Thus PEGylated liposomes are characterised by a significantly extended circulation time. This property is attributed to the decreased adsorption of opsonins from the blood on the liposomal surface, due to the highly flexible hydrophilic steric barrier provided by the polymer brushes. The development of long-circulating liposomes in the early 1990's was considered a breakthrough in the liposomal field, and resulted, among others, in a liposomal formulation of doxorubicin approved for regular clinical use (Doxil/Cealyx) (Allen and Cullis, 2004).

2.6.7.3 Targeting Liposomes to Liver Endothelial Cells

Although LEC have direct contact with blood, significant accumulation of conventional liposomes in these cells does not occur (Spanjer et al., 1986). Interesting results were observed when the uptake of negatively charged liposomes containing PS in vivo was compared with that in primary cultures of LEC. The contribution of LEC in the uptake of PS-containing liposomes after intravenous injection was minimal, while accumulation of these liposomes by cultured LEC was almost equal to that of KCs (Kamps et al., 1999). These in vitro observations were confirmed when uptake of PS-containing liposomes was studied in the serum-free perfused rat liver (Rothkopf et al., 2005). Polyinosinic acid, a competitive inhibitor of ScR reduced the association of PS containing liposomes with cultured LEC, as well as the uptake in the serum-free perfused livers, suggesting involvement of ScR in this process. These findings demonstrated that LEC have a high capacity to take up liposomes. However,

accumulation of PS-containing liposomes by LEC *in vivo* might be inhibited by “dysopsonins”, that mask the PS for receptor recognition.

LEC are known to abundantly express different classes of scavenger receptors (ScR) including class A I and II, class B ScR-B I and CD 36, all known to recognise anionic domains. As a matter of fact, massive targeting of liposomes to LEC *in vivo* was achieved by coupling a poly-anionic molecule, aconitylated human serum albumin (AcoHSA), to the liposomal surface (Kamps et al., 1997). Inhibition of the *in vivo* uptake of AcoHSA by polyinosinic acid also indicated that this association is specifically mediated by ScR. Application of AcoHSA as a targeting ligand to LEC was successfully applied in the preparation of stabilised lipid coated lipoplexes, that were shown to efficiently deliver functionally active antisense oligonucleotides to LEC *in vivo* (Bartsch et al., 2004).

Injured hepatocytes, activated KCs and endothelial cells release broad spectrum of cytokines and other substances such as ROS which induce inflammation and oxidative stress as well as activate HSC in the fibrotic liver. These processes perpetuate development of fibrosis and contribute to the liver failure. Liposomal drugs selectively targeted to hepatocytes, KCs and endothelial cells may be used for specific inhibition of proinflammatory actions in these cells simultaneously with antifibrotic compounds directed to HSC.

2.7 FORMULATION OPTIMIZATION

An experimental approach to Design of Experiment (DoE) optimization of drug delivery systems (DDS) comprises several phases. (Kannan et al., 2003(a); Singh et al., 2004(b); Doornbos and de Haan, 1995; Myers et al., 2003(b)). Broadly, these phases can be sequentially summed up in seven salient steps. Figure 2.7 delineates these steps pictographically.

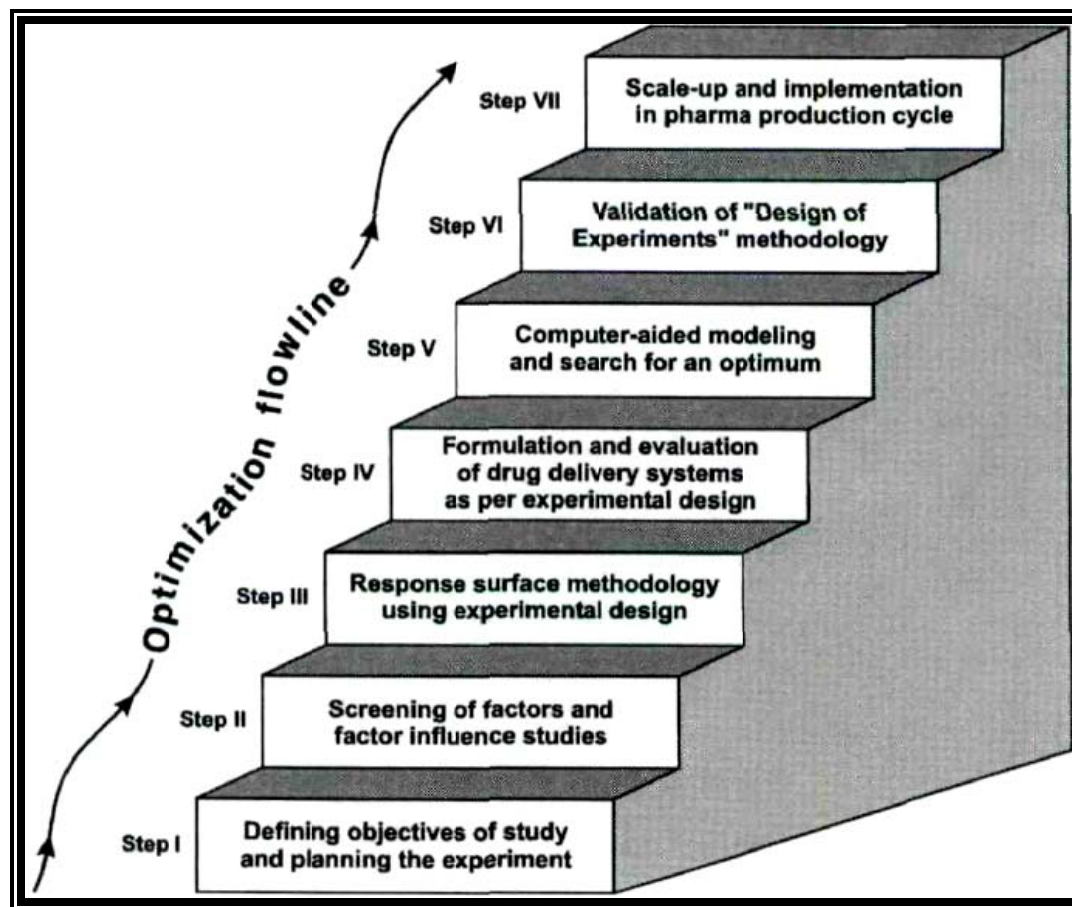


Figure 2.7 Seven-step ladder for optimizing drug delivery systems

The optimization study begins with:

- **Step I**, where an endeavor is made to ascertain the initial drug delivery objective(s) in an explicit manner. Various main response parameters, which closely and pragmatically epitomize the objective(s), are chosen for the purpose.
- In **Step II**, the experimenter has several potential independent product and/or process variables to choose from. By executing a set of suitable screening techniques and designs, the formulator selects the “vital few” influential factors among the possible “so many” input variables. Following selection of these factors, a factor influence study is carried out to quantitatively estimate the main effects and interactions. Before going to the more detailed study, experimental studies are undertaken to define the broad range of factor levels as well.

- During **Step III**, an opposite experimental design is worked out on the basis of the study objective(s), and the number and the type of factors, factor levels, and responses being explored. Working details on variegated vistas of the experimental designs, customarily required to implement DoE optimization of drug delivery, have been elucidated in the subsequent section. Afterwards, response surface modeling (RSM) is characteristically employed to relate a response variable to the levels of input variables, and a design matrix is generated to guide the drug delivery scientist to choose optimal formulations.
- In **Step IV**, the drug delivery formulations are experimentally prepared according to the approved experimental design, and the chosen responses are evaluated.
- Later in **Step V**, a suitable mathematical model for the objective(s) under exploration is proposed, the experimental data thus obtained are analyzed accordingly, and the statistical significance of the proposed model discerned. Optimal formulation compositions are searched within the experimental domain, employing graphical or numerical techniques. This entire exercise is invariably executed with the help of pertinent computer software.
- **Step VI** is the penultimate phase of the optimization exercise, involving validation of response prognostic ability of the model put forward. Drug delivery performance of some studies, taken as the checkpoints, is assessed vis-a-vis that predicted using RSM, and the results are critically compared.
- Finally, during **Step VII**, which is carried out in the industrial milieu, the process is scaled up and set forth ultimately for the production cycle.

The niceties of the significance and execution of each of these seven steps is discussed in greater detail below.

The foremost step while executing systematic DoE methodology is to understand the deliverables of the finished product. This step is not merely confined to understanding the process performance and the product composition, but it usually goes beyond to enfold the concepts of economics, quality control, packaging, market research, etc.

The term objective (also called criterion) has been used to indicate either the goal of an optimization experiment or the property of interest (Schwartz and Connor, 1996; Doornbos and de Haan, 1995). The objectives for an experiment should be clearly

determined after discussion among the project team members having sound expertise and empiricism on product development, optimization, production, and/or quality control. The group of scientists contemplates the key objectives and identifies the trivial ones. Prioritizing the objectives helps in determining the direction to proceed with regard to the selection of the factors, the responses, and the particular design (Kannan et al., 2003(a); Myers et al., 2003(b); Kannan et al., 2003(b)). This step can be very time consuming and may not furnish rapid results. However, unless the objectives are accurately defined, it may be necessary to repeat the entire work that is to follow. The response variables, selected with dexterity, should be such that they provide maximal information with the minimal experimental effort and time. Such response variables are usually the performance objectives, such as the extent and rate of drug release, or are occasionally related to the visual aesthetics, such as chipping, grittiness, or mottling (Singh et al., 2004(b)).

The word 'optimize' simply means to make as perfect, effective, or functional as possible (Lewis et al., 2002; Schwartz and Connor, 1996). The term optimized has been used in the past to suggest that a product has been improved to accomplish the objectives of a development scientist. However, today the term implies that DoE and computers have been used to achieve the objective(s). With respect to drug formulations or pharmaceutical processes, optimization is a phenomenon of finding the best possible composition or operating conditions (Lewis et al., 2002; Lewis et al., 1999). Accordingly, optimization has been defined as the implementation of systematic approaches to achieve the best combination of product and/or process characteristics under a given set of conditions (Singh and Ahuja, 2004(a)).

2.7.1 Variables

Design and development of any drug formulation or pharmaceutical process invariably involves several variables (Lewis et al., 2002; Schwartz et al., 1973; Stetsko, 1986). The input variables, which are directly under the control of the product development scientist, are known as independent variables - e.g., drug content, polymer composition, compression force, percentage of penetration enhancer, hydration volume, agitation speed. Such variables can either be quantitative or qualitative (Doornbos and de Haan, 1995; Bolton, 1997(a)). Quantitative variables are those that can take numeric values (e.g., time, temperature, amount of polymer,

osmogent, plasticizer, super disintegrants) and are continuous. Instances of qualitative variables, on the other hand, include the type of polymer, lipid, excipient, or tableting machine. These are also known as categorical variables (Lewis et al., 1999; Anderson et al., 2002). Their influence can be evaluated by assigning discrete dummy values to them. The independent variables, which influence the formulation characteristics or output of the process, are labeled factors (Lewis et al., 1999; Cochran and Cox, 1992; Bolton, 1997(a)). The values assigned to the factors are termed levels - e.g., 100 mg and 200 mg are the levels for the factor, release rate controlling polymer in the compressed matrices. Restrictions imposed on the factor levels are known as constraints (Schwartz and Connor, 1996; Bolton, 1997(a)).

The characteristics of the finished drug product or the in-process material are known as dependent variables - e.g., drug release profile, percent drug entrapment, pellet size distribution, moisture uptake (Lewis et al., 1999; Doornbos and de Haan, 1995; Box et al., 1960). Popularly termed response variables, these are the measured properties of the system to estimate the outcome of the experiment. Usually, these are direct function(s) of any change(s) in the independent variables.

Accordingly, a drug formulation (product), with respect to optimization techniques, can be considered as a system whose output (Y) is influenced by a set of input variables via a transfer function (T) (Montgomery, 2001). These input variables may either be controllable (X; signal factors) or uncontrollable (U; noise factors) (Doornbos and de Haan, 1995; Taguchi, 1987). Figure 2.8 depicts the same graphically.

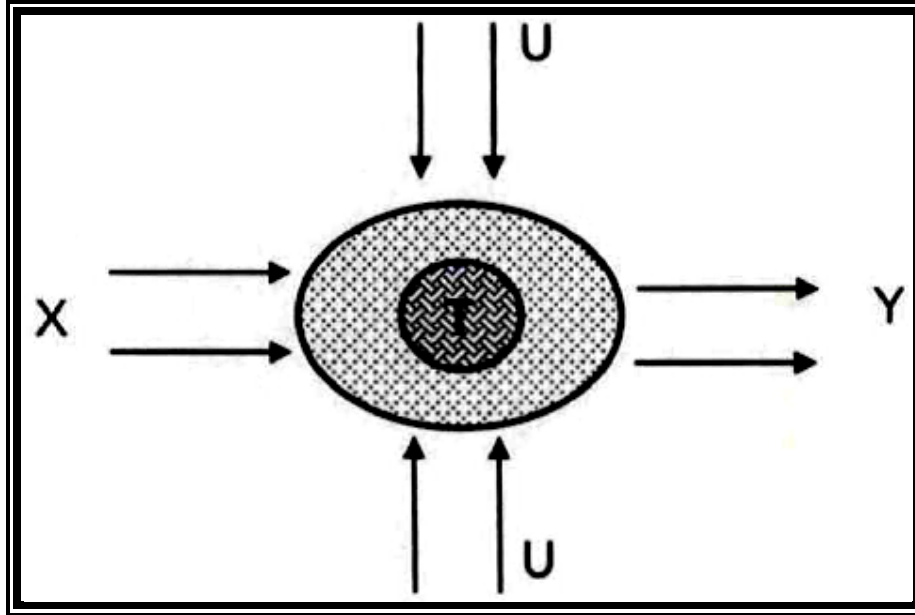


Figure 2.8 System with controllable input variables (X), uncontrollable input variables (U), transfer function (T), and output variables (Y)

The nomenclature of T depends upon the predictability of the output as an effect of the change of input variables. If the output is totally unpredictable from the previous studies, T is termed the black box. The term white box is used for a system with absolutely true predictability, while the term gray box is used for moderate predictability. Using optimization methods, the attempt of the formulator is to attain a white box or nearly white box status from the erstwhile black or gray box status observed in the traditional studies (Singh and Ahuja, 2004(a)). The greater the number of variables in a given system, the more complicated becomes the job of DoE optimization. Nevertheless, regardless of the number of variables, a distinct relationship exists between a given response and the factors studied (Lewis et al., 1999).

2.7.2 Effect, Interaction, and Confounding

The magnitude of the change in response caused by varying the factor level(s) is termed as an effect (Cochran and Cox, 1992; Bolton, 1997(a)). The main effect is the effect of a factor averaged over all the levels of other factors.

However, an interaction is said to occur when there is "lack of additivity of factor effects." This implies that the effect is not directly proportional to the change in the

factor levels (Bolton, 1997(a)). In other words, the influence of a factor on the response is nonlinear (Lewis et al., 2002; Lewis et al., 1999; Montgomery, 2001; Stack, 2003). In addition, an interaction may be said to take place when the effect of two or more factors are dependent on each other - e.g., the effect of factor A changes on changing factor B by one unit. The measured property' of the interacting variables depends not only on their fundamental levels, but also on the degree of interaction between them. Depending upon whether the change in the response is desired (positive) or undesired (negative), the phenomenon of interaction may be described as synergism or antagonism, respectively (Lewis et al., 1999; Bolton, 1997(a)). Figure 2.9 illustrates the concept of interaction graphically.

Effects plot is plotted between the magnitude of various coefficients for the effects and/or interactions against the response variable (Lewis et al., 1999). The plot is drawn during the initial stages of DoE to determine the influence of each term.

The term orthogonality is used if the estimated effects are due to the main factor of interest and are independent of interactions (Kettaneh-Wold, 1991; Bolton, 1997(a); Myers and Montgomery, 1995; Box and Draper, 1987). Conversely, lack of orthogonality (or independence) is termed confounding or aliasing (Bolton, 1997(a); Stack, 2003). When an effect is confounded (or aliased, or mixed up, or equalled), one cannot assess how much of the observed effect is due to the factor under consideration. The effect is influenced by other factors in a manner that cannot easily be explored. The measure of the degree of confounding is known as resolution (Montgomery, 2001; Myers and Montgomery, 1995). At times, there is confusion between confounding and interaction. Confounding, in fact, is a bias that must be controlled by suitable selection of the design and data analysis. Interaction, on the other hand, is an inherent quality of the data, which must be explored. Confounding must be assessed qualitatively, while interaction may be tested more quantitatively (Stack, 2003).

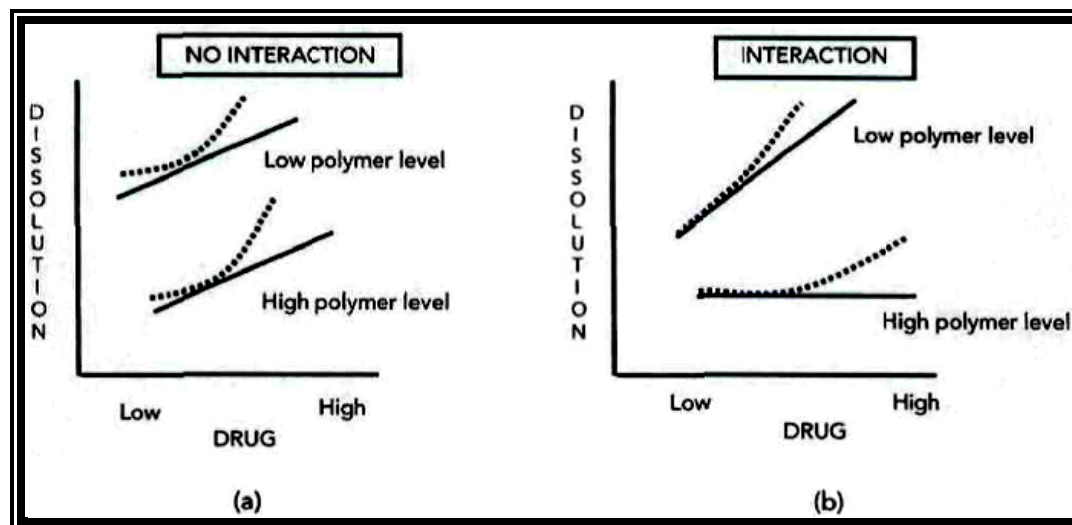


Figure 2.9 Diagrammatic depiction of interaction. Unparallel lines in (b) describe the phenomenon of interaction between the levels of drug and polymer amount affecting drug dissolution [(—); Linear response-factor relationship; (.....): nonlinear response-factor relationship]

Subsequent to ascertaining the study objectives and responses, "several possible" factors are envisioned and screening of a "few important" ones is done. The influence of the important factors - i.e., the main effects and the possible interactions are also studied. Collectively, screening and factor influence studies are also known as factor studies (Lewis et al., 2002). Often carried out as a prelude to finding the optimum, these are sequential stages in the development process. Screening methods are used to identify important and critical effects (Lewis et al., 1999; Myers et al., 2003(b)). Factor studies aim at quantitative determination of the effects as a result of a change in the potentially critical formulation or process parameter(s). Such factor studies usually involve statistical experimental designs, and the results so obtained provide useful leads for further response optimization studies. 1. Screening of Influential Factors

As the term suggests, screening is analogous to separating "rice" from "rice husk," where rice is a group of factors with significant influence on response, and husk is a group of the rest of the noninfluential factors (Singh et al., 2004(b)). A product development scientist normally has numerous possible input variables to be investigated for their impact on the response variables. During the initial stages of optimization, such input variables are explored for their influence on the outcome of

the finished product to see if they are factors (Lewis et al., 2002; Lewis et al., 1999; Murphy, 2003). The process, called screening of influential variables, is a paramount step. An input variable, identified as a factor, increases the chance of success, while an input variable that is not a factor has no consequence (Doornbos and de Haan, 1995). Furthermore, an input variable falsely identified as a factor unduly increases the effort and cost, while an unrecognized factor leads to an erroneous picture, and a true optimum may be missed.

Principally, screening embarks upon the phenomenon of sparsity effect - i.e., only a few of the factors among the numerous envisioned ones truly explain a larger proportion of the experimental variation (Montgomery, 2001; Anonymous, 2002). The factors responsible for the variability are the active or influential variables, while others are termed inactive or less influential variables. The entire exercise aims solely at selecting the active factors and excluding the redundant variables, but not at obtaining complete and exact numerical data on the system properties. Such a reduction in the number of factors becomes necessary before the pharmaceutical scientist invests the human, financial, and industrial resources in more elaborate studies (Lewis et al., 2002; Myers et al., 2003(b)). This phase may be omitted if the process is known well enough from the analogous studies. Even after elimination of the non influential variables, the number of factors may, at times, still be too large to optimize in terms of available resources of time, money, manpower, equipment, etc (Lewis et al., 2002). In such cases, more influential variables are optimized, keeping less influential ones as constant at their best levels. The number of experiments is kept as small as possible to limit the volume of work carried out during the initial stages.

2.7.2.1 Screening Designs

The experimental designs employed for this purpose are commonly termed screening designs (Myers et al., 2003(b); Murphy, 2003). Screening presumes considerable approximation of the additivity of the different factors and the absence of interaction. Therefore, the primary purpose of the screening design is to identify significant main effects, rather than interaction effects. Thus, these are usually first-order designs with low resolution (Armstrong and James, 1990). These designs are also sometimes termed main effects designs or orthogonal main effect plans or simply orthogonal arrays (Lewis et al., 1999). The number of experiments in the screening process is

kept small, but it must at least be equal to the number of independent coefficients (P) required to be calculated, as in following equation:

$$P = 1 + \sum_{i=1}^k (S_i - 1)$$

where S_i is the number of levels of the i^{th} factor, when there are k factors in all (Lewis et al., 1999). The estimators of the coefficients should be orthogonal and be estimated with minimum possible error. In general, in order to determine main effects independently, the number of runs should be four times the number of factors to be estimated. The experimental designs are said to be saturated if the number of runs equals the number of model terms to be estimated (Anonymous, 2002). In cases where a larger number of factors need to be screened, the number of runs becomes exorbitantly high. In such circumstances, supersaturated designs, which possess fewer runs than factors, are used. Supersaturated designs can be attractive for factor screening, especially when there are many factors and/or the experimental runs are expensive. A supersaturated design can examine dozens of factors using fewer than half the number of runs. This is usually at the expense of the precision and accuracy of the information. The mathematical models normally considered for screening include the linear and interaction models already described by Eqs. (1) and (2). (Lewis et al., 2002; Myers et al., 2003(b); Murphy, 2003). A two-level screening design can be augmented to a high-level design by adding axial points along with center points.

2.7.2.2 Factor Influence Study

Having screened the influential variables, a more comprehensive study is subsequently undertaken, with the main aim to quantify the effect of factors and to determine the interactions, if any (Lewis et al., 2002; Lewis et al., 1999; Myers and Montgomery, 1995). Herein, the studied experimental domain is less extensive, as many fewer active factors are studied. The models used for this study are neither predictive nor capable of generating a response surface. The number of levels is usually limited to two (i.e, the factors are investigated at the extreme values). However, sufficient experimentation is carried out to allow for the detection of interactions among factors (Lewis et al., 1999; Box et al., 1978). The experimental designs used are generally of the same kind as used for screening. The experiments

conducted at this step may often be "reused" during the optimization or response modeling phase by augmenting the experimental designs with additional design points at the center or the axes. Central points (i.e., at the intermediate level), if added at this stage, are not included in the calculation of model equations (Lewis et al., 2002). Nevertheless, they may prove to be useful in identifying the curvature in the response, in allowing the reuse of the experiments at various stages, and if replicated, in validating the reproducibility of the experimental study.

2.7.3 Coding

The process of transforming a natural variable into a nondimensional coded variable, X_i , so that the central value of experimental domain is zero is known as coding (or normalization) (Cochran and Cox, 1992; Bolton, 1997(a); Das and Giri, 1994).

Generally, the various levels of a factor are designated as -1, 0, and +1, representing the lowest, intermediate (central), and highest factor levels investigated, respectively (Lewis et al., 1999; Bolton, 1997(a)). For instance, if sodium carboxymethyl cellulose, a hydrophilic polymer, is studied as a factor in the range of 120-240 mg, then codes -1 and +1 signify 120 mg and 240 mg amounts, respectively. The code 0 would represent the central point at the arithmetic mean of the two extremes - i.e., 180 mg. Alternatively, for convenience, the factors and their levels have been denoted by alphabetic notation (symbol) to express various combinations investigated in the study. For example, a factor is denoted by a capital alphabet letter (say factor A), the high level by a, and low level as (-1). Table 2.6 illustrates the alphabetic denotations used in pharmaceutical literature for coding factors and their factor combinations at the respective levels.

Although the terminology for factors as A and B and their levels as (1), a, b, etc. is comprehensive in the text format, their translation into mathematical equation(s) is neither practical nor easy to comprehend (Singh and Ahuja, 2004(a)). Therefore, the symbol X_k is normally used for representing the factor X, where the subscript k depicts the number of factors (Doornbos and de Haan, 1995). Analogously, the subscripted p values are employed to denote the coefficient values in the mathematical equations.

Coding involves the orthogonality of effects and depicts effects and interaction(s) using (+) or (-) signs (Schwartz and Connor, 1996; Bolton, 1997(a)). It assigns equal

significance to each axis and allows not only easier calculation of coefficients and coefficient variances, but easier depiction of response surfaces as well.

Table 2.6 Denotation of various levels of two factors

Factor	Level notation	
	Low level	High level
A	-1	a
B	-1	b
AB	-1	ab

To circumvent any anomaly in factor sensitivity with change in levels, it is recommended that the factor coding must be carried out judiciously (Doornbos and de Haan, 1995; Bolton, 1997(a)). For instance, in the case of microsphere production, if one factor is stirring speed (say, within the range of 1500-3000 rpm) and the other is pH (say within the range of 1-5), a change of 1 pH unit is far more significant than a change of 1 rpm.

2.7.4 Experimental Domain

The dimensional space defined by the coded variables is known as factor space (Lewis et al., 1999; Armstrong and James, 1990). Figure 2.10 illustrates the factor space for two factors on a bi-dimensional (2-D) plane during the formulation of controlled release microspheres. The part of the factor space, investigated experimentally for optimization, is the experimental domain (Lewis et al., 1999; Das and Giri, 1994). Also known as the region of interest, it is enclosed by the upper and lower levels of the variables, the factor space covers the entire figure area and extends even beyond it, whereas the design space of the experimental domain is the square enclosed by $X_1 = \pm 1$, $X_2 = \pm 1$.

2.7.5 Experimental Design

The conduct of an experiment and the subsequent interpretation of its experimental outcome are the twin essential features of the general scientific methodology (Lewis et al., 2002; Armstrong and James, 1990). This can be accomplished only if the experiments are carried out in a systematic way and the inferences are drawn accordingly.

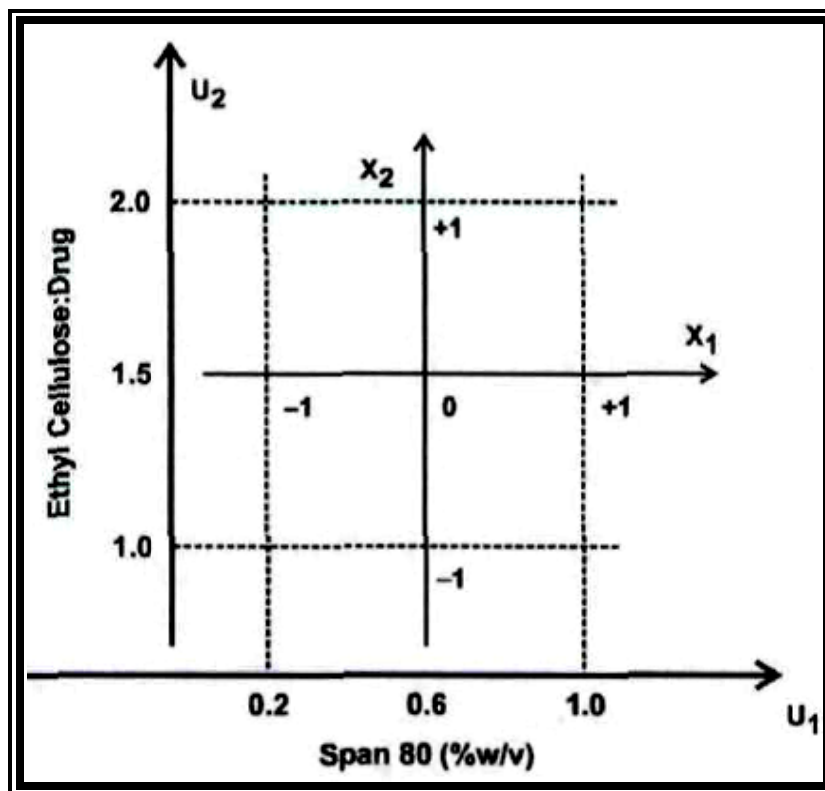


Figure 2.10 Quantitative factors and factor space (The axes for the natural variables, ethyl cellulose:drug ratio and Span 80 are labeled U_1 and U_2 and those of the corresponding coded variables X_1 and X_2)

An experimental design is the statistical strategy for organizing the experiments in such a manner that the required information is obtained as efficiently and precisely as possible (Haaland, 1989; Kettaneh-Wold, 1991; Cochran and Cox, 1992; Wehrle and Stamm, 1994). Runs or trials are the experiments conducted according to the selected experimental design (Lewis et al., 1999; Doornbos and de Haan, 1995). Such DoE trials are arranged in the design space so that the reliable and consistent information is attainable with minimum experimentation. The layout of the experimental runs in a matrix form, according to the experimental design, is known as the design matrix (Lewis et al., 1999). The choice of design depends upon the proposed model, the shape of the domain, and the objective of the study. Primarily, the experimental (or statistical) designs are based on the principles of randomization (i.e., the manner of allocations of treatments to the experimental units), replication (i.e., the number of units employed for each treatment), and error control or local control (i.e., the

grouping of specific types of experiments to increase the precision) (Montgomery, 2001; Cochran and Cox, 1992; Das and Giri, 1994).

DoE is an efficient procedure for planning experiments in such a way that the data obtained can be analyzed to yield valid and unbiased conclusions (Tye, 2004; Porter et al., 1997). An experimental design is a strategy for laying out a detailed experimental plan in advance to the conduct of the experimental studies (Araujo and Brereton, 1996; Armstrong and James, 1990; Haaland, 1989). Before the selection of experimental design, it is essential to demarcate the experimental domain within the factor space - i.e, the broad range of factor studies. To accomplish this task, first a pragmatic range of experimental domain is embarked upon and the levels and their number are selected so that the optimum lies within its realm (Singh and Ahuja, 2004(a)). While selecting the levels, one must see that the increments between them should be realistic. Too wide increments may miss finding the useful information between the levels, while a too narrow range may not yield accurate results (Singh et al., 2004(b)).

There are numerous types of experimental designs. Various commonly employed experimental designs for RSM, screening, and factor-influence studies in pharmaceutical product development are

- a) Factorial designs
- b) Fractional factorial designs
- c) Plackett-Burman designs
- d) Star designs
- e) Central composite designs
- f) Box-Behnken designs
- g) Center of gravity designs
- h) Equiradial designs
- i) Mixture designs
- j) Taguchi designs
- k) Optimal designs
- l) Rechtschaffner designs
- m) Cotter designs

For a three-factor study, an experimental design can invariably be envisaged as a "cube," with the possible combinations of the factor levels (low or high) represented at its respective corners (Tye, 2004). The cube thus can be the most appropriate representation of the experimental region being explored. Most design types discussed in the current article are, therefore, being depicted pictorially using this cubic model, with experimental points at the corners, centers of faces, centers of edges, and so forth. Such depiction facilitates easier comprehension of various designs and comparisons among them. For designs in which more than three factors are adjusted, the same concept is applicable except that a hypercube represents the experimental region. Such cubic designs are popular because they are symmetrical and straightforward for conceptualizing and envisioning the model.

2.7.5.1 Factorial Designs

Factorial designs (FDs) are very frequently used response surface designs (Araujo and Brereton, 1996; Bolton, 1997(a); Li et al., 2003(a)). A factorial experiment is one in which all levels of a given factor are combined with all levels of every other factor in the experiment (Lewis et al., 1999; Bolton, 1997(a); Acikgoz et al., 1996). These are generally based upon first-degree mathematical models. Full FDs involve studying the effect of all the factors (k) at various levels (x), including the interactions among them, with the total number of experiments being xr . FDs can be investigated at either two levels (2^k FD) or more than two levels. If the number of levels is the same for each factor in the optimization study, the FDs are said to be symmetric, whereas in cases of a different number of levels for different factors, FDs are termed asymmetric (Lewis et al., 1999).

2.7.5.2 2^k Factorial Designs

The two-level FDs are the simplest form of orthogonal design, commonly employed for screening and factor influence studies (Bolton, 1997(a); Das and Giri, 1994). They involve the study of k factors at two levels only - i.e., at high (+) and low (-) levels. The simplest FD involves investigation of two factors at two levels only. Characteristically, these represent first-order models with linear response, as demonstrated in Figure 11 portrays a 2^2 and 2^3 FD, in which each point represents an individual experiment.

The design matrix for a two-level full factorial with k factors in the standard order can be generated in the following manner. The first column (X_1) starts with -1 followed by alternate sign for all 2^k runs. The second column (X_2) starts with -1 repeated twice, then alternates with 2 in a row of the opposite sign until all 2^k places are filled. The third column (X_3) starts with -1 repeated four times, then four repeats of +1, and so on. In general, the i^{th} column (X_i) starts with 2^{i-1} repeats of -1 followed by 2^{i-1} repeats of +1.

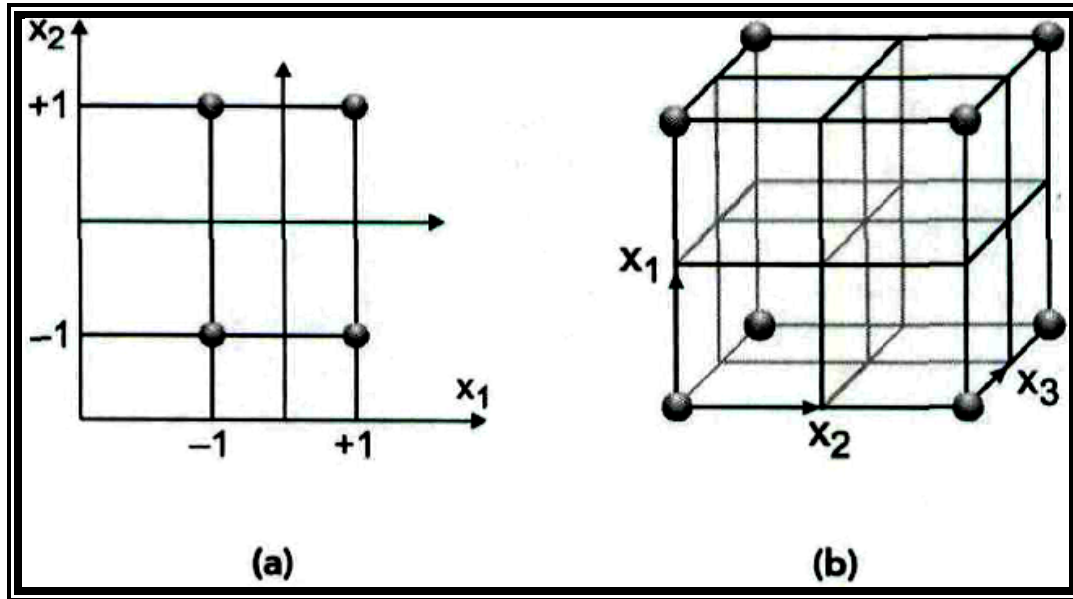


Figure 2.11 Diagrammatic representation of (a) 2^2 factorial design; (b) 2^3 factorial design

The mathematical model associated with the design consists of the main effects of each variable plus all the possible interaction effects - i.e., interactions between the two variables, and in fact, between as many factors as there are in the model (Lewis et al., 2002; Lewis et al., 1999; Box and Draper, 1987). Below equation is the general mathematical relationship for the FDs involving main effect and interaction terms.

$$Y = \beta_0 + \sum_{i=1}^n \beta_i X_i + \sum_{i=1}^n \sum_{j=i+1}^n \beta_{ij} X_i X_j + \sum_{i=1}^n \sum_{j=i+1}^n \sum_{k=i+2}^n \beta_{ijk} X_i X_j X_k$$

where n is the number of factors (3 in the above equation), X is +1 or -1 as per coding, Y is the measured response, and β_i , β_{ij} , β_{ijk} represent the coefficients

computed from the responses of the formulation in the design. For a 2^3 FD, the above equation can be written as:

$$Y = \beta_0 + \beta_1 X_1 + \beta_2 X_2 + \beta_3 X_3 + \beta_{12} X_1 X_2 + \beta_{13} X_1 X_3 + \beta_{23} X_2 X_3 + \beta_{123} X_1 X_2 X_3$$

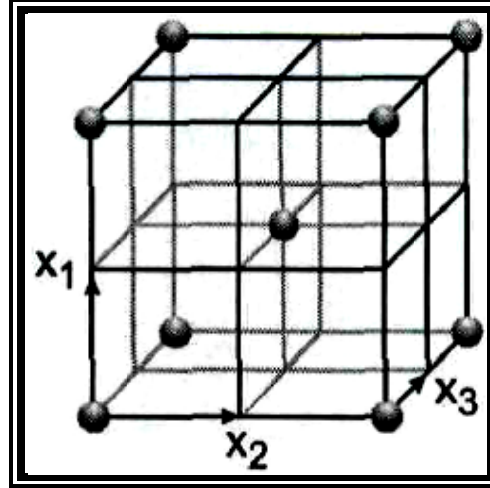


Figure 2.12 Diagrammatic representation of 2^3 factorial design with added center point

Center points can be added to 2^k FDs to allow identification of the curvature in the response and, upon replication, validate the reproducibility of the experimental study (Li et al., 2003(a)). Figure 2.12 shows the cubic model for 2^3 FD with an added center point.

2.7.5.3 Higher Level Factorial Designs

FDs at three or more number of levels are employed mainly for response surface optimization (Doornbos and de Haan, 1995; Myers and Montgomery, 1995; Li et al., 2003(a)). Simple to generate, these designs can detect and estimate nonlinear or quadratic effects. The main strength of the design is orthogonality, because it allows independent estimation of the main effects and interactions (Bolton, 1997(a); Li et al., 2003(a)). On the other hand, the major limitation associated with high-level FDs is the increased number of experiments required with the increase in the number of factors (k). Even at a modest number of factors, the number of runs is quite large. For instance, the absolute minimum number of runs required to estimate all the terms present in a four-factor, three-level quadratic model is 15, involving the intercept term, four main effects, six two-factor interactions, and four quadratic terms. The

corresponding 3^k FD for $k = 4$ requires 81 runs. Another disadvantage of x^k FDs is the lack of rotatability (Montgomery, 2001).

For deriving maximal benefits from DoE, an experimenter has invariably to know, comprehend and apply some or all of the following aspects.

2.7.5.4 Blocking in Experimental Designs

Often the estimation of "effects" and "interaction" becomes complicated as a result of variability in the results caused by some uncontrollable factors, commonly termed nuisance factors or extraneous factors (Montgomery, 2001). Although these nuisance factors are the factors that may affect the measured result, they are not of primary interest. In such situations, blocks are generated in the experimental domain. Each block is a set of relatively homogenous experimental conditions, wherein every level of the primary factor occurs the same number of times with each level of nuisance factor (Montgomery, 2001; Box and Draper, 1987). These uncontrollable factors, therefore, are usually taken as the blocking factors. This technique of blocking is used to reduce or eliminate the variability transmitted by the nuisance factors. Accordingly, the analysis of the experiment focuses on the effect of varying levels of the primary factor "within each block" of the experiment. Runs are distributed over blocks in such a way that any difference between the blocks does not bias the results for the factors of interest. This is accomplished by treating the blocking factor as another factor in the design. The inclusion of blocking factors as additional factors in the design results in loss of estimation of some interaction terms, eventually lowering the resolution of the design. Nonetheless, the technique of blocking makes the design statistically more powerful. It allows simultaneous estimation and control of variability stemming from the difference(s) between the blocks during optimization of a process or formulation. Blocking considerably improves the precision with which comparisons are made among the factors of interest.

2.7.5.5 Resolution of Experimental Designs

One of the important features of the experimental designs is their resolution - i.e., the ability to describe the degree to which the estimated main effects are aliased (or confounded) with the estimated two-, three-, or higher level interactions (Lewis et al., 1999; Montgomery, 2001; Singh et al., 2004(b); Myers and Montgomery, 1995). In general, the resolution of a design is one more than the smallest order interaction that

some main effect is confounded with (Anderson et al., 2002). For instance, if some main effects are confounded with some two-level interactions, then the resolution is III. The most prevalent design resolutions in the pharmaceutical arena are III, IV, and V (Lewis et al., 1999). These designs imply that

- a) **Resolution III Designs:** In such designs, the main effects are confounded (aliased) with two-factor interactions.
- b) **Resolution IV Designs:** No main effects are aliased with two-factor interactions, but two-factor interactions are aliased with each other.
- c) **Resolution V Designs:** No main effect or two-factor interaction is aliased with any other main effect or two-factor interaction, but two-factor interactions are aliased with three-factor interactions.

The orthogonal designs, where the estimation of main effects and interactions are independent of each other, are said to possess “infinite resolution.” For most practical purposes, when the number of factors is quite large in pharmaceutical product development, a resolution IV design may be adequate, while a resolution V design is an excellent choice. Resolution III designs, on the other hand, are also useful in conditions where the number of factors is large and interactions among them are assumed to be negligible.

The resolution of experimental designs can be improved upon by the fold over technique (Montgomery, 2001; Box and Draper, 1987; Loukas, 1997). The procedure involves the generation or addition of a second block of experiments, in which the levels of each factor are reversed from the original block. For a resolution III design, this will improve the alias structure for all the factors. Fold over designs can either be mirror-image fold over designs (resulting in complete dealiasing of main effects and all interactions) or alternative fold over designs (involving break-up of specific alias patterns).

2.7.5.6 Design Augmentation

In the whole DoE endeavor, a situation sometimes arrives in which a study, conducted at some stage, is found to be inadequate and needs to be investigated further, or when the study carried out during the initial stages needs to be “reused” (Singh et al., 2004(b)). In either situation, more design points can be added systematically to the erstwhile design. Thus, the erstwhile primitive design can be enhanced to a more

advanced design furnishing more information, better reliability', and higher resolution. This process of extension of a statistical design, by adding some more rational design points, is known as design augmentation (Anderson et al., 2002). For instance, a design involving study at two levels can be augmented to a three-level design by adding some more design points. A design can be augmented in a number of ways, such as by replicating, adding center points to two-level designs, adding axial points (i.e., design points at various axes of the experimental domain), or by folding over.

2.7.6 Response Surfaces

During this crucial stage in DoE, one or more selected experimental responses are recorded for a set of experiments carried out in a systematic way to develop a mathematical model (Araujo and Brereton, 1996; Podczec, 1996; Haaland, 1989; Bolton, 1997(b); Das and Giri, 1994; Abu-Izza et al., 1996; Wehrle et al., 1993). These approaches comprise the postulation of an empirical mathematical model for each response, which adequately represents change in the response within the zone of interest. Rather than estimating the effects of each variable directly, response surface modeling (RSM) involves fitting the coefficients into the model equation of a particular response variable and mapping the response over the whole of the experimental domain in the form of a surface (Lewis et al., 1999; Singh and Ahuja, 2004(a); Doornbos, 1981; Box and Draper, 1987; Myers et al., 2003(b)).

Principally, RSM is a group of statistical techniques for empirical model building and model exploitation (Box and Draper, 1987; Myers et al., 2003(b)). By careful design and analysis of experiments, it seeks to relate a response to a number of predictors affecting it by generating a response surface, which is an area of space defined within upper and lower limits of the independent variables depicting the relationship of these variables to the measured response.

Experimental designs, which allow the estimation of main effects, interaction effects, and even quadratic effects, and, hence, provide an idea of the (local) shape of the response surface being investigated, are termed response surface designs (Lewis et al., 1999; Doornbos and de Haan, 1995; Myers and Montgomery, 1995; Wehrle et al., 1993). Under some circumstances, a model involving only main effects and interactions may be appropriate to describe a response surface. Such circumstances arise when analysis of the results reveals no evidence of "pure quadratic" curvature in

the response of interest - i.e., the response at the center approximately equals the average of the responses at the two extreme levels, +1 and -1.

In each part of Figure 2.13 (a, b, and c), the value of the response increases from the bottom of the figure to the top and those of the factor settings increase from left to right. If a response behaves as in Figure 2.13a, the design matrix to quantify that behavior needs only to contain factors with two levels - low and high. This model is a basic assumption of simple two-level screening or factor-influence designs. If a response behaves as in Figure 2.13b, the minimum number of levels required for a factor to quantify that behavior is three.

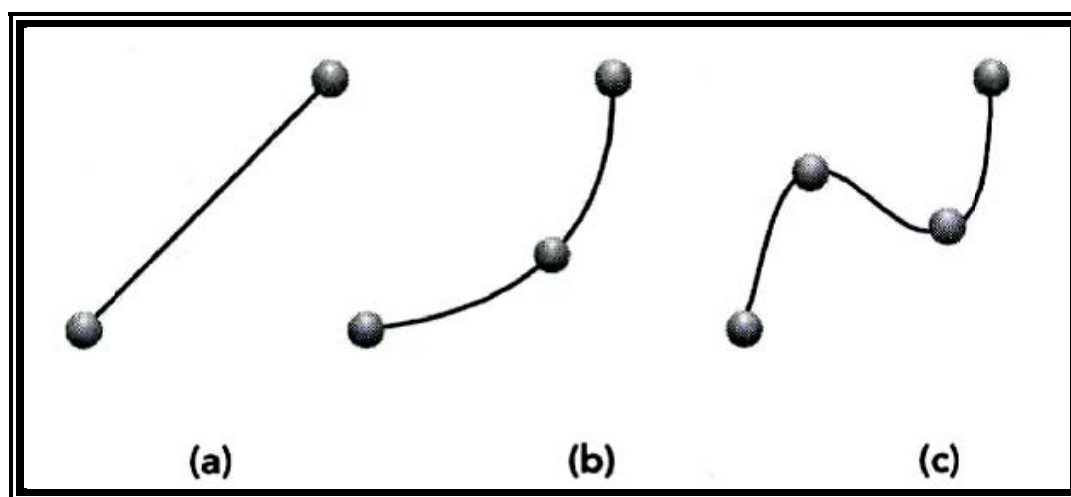


Figure 2.13 Different types of responses as functions of factor settings; (a) linear; (b) quadratic; (c) cubic

Addition of center points to a two-level design appears to be a logical step at this point, but the arrangement of the treatments in such a matrix may confound all the quadratic effects with each other (Myers and Montgomery, 1995; Box and Draper, 1987). A two-level design with center points can only detect the quadratic nature of the response, but not estimate the individual pure quadratic effects. Generally, the quadratic models are proposed for optimization of drug delivery devices (Lewis et al., 2002; Lewis et al., 1999; Armstrong and James, 1990). Therefore, response surface designs involving studies at three or more than three levels are employed for DoE optimization purposes. These response surface designs are used to find improved or optimal process settings, troubleshoot the process problems and weak points, and make a formulation or process more robust (i.e., less variable) against external and

non-controllable influences (Myers and Montgomery, 1995). Relatively more complicated cubic responses (Figure 2.13c) are quite infrequent in pharmaceutical practice (Lewis et al., 1999; Armstrong and James, 1990).

The prediction ability of response surface designs can be determined by prediction variance, which is a function of experimental variance (σ^2) and variance function (d) as described by equation (Lewis et al., 1999; Montgomery, 2001; Myers and Montgomery, 1995):

$$\text{var}(\hat{y}) = d \cdot \sigma^2$$

where $\text{var}(\hat{y})$ is the prediction variance. The variance function (d) further depends upon the levels of a factor and the experimental design. When the prediction variance of a response is constant in all the directions at a given distance from the center point of the domain, the design is termed rotatable (Montgomery, 2001; Araujo and Brereton, 1996). Ideally, all response surface designs should possess the characteristic of rotatability - i.e., the ability' of a design to be run in any direction without any change in response prediction variance.

Conduct of DoE trials, according to the chosen statistical design, yields a series of data on the response variables explored. Such data can be suitably modeled to generate mathematical relationships between the independent variables and the dependent variables. Graphical depiction of the mathematical relationship is known as a response surface (Singh and Ahuja, 2004(a); Myers and Montgomery, 1995; Wehrle and Stamm, 1994). A response surface plot is a 3-D graphical representation of a response plotted between two independent variables and one response variable. The use of 3-D response surface plots allows us to understand the behavior of the system by demonstrating the contribution of the independent variables.

The geometric illustration of a response obtained by plotting one independent variable against another, while holding the magnitude of response and other variables as constant, is known as a contour plot (Doornbos and de Haan, 1995). Such contour plots represent the 2-D slices of the corresponding 3-D response surfaces. The resulting curves are called contour lines. Figure 2.14 depicts a typical response surface and contour plot for a diffusional release exponent (Korsemeier et al., 1983) as the response variable, reported with mucoadhesive compressed matrices of atenolol (Singh et al., 2003). For complete response depiction among k independent variables,

a total of kC_2 number of response surfaces and contour plots may be required. In other words, 1, 3, 6, or 10 number of 3-D and 2-D plots are needed to provide depiction of each response for 2, 3, 4, or 5 number of variables, respectively (Singh et al., 2004(b)).

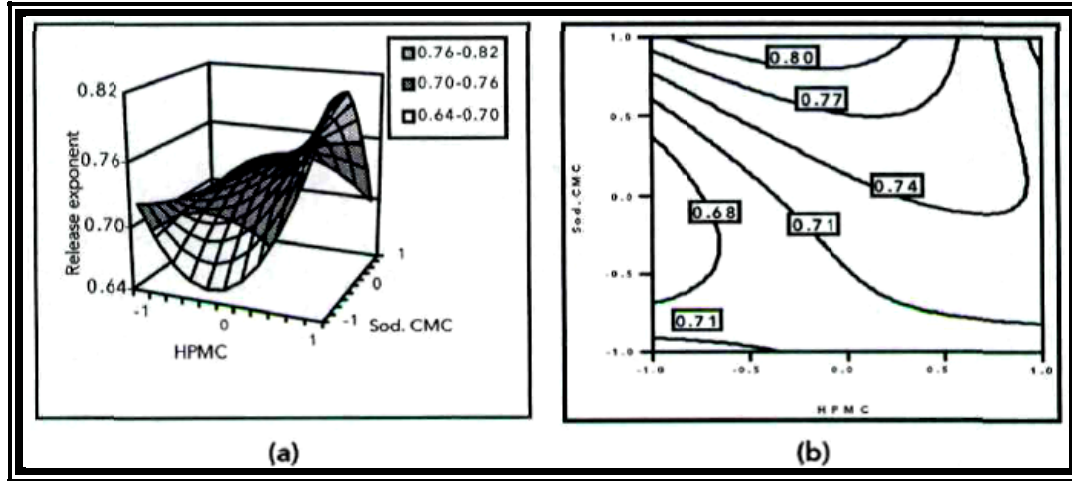


Figure 2.14 (a) A typical response surface plotted between a response variable, release exponent, and two factors, HPMC and sodium CMC, in case of mucoadhesive compressed matrices; (b) the corresponding contour plot

2.7.7 Mathematical Models

The mathematical model, simply referred to as the model, is an algebraic expression defining the dependence of a response variable on the independent variable(s) (Box and Draper, 1987; Box et al., 1978). Mathematical models can either be empirical or theoretical (Doornbos and de Haan, 1995). An empirical model provides a way to describe the factor/response relationship. It is most frequently, but not invariably, a set of polynomial equations of a given order (Montgomery, 2001; Box and Draper, 1987). Most commonly used linear models are shown in following equations:

$$Y = \beta_0 + \beta_1 X_1 + \beta_2 X_2 + \dots + \epsilon$$

$$Y = \beta_0 + \beta_1 X_1 + \beta_2 X_2 + \beta_{12} X_1 X_2 + \dots + \epsilon$$

$$Y = \beta_0 + \beta_1 X_1 + \beta_2 X_2 + \beta_{12} X_1 X_2 + \beta_{11} X_1^2 + \beta_{22} X_2^2 + \dots + \epsilon$$

where y represents the estimated response, sometimes also denoted as E(y). The symbols X, represent the value of the factors, and β_0 , β_i , β_{ii} and β_{ij} are the constants representing the intercept, coefficients of first-order (first-degree) terms, coefficients

of second-order quadratic terms, and coefficients of second-order interaction terms, respectively. The symbol implies pure error. First two equations are linear in variables, representing a flat surface and a twisted plane in 3-D space, respectively. Third equation represents a linear second-order model that describes a twisted plane with curvature, arising from the quadratic terms.

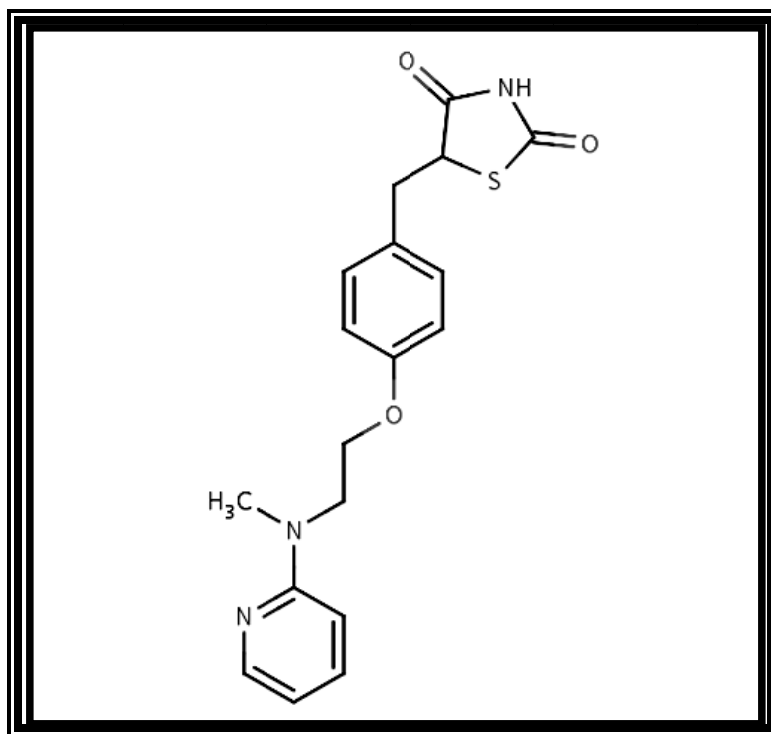
A theoretical model or mechanistic model may also exist or be proposed. It is most often a nonlinear model, where transformation to a linear function is not usually possible (Doornbos and de Haan, 1995). Such theoretical relationships are, however, rarely employed in pharmaceutical product development.

2.8 DRUG PROFILE

2.8.1 Rosiglitazone (RGZ)

Rosiglitazone is an oral diabetes medicine that helps control blood sugar levels. Rosiglitazone is for people with type-2 (non insulin dependent) diabetes. Rosiglitazone is sometimes used in combination with insulin or other medications, but it is not for treating type-1 diabetes. Taking rosiglitazone may increase your risk of serious heart problems, such as heart attack or stroke. Therefore, rosiglitazone is available only to certain people with type 2 diabetes that cannot be controlled with other diabetes medications. Rosiglitazone is not recommended for use with insulin. Apart from its effect on insulin resistance, it appears to have an anti-inflammatory effect: nuclear factor kappa-B (NF κ B) levels fall and inhibitor (I κ B) levels increase in patients on rosiglitazone. Recent research has suggested that rosiglitazone may also be of benefit to a subset of patients with Alzheimer's disease not expressing the ApoE4 allele. Thiazolidinediones class drugs also modulate the biology of fibrogenic cells and hence, studied to treat liverfibrosis. This is the subject of a clinical trial currently underway. The chemical name is 5-[(4-{2-[methyl(pyridin-2-yl)amino]ethoxy}phenyl)methyl]-1,3-thiazolidine-2,4-dione with the following structural formula:

2.8.1.1 Chemical Structure



Empirical Formula: C₁₈H₁₉N₃O₃S

CAS Number: 122320-73-4

Mol. Wt.: 357.43

2.8.1.2 Physical Properties

It is a white or almost white, crystalline, odorless, tasteless powder, practically insoluble in water (30µg/ml), freely soluble in organic solvents such as ethanol, DMSO, dimethyl formamide, methanol and chloroform. It has Log P value of 2.95 and melting point 153-155 °C.

2.8.1.3 Mechanism of Action

Rosiglitazone acts as an agonist at PPAR in target tissues such as adipose tissue, skeletal muscle, and liver. PPAR γ activation reduces expression of interstitial collagens and other matrix proteins, downregulates the ability to proliferate and migrate in response to PDGF, blocks the secretion of proinflammatory chemokines such as monocyte chemoattractant protein 1, and induces apoptosis. Moreover, exposure TNF- α or PDGF reduces PPAR γ expression or transcriptional activity while

PPAR γ ligands counteract these effects. In some systems the actions of TZDs have been shown to be independent of PPAR γ . However, ectopic expression of PPAR γ in activated HSCs recapitulates the effects of TZD treatment, indicating that these drugs modulate the biology of fibrogenic cells due to their ability to ligate PPAR γ .

2.8.1.4 Pharmacokinetics

The absolute bioavailability of rosiglitazone is 99%. Peak plasma concentrations are observed about 1 hour after dosing. Administration of rosiglitazone with food resulted in no change in overall exposure (AUC), but there was an approximately 28% decrease in C_{max} and a delay in T_{max} (1.75 hours). These changes are not likely to be clinically significant; therefore, rosiglitazone may be administered with or without food. About 99.8% of rosiglitazone is bound to plasma proteins, primarily to albumin and hence, volume of distribution is 6L. Rosiglitazone is extensively metabolized in the liver to inactive metabolites via N-demethylation, hydroxylation, and conjugation with sulfate and glucuronic acid. In vitro data have shown that Cytochrome (CYP) P450 isoenzyme 2C8 (CYP2C8) and to a minor extent CYP2C9 are involved in the hepatic metabolism of rosiglitazone. Following oral or intravenous administration of [¹⁴C] rosiglitazone, approximately 64% and 23% of the dose was eliminated in the urine and in the feces, respectively with elimination half life of 3-4 hours.

2.8.1.5 Side Effects

serious side effect includes: feeling short of breath, even with mild exertion; swelling or rapid weight gain; chest pain or heavy feeling, pain spreading to the arm or shoulder, sweating, general ill feeling; nausea, stomach pain, low fever, loss of appetite, dark urine, clay-colored stools, jaundice (yellowing of the skin or eyes); blurred vision; increased thirst or hunger, urinating more than usual; or pale skin, easy bruising or bleeding, weakness.

Less serious side effects may include: sneezing, runny nose, cough or other signs of a cold; headache; gradual weight gain; mild diarrhea; or back pain.

2.8.1.6 Interaction

Rosiglitazone has following drug interactions:

Drug	Interaction
Gemfibrozil	Increases the effect and toxicity of rosiglitazone/pioglitazone
Ketoconazole	Ketoconazole increases the effect of rosiglitazone
Pregabalin	Increased risk of edema
Rifampin	Rifampin reduces levels and efficacy of rosiglitazone
Somatropin recombinant	Somatropin may antagonize the hypoglycemic effect of rosiglitazone. Monitor for changes in fasting and postprandial blood sugars.
Tretinoin	The moderate CYP2C8 inhibitor, Rosiglitazone, may decrease the metabolism and clearance of oral Tretinoin. Monitor for changes in Tretinoin effectiveness and adverse/toxic effects if Rosiglitazone is initiated, discontinued to dose changed.

2.8.1.7 Contraindication

RGZ is contraindicated in patients with known hypersensitivity to RGZ and in conditions like Diabetic ketoacidosis.

2.8.1.8 Methods for Estimation

2.8.1.8.1 Ultraviolet Spectroscopy

UV spectra of RGZ gave absorption maxima at 311.8 nm in methanol and at 313.8 nm in diffusion medium (50 mM HPBCD, 20 mM HEPES, pH 7.4).

2.8.1.8.2 Chromatographic Analysis:

HPLC

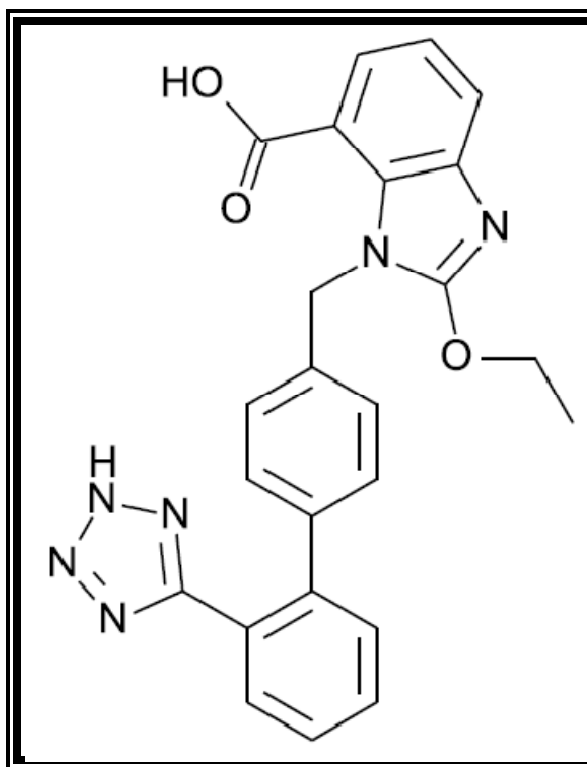
The chromatographic analysis was carried out on a GRACE Brava™ BDS C18 (5 μ m, 25 cm \times 4.6 mm) column maintained at 30 \pm 0.5°C. RGZ was eluted using a mobile phase composition of 10mM sodium acetate (pH 5): acetonitrile: methanol (40:40:20, v/v/v) at a flow rate 1.0 mL·min⁻¹. The mobile phase was premixed, filtered through a 0.45 mm Nylon 66 membrane filter and degassed before use. RGZ was detected at 245.0 nm and was eluted in 6.7 min after injection.

2.8.2 Candesartan (CDS)

Candesartan, a angiotensin-receptor blocker (ARB), is used alone or with other antihypertensive agents to treat hypertension. Candesartan competes with angiotensin II for binding at the AT1 receptor subtype. Recent research has suggested that HSCs with contractile and fibrogenic properties are the principal site of ECM production.

These cells are stimulated by fibrogenic cytokines, one of which is angiotensin II (ATII). The role of the renin-angiotensin system is supported by the observation that angiotensin type 1 (AT1) receptor antagonists attenuate the progression of liver fibrosis and reduce portal pressure. The chemical name is 2-ethoxy-1-({4-[2-(2H-1,2,3,4-tetrazol-5-yl)phenyl]phenyl}methyl)-1H-1,3-benzodiazole-7-carboxylic acid with the following structural formula:

2.8.2.1 Structure



Empirical Formula: C₂₄H₂₀N₆O₃

CAS Number: 139481-59-7

Mol. Wt.: 440.45

2.8.2.2 Physical Properties

It is a white or almost white crystalline powder; odorless; tasteless; practically insoluble in water (7.7µg/ml), freely soluble in chloroform, soluble in acetone, sparingly soluble in methanol, slightly soluble in ethanol. It has Log P value of 4.02 and melting point 183-185°C.

2.8.2.3 Mechanism of Action

Angiotensin II, the principal pressor agent of the renin-angiotensin system, is responsible for effects such as vasoconstriction, stimulation of synthesis and release of aldosterone, cardiac stimulation, and renal reabsorption of sodium. Candesartan selectively blocks the binding of angiotensin II to the AT1 receptor, which in turn leads to multiple effects including vasodilation, a reduction in the secretion of vasopressin, and reduction in the production and secretion of aldosterone. The resulting effect is a decrease in blood pressure. Candesartan's action is independent of the pathways for angiotensin II synthesis. The drug blocks the vasoconstrictor and aldosterone-secreting effects of angiotensin II by selectively blocking the binding of angiotensin II to the AT1 receptor in many tissues. This action is different from ACE inhibitors, which block the conversion of angiotensin I to angiotensin II, meaning that the production of angiotensin II is not completely inhibited, as the hormone can be formed via other enzymes. AT-II has also been shown to induce contraction and proliferation of HSCs, which play a pivotal role in liver fibrosis development. Accordingly, it has been suggested that AT-II plays a role in liver fibrosis development. The inhibition of angiotensin II synthesis and/or blockade of AT1 receptors attenuate experimental liver fibrosis.

2.8.2.4 Pharmacokinetics

Oral absorption of Candesartan is found to be 45% \pm 11. Volume of distribution is found to be 0.13l/kg and plasma protein binding is 99.8%. Renal Excretion accounts for 52% and plasma half life is 9.7hr.

2.8.2.5 Side Effects

serious side effect includes: rash; hives; itching; difficulty breathing; tightness in the chest; swelling of the mouth, face, lips, or tongue; hoarseness; change in the amount of urine produced; chest pain; dark urine; difficulty swallowing; fast, slow, or irregular heartbeat; fever, chills, or persistent sore throat; muscle pain or cramps; severe or persistent stomach pain (with or without nausea or vomiting); symptoms of low blood pressure (eg, fainting, lightheadedness, severe dizziness); unusual bruising or bleeding; yellowing of the eyes or skin.

Less serious side effects may include: Back pain; dizziness; upper respiratory tract infection.

2.8.2.6 Interaction

Candesartan has following drug interactions:

Drug	Interaction
Amiloride	Increased risk of hyperkalemia
Drospirenone	Increased risk of hyperkalemia
Lithium	The ARB increases serum levels of lithium
Potassium	Increased risk of hyperkalemia
Spirolactone	Increased risk of hyperkalemia
Tobramycin	Increased risk of nephrotoxicity
Trandolapril	The angiotensin II receptor blocker, Candesartan, may increase the adverse effects of Trandolapril.
Treprostinil	Additive hypotensive effect. Monitor antihypertensive therapy during concomitant use.
Triamterene	Increased risk of hyperkalemia

2.8.2.7 Contraindication

CDS is contraindicated in patients with hypersensitivity and in pregnancy (2nd and 3rd trimester) and lactation.

2.8.2.8 Methods for Estimation

2.8.2.8.1 Ultraviolet Spectroscopy

UV spectra of FRL gave absorption maxima at 304.8 nm in methanol and at 306.2 nm in diffusion medium (100 mM HPBCD, 20 mM HEPES, pH 7.4).

2.8.2.8.2 Chromatographic Analysis:

HPLC

The chromatographic analysis was carried out on a GRACE Brava™ BDS C18 (5 μ m, 25 cm \times 4.6 mm) column maintained at $30 \pm 0.5^\circ\text{C}$. CDS was eluted using a mobile phase composition of methanol: acetonitrile: 10mM sodium acetate pH 5 (74 : 16 : 10, v/v/v) (pH 2.5) at a flow rate $1.0 \text{ mL}\cdot\text{min}^{-1}$. The mobile phase was premixed, filtered through a 0.45 μ m Nylon 66 membrane filter and degassed before use. CDS was detected at 260.0 nm and was eluted in 4.5 min after injection.

2.9 REFERENCES

- Abdi W**, Millan JC, Mezey E. Sampling variability on percutaneous liver biopsy. *Arch Intern Med.* 1979 Jun;139(6):667-9.
- Abu-Izza KA**, Garcia-Contreras L, Lu DR. Preparation and evaluation of sustained release AZT-loaded microspheres: optimization of the release characteristics using response surface methodology. *J Pharm Sci.* 1996 Feb;85(2):144-9.
- Acikgoz M**, Kas H, Orman M, Hincal A. Chitosan microspheres of diclofenac sodium: I. Application of factorial design and evaluation of release kinetics. *J Microencapsul.* 1996 Mar-Apr;13(2):141-59.
- Afdhal NH**, Nunes D. Evaluation of liver fibrosis: a concise review. *Am J Gastroenterol.* 2004 Jun;99(6):1160-74.
- Albanis E**, Friedman SL. Non-invasive markers of hepatic fibrosis. *Clin Perspect Gastroenterol.* 2002;5(3):182-7.
- Allen TM**, Cullis PR. Drug delivery systems: entering the mainstream. *Science.* 2004 Mar 19;303(5665):1818-22.
- ANAES** (Agence Nationale d'Accreditation et d'Evaluation en Sante). Consensus conference: treatment of hepatitis C. *Gastroenterol Clin Biol.* 2002;26 Spec No 2:B303-20.
- Anderson M**, Kraber S, Hansel H, Klick S, Beckenbach R, Cianca-Bctancourt H. *Design Expert® Software Version 6 User's Guide.* MN: Statease Inc., 2002.
- Angulo P**. Nonalcoholic fatty liver disease. *N Engl J Med.* 2002 Apr 18;346(16):1221-31.
- Ankoma-Sey V**, Wang Y, Dai Z. Hypoxic stimulation of vascular endothelial growth factor expression in activated rat hepatic stellate cells. *Hepatology.* 2000 Jan;31(1):141-8.
- Anonymous.** JMP® Design of Experiments, Version 5 User's Guide. Cary: SAS International, 2002.
- Aoyagi M**, Sakaida I, Suzuki C, Segawa M, Fukumoto Y, Okita K. Prolyl 4-hydroxylase inhibitor is more effective for the inhibition of proliferation than for inhibition of collagen synthesis of rat hepatic stellate cells. *Hepatol Res.* 2002 May;23(1):1-6.
- Aparicio T**, Lehy T. Matrix metalloproteases in digestive pathology. *Gastroenterol Clin Biol.* 1999 Mar;23(3):330-41.
- Araujo PW**, Breton RG. Experimental design II. Optimization. *TrAC, Trends Anal Chem.* 1996 Feb; 15(2):63-70.
- Arena U**, Vizzutti F, Corti G, Ambu S, Stasi C, Bresci S, Moscarella S, Boddi V, Petrarca A, Laffi G, Marra F, Pinzani M. Acute viral hepatitis increases liver stiffness values measured by transient elastography. *Hepatology.* 2008 Feb;47(2):380-4.
- Armstrong NA**, James K.C. *Understanding Experimental Design and Interpretation in Pharmaceuticals.* Ellis Horwood, London, 1990; pp. 27-54, and pp. 136-157.

Arthur MJ, Stanley A, Iredale JP, Rafferty JA, Hembry RM, Friedman SL. Secretion of 72 kDa type IV collagenase/gelatinase by cultured human lipocytes. Analysis of gene expression, protein synthesis and proteinase activity. *Biochem J.* 1992 Nov 1;287(Pt 3):701-7.

Arthur MJ. Fibrosis and altered matrix degradation. *Digestion.* 1998 Jul-Aug;59(4):376-80.

Aube C, Oberti F, Korali N, Namour MA, Loisel D, Tanguy JY, Valsesia E, Pilette C, Rousselet MC, Bedossa P, Rifflet H, Maiga MY, Penneau-Fontbonne D, Caron C, Cales P. Ultrasonographic diagnosis of hepatic fibrosis or cirrhosis. *J Hepatol.* 1999 Mar;30(3):472-8.

Aube C, Racineux PX, Lebigot J, Oberti F, Croquet V, Argaud C, Cales P, Caron C. Diagnosis and quantification of hepatic fibrosis with diffusion weighted MR imaging: preliminary results. *J Radiol.* 2004 Mar;85(3):301-6.

Auwerx J. PPARgamma, the ultimate thrifty gene. *Diabetologia.* 1999 Sep;42(9):1033-49.

Babbs C, Hunt LP, Haboubi NY, Smith A, Rowan BP, Warnes TW. Type III procollagen peptide: a marker of disease activity and prognosis in primary biliary cirrhosis. *Lancet.* 1988 May 7;331(8593):1021-4.

Bachem MG, Melchior R, Gressne AM. The role of thrombocytes in liver fibrogenesis: effects of platelet lysate and thrombocyte-derived growth factors on the mitogenic activity and glycosaminoglycan synthesis of cultured rat liver fat storing cells. *J Clin Chem Clin Biochem.* 1989 Sep;27(9):555-65.

Bacon B, Goodman Z, Brunt E. Liver disease in the 21st century: clinico pathologic correlates. Report of the postgraduate course held october 24-25, 2003 by the American Association for the study of Liver Diseases. 2003.

Bacq Y, Schillio Y, Brechot JF, De Muret A, Dubois F, Metman EH. Decrease of haptoglobin serum level in patients with chronic viral hepatitis C. *Gastroenterol Clin Biol.* 1993;17(5):364-9.

Baik SK, Jo HS, Suk KT, Kim JM, Lee BJ, Choi YJ, Kim HS, Lee DK, Kwon SO, Lee KI, Cha SK, Park KS, Kong ID. Inhibitory effect of angiotensin II receptor antagonist on the contraction and growth of hepatic stellate cells. *Korean J Gastroenterol.* 2003 Aug;42(2):134-41.

Bangham AD, Hill MV, Miller MGA In: Korn ED (Eds.), *Methods in Membrane Biology*, Plenum Press, New York, 1974, pp. 1-68.

Bangham AD, Standish MM, Watkins JC. Diffusion of univalent ions across the lamellae of swollen phospholipids. *J Mol Biol.* 1965 Aug;13(1):238-52.

Barenholz Y, Amselem S, Lichtenberg D. A new method for preparation of phospholipid vesicles (liposomes) - French press. *FEBS Lett.* 1979 Mar 1;99(1):210-4.

Bartsch M, Weeke-Klimp AH, Hoenselaar EP, Stuart MC, Meijer DK, Scherphof GL, Kamps JA. Stabilized lipid coated lipoplexes for the delivery of antisense oligonucleotides to liver endothelial cells in vitro and in vivo. *J Drug Target.* 2004;12(9-10):613-21.

Bataller R, Brenner DA. Hepatic stellate cells as a target for the treatment of liver fibrosis. *Semin Liver Dis.* 2001 Aug;21(3):437-51.

Bataller R, Brenner DA. Liver fibrosis. *J Clin Invest.* 2005 Feb;115(2):209-18.

Bataller R, Gines P, Nicolas JM, Gorbic MN, Garcia-Ramallo E, Gasull X, Bosch J, Arroyo V, Rodes J. Angiotensin II induces contraction and proliferation of human hepatic stellate cells. *Gastroenterology.* 2000 Jun;118(6):1149-56.

Bataller R, North KE, Brenner DA. Genetic polymorphisms and the progression of liver fibrosis: a critical appraisal. *Hepatology.* 2003(a) Mar;37(3):493-503.

Bataller R, Paik YH, Lindquist JN, Lemasters JJ, Brenner DA. Hepatitis C virus core and nonstructural proteins induce fibrogenic effects in hepatic stellate cells. *Gastroenterology.* 2004 Feb;126(2):529-40.

Bataller R, Schwabe RF, Choi YH, Yang L, Paik YH, Lindquist J, Qian T, Schoonhoven R, Hagedorn CH, Lemasters JJ, Brenner DA. NADPH oxidase signal transduces angiotensin II in hepatic stellate cells and is critical in hepatic fibrosis. *J Clin Invest.* 2003(b) Nov;112(9):1383-94.

Batzri S, Korn ED. Single bilayer liposomes prepared without sonication. *Biochim Biophys Acta.* 1973 Apr 16;298(4):1015-9.

Bedossa P, Dargere D, Paradis V. Sampling variability of liver fibrosis in chronic hepatitis C. *Hepatology.* 2003 Dec;38(6):1449-57.

Bedossa P, Poynard T. An algorithm for the grading of activity in chronic hepatitis C. The METAVIR Cooperative Study Group. *Hepatology.* 1996 Aug;24(2):289-93.

Beljaars L, Molema G, Schuppan D, Geerts A, De Bleser PJ, Weert B, Meijer DK, Poelstra K. Successful targeting to rat hepatic stellate cells using albumin modified with cyclic peptides that recognize the collagen type VI receptor. *J Biol Chem* 2000 Apr 28; 275(17): 12743-51.

Beljaars L, Molema G, Weert B, Bonnema H, Olinga P, Groothuis GM, Meijer DKF, Poelstra K. Albumin modified with mannose 6-phosphate: A potential carrier for selective delivery of antifibrotic drugs to rat and human hepatic stellate cells. *Hepatology* 1999 May; 29(5): 1486-93.

Beljaars L, Olinga P, Molema G, de Bleser P, Geerts A, Groothuis GM, Meijer DKF, Poelstra K. Characteristics of the hepatic stellate cell-selective carrier mannose 6-phosphate modified albumin (M6P(28)-HSA). *Liver.* 2001 Oct; 21(5): 320-8.

Beljaars L, Weert B, Geerts A, Meijer DK, Poelstra K. The preferential homing of a platelet derived growth factor receptor-recognizing macromolecule to fibroblast-like cells in fibrotic tissue. *Biochem Pharmacol.* 2003 Oct 1;66(7):1307-17.

Benedetti A, Di Sario A, Casini A, Ridolfi F, Bendia E, Pignini P, Tonnini C, D'Ambrosio L, Feliciangeli G, Macarri G, Svegliati-Baroni G. Inhibition of the NA(+)/H(+) exchanger reduces rat hepatic stellate cell activity and liver fibrosis: an in vitro and in vivo study. *Gastroenterology.* 2001 Feb;120(2):545-56.

Bennett RG, Kharbanda KK, Tuma DJ. Inhibition of markers of hepatic stellate cell activation by the hormone relaxin. *Biochem Pharmacol.* 2003 Sep 1;66(5):867-74.

- Bentsen KD**, Horslev-Petersen K, Junker P, Juhl E, Lorenzen I. Serum aminoterminal procollagen type III peptide in acute viral hepatitis. A long-term follow-up study. *Liver*. 1987 Apr;7(2):96-105.
- Benyon RC**, Arthur MJ. Extracellular matrix degradation and the role of hepatic stellate cells. *Semin Liver Dis*. 2001 Aug;21(3):373-84.
- Betageri GV**. Liposomal Encapsulation and Stability of Dideoxyinosine Triphosphate. *Drug Dev Ind Pharm*. 1993 Jan; 19(5): 531-39.
- Beuers U**. Hepatic overlap syndromes. *J Hepatol*. 2005; 42 Suppl(1): S93-9.
- Bickel M**, Baringhaus KH, Gerl M, Günzler V, Kanta J, Schmidts L, Stapf M, Tschank G, Weidmann K, Werner U. Selective inhibition of hepatic collagen accumulation in experimental liver fibrosis in rats by a new prolyl 4-hydroxylase inhibitor. *Hepatology*. 1998 Aug;28(2):404-11.
- Boeker KH**, Haberkorn CI, Michels D, Flemming P, Manns MP, Lichtinghagen R. Diagnostic potential of circulating TIMP-1 and MMP-2 as markers of liver fibrosis in patients with chronic hepatitis C. *Clin Chim Acta*. 2002 Feb;316(1-2):71-81.
- Bolton S**. Factorial designs. In: *Pharmaceutical Statistics: Practical and Clinical Applications*. 3rd ed. New York: Marcel Dekker, 1997(a).
- Bolton S**. Optimization techniques. In: *Pharmaceutical Statistics: Practical and Clinical Applications*. 3rd ed. New York: Marcel Dekker, 1997(b).
- Bonacchi A**, Petrai I, Defranco RM, Lazzeri E, Annunziato F, Efsen E, Cosmi L, Romagnani P, Milani S, Failli P, Batignani G, Liotta F, Laffi G, Pinzani M, Gentilini P, Marra F. The chemokine CCL21 modulates lymphocyte recruitment and fibrosis in chronic hepatitis C. *Gastroenterology*. 2003 Oct;125(4):1060-76.
- Bonis PA**, Friedman SL, Kaplan MM. Is liver fibrosis reversible? *N Engl J Med*. 2001 Feb 8;344(6):452-4.
- Borkham-Kamphorst E**, Stoll D, Gressner AM, Weiskirchen R. Antisense strategy against PDGF B-chain proves effective in preventing experimental liver fibrogenesis. *Biochem Biophys Res Commun*. 2004 Aug 20;321(2):413-23.
- Boulanger Y**, Amara M, Lepanto L, Beaudoin G, Nguyen BN, Allaire G, Poliquin M, Nicolet V. Diffusion-weighted MR imaging of the liver of hepatitis C patients. *NMR Biomed*. 2003 May;16(3):132-6.
- Box GEP**, Draper NR. *Empirical Model-Building and Response Surfaces*. 1st ed. New York: Wiley, 1987.
- Box GEP**, Hunter WG, Hunter JS. *Statistics for Experimenters*. New York: Wiley, 1978.
- Box GEP**, Connor LR, Cousins WR, Davies OL, Hunsworth FR, Sulitto GP, editors. *The Design and Analysis of Industrial Experiments*. 2nd ed. London: Oliver and Boyd, 1960.
- Boyer N**, Marcellin P. Pathogenesis, diagnosis and management of hepatitis C. *J Hepatol*. 2000;32(1 Suppl):98-112.
- Bravo AA**, Sheth SG, Chopra S. Liver biopsy. *N Engl J Med*. 2001 Feb 15;344(7):495-500.

Breitkopf K, Lahme B, Tag CG, Gressner AM. Expression and matrix deposition of latent transforming growth factor beta binding proteins in normal and fibrotic rat liver and transdifferentiating hepatic stellate cells in culture. *Hepatology*. 2001 Feb;33(2):387-96.

Brewer GJ, Askari FK. Wilson's disease: clinical management and therapy. *J Hepatol*. 2005;42 Suppl(1):S13-21.

Bruck R, Genina O, Aeed H, Alexiev R, Nagler A, Avni Y, Pines M. Halofuginone to prevent and treat thioacetamide-induced liver fibrosis in rats. *Hepatology*. 2001 Feb;33(2):379-86.

Brunt EM. Grading and staging the histopathological lesions of chronic hepatitis: the Knodell histology activity index and beyond. *Hepatology*. 2000 Jan;31(1):241-6.

Cadranel JF, Rufat P, Degos F. Practices of liver biopsy in France: results of a prospective nationwide survey. For the Group of Epidemiology of the French Association for the Study of the Liver (AFEF). *Hepatology*. 2000 Sep;32(3):477-81.

Caligiuri A, De Franco RM, Romanelli RG, Gentilini A, Meucci M, Failli P, Mazzetti L, Rombouts K, Geerts A, Vanasia M, Gentilini P, Marra F, Pinzani M. Antifibrogenic effects of canrenone, an antialdosteronic drug, on human hepatic stellate cells. *Gastroenterology*. 2003 Feb;124(2):504-20.

Callewaert N, Van Vlierberghe H, Van Hecke A, Laroy W, Delanghe J, Contreras R. Noninvasive diagnosis of liver cirrhosis using DNA sequencer-based total serum protein glycomics. *Nat Med*. 2004 Apr;10(4):429-34.

Camps J, Garcia-Granero M, Riezu-Boj JI, Larrea E, de Alava E, Civeira MP, Castilla A, Prieto J. Prediction of sustained remission of chronic hepatitis C after a 12-month course of alfa interferon. *J Hepatol*. 1994 Jul;21(1):4-11.

Canbay A, Higuchi H, Bronk SF, Taniai M, Sebo TJ, Gores GJ. Fas enhances fibrogenesis in the bile duct ligated mouse: a link between apoptosis and fibrosis. *Gastroenterology*. 2002 Oct;123(4):1323-30.

Canbay A, Taimr P, Torok N, Higuchi H, Friedman S, Gores GJ. Apoptotic body engulfment by a human stellate cell line is profibrogenic. *Lab Invest*. 2003 May;83(5):655-63.

Cao Q, Mak KM, Lieber CS. DLPC decreases TGF-beta1-induced collagen mRNA by inhibiting p38 MAPK in hepatic stellate cells. *Am J Physiol Gastrointest Liver Physiol*. 2002 Nov;283(5):G1051-61.

Casini A, Ceni E, Salzano R, Biondi P, Parola M, Galli A, Foschi M, Caligiuri A, Pinzani M, Surrenti C. Neutrophil-derived superoxide anion induces lipid peroxidation and stimulates collagen synthesis in human hepatic stellate cells: role of nitric oxide. *Hepatology*. 1997 Feb;25(2):361-7.

Cassiman D, Libbrecht L, Desmet V, Denef C, Roskams T. Hepatic stellate cell/myofibroblast subpopulations in fibrotic human and rat livers. *J Hepatol*. 2002 Feb;36(2):200-9.

Castilla A, Prieto J, Fausto N. Transforming growth factors beta 1 and alpha in chronic liver disease. Effects of interferon alfa therapy. *N Engl J Med*. 1991 Apr 4;324(14):933-40.

Chen A, Zhang L, Xu J, Tang J. The antioxidant (-)-epigallocatechin-3-gallate inhibits activated hepatic stellate cell growth and suppresses acetaldehyde-induced gene expression. *Biochem J*. 2002 Dec 15;368(Pt 3):695-704.

Cheng J, Imanishi H, Liu W, Iwasaki A, Ueki N, Nakamura H, Hada T. Inhibition of the expression of alpha-smooth muscle actin in human hepatic stellate cell line, LI90, by a selective cyclooxygenase 2 inhibitor, NS-398. *Biochem Biophys Res Commun*. 2002 Oct 11;297(5):1128-34.

Cheng ML, Wu J, Zhang WS, Wang HQ, Li CX, Huang NH, Yao YM, Ren LG, Ye L, Li L. Effect of Maotai liquor on the liver: an experimental study. *Hepatobiliary Pancreat Dis Int*. 2004 Feb;3(1):93-8.

Cho JJ, Hocher B, Herbst H, Jia JD, Ruehl M, Hahn EG, Riecken EO, Schuppan D. An oral endothelin-A receptor antagonist blocks collagen synthesis and deposition in advanced rat liver fibrosis. *Gastroenterology*. 2000 Jun;118(6):1169-78.

Cochran WC, Cox GM. *Experimental Design*. 2nd ed. New York: Wiley, 1992.

Cohen BE. The permeability of liposomes to nonelectrolytes. I. Activation energies for permeation. *J Membr Biol*. 1975;20(3-4):205-34.

Colloredo G, Guido M, Sonzogni A, Leandro G. Impact of liver biopsy size on histological evaluation of chronic viral hepatitis: the smaller the sample, the milder the disease. *J Hepatol*. 2003 Aug;39(2):239-44.

Colombo M, Del Ninno E, de Franchis R, De Fazio C, Festorazzi S, Ronchi G, Tommasini MA. Ultrasound-assisted percutaneous liver biopsy: superiority of the Tru-Cut over the Menghini needle for diagnosis of cirrhosis. *Gastroenterology*. 1988 Aug;95(2):487-9.

Colombo M, Sangiovanni A. Etiology, natural history and treatment of hepatocellular carcinoma. *Antiviral Res*. 2003 Oct;60(2):145-50.

Conley J, Yang H, Wilson T, Blasetti K, Di Ninno V, Schnell G, Wong JP. Aerosol delivery of liposome-encapsulated ciprofloxacin: aerosol characterization and efficacy against *Francisella tularensis* infection in mice. *Antimicrob Agents Chemother*. 1997 Jun;41(6):1288-92.

Corpechot C, Barbu V, Wendum D, Kinnman N, Rey C, Poupon R, Housset C, Rosmorduc O. Hypoxia-induced VEGF and collagen I expressions are associated with angiogenesis and fibrogenesis in experimental cirrhosis. *Hepatology*. 2002 May;35(5):1010-21.

Cortesi R, Esposito E, Gambarin S, Telloli P, Menegatti E, Nastruzzi C. Preparation of liposomes by reverse-phase evaporation using alternative organic solvents. *J Microencapsul*. 1999 Mar-Apr;16(2):251-6.

Crommelin DJA, Van Bommel EMG. Stability of liposome on storage; freeze dried, frozen or as an aqueous dispersion. *Pharm Res*. 1984;1(4), 159-64.

Croquet V, Vuillemin E, Ternisien C, Pilette C, Oberti F, Gallois Y, Trossaert M, Rousselet MC, Chappard D, Cales P. Prothrombin index is an indirect marker of severe liver fibrosis. *Eur J Gastroenterol Hepatol*. 2002 Oct;14(10):1133-41.

Cullen SN, Chapman RW. Review article: current management of primary sclerosing cholangitis. *Aliment Pharmacol Ther*. 2005 Apr 15;21(8):933-48.

Czaja AJ, Bianchi FB, Carpenter HA, Krawitt EL, Lohse AW, Manns MP, McFarlane IG, Mieli-Vergani G, Toda G, Vergani D, Vierling J, Zeniya M. Treatment challenges and investigational opportunities in autoimmune hepatitis. *Hepatology*. 2005 Jan;41(1):207-15.

Daemen T, Velinova M, Regts J, de Jager M, Kalicharan R, Donga J, van der Want JJ, Scherphof GL. Different intrahepatic distribution of phosphatidylglycerol and phosphatidylserine liposomes in the rat. *Hepatology*. 1997 Aug;26(2):416-23.

Das MN, Giri NC. *Design and Analysis of Experiments*. 2nd ed- New Delhi: Wiley Eastern Limited, New Age International Limited, 1994.

De Bleser PJ, Niki T, Rogiers V, Geerts A. Transforming growth factor-beta gene expression in normal and fibrotic rat liver. *J Hepatol*. 1997 Apr;26(4):886-93.

Deamer D, Bangham AD. Large volume liposomes by an ether vaporization method. *Biochim Biophys Acta*. 1976 Sep 7;443(3):629-34.

Deasy PB (Ed), *Microencapsulation and related drug Processes*, Marcel Dekker Inc., New York, 1984.

Denzer U, Arnoldy A, Kanzler S, Galle PR, Dienes HP, Lohse AW. Prospective randomized comparison of minilaparoscopy and percutaneous liver biopsy: diagnosis of cirrhosis and complications. *J Clin Gastroenterol*. 2007 Jan;41(1):103-10.

Desmet VJ, Roskams T. Cirrhosis reversal: a duel between dogma and myth. *J Hepatol*. 2004 May;40(5):860-7.

Di Sario A, Bendia E, Taffetani S, Marzioni M, Candelaresi C, Pigni P, Schindler U, Kleemann HW, Trozzi L, Macarri G, Benedetti A. Selective Na⁺/H⁺ exchange inhibition by cariporide reduces liver fibrosis in the rat. *Hepatology*. 2003 Feb;37(2):256-66.

Dienstag JL, Goldin RD, Heathcote EJ, Hann HW, Woessner M, Stephenson SL, Gardner S, Gray DF, Schiff ER. Histological outcome during long-term lamivudine therapy. *Gastroenterology*. 2003 Jan;124(1):105-17.

Doornbos DA, de Haan P. Optimization techniques in formulation and processing. In: Swarbrick J, Boylan JC, editors. *Encyclopedia of Pharmaceutical Technology*. New York- Marcel Dekker. 1995.

Doornbos DA. Optimization in pharmaceutical sciences. *Pharm Week Sci*. 1981;3:33-61.

Edwards AM, Lucas CM, Baddams HM. Modulation of gamma-glutamyltranspeptidase in normal rat hepatocytes in culture by cell density, epidermal growth factor and agents which alter cell differentiation. *Carcinogenesis*. 1987 Dec;8(12):1837-42.

Efsen E, Bonacchi A, Pastacaldi S, Valente AJ, Wenzel UO, Tosti-Guerra C, Pinzani M, Laffi G, Abboud HE, Gentilini P, Marra F. Agonist-specific regulation of monocyte chemoattractant protein-1 expression by cyclooxygenase metabolites in hepatic stellate cells. *Hepatology*. 2001 Mar;33(3):713-21.

Efsen E, Grappone C, DeFranco RM, Milani S, Romanelli RG, Bonacchi A, Caligiuri A, Failli P, Annunziato F, Pagliai G, Pinzani M, Laffi G, Gentilini P, Marra F. Up-

regulated expression of fractalkine and its receptor CX3CR1 during liver injury in humans. *J Hepatol.* 2002 Jul;37(1):39-47.

Engstrom-Laurent A, Loof L, Nyberg A, Schroder T. Increased serum levels of hyaluronate in liver disease. *Hepatology.* 1985 Jul-Aug;5(4):638-42.

Eriksson S, Fraser JR, Laurent TC, Pertoft H, Smedsrod B. Endothelial cells are a site of uptake and degradation of hyaluronic acid in the liver. *Exp Cell Res.* 1983 Mar;144(1):223-8.

Everett L, Galli A, Crabb D. The role of hepatic peroxisome proliferator-activated receptors (PPARs) in health and disease. *Liver.* 2000 Jun;20(3):191-9.

Everson GT. Management of cirrhosis due to chronic hepatitis C. *J Hepatol.* 2005;42 Suppl(1):S65-74.

Fabris C, Falletti E, Federico E, Toniutto P, Pirisi M. A comparison of four serum markers of fibrosis in the diagnosis of cirrhosis. *Ann Clin Biochem.* 1997 Mar;34 (Pt 2):151-5.

Fabris P, Marranconi F, Bozzola L, Biasin MR, De Lazzari F, Plebani M, Benedetti P, Tositti G, Pellizzer G, Stecca C, de Lalla F. Fibrogenesis serum markers in patients with chronic hepatitis C treated with alpha-IFN. *J Gastroenterol.* 1999 Jun;34(3):345-50.

Failli P, DeFRANCO RM, Caligiuri A, Gentilini A, Romanelli RG, Marra F, Batignani G, Guerra CT, Laffi G, Gentilini P, Pinzani M. Nitrovasodilators inhibit platelet-derived growth factor-induced proliferation and migration of activated human hepatic stellate cells. *Gastroenterology.* 2000 Aug;119(2):479-92.

Fiorucci S, Antonelli E, Morelli O, Mencarelli A, Casini A, Mello T, Palazzetti B, Tallet D, del Soldato P, Morelli A. NCX-1000, a NO-releasing derivative of ursodeoxycholic acid, selectively delivers NO to the liver and protects against development of portal hypertension. *Proc Natl Acad Sci U S A.* 2001 Jul 17;98(15):8897-902.

Fiorucci S, Antonelli E, Rizzo G, Renga B, Mencarelli A, Riccardi L, Orlandi S, Pellicciari R, Morelli A. The nuclear receptor SHP mediates inhibition of hepatic stellate cells by FXR and protects against liver fibrosis. *Gastroenterology.* 2004 Nov;127(5):1497-512.

Fontana RJ, Lok AS. Noninvasive monitoring of patients with chronic hepatitis C. *Hepatology.* 2002 Nov;36(5 Suppl 1):S57-64.

Forbes SJ, Russo FP, Rey V, Burra P, Rugge M, Wright NA, Alison MR. A significant proportion of myofibroblasts are of bone marrow origin in human liver fibrosis. *Gastroenterology.* 2004 Apr;126(4):955-63.

Forman BM, Chen J, Evans RM. The peroxisome proliferator-activated receptors: ligands and activators. *Ann N Y Acad Sci.* 1996 Dec 27;804:266-75.

Forns X, Ampurdanes S, Llovet JM, Aponte J, Quinto L, Martinez-Bauer E, Bruguera M, Sanchez-Tapias JM, Rodes J. Identification of chronic hepatitis C patients without hepatic fibrosis by a simple predictive model. *Hepatology.* 2002 Oct;36(4 Pt 1):986-92.

Fortunato G, Castaldo G, Oriani G, Cerini R, Intrieri M, Molinaro E, Gentile I, Borgia G, Piazza M, Salvatore F, Sacchetti L. Multivariate discriminant function based on six biochemical markers in blood can predict the cirrhotic evolution of chronic hepatitis. *Clin Chem*. 2001 Sep;47(9):1696-700.

Foucher J, Chanteloup E, Vergniol J, Castera L, Le Bail B, Adhoute X, Bertet J, Couzigou P, de Ledinghen V. Diagnosis of cirrhosis by transient elastography (FibroScan): a prospective study. *Gut*. 2006 Mar;55(3):403-8.

Fresta M, Puglisi G. Corticosteroid dermal delivery with skin-lipid liposomes. *J Controlled Release*. 1997 Feb;44(2-3):141-51.

Friedman SL, Arthur MJ. Activation of cultured rat hepatic lipocytes by Kupffer cell conditioned medium. Direct enhancement of matrix synthesis and stimulation of cell proliferation via induction of platelet-derived growth factor receptors. *J Clin Invest*. 1989 Dec;84(6):1780-5.

Friedman SL. Cytokines and fibrogenesis. *Semin Liver Dis*. 1999;19(2): 129-40.

Friedman SL. Hepatic stellate cells. *Prog Liver Dis*. 1996;14:101-30.

Friedman SL. Liver fibrosis - from bench to bedside. *J Hepatol*. 2003;38 Suppl 1:S38-53.

Friedman SL. Mechanisms of Hepatic Fibrogenesis. *Gastroenterology* 2008 May;134(6):1655-69.

Friedman SL. Molecular regulation of hepatic fibrosis, an integrated cellular response to tissue injury. *J Biol Chem*. 2000 Jan 28; 275(4):2247-50.

Friedrich-Rust M, Ong MF, Martens S, Sarrazin C, Bojunga J, Zeuzem S, Herrmann E. Performance of transient elastography for the staging of liver fibrosis: a meta-analysis. *Gastroenterology*. 2008 Apr;134(4):960-74.

Fu M, Zhu X, Wang Q, Zhang J, Song Q, Zheng H, Ogawa W, Du J, Chen YE. Platelet-derived growth factor promotes the expression of peroxisome proliferator-activated receptor gamma in vascular smooth muscle cells by a phosphatidylinositol 3-kinase/Akt signaling pathway. *Circ Res*. 2001 Nov 23;89(11):1058-64.

Fukuzawa K, Chida H, Tokumura A, Tsukatani H. Antioxidative effect of alpha-tocopherol incorporation into lecithin liposomes on ascorbic acid-Fe²⁺-induced lipid peroxidation. *Arch Biochem Biophys*. 1981 Jan;206(1):173-80.

Fung SK, Lok AS. Management of patients with hepatitis B virus-induced cirrhosis. *J Hepatol*. 2005; 42 Suppl(1): S54-64.

Galli A, Crabb D, Price D, Ceni E, Salzano R, Surrenti C, Casini A. Peroxisome proliferator-activated receptor gamma transcriptional regulation is involved in platelet-derived growth factor-induced proliferation of human hepatic stellate cells. *Hepatology*. 2000 Jan;31(1):101-8.

Geerts A. History, heterogeneity, developmental biology, and functions of quiescent hepatic stellate cells. *Semin Liver Dis*. 2001 Aug; 21(3): 311-35.

George J, Roulot D, Kotliansky VE, Bissell DM. In vivo inhibition of rat stellate cell activation by soluble transforming growth factor beta type II receptor: a potential new therapy for hepatic fibrosis. *Proc Natl Acad Sci U S A*. 1999 Oct 26;96(22):12719-24.

Germano MP, D'Angelo V, Sanogo R, Morabito A, Pergolizzi S, De Pasquale R. Hepatoprotective activity of *Trichilia roka* on carbon tetrachloride-induced liver damage in rats. *J Pharm Pharmacol*. 2001 Nov;53(11):1569-74.

Giannini E, Risso D, Botta F, Chiarbonello B, Fasoli A, Malfatti F, Romagnoli P, Testa E, Ceppa P, Testa R. Validity and clinical utility of the aspartate aminotransferase-alanine aminotransferase ratio in assessing disease severity and prognosis in patients with hepatitis C virus-related chronic liver disease. *Arch Intern Med*. 2003 Jan 27;163(2):218-24.

Godichaud S, Krisa S, Couronne B, Dubuisson L, Merillon JM, Desmouliere A, Rosenbaum J. Deactivation of cultured human liver myofibroblasts by trans-resveratrol, a grapevine-derived polyphenol. *Hepatology*. 2000 Apr;31(4):922-31.

Gonzalo T, Talman EG, van de Ven A, Temming K, Greupink R, Beljaars L, Reker-Smit C, Meijer DKF, Molema G, Poelstra K, Kok RJ. Selective targeting of pentoxifylline to hepatic stellate cells using a novel platinum-based linker technology. *J Control Release*. 2006 Mar 10; 111(1-2): 193-203.

Gordon SC, Fang JW, Silverman AL, McHutchison JG, Albrecht JK. The significance of baseline serum alanine aminotransferase on pretreatment disease characteristics and response to antiviral therapy in chronic hepatitis C. *Hepatology*. 2000 Aug;32(2):400-4.

Green S, Wahli W. Peroxisome proliferator-activated receptors: finding the orphan a home. *Mol Cell Endocrinol*. 1994 Apr;100(1-2):149-53.

Gregoriadis G, Davis C. Stability of liposomes in vivo and in vitro is promoted by their cholesterol content and the presence of blood cells. *Biochem Biophys Res Commun*. 1979 Aug 28;89(4):1287-93.

Gressner AM, Lotfi S, Gressner G, Haltner E, Kropf J. Synergism between hepatocytes and Kupffer cells in the activation of fat storing cells (perisinusoidal lipocytes). *J Hepatol*. 1993 Aug;19(1):117-32.

Gressner AM. Cytokines and cellular crosstalk involved in the activation of fat-storing cells. *J Hepatol*. 1995;22(2 Suppl):28-36.

Gressner AM. The cell biology of liver fibrogenesis-an imbalance of proliferation, growth arrest and apoptosis of myofibroblast. *Cell Tissue Res*. 1998 Jun;292(3):447-52.

Greupink R, Bakker HI, Bouma W, Reker-Smit C, Meijer DKF, Beljaars L, Poelstra K. The antiproliferative drug doxorubicin inhibits liver fibrosis in bile duct-ligated rats and can be selectively delivered to hepatic stellate cells in vivo. *J Pharmacol Exp Ther*. 2006 May;317(2):514-21.

Greupink R, Bakker HI, Reker-Smit C, Loenen-Weemaes AM, Kok RJ, Meijer DKF, Beljaars L, Poelstra K. Studies on the targeted delivery of the antifibrogenic compound mycophenolic acid to the hepatic stellate cell. *J Hepatol*. 2005 Nov;43(5):884-92.

Gronbaek K, Christensen PB, Hamilton-Dutoit S, Federspiel BH, Hage E, Jensen OJ, Vyberg M. Interobserver variation in interpretation of serial liver biopsies from patients with chronic hepatitis C. *J Viral Hepat*. 2002 Nov;9(6):443-9.

Guechot J, Laudat A, Loria A, Serfaty L, Poupon R, Giboudeau J. Diagnostic accuracy of hyaluronan and type III procollagen amino-terminal peptide serum assays as markers of liver fibrosis in chronic viral hepatitis C evaluated by ROC curve analysis. *Clin Chem*. 1996 Apr;42(4):558-63.

Guechot J, Loria A, Serfaty L, Giral P, Giboudeau J, Poupon R. Serum hyaluronan as a marker of liver fibrosis in chronic viral hepatitis C: effect of alpha-interferon therapy. *J Hepatol*. 1995(a) Jan;22(1):22-6.

Guechot J, Poupon RE, Poupon R. Serum hyaluronan as a marker of liver fibrosis. *J Hepatol*. 1995(b);22(suppl 2):103-6.

Gulati M, Grover M, Singh M, Singh S. Study of azathioprine encapsulation into liposomes. *J Microencapsul*. 1998 Jul-Aug;15(4):485-94.

Guler ML, Gorham JD, Hsieh CS, Mackey AJ, Steen RG, Dietrich WF, Murphy KM. Genetic susceptibility to Leishmania: IL-12 responsiveness in TH1 cell development. *Science*. 1996 Feb 16;271(5251):984-7.

Gutierrez-Ruiz MC, Bucio L, Correa A, Souza V, Hernandez E, Gomez-Quiroz LE, Kershenovich D. Metadoxine prevents damage produced by ethanol and acetaldehyde in hepatocyte and hepatic stellate cells in culture. *Pharmacol Res*. 2001 Nov;44(5):431-6.

Haaland PD. *Experimental Design in Biotechnology*. Marcel Dekker, New York, 1989.

Hadziyannis SJ, Tassopoulos NC, Heathcote EJ, Chang TT, Kitis G, Rizzetto M, Marcellin P, Lim SG, Goodman Z, Wulfsohn MS, Xiong S, Fry J, Brosgart CL; Adefovir Dipivoxil 438 Study Group. Adefovir dipivoxil for the treatment of hepatitis B e antigen-negative chronic hepatitis B. *N Engl J Med*. 2003 Feb 27;348(9):800-7.

Hagens WI, Olinga P, Meijer DK, Groothuis GM, Beljaars L, Poelstra K. Gliotoxin non-selectively induces apoptosis in fibrotic and normal livers. *Liver Int*. 2006 Mar;26(2):232-9.

Harada N, Soejima Y, Taketomi A, Yoshizumi T, Ikegami T, Yamashita Y, Itoh S, Kuroda Y, Maehara Y. Assessment of graft fibrosis by transient elastography in patients with recurrent hepatitis C after living donor liver transplantation. *Transplantation*. 2008 Jan 15;85(1):69-74.

Hardman J, Limbird L, Goodman Gilman A. *Goodman and Gilman's the Pharmacological basis of therapeutics*. 10th ed, McGraw-Hill publishers, 2001.

Hattori Y, Kawakami S, Yamashita F, Hashida M. Controlled biodistribution of galactosylated liposomes and incorporated probucol in hepatocyte-selective drug targeting. *J Control Release*. 2000 Dec 3;69(3):369-77.

Hauser H, Strauss G. Stabilization of small unilamellar phospholipid vesicles during spray-drying. *Biochim Biophys Acta*. 1987 Feb 26;897(2):331-4.

Hayasaka A, Schuppan D, Ohnishi K, Okuda K, Hahn EG. Serum concentrations of the carboxyterminal cross-linking domain of procollagen type IV (NC1) and the aminoterminal propeptide of procollagen type III (PIIIP) in chronic liver disease. *J Hepatol*. 1990 Jan;10(1):17-22.

Heinzel FP, Sadick MD, Holaday BJ, Coffman RL, Locksley RM. Reciprocal expression of interferon gamma or interleukin 4 during the resolution or progression of murine leishmaniasis. Evidence for expansion of distinct helper T cell subsets. *J Exp Med*. 1989 Jan 1;169(1):59-72.

Hellemans K, Grinko I, Rombouts K, Schuppan D, Geerts A. All-trans and 9-cis retinoic acid alter rat hepatic stellate cell phenotype differentially. *Gut*. 1999 Jul;45(1):134-42.

Hellemans K, Michalik L, Dittie A, Knorr A, Rombouts K, De Jong J, Heirman C, Quartier E, Schuit F, Wahli W, Geerts A. Peroxisome proliferator-activated receptor-beta signaling contributes to enhanced proliferation of hepatic stellate cells. *Gastroenterology*. 2003 Jan;124(1):184-201.

Hellemans K, Verbuyst P, Quartier E, Schuit F, Rombouts K, Chandraratna RA, Schuppan D, Geerts A. Differential modulation of rat hepatic stellate phenotype by natural and synthetic retinoids. *Hepatology*. 2004 Jan;39(1):97-108.

Herbst H, Wege T, Milani S, Pellegrini G, Orzechowski HD, Bechstein WO, Neuhaus P, Gressner AM, Schuppan D. Tissue inhibitor of metalloproteinase-1 and -2 RNA expression in rat and human liver fibrosis. *Am J Pathol*. 1997 May;150(5):1647-59.

Hernandez-Caselles T, Villalain J, Gomez-Fernandez JC. Stability of liposomes on long term storage. *J Pharm Pharmacol*. 1990 Jun;42(6):397-400.

Hillebrandt S, Goos C, Matern S, Lammert F. Genome-wide analysis of hepatic fibrosis in inbred mice identifies the susceptibility locus Hfib1 on chromosome 15. *Gastroenterology*. 2002 Dec;123(6):2041-51.

Hirayama C, Suzuki H, Takada A, Fujisawa K, Tanikawa K, Igarashi S. Serum type IV collagen in various liver diseases in comparison with serum 7S collagen, laminin, and type III procollagen peptide. *J Gastroenterol*. 1996 Apr;31(2):242-8.

Honda H, Onitsuka H, Masuda K, Nishitani H, Nakata H, Watanabe K. Chronic liver disease: value of volumetry of liver and spleen with computed tomography. *Radiat Med*. 1990 Nov-Dec;8(6):222-6.

Housset C, Rockey DC, Bissell DM. Endothelin receptors in rat liver: lipocytes as a contractile target for endothelin 1. *Proc Natl Acad Sci U S A*. 1993 Oct 15;90(20):9266-70.

Huang Z, Li Q, Wang Z. Observation on dynamic changes of serum procollagen III, hyaluronic acid and laminin in rats with hepatic fibrosis treated with Hujin pill. *Zhongguo Zhong Xi Yi Jie He Za Zhi*. 2000 Jun;20(6):447-9.

Hui AY, Dannenberg AJ, Sung JJ, Subbaramaiah K, Du B, Olinga P, Friedman SL. Prostaglandin E2 inhibits transforming growth factor beta 1-mediated induction of collagen alpha 1(I) in hepatic stellate cells. *J Hepatol*. 2004 Aug;41(2):251-8.

Ikeda H, Nagoshi S, Ohno A, Yanase M, Maekawa H, Fujiwara K. Activated rat stellate cells express c-met and respond to hepatocyte growth factor to enhance transforming growth factor beta1 expression and DNA synthesis. *Biochem Biophys Res Commun*. 1998 Sep 29;250(3):769-75.

Ikejima K, Takei Y, Honda H, Hirose M, Yoshikawa M, Zhang YJ, Lang T, Fukuda T, Yamashina S, Kitamura T, Sato N. Leptin receptor-mediated signaling regulates

hepatic fibrogenesis and remodeling of extracellular matrix in the rat. *Gastroenterology*. 2002 May;122(5):1399-410.

Imanishi Y, Maeda N, Otogawa K, Seki S, Matsui H, Kawada N, Arakawa T. Herb medicine Inchin-ko-to (TJ-135) regulates PDGF-BB-dependent signaling pathways of hepatic stellate cells in primary culture and attenuates development of liver fibrosis induced by thioacetamide administration in rats. *J Hepatol*. 2004 Aug;41(2):242-50.

Imbert-Bismut F, Ratziu V, Pieroni L, Charlotte F, Benhamou Y, Poynard T; MULTIVIRC Group. Biochemical markers of liver fibrosis in patients with hepatitis C virus infection: a prospective study. *Lancet*. 2001 Apr 7;357(9262):1069-75.

Iredale JP, Benyon RC, Pickering J, McCullen M, Northrop M, Pawley S, Hovell C, Arthur MJ. Mechanisms of spontaneous resolution of rat liver fibrosis. Hepatic stellate cell apoptosis and reduced hepatic expression of metalloproteinase inhibitors. *J Clin Invest*. 1998 Aug 1;102(3):538-49.

Iredale JP, Murphy G, Hembry RM, Friedman SL, Arthur MJ. Human hepatic lipocytes synthesize tissue inhibitor of metalloproteinases-1. Implications for regulation of matrix degradation in liver. *J Clin Invest*. 1992 Jul;90(1):282-7.

Ishak K, Baptista A, Bianchi L, Callea F, De Groote J, Gudat F, Denk H, Desmet V, Korb G, MacSween RNM, Phillips MJ, Portmann BG, Poulsen H, Scheuer PJ, Schmid M, Thaler H. Histological grading and staging of chronic hepatitis. *J Hepatol*. 1995 Jun;22(6):696-9.

Ishikawa K, Mochida S, Mashiba S, Inao M, Matsui A, Ikeda H, Ohno A, Shibuya M, Fujiwara K. Expressions of vascular endothelial growth factor in nonparenchymal as well as parenchymal cells in rat liver after necrosis. *Biochem Biophys Res Commun*. 1999 Jan 27;254(3):587-93.

Issa R, Williams E, Trim N, Kendall T, Arthur MJ, Reichen J, Benyon RC, Iredale JP. Apoptosis of hepatic stellate cells: involvement in resolution of biliary fibrosis and regulation by soluble growth factors. *Gut*. 2001 Apr;48(4):548-57.

Issa R, Zhou X, Constandinou CM, Fallowfield J, Millward-Sadler H, Gaca MD, Sands E, Suliman I, Trim N, Knorr A, Arthur MJ, Benyon RC, Iredale JP. Spontaneous recovery from micronodular cirrhosis: evidence for incomplete resolution associated with matrix cross-linking. *Gastroenterology*. 2004 Jun;126(7):1795-808.

Iwamoto H, Sakai H, Kotoh K, Nakamuta M, Nawata H. Soluble Arg-Gly-Asp peptides reduce collagen accumulation in cultured rat hepatic stellate cells. *Dig Dis Sci*. 1999(a) May;44(5):1038-45.

Iwamoto H, Sakai H, Tada S, Nakamuta M, Nawata H. Induction of apoptosis in rat hepatic stellate cells by disruption of integrin-mediated cell adhesion. *J Lab Clin Med*. 1999(b) Jul;134(1):83-9.

Ji G, Wang YQ, Cao CL. Clinical study on treatment of alcoholic liver disease by qinggan huoxue recipe. *Zhongguo Zhong Xi Yi Jie He Za Zhi*. 2004 Jan;24(1):13-6.

Jia JD, Bauer M, Cho JJ, Ruehl M, Milani S, Boigk G, Riecken EO, Schuppan D. Antifibrotic effect of silymarin in rat secondary biliary fibrosis is mediated by downregulation of procollagen alpha1(I) and TIMP-1. *J Hepatol*. 2001 Sep;35(3):392-8.

Jiang W, Yang CQ, Liu WB, Wang YQ, He BM, Wang JY. Blockage of transforming growth factor beta receptors prevents progression of pig serum-induced rat liver fibrosis. *World J Gastroenterol*. 2004 Jun 1;10(11):1634-8.

Johansen JS, Christoffersen P, Moller S, Price PA, Henriksen JH, Garbarsch C, Bendtsen F. Serum YKL-40 is increased in patients with hepatic fibrosis. *J Hepatol*. 2000 Jun;32(6):911-20.

Johnston DS, Chapman D. Preparation of liposomes, In: Gregoriadis G (Ed). *Liposomal Technology*. Vol. I, CRC Press Inc, BocaRaton, FL, 1984.

Jonsson JR, Clouston AD, Ando Y, Kelemen LI, Horn MJ, Adamson MD, Purdie DM, Powell EE. Angiotensin-converting enzyme inhibition attenuates the progression of rat hepatic fibrosis. *Gastroenterology*. 2001 Jul;121(1):148-55.

Kagawa Y, Racker E. Partial resolution of the enzymes catalysing oxidative phosphorylation. XXV Reconstitution of vesicles catalysing ^{32}P -adenosine triphosphate exchange. *J Biol Chem*. 1971 Sep 10;246(17):5477-87.

Kalinichenko VV, Bhattacharyya D, Zhou Y, Gusarova GA, Kim W, Shin B, Costa RH. Foxf1 +/- mice exhibit defective stellate cell activation and abnormal liver regeneration following CCl4 injury. *Hepatology*. 2003 Jan;37(1):107-17.

Kalluri R, Neilson EG. Epithelial-mesenchymal transition and its implications for fibrosis. *J Clin Invest*. 2003 Dec;112(12):1776-84.

Kamada Y, Tamura S, Kiso S, Matsumoto H, Saji Y, Yoshida Y, Fukui K, Maeda N, Nishizawa H, Nagaretani H, Okamoto Y, Kihara S, Miyagawa J, Shinomura Y, Funahashi T, Matsuzawa Y. Enhanced carbon tetrachloride-induced liver fibrosis in mice lacking adiponectin. *Gastroenterology*. 2003 Dec;125(6):1796-807.

Kamps JA, Morselt HW, Scherphof GL. Uptake of liposomes containing phosphatidylserine by liver cells in vivo and by sinusoidal liver cells in primary culture: in vivo-in vitro differences. *Biochem Biophys Res Commun*. 1999 Mar 5;256(1):57-62.

Kamps JA, Morselt HW, Swart PJ, Meijer DK, Scherphof GL. Massive targeting of liposomes, surface-modified with anionized albumins, to hepatic endothelial cells. *Proc Natl Acad Sci U S A*. 1997 Oct 14;94(21):11681-5.

Kannan V, Kandrapu R, Garg S. Optimization techniques for the design and development of novel drug delivery systems, part I. *Pharm Tech*. 2003(a) Feb;74-90.

Kannan V, Kandrapu R, Garg S. Optimization techniques for the design and development of novel drug delivery systems, part II. *Pharm Tech*. 2003(b) Mar;102-18.

Kanzler S, Baumann M, Schirmacher P, Dries V, Bayer E, Gerken G, Dienes HP, Lohse AW. Prediction of progressive liver fibrosis in hepatitis C infection by serum and tissue levels of transforming growth factor-beta. *J Viral Hepat*. 2001 Nov;8(6):430-7.

Kaplan MM, Gershwin ME. Primary biliary cirrhosis. *N Engl J Med*. 2005 Sep 22;353(12):1261-73.

Kaplowitz N. Mechanisms of liver cell injury. *J Hepatol*. 2000;32(1 Suppl):39-47.

Kawada N, Klein H, Decker K. Eicosanoid-mediated contractility of hepatic stellate cells. *Biochem J.* 1992(a) Jul 15;285 (Pt 2):367-71.

Kawada N, Mizoguchi Y, Kobayashi K, Monna T, Liu P, Morisawa S. Enhancement of prostaglandin E2 production by liver macrophages (Kupffer cells) after stimulation with biological response modifiers. *Prostaglandins Leukot Essent Fatty Acids.* 1992(b) Jun;46(2):105-10.

Kayano K, Sakaida I, Uchida K, Okita K. Inhibitory effects of the herbal medicine Sho-saiko-to (TJ-9) on cell proliferation and procollagen gene expressions in cultured rat hepatic stellate cells. *J Hepatol.* 1998 Oct;29(4):642-9.

Kettaneh A, Marcellin P, Douvin C, Poupon R, Zioli M, Beaugrand M, de Ledinghen V. Features associated with success rate and performance of FibroScan measurements for the diagnosis of cirrhosis in HCV patients: a prospective study of 935 patients. *J Hepatol.* 2007 Apr;46(4):628-34.

Kettaneh-Wold N. Use of experimental design in the pharmaceutical industry. *J Pharm Biomed Anal.* 1991;9(8):605-10.

Kinnman N, Francoz C, Barbu V, Wendum D, Rey C, Hultcrantz R, Poupon R, Housset C. The myofibroblastic conversion of peribiliary fibrogenic cells distinct from hepatic stellate cells is stimulated by platelet-derived growth factor during liver fibrogenesis. *Lab Invest.* 2003 Feb;83(2):163-73.

Kliwer SA, Forman BM, Blumberg B, Ong ES, Borgmeyer U, Mangelsdorf DJ, Umesono K, Evans RM. Differential expression and activation of a family of murine peroxisome proliferator-activated receptors. *Proc Natl Acad Sci U S A.* 1994 Jul 19;91(15):7355-9.

Knittel T, Mehde M, Kobold D, Saile B, Dinter C, Ramadori G. Expression patterns of matrix metalloproteinases and their inhibitors in parenchymal and non-parenchymal cells of rat liver: regulation by TNF-alpha and TGF-beta1. *J Hepatol.* 1999 Jan;30(1):48-60.

Knolle PA, Loser E, Protzer U, Duchmann R, Schmitt E, zum Büschenfelde KH, Rose-John S, Gerken G. Regulation of endotoxin-induced IL-6 production in liver sinusoidal endothelial cells and Kupffer cells by IL-10. *Clin Exp Immunol.* 1997 Mar;107(3):555-61.

Kobayashi S, Seki S, Kawada N, Morikawa H, Nakatani K, Uyama N, Ikeda K, Nakajima Y, Arakawa T, Kaneda K. Apoptosis of T cells in the hepatic fibrotic tissue of the rat: a possible inducing role of hepatic myofibroblast-like cells. *Cell Tissue Res.* 2003 Mar;311(3):353-64.

Korner T, Kropf J, Gressner AM. Serum laminin and hyaluronan in liver cirrhosis: markers of progression with high prognostic value. *J Hepatol.* 1996 Nov;25(5):684-8.

Korsemeier RW, Gumy R, Doelker E, Buri P, Peppas NA. Mechanisms of solute release from porous hydrophilic polymers. *Int J Pharm.* 1983 May;15(1):25-35.

Koukoulis GK, Koso-Thomas AK, Zardi L, Gabbiani G, Gould VE. Enhanced tenascin expression correlates with inflammation in primary sclerosing cholangitis. *Pathol Res Pract.* 1999;195(11):727-31.

Koukoulis GK, Shen J, Virtanen I, Gould VE. Vitronectin in the cirrhotic liver: an immunomarker of mature fibrosis. *Hum Pathol.* 2001 Dec;32(12):1356-62.

Kropf J, Gressner AM, Negwer A. Efficacy of serum laminin measurement for diagnosis of fibrotic liver diseases. *Clin Chem*. 1988 Oct;34(10):2026-30.

Lai CL, Chien RN, Leung NW, Chang TT, Guan R, Tai DI, Ng KY, Wu PC, Dent JC, Barber J, Stephenson SL, Gray DF. A one-year trial of lamivudine for chronic hepatitis B. Asia Hepatitis Lamivudine Study Group. *N Engl J Med*. 1998 Jul 9;339(2):61-8.

Larrey D. Drug-induced liver diseases. *J Hepatol*. 2000;32(1 Suppl):77-88.

Lasic DD (Ed). *Liposomes: From Physics to Applications*. Elsevier, Amsterdam, 1993.

Lau GK, Piratvisuth T, Luo KX, Marcellin P, Thongsawat S, Cooksley G, Gane E, Fried MW, Chow WC, Paik SW, Chang WY, Berg T, Flisiak R, McCloud P, Pluck N; Peginterferon Alfa-2a HBeAg-Positive Chronic Hepatitis B Study Group. Peginterferon Alfa-2a, lamivudine, and the combination for HBeAg-positive chronic hepatitis B. *N Engl J Med*. 2005 Jun 30;352(26):2682-95.

Law SL, Lo WY, Lin M. Increase of liposome stability by incorporation of bovine serum albumin. *Drug Dev Ind Pharm*. 1994 Jan;20(8):1411-23.

Leclercq IA, Farrell GC, Schriemer R, Robertson GR. Leptin is essential for the hepatic fibrogenic response to chronic liver injury. *J Hepatol*. 2002 Aug;37(2):206-13.

LeCouter J, Moritz DR, Li B, Phillips GL, Liang XH, Gerber HP, Hillan KJ, Ferrara N. Angiogenesis-independent endothelial protection of liver: role of VEGFR-1. *Science*. 2003 Feb 7;299(5608):890-3.

Lee KS, Buck M, Houghlum K, Chojkier M. Activation of hepatic stellate cells by TGF alpha and collagen type I is mediated by oxidative stress through c-myc expression. *J Clin Invest*. 1995 Nov;96(5):2461-8.

Lee KS, Lee SJ, Park HJ, Chung JP, Han KH, Chon CY, Lee SI, Moon YM. Oxidative stress effect on the activation of hepatic stellate cells. *Yonsei Med J*. 2001 Feb;42(1):1-8.

Lee SJ, Kim YG, Kang KW, Kim CW, Kim SG. Effects of colchicine on liver functions of cirrhotic rats: beneficial effects result from stellate cell inactivation and inhibition of TGF beta1 expression. *Chem Biol Interact*. 2004 Jan 15;147(1):9-21.

Leroy V, De Traversay C, Barnoud R, Hartmann JD, Baud M, Ouzan D, Zarski JP. Changes in histological lesions and serum fibrogenesis markers in chronic hepatitis C patients non-responders to interferon alpha. *J Hepatol*. 2001 Jul;35(1):120-6.

Leung NW, Lai CL, Chang TT, Guan R, Lee CM, Ng KY, Lim SG, Wu PC, Dent JC, Edmundson S, Condreay LD, Chien RN; Asia Hepatitis Lamivudine Study Group. Extended lamivudine treatment in patients with chronic hepatitis B enhances hepatitis B e antigen seroconversion rates: results after 3 years of therapy. *Hepatology*. 2001 Jun;33(6):1527-32.

Levy MT, McCaughan GW, Abbott CA, Park JE, Cunningham AM, Müller E, Rettig WJ, Gorrell MD. Fibroblast activation protein: a cell surface dipeptidyl peptidase and gelatinase expressed by stellate cells at the tissue remodelling interface in human cirrhosis. *Hepatology*. 1999 Jun;29(6):1768-78.

Lewis GA, Mathieu D, Phan-Tan-Luu R. *Pharmaceutical Experimental Design*. 1st ed. New York Marcel Dekker, 1999.

Lewis GA. Optimization methods. In: Swarbrick J, Boylan JC (ed). *Encyclopedia of Pharmaceutical Technology*. 2nd ed. Marcel Dekker, New York, 2002.

Li J. Factorial designs. In: Chow S-C (ed). *Encyclopedia of Biopharmaceutical Statistics*. Marcel Dekker, New York, 2003(a).

Li L, Xu M, Liu ZL. Effect of dahuang zhechong pill on transforming growth factor-beta 1 in hepatic stellate cells in rats. *Zhongguo Zhong Xi Yi Jie He Za Zhi*. 2003(b) Oct;23(10):763-6.

Li W, Wang C, Zhang J. Effects of da ding feng zhu decoction in 30 cases of liver fibrosis. *J Tradit Chin Med*. 2003(c) Dec;23(4):251-4.

Liaw YF, Leung NW, Chang TT, Guan R, Tai DI, Ng KY, Chien RN, Dent J, Roman L, Edmundson S, Lai CL. Effects of extended lamivudine therapy in Asian patients with chronic hepatitis B. Asia Hepatitis Lamivudine Study Group. *Gastroenterology*. 2000 Jul;119(1):172-80.

Liu CH, Liu P, Hu YY, Xu LM, Tan YZ, Wang ZN, Liu C. Effects of salvianolic acid-A on rat hepatic stellate cell proliferation and collagen production in culture. *Acta Pharmacol Sin*. 2000(a) Aug;21(8):721-6.

Liu WB, Yang CQ, Jiang W, Wang YQ, Guo JS, He BM, Wang JY. Inhibition on the production of collagen type I, III of activated hepatic stellate cells by antisense TIMP-1 recombinant plasmid. *World J Gastroenterol*. 2003 Feb;9(2):316-9.

Liu X, Zhang Z, Yang L, Chen D, Wang Y. [Inhibition of the activation and collagen production of cultured rat hepatic stellate cells by antisense oligonucleotides against transforming growth factor-beta 1 is enhanced by cationic liposome delivery]. *Hua Xi Yi Ke Da Xue Xue Bao*. 2000(b) Jun;31(2):133-5, 142.

Lok AS. Hepatitis B infection: pathogenesis and management. *J Hepatol*. 2000;32(1 Suppl):89-97.

Longmuir KJ, Robertson RT, Haynes SM, Baratta JL, Waring AJ. Effective targeting of liposomes to liver and hepatocytes in vivo by incorporation of a Plasmodium amino acid sequence. *Pharm Res*. 2006 Apr;23(4):759-69.

Loukas YL. 2(k-p) fractional factorial design via fold over: application to optimization of novel multicomponent vesicular systems. *Analyst*. 1997 Oct;122(10):1023-7.

Lu Y, Lu T, Cheng M. Changes of collagenase activity in immune hepatic fibrosis following pig's serum injection and therapeutic effect of HanDanGanLe. *Zhonghua Gan Zang Bing Za Zhi*. 2000 Apr;8(2):108-9.

Luster MI, Germolec DR, Yoshida T, Kayama F, Thompson M. Endotoxin-induced cytokine gene expression and excretion in the liver. *Hepatology*. 1994 Feb;19(2):480-8.

Macias J, Giron-Gonzalez JA, Gonzalez-Serrano M, Merino D, Cano P, Mira JA, Arizcorreta-Yarza A, Ruiz-Morales J, Lomas-Cabeza JM, Garcia-Garcia JA, Corzo JE, Pineda JA. Prediction of liver fibrosis in human immunodeficiency virus/hepatitis

C virus coinfecting patients by simple non-invasive indexes. *Gut*. 2006 Mar;55(3):409-14.

Magness ST, Bataller R, Yang L, Brenner DA. A dual reporter gene transgenic mouse demonstrates heterogeneity in hepatic fibrogenic cell populations. *Hepatology*. 2004 Nov;40(5):1151-9.

Maharaj B, Maharaj RJ, Leary WP, Cooppan RM, Naran AD, Pirie D, Pudifin DJ. Sampling variability and its influence on the diagnostic yield of percutaneous needle biopsies of the liver. *Lancet*. 1986 Mar 8;1(8480):523-5.

Maher JJ, McGuire RF. Extracellular matrix gene expression increases preferentially in rat lipocytes and sinusoidal endothelial cells during hepatic fibrosis in vivo. *J Clin Invest*. 1990 Nov;86(5):1641-8.

Maher JJ. Interactions between hepatic stellate cells and the immune system. *Semin Liver Dis*. 2001 Aug;21(3):417-26.

Malinda KM, Ponce L, Kleinman HK, Shackelton LM, Millis AJ. Gp38k, a protein synthesized by vascular smooth muscle cells, stimulates directional migration of human umbilical vein endothelial cells. *Exp Cell Res*. 1999 Jul 10;250(1):168-73.

Mann DA, Smart DE. Transcriptional regulation of hepatic stellate cell activation. *Gut*. 2002 Jun;50(6):891-6.

Marcellin P, Chang TT, Lim SG, Tong MJ, Sievert W, Shiffman ML, Jeffers L, Goodman Z, Wulfsohn MS, Xiong S, Fry J, Brosgart CL; Adefovir Dipivoxil 437 Study Group. Adefovir dipivoxil for the treatment of hepatitis B e antigen-positive chronic hepatitis B. *N Engl J Med*. 2003 Feb 27;348(9):808-16.

Marra F, DeFranco R, Grappone C, Parola M, Milani S, Leonarduzzi G, Pastacaldi S, Wenzel UO, Pinzani M, Dianzani MU, Laffi G, Gentilini P. Expression of monocyte chemoattractant protein-1 precedes monocyte recruitment in a rat model of acute liver injury, and is modulated by vitamin E. *J Investig Med*. 1999 Jan;47(1):66-75.

Marra F, Efsen E, Romanelli RG, Caligiuri A, Pastacaldi S, Batignani G, Bonacchi A, Caporale R, Laffi G, Pinzani M, Gentilini P. Ligands of peroxisome proliferator-activated receptor gamma modulate profibrogenic and proinflammatory actions in hepatic stellate cells. *Gastroenterology*. 2000 Aug;119(2):466-78.

Marra F. Chemokines in liver inflammation and fibrosis. *Front Biosci*. 2002 Sep 1;7:d1899-914.

Martin FJ. Specialized Drug Delivery Systems Manufacturing and Production Technology. In: Tyle P (Ed). Marcel Dekker Inc., New York and Basel, 1990.

Maxwell PH, Ferguson DJ, Osmond MK, Pugh CW, Heryet A, Doe BG, Johnson MH, Ratcliffe PJ. Expression of a homologously recombined erythropoietin-SV40 T antigen fusion gene in mouse liver: evidence for erythropoietin production by Ito cells. *Blood*. 1994 Sep 15;84(6):1823-30.

McGary CT, Yannariello-Brown J, Kim DW, Stinson TC, Weigel PH. Degradation and intracellular accumulation of a residualizing hyaluronan derivative by liver endothelial cells. *Hepatology*. 1993 Dec;18(6):1465-76.

McHutchison JG, Blatt LM, de Medina M, Craig JR, Conrad A, Schiff ER, Tong MJ. Measurement of serum hyaluronic acid in patients with chronic hepatitis C and its relationship to liver histology. Consensus Interferon Study Group. *J Gastroenterol Hepatol.* 2000 Aug;15(8):945-51.

Meeren PV, Laethem MV, Vanderdeelen J, Baert L. Particle Sizing of Liposomal Dispersions: A Critical Evaluation of Some Quasi-Elastic Light-Scattering Data-Analysis Software Programs. 1992;2(1):23-42.

Milani S, Herbst H, Schuppan D, Grappone C, Pellegrini G, Pinzani M, Casini A, Calabro A, Ciancio G, Stefanini F. Differential expression of matrix-metalloproteinase-1 and -2 genes in normal and fibrotic human liver. *Am J Pathol.* 1994 Mar;144(3):528-37.

Millonig G, Reimann FM, Friedrich S, Fonouni H, Mehrabi A, Büchler MW, Seitz HK, Mueller S. Extrahepatic cholestasis increases liver stiffness (FibroScan) irrespective of fibrosis. *Hepatology.* 2008 Nov;48(5):1718-23.

Miyahara T, Schrum L, Rippe R, Xiong S, Yee HF Jr, Motomura K, Anania FA, Willson TM, Tsukamoto H. Peroxisome proliferator-activated receptors and hepatic stellate cell activation. *J Biol Chem.* 2000 Nov 17;275(46):35715-22.

Montgomery DC. Design and Analysis of Experiments. 5th ed. Wiley, New York, 2001.

Murawaki Y, Ikuta Y, Idobe Y, Kitamura Y, Kawasaki H. Tissue inhibitor of metalloproteinase-1 in the liver of patients with chronic liver disease. *J Hepatol.* 1997 Jun;26(6):1213-9.

Murawaki Y, Ikuta Y, Nishimura Y, Koda M, Kawasaki H. Serum markers for connective tissue turnover in patients with chronic hepatitis B and chronic hepatitis C: a comparative analysis. *J Hepatol.* 1995 Aug;23(2):145-52.

Murawaki Y, Ikuta Y, Okamoto K, Koda M, Kawasaki H. Diagnostic value of serum markers of connective tissue turnover for predicting histological staging and grading in patients with chronic hepatitis C. *J Gastroenterol.* 2001(a) Jun;36(6):399-406.

Murawaki Y, Koda M, Okamoto K, Mimura K, Kawasaki H. Diagnostic value of serum type IV collagen test in comparison with platelet count for predicting the fibrotic stage in patients with chronic hepatitis C. *J Gastroenterol Hepatol.* 2001(b) Jul;16(7):777-81.

Muriel P, Castro V. Effects of S-adenosyl-L-methionine and interferon-alpha2b on liver damage induced by bile duct ligation in rats. *J Appl Toxicol.* 1998 Mar-Apr;18(2):143-7.

Muriel P, Suarez OR, Gonzalez P, Zuniga L. Protective effect of S-adenosyl-L-methionine on liver damage induced by biliary obstruction in rats: a histological, ultrastructural and biochemical approach. *J Hepatol.* 1994 Jul;21(1):95-102.

Murphy FR, Issa R, Zhou X, Ratnarajah S, Nagase H, Arthur MJ, Benyon C, Iredale JP. Inhibition of apoptosis of activated hepatic stellate cells by tissue inhibitor of metalloproteinase-1 is mediated via effects on matrix metalloproteinase inhibition: implications for reversibility of liver fibrosis. *J Biol Chem.* 2002 Mar 29;277(13):11069-76.

Murphy JR. Screening design. In: Chow S-C (ed). Encyclopedia of Biopharmaceutical Statistics. Marcel Dekker, New York, 2003.

Myers RH, Montgomery DC. Response Surface Methodology: Process and Product Optimization using Designed Experiments. Wiley, New York, 1995.

Myers RP, Benhamou Y, Imbert-Bismut F, Thibault V, Bochet M, Charlotte F, Ratzu V, Bricaire F, Katlama C, Poynard T. Serum biochemical markers accurately predict liver fibrosis in HIV and hepatitis C virus co-infected patients. AIDS. 2003(a) Mar 28;17(5):721-5.

Myers WR. Response surface methodology. In: Chow S-C (ed). Encyclopedia of Biopharmaceutical Statistics. Marcel Dekker, New York, 2003(b).

Nagano T, Kita T, Tanaka N. The immunocytochemical localization of tumour necrosis factor and leukotriene in the rat liver after treatment with lipopolysaccharide. Int J Exp Pathol. 1992 Oct;73(5):675-83.

Nakamura T, Tomita Y, Hirai R, Yamaoka K, Kaji K, Ichihara A. Inhibitory effect of transforming growth factor-beta on DNA synthesis of adult rat hepatocytes in primary culture. Biochem Biophys Res Commun. 1985 Dec 31;133(3):1042-50.

Naveau S, Poynard T, Benattar C, Bedossa P, Chaput JC. Alpha-2-macroglobulin and hepatic fibrosis. Diagnostic interest. Dig Dis Sci. 1994 Nov;39(11):2426-32.

Naveau S, Raynard B, Ratzu V, Abella A, Imbert-Bismut F, Messous D, Beuzen F, Capron F, Thabut D, Munteanu M, Chaput JC, Poynard T. Biomarkers for the prediction of liver fibrosis in patients with chronic alcoholic liver disease. Clin Gastroenterol Hepatol. 2005 Feb;3(2):167-74.

Nelson DR, Gonzalez-Peralta RP, Qian K, Xu Y, Marousis CG, Davis GL, Lau JY. Transforming growth factor-beta 1 in chronic hepatitis C. J Viral Hepat. 1997 Jan;4(1):29-35.

New RRC (ed). Liposomes: A Practical Approach. Oxford University Press, UK, 1990.

Nie QH, Cheng YQ, Xie YM, Zhou YX, Cao YZ. Inhibiting effect of antisense oligonucleotides phosphorothioate on gene expression of TIMP-1 in rat liver fibrosis. World J Gastroenterol. 2001 Jun;7(3):363-9.

Nieto N, Friedman SL, Greenwel P, Cederbaum AI. CYP2E1-mediated oxidative stress induces collagen type I expression in rat hepatic stellate cells. Hepatology. 1999 Oct;30(4):987-96.

Nieto N, Greenwel P, Friedman SL, Zhang F, Dannenberg AJ, Cederbaum AI. Ethanol and arachidonic acid increase alpha 2(I) collagen expression in rat hepatic stellate cells overexpressing cytochrome P450 2E1. Role of H₂O₂ and cyclooxygenase-2. J Biol Chem. 2000 Jun 30;275(26):20136-45.

NIH Consensus Statement on Management of Hepatitis C: 2002. NIH Consensus State Sci Statements. 2002 Jun 10-12;19(3):1-46.

Niki T, Rombouts K, De Bleser P, De Smet K, Rogiers V, Schuppan D, Yoshida M, Gabbiani G, Geerts A. A histone deacetylase inhibitor, trichostatin A, suppresses myofibroblastic differentiation of rat hepatic stellate cells in primary culture. Hepatology. 1999 Mar;29(3):858-67.

Nojgaard C, Johansen JS, Christensen E, Skovgaard LT, Price PA, Becker U; EMALD Group. Serum levels of YKL-40 and PIIINP as prognostic markers in patients with alcoholic liver disease. *J Hepatol*. 2003(a) Aug;39(2):179-86.

Nojgaard C, Johansen JS, Krarup HB, Holten-Andersen M, Moller A, Bendtsen F; Danish Viral Hepatitis Study Group. Effect of antiviral therapy on markers of fibrogenesis in patients with chronic hepatitis C. *Scand J Gastroenterol*. 2003(b) Jun;38(6):659-65.

Oberti F, Valsesia E, Pilette C, Rousselet MC, Bedossa P, Aube C, Gallois Y, Rifflet H, Maïga MY, Penneau-Fontbonne D, Cales P. Noninvasive diagnosis of hepatic fibrosis or cirrhosis. *Gastroenterology*. 1997 Nov;113(5):1609-16.

O'Brien MJ, Keating NM, Elderiny S, Cerda S, Keaveny AP, Afdhal NH, Nunes DP. An assessment of digital image analysis to measure fibrosis in liver biopsy specimens of patients with chronic hepatitis C. *Am J Clin Pathol*. 2000 Nov;114(5):712-8.

Okuno M, Akita K, Moriwaki H, Kawada N, Ikeda K, Kaneda K, Suzuki Y, Kojima S. Prevention of rat hepatic fibrosis by the protease inhibitor, camostat mesilate, via reduced generation of active TGF-beta. *Gastroenterology*. 2001 Jun;120(7):1784-800.

Okuyama H, Shimahara Y, Kawada N, Seki S, Kristensen DB, Yoshizato K, Uyama N, Yamaoka Y. Regulation of cell growth by redox-mediated extracellular proteolysis of platelet-derived growth factor receptor beta. *J Biol Chem*. 2001 Jul 27;276(30):28274-80.

Olaso E, Salado C, Egilegor E, Gutierrez V, Santisteban A, Sancho-Bru P, Friedman SL, Vidal-Vanaclocha F. Proangiogenic role of tumor-activated hepatic stellate cells in experimental melanoma metastasis. *Hepatology*. 2003 Mar;37(3):674-85.

Orr JG, Leel V, Cameron GA, Marek CJ, Haughton EL, Elrick LJ, Trim JE, Hawksworth GM, Halestrap AP, Wright MC. Mechanism of action of the antifibrogenic compound gliotoxin in rat liver cells. *Hepatology*. 2004 Jul;40(1):232-42.

Ostro MJ. *Liposomes as Drug Carriers: Recent Trends and Progress*, ed. Gregoriadis G, John Wiley and sons, Toronto, 1988.

Pagliari L, Rinaldi F, Craxi A, Di Piazza S, Filippazzo G, Gatto G, Genova G, Magrin S, Maringhini A, Orsini S, Palazzo U, Spinello M, Vinci M. Percutaneous blind biopsy versus laparoscopy with guided biopsy in diagnosis of cirrhosis. A prospective, randomized trial. *Dig Dis Sci*. 1983 Jan;28(1):39-43.

Paik YH, Schwabe RF, Bataller R, Russo MP, Jobin C, Brenner DA. Toll-like receptor 4 mediates inflammatory signaling by bacterial lipopolysaccharide in human hepatic stellate cells. *Hepatology*. 2003 May;37(5):1043-55.

Papahadjopoulos D, Jacobson K, Nir S, Isac T. Phase transitions in phospholipid vesicles. Fluorescence polarization and permeability measurements concerning the effect of temperature and cholesterol. *Biochim Biophys Acta*. 1973 Jul 6;311(3):330-48.

Paradis V, Laurent A, Mathurin P, Poynard T, Vidaud D, Vidaud M, Bedossa P. Role of liver extracellular matrix in transcriptional and post-transcriptional regulation of apolipoprotein A-I by hepatocytes. *Cell Mol Biol (Noisy-le-grand)*. 1996 Jun;42(4):525-34.

Pares A, Deulofeu R, Gimenez A, Caballeria L, Bruguera M, Caballeria J, Ballesta AM, Rodes J. Serum hyaluronate reflects hepatic fibrogenesis in alcoholic liver disease and is useful as a marker of fibrosis. *Hepatology*. 1996 Dec;24(6):1399-403.

Park EJ, Ko G, Kim J, Sohn DH. Antifibrotic effects of a polysaccharide extracted from *Ganoderma lucidum*, glycyrrhizin, and pentoxifylline in rats with cirrhosis induced by biliary obstruction. *Biol Pharm Bull*. 1997 Apr;20(4):417-20.

Parola M, Leonarduzzi G, Biasi F, Albano E, Biocca ME, Poli G, Dianzani MU. Vitamin E dietary supplementation protects against carbon tetrachloride-induced chronic liver damage and cirrhosis. *Hepatology*. 1992 Oct;16(4):1014-21.

Patel K, Gordon SC, Jacobson I, Hezode C, Oh E, Smith KM, Pawlotsky JM, McHutchison JG. Evaluation of a panel of non-invasive serum markers to differentiate mild from moderate-to-advanced liver fibrosis in chronic hepatitis C patients. *J Hepatol*. 2004 Dec;41(6):935-42.

Patel K, Muir AJ, McHutchison JG. Validation of a simple predictive model for the identification of mild hepatic fibrosis in chronic hepatitis C patients. *Hepatology*. 2003 May;37(5):1222; author reply 1222-3.

Pavanato A, Tunon MJ, Sanchez-Campos S, Marroni CA, Llesuy S, Gonzalez-Gallego J, Marroni N. Effects of quercetin on liver damage in rats with carbon tetrachloride-induced cirrhosis. *Dig Dis Sci*. 2003 Apr;48(4):824-9.

Peck-Radosavljevic M. Hypersplenism. *Eur J Gastroenterol Hepatol*. 2001 Apr;13(4):317-23.

Perrault J, McGill DB, Ott BJ, Taylor WF. Liver biopsy: complications in 1000 inpatients and outpatients. *Gastroenterology*. 1978 Jan;74(1):103-6.

Perrillo RP. The role of liver biopsy in hepatitis C. *Hepatology*. 1997 Sep;26(3 Suppl 1):57S-61S.

Perugini P, Pavanetto F. Liposomes containing boronophenylalanine for boron neutron capture therapy. *J Microencapsul*. 1998 Jul-Aug;15(4):473-83.

Peters KM, Dommaschk J, Grundmann R, Schaadt M, Schicha H. Monitoring of tumor necrosis factor therapy with neopterin. *Arzneimittelforschung*. 1990 Apr;40(4):508-10.

Pietrangelo A. Hereditary hemochromatosis--a new look at an old disease. *N Engl J Med*. 2004 Jun 3;350(23):2383-97.

Pilette C, Oberti F, Aube C, Rousselet MC, Bedossa P, Gallois Y, Rifflet H, Cales P. Non-invasive diagnosis of esophageal varices in chronic liver diseases. *J Hepatol*. 1999 Nov;31(5):867-73.

Pinzani M, Marra F. Cytokine receptors and signaling in hepatic stellate cells. *Semin Liver Dis*. 2001 Aug;21(3):397-416.

Pinzani M, Rombouts K, Colagrande S. Fibrosis in chronic liver diseases: diagnosis and management. *J Hepatol*. 2005;42 Suppl(1):S22-36.

Podczeczek F. The development and optimization of tablet formulations using mathematical methods. In: Banker GS, Rhodes CT (ed). *Modern Pharmaceutics*. Marcel Dekker, New York, 1996.

Pohlmann S, Zhang J, Baribaud F, Chen Z, Leslie GJ, Lin G, Granelli-Piperno A, Doms RW, Rice CM, McKeating JA. Hepatitis C virus glycoproteins interact with DC-SIGN and DC-SIGNR. *J Virol*. 2003 Apr;77(7):4070-80.

Poniachik J, Bernstein DE, Reddy KR, Jeffers LJ, Coelho-Little ME, Civantos F, Schiff ER. The role of laparoscopy in the diagnosis of cirrhosis. *Gastrointest Endosc*. 1996 Jun;43(6):568-71.

Porter SC, Verseput RP, Cunnigham CR. Process optimization using design of experimnts. *Pharm Tech* 1997 Oct;1-7.

Poupon RE, Huet PM, Poupon R, Bonnard AM, Nhieu JT, Zafrani ES. A randomized trial comparing colchicine and ursodeoxycholic acid combination to ursodeoxycholic acid in primary biliary cirrhosis. UDCA-PBC Study Group. *Hepatology*. 1996 Nov;24(5):1098-103.

Poynard T, Imbert-Bismut F, Munteanu M, Messous D, Myers RP, Thabut D, Ratziu V, Mercadier A, Benhamou Y, Hainque B. Overview of the diagnostic value of biochemical markers of liver fibrosis (FibroTest, HCV FibroSure) and necrosis (ActiTest) in patients with chronic hepatitis C. *Comp Hepatol*. 2004(a) Sep 23;3(1):8.

Poynard T, Imbert-Bismut F, Ratziu V. Serum markers of fibrosis. *Hepatology Rev*. 2004(b) Jan-Mar;1(1):23-31.

Poynard T, McHutchison J, Manns M, Trepo C, Lindsay K, Goodman Z, Ling MH, Albrecht J. Impact of pegylated interferon alfa-2b and ribavirin on liver fibrosis in patients with chronic hepatitis C. *Gastroenterology*. 2002 May;122(5):1303-13.

Poynard T, Ratziu V, Benmanov Y, Di Martino V, Bedossa P, Opolon P. Fibrosis in patients with chronic hepatitis C: detection and significance. *Semin Liver Dis*. 2000;20(1):47-55.

Pradat P, Alberti A, Poynard T, Esteban JI, Weiland O, Marcellin P, Badalamenti S, Trepo C. Predictive value of ALT levels for histologic findings in chronic hepatitis C: a European collaborative study. *Hepatology*. 2002 Oct;36(4 Pt 1):973-7.

Qi Z, Atsuchi N, Ooshima A, Takeshita A, Ueno H. Blockade of type beta transforming growth factor signaling prevents liver fibrosis and dysfunction in the rat. *Proc Natl Acad Sci U S A*. 1999 Mar 2;96(5):2345-9.

Rachfal AW, Brigstock DR. Connective tissue growth factor (CTGF/CCN2) in hepatic fibrosis. *Hepatol Res*. 2003 May;26(1):1-9.

Raetsch C, Jia JD, Boigk G, Bauer M, Hahn EG, Riecken EO, Schuppan D. Pentoxifylline downregulates profibrogenic cytokines and procollagen I expression in rat secondary biliary fibrosis. *Gut*. 2002 Feb;50(2):241-7.

Ramadori G, Neubauer K, Odenthal M, Nakamura T, Knittel T, Schwogler S, Meyer zum Büschenfelde KH. The gene of hepatocyte growth factor is expressed in fat-storing cells of rat liver and is downregulated during cell growth and by transforming growth factor-beta. *Biochem Biophys Res Commun*. 1992 Mar 16;183(2):739-42.

Ramadori G, Zohrens G, Manns M, Rieder H, Dienes HP, Hess G, Meyer KH, Büschenfelde Z. Serum hyaluronate and type III procollagen aminoterminal propeptide concentration in chronic liver disease. Relationship to cirrhosis and disease activity. *Eur J Clin Invest*. 1991 Jun;21(3):323-30.

Regev A, Berho M, Jeffers LJ, Milikowski C, Molina EG, Pyrsopoulos NT, Feng ZZ, Reddy KR, Schiff ER. Sampling error and intraobserver variation in liver biopsy in patients with chronic HCV infection. *Am J Gastroenterol*. 2002 Oct;97(10):2614-8.

Reif S, Aeed H, Shilo Y, Reich R, Kloog Y, Kweon YO, Bruck R. Treatment of thioacetamide-induced liver cirrhosis by the Ras antagonist, farnesylthiosalicylic acid. *J Hepatol*. 2004 Aug;41(2):235-41.

Rensen PC, Sliedregt LA, Ferns M, Kieviet E, van Rossenberg SM, van Leeuwen SH, van Berkel TJ, Biessen EA. Determination of the upper size limit for uptake and processing of ligands by the asialoglycoprotein receptor on hepatocytes in vitro and in vivo. *J Biol Chem*. 2001 Oct 5;276(40):37577-84.

Riaz M, Weiner N, Martin F. *Pharmaceutical Dosage Forms: disperse Systems* (vol. 2), Leiberman HA, Reiger MA and Banker GS (Ed). Marcel Dekker Inc., New York, 1988.

Rigamonti C, Donato MF, Fraquelli M, Agnelli F, Ronchi G, Casazza G, Rossi G, Colombo M. Transient elastography predicts fibrosis progression in patients with recurrent hepatitis C after liver transplantation. *Gut*. 2008 Jun;57(6):821-7.

Ringdorf H, Schlarb B, Venzmer J *Molecular Architecture and Function of Polymeric Oriented Systems: Models for the Study of Organization, Surface Recognition, and Dynamics of Biomembranes*. *Angewandte Chemie International Edition*, 1988; 27(1):113-58.

Rocchi S, Auwerx J. Peroxisome proliferator-activated receptor-gamma: a versatile metabolic regulator. *Ann Med*. 1999 Oct;31(5):342-51.

Rockey DC. Hepatic blood flow regulation by stellate cells in normal and injured liver. *Semin Liver Dis*. 2001 Aug;21(3):337-49.

Rockey DC. Vascular mediators in the injured liver. *Hepatology*. 2003 Jan;37(1):4-12.

Romanelli RG, Caligiuri A, Carloni V, DeFranco R, Montalto P, Ceni E, Casini A, Gentilini P, Pinzani M. Effect of pentoxifylline on the degradation of procollagen type I produced by human hepatic stellate cells in response to transforming growth factor-beta 1. *Br J Pharmacol*. 1997 Nov;122(6):1047-54.

Rombouts K, Kisanga E, Hellemans K, Wielant A, Schuppan D, Geerts A. Effect of HMG-CoA reductase inhibitors on proliferation and protein synthesis by rat hepatic stellate cells. *J Hepatol*. 2003 May;38(5):564-72.

Romero EL, Morilla MJ, Regts J, Koning GA, Scherphof GL. On the mechanism of hepatic transendothelial passage of large liposomes. *FEBS Lett*. 1999 Apr 1;448(1):193-6.

Rosenberg WM, Voelker M, Thiel R, Becka M, Burt A, Schuppan D, Hubscher S, Roskams T, Pinzani M, Arthur MJ; European Liver Fibrosis Group. Serum markers detect the presence of liver fibrosis: a cohort study. *Gastroenterology*. 2004 Dec;127(6):1704-13.

Rossi E, Adams L, Prins A, Bulsara M, de Boer B, Garas G, MacQuillan G, Speers D, Jeffrey G. Validation of the FibroTest biochemical markers score in assessing liver fibrosis in hepatitis C patients. *Clin Chem*. 2003 Mar;49(3):450-4.

Rothkopf C, Fahr A, Fricker G, Scherphof GL, Kamps JA. Uptake of phosphatidylserine-containing liposomes by liver sinusoidal endothelial cells in the serum-free perfused rat liver. *Biochim Biophys Acta*. 2005 Feb 1;1668(1):10-6.

Rousselet MC, Michalak S, Dupre F, Croue A, Bedossa P, Saint-Andre JP, Cales P; Hepatitis Network 49. Sources of variability in histological scoring of chronic viral hepatitis. *Hepatology*. 2005 Feb;41(2):257-64.

Safadi R, Ohta M, Alvarez CE, Fiel MI, Bansal M, Mehal WZ, Friedman SL. Immune stimulation of hepatic fibrogenesis by CD8 cells and attenuation by transgenic interleukin-10 from hepatocytes. *Gastroenterology*. 2004 Sep;127(3):870-82.

Sagir A, Erhardt A, Schmitt M, Häussinger D. Transient elastography is unreliable for detection of cirrhosis in patients with acute liver damage. *Hepatology*. 2008 Feb;47(2):592-5.

Saitou Y, Shiraki K, Yamanaka Y, Yamaguchi Y, Kawakita T, Yamamoto N, Sugimoto K, Murata K, Nakano T. Noninvasive estimation of liver fibrosis and response to interferon therapy by a serum fibrogenesis marker, YKL-40, in patients with HCV-associated liver disease. *World J Gastroenterol*. 2005 Jan 28;11(4):476-81.

Sakugawa H, Nakayoshi T, Kobashigawa K, Yamashiro T, Maeshiro T, Miyagi S, Shiroma J, Toyama A, Nakayoshi T, Kinjo F, Saito A. Clinical usefulness of biochemical markers of liver fibrosis in patients with nonalcoholic fatty liver disease. *World J Gastroenterol*. 2005 Jan 14;11(2):255-9.

Sandrin L, Tanter M, Gennisson JL, Catheline S, Fink M. Shear elasticity probe for soft tissues with 1-D transient elastography. *IEEE Trans Ultrason Ferroelectr Freq Control*. 2002 Apr;49(4):436-46.

Santos VN, Leite-Mor MM, Kondo M, Martins JR, Nader H, Lanzoni VP, Parise ER. Serum laminin, type IV collagen and hyaluronan as fibrosis markers in non-alcoholic fatty liver disease. *Braz J Med Biol Res*. 2005 May;38(5):747-53.

Sasaki H, Pollard RB, Schmitt D, Suzuki F. Transforming growth factor-beta in the regulation of the immune response. *Clin Immunol Immunopathol*. 1992 Oct;65(1):1-9.

Saxena NK, Saliba G, Floyd JJ, Anania FA. Leptin induces increased alpha2(I) collagen gene expression in cultured rat hepatic stellate cells. *J Cell Biochem*. 2003 May 15;89(2):311-20.

Scherphof G, Dame J, Wilschut J. Interactions of Liposome with Plasma Proteins. In: Gregoriadis G (Ed). *Liposome Technology*, Vol. III, CRC Press Inc., BocaRaton, FL, 1984.

Scherphof G, Damen J, Hoekstra D. In: Knight CG (Ed). *Liposomes: From Physical structure to Therapeutic Applications*. Elsevier/North Holland Biomedical Press, Amsterdam, 1981.

Scherphof GL, Kamps JA. The role of hepatocytes in the clearance of liposomes from the blood circulation. *Prog Lipid Res*. 2001 May;40(3):149-66.

Schoemaker MH, Conde de la Rosa L, Buist-Homan M, Vrenken TE, Havinga R, Poelstra K, Haisma HJ, Jansen PL, Moshage H. Tauroursodeoxycholic acid protects

rat hepatocytes from bile acid-induced apoptosis via activation of survival pathways. *Hepatology*. 2004 Jun;39(6):1563-73.

Schuppan D, Ruehl M, Somasundaram R, Hahn EG. Matrix as a modulator of hepatic fibrogenesis. *Semin Liver Dis*. 2001 Aug;21(3):351-72.

Schuppan D, Stolzel U, Oesterling C, Somasundaram R. Serum assays for liver fibrosis. *J Hepatol*. 1995;22(2 Suppl):82-8.

Schuppan D. Connective tissue polypeptides in serum as parameters to monitor antifibrotic treatment in hepatic fibrogenesis. *J Hepatol*. 1991;13 Suppl 3:S17-25.

Schwabe RF, Bataller R, Brenner DA. Human hepatic stellate cells express CCR5 and RANTES to induce proliferation and migration. *Am J Physiol Gastrointest Liver Physiol*. 2003 Nov;285(5):G949-58.

Schwartz JB, Connor RE. Optimization techniques in pharmaceutical formulation and processing. In: Banker GS, Rhodes CT (eds). *Modern Pharmaceutics*. 3rd ed. Marcel Dekker, New York, 1996.

Schwartz JB, Flamholz JR, Press RH. Computer optimization of pharmaceutical formulations. I. General procedure. *J Pharm Sci*. 1973 Jul;62(7):1165-70.

Sebastiani G, Vario A, Guido M, Noventa F, Plebani M, Pistis R, Ferrari A, Alberti A. Stepwise combination algorithms of non-invasive markers to diagnose significant fibrosis in chronic hepatitis C. *J Hepatol*. 2006 Apr;44(4):686-93.

Shahin M, Schuppan D, Waldherr R, Risteli J, Risteli L, Savolainen ER, Oesterling C, Abdel Rahman HM, El Sahly AM, Abdel Razek SM, El Ruby O, Koch A, Seitz HK. Serum procollagen peptides and collagen type VI for the assessment of activity and degree of hepatic fibrosis in schistosomiasis and alcoholic liver disease. *Hepatology*. 1992 Apr;15(4):637-44.

Shao R, Yan W, Rockey DC. Regulation of endothelin-1 synthesis by endothelin-converting enzyme-1 during wound healing. *J Biol Chem*. 1999 Jan 29;274(5):3228-34.

Shew RL, Deamer DW. A novel method for encapsulation of macromolecules in liposomes. *Biochim Biophys Acta*. 1985 Jun 11;816(1):1-8.

Shi Z, Wakil AE, Rockey DC. Strain-specific differences in mouse hepatic wound healing are mediated by divergent T helper cytokine responses. *Proc Natl Acad Sci U S A*. 1997 Sep 30;94(20):10663-8.

Shimizu E, Kobayashi Y, Oki Y, Kawasaki T, Yoshimi T, Nakamura H. OPC-13013, a cyclic nucleotide phosphodiesterase type III, inhibitor, inhibits cell proliferation and transdifferentiation of cultured rat hepatic stellate cells. *Life Sci*. 1999;64(23):2081-8.

Singh B, Ahuja N. Response surface optimization of drug delivery system. In: Jain NK (ed). *Progress in Controlled and Novel Drug Delivery Systems*. 1st ed. CBS Publishers, New Delhi, 2004(a).

Singh B, Chakkal SK, Ahuja N. Computer-aided design, development and optimization of controlled release mucoadhesive formulations of atenolol. In: *Proceedings of National Seminar on Pharmaceutics in the Light of Drug Delivery Challenges*; Chandigarh, India, 2003.

Singh B, Gupta RK, Ahuja N. Computer-assisted optimization of pharmaceutical formulations. In: Jain NK (ed). *Pharmaceutical Product Development*. CBS Publishers, New Delhi, 2004(b).

Sliedregt LA, Rensen PC, Rump ET, van Santbrink PJ, Bijsterbosch MK, Valentijn AR, van der Marel GA, van Boom JH, van Berkel TJ, Biessen EA. Design and synthesis of novel amphiphilic dendritic galactosides for selective targeting of liposomes to the hepatic asialoglycoprotein receptor. *J Med Chem.* 1999 Feb 25;42(4):609-18.

Smedsrod B, De Bleser PJ, Braet F, Lovisetti P, Vanderkerken K, Wisse E, Geerts A. Cell biology of liver endothelial and Kupffer cells. *Gut.* 1994 Nov;35(11):1509-16.

Sougioultzis S, Dalakas E, Hayes PC, Plevris JN. Alcoholic hepatitis: from pathogenesis to treatment. *Curr Med Res Opin.* 2005 Sep;21(9):1337-46.

Spanjer HH, van Galen M, Roerdink FH, Regts J, Scherphof GL. Intrahepatic distribution of small unilamellar liposomes as a function of liposomal lipid composition. *Biochim Biophys Acta.* 1986 Dec 16;863(2):224-30.

Stack CB. Confounding and interaction. In: Chow S-C (ed). *Encyclopedia of Biopharmaceutical Statistics*. Marcel Dekker, New York, 2003.

Stamp D, Juliano RL. Factors affecting the encapsulation of drugs within liposomes. *Can J Physiol Pharmacol.* 1979 May;57(5):535-9.

Stetsko G. Statistical experimental design and its application to pharmaceutical development problem. *Drug Dev Ind Pharm.* 1986 Jan; 12(8-9):1109-23.

Sugarman SM, Perez-Soler R. Liposomes in the treatment of malignancy: a clinical perspective. *Crit Rev Oncol Hematol.* 1992;12(3):231-42.

Suzuki A, Angulo P, Lymp J, Li D, Satomura S, Lindor K. Hyaluronic acid, an accurate serum marker for severe hepatic fibrosis in patients with non-alcoholic fatty liver disease. *Liver Int.* 2005 Aug;25(4):779-86.

Svegliati-Baroni G, Saccomanno S, van Goor H, Jansen P, Benedetti A, Moshage H. Involvement of reactive oxygen species and nitric oxide radicals in activation and proliferation of rat hepatic stellate cells. *Liver.* 2001 Feb;21(1):1-12.

Sveinsson SJ, Holbrook WP. Oral mucosal adhesive ointment containing liposomal corticosteroid. *Int J Pharm.* 1993 June 30;95(1-3): 105-9.

Taguchi G. *System of Experimental Designs*. UNIPUB/Krauss International, New York, 1987.

Talsma H, Crommelin DJA. Liposomes as Drug Delivery Systems: Part I: Preparation. *Pharma Tech.* 1992(a);16, 96-106.

Talsma H, Crommelin DJ. Liposome as drug delivery system: part-III: Stabilization. *Pharm. Tech.* 1993;16, 48-59.

Talsma H, Van Steenberg MJ, Crommelin DJA. The cryopreservation of liposomes. 2. Effect of particle size on crystallization behavior and marker retention. *Cryobiology.* 1992(b) Feb;29(1):80-6.

Teare JP, Sherman D, Greenfield SM, Simpson J, Bray G, Catterall AP, Murray-Lyon IM, Peters TJ, Williams R, Thompson RP. Comparison of serum procollagen III

peptide concentrations and PGA index for assessment of hepatic fibrosis. *Lancet*. 1993 Oct 9;342(8876):895-8.

Thabut D, Simon M, Myers RP, Messous D, Thibault V, Imbert-Bismut F, Poynard T. Noninvasive prediction of fibrosis in patients with chronic hepatitis C. *Hepatology*. 2003 May;37(5):1220-1; author reply 1221.

The French METAVIR Cooperative Study Group. Intraobserver and interobserver variations in liver biopsy interpretation in patients with chronic hepatitis C. *Hepatology*. 1994 Jul;20(1 Pt 1):15-20.

Tiegs G, Hentschel J, Wendel A. A T cell-dependent experimental liver injury in mice inducible by concanavalin A. *J Clin Invest*. 1992 Jul;90(1):196-203.

Tiggelman AM, Linthorst C, Boers W, Brand HS, Chamuleau RA. Transforming growth factor-beta-induced collagen synthesis by human liver myofibroblasts is inhibited by alpha2-macroglobulin. *J Hepatol*. 1997 Jun;26(6):1220-8.

Tilg H, Diehl AM. Cytokines in alcoholic and nonalcoholic steatohepatitis. *N Engl J Med*. 2000 Nov 16;343(20):1467-76.

Tolstoshev P. Gene therapy, concepts, current trials and future directions. *Annu Rev Pharmacol Toxicol*. 1993;33:573-96.

Tontonoz P, Hu E, Spiegelman BM. Regulation of adipocyte gene expression and differentiation by peroxisome proliferator activated receptor gamma. *Curr Opin Genet Dev*. 1995 Oct;5(5):571-6.

Torriani FJ, Rodriguez-Torres M, Rockstroh JK, Lissen E, Gonzalez-Garcia J, Lazzarin A, Carosi G, Sasadeusz J, Katlama C, Montaner J, Sette H Jr, Passe S, De Pampphilis J, Duff F, Schrenk UM, Dieterich DT; APRICOT Study Group. Peginterferon Alfa-2a plus ribavirin for chronic hepatitis C virus infection in HIV-infected patients. *N Engl J Med*. 2004 Jul 29;351(5):438-50.

Trafny EA, Antos-Bielska M, Grzybowski J. Antibacterial activity of liposome-encapsulated antibiotics against *Pseudomonas aeruginosa* attached to the matrix of human dermis. *J Microencapsul*. 1999 Jul-Aug;16(4):419-29.

Tran A, Benzaken S, Saint-Paul MC, Guzman-Granier E, Hastier P, Pradier C, Barjoan EM, Demuth N, Longo F, Rampal P. Chondrex (YKL-40), a potential new serum fibrosis marker in patients with alcoholic liver disease. *Eur J Gastroenterol Hepatol*. 2000 Sep;12(9):989-93.

Tsukamoto H. Redox regulation of cytokine expression in Kupffer cells. *Antioxid Redox Signal*. 2002 Oct;4(5):741-8.

Tuma DJ. Role of malondialdehyde-acetaldehyde adducts in liver injury. *Free Radic Biol Med*. 2002 Feb 15;32(4):303-8.

Tye H. Application of statistical 'design of experiments' methods in drug discovery. *Drug Discov Today*. 2004 Jun 1;9(11):485-91.

Ueki T, Kaneda Y, Tsutsui H, Nakanishi K, Sawa Y, Morishita R, Matsumoto K, Nakamura T, Takahashi H, Okamoto E, Fujimoto J. Hepatocyte growth factor gene therapy of liver cirrhosis in rats. *Nat Med*. 1999 Feb;5(2):226-30.

Ueno T, Tamaki S, Sugawara H, Inuzuka S, Torimura T, Sata M, Tanikawa K. Significance of serum tissue inhibitor of metalloproteinases-1 in various liver diseases. *J Hepatol*. 1996 Feb;24(2):177-84.

Van Berkel TJ, Van Eck M, Herijgers N, Fluiters K, Nion S. Scavenger receptor classes A and B. Their roles in atherogenesis and the metabolism of modified LDL and HDL. *Ann N Y Acad Sci*. 2000 May;902:113-26; discussion 126-7.

van Oosten M, van de Bilt E, de Vries HE, van Berkel TJ, Kuiper J. Vascular adhesion molecule-1 and intercellular adhesion molecule-1 expression on rat liver cells after lipopolysaccharide administration in vivo. *Hepatology*. 1995 Nov;22(5):1538-46.

Vargas-Tank L, Martinez V, Jiron MI, Soto JR, Armas-Merino R. Tru-cut and Menghini needles: different yield in the histological diagnosis of liver disease. *Liver*. 1985 Jun;5(3):178-81.

Velupandian T, Gupta SK, Gupta YK, Biswas NR, Agarwal HC. Ocular drug targeting by liposomes and their corneal interactions. *J Microencapsul*. 1999 Mar-Apr;16(2):243-50.

Venkataram S, Awni WM, Jordan K, Rahman YE. Pharmacokinetics of two alternative dosage forms for cyclosporine: liposomes and intralipid. *J Pharm Sci*. 1990 Mar;79(3):216-9.

Villalain J, Aranda FJ, Gomez-Fernandez JC. Calorimetric and infrared spectroscopic studies of the interaction of alpha-tocopherol and alpha-tocopheryl acetate with phospholipid vesicles. *Eur J Biochem*. 1986 Jul 1;158(1):141-7.

Vizzutti F, Arena U, Romanelli RG, Rega L, Foschi M, Colagrande S, Petrarca A, Moscarella S, Belli G, Zignego AL, Marra F, Laffi G, Pinzani M. Liver stiffness measurement predicts severe portal hypertension in patients with HCV-related cirrhosis. *Hepatology*. 2007 May;45(5):1290-7.

Wai CT, Greenson JK, Fontana RJ, Kalbfleisch JD, Marrero JA, Conjeevaram HS, Lok AS. A simple noninvasive index can predict both significant fibrosis and cirrhosis in patients with chronic hepatitis C. *Hepatology*. 2003 Aug;38(2):518-26.

Walsh KM, Fletcher A, MacSween RN, Morris AJ. Basement membrane peptides as markers of liver disease in chronic hepatitis C. *J Hepatol*. 2000 Feb;32(2):325-30.

Walsh KM, Fletcher A, MacSween RN, Morris AJ. Comparison of assays for N-amino terminal propeptide of type III procollagen in chronic hepatitis C by using receiver operating characteristic analysis. *Eur J Gastroenterol Hepatol*. 1999(a) Aug;11(8):827-31.

Walsh KM, Timms P, Campbell S, MacSween RN, Morris AJ. Plasma levels of matrix metalloproteinase-2 (MMP-2) and tissue inhibitors of metalloproteinases -1 and -2 (TIMP-1 and TIMP-2) as noninvasive markers of liver disease in chronic hepatitis C: comparison using ROC analysis. *Dig Dis Sci*. 1999(b) Mar;44(3):624-30.

Wang JY, Guo JS, Li H, Liu SL, Zern MA. Inhibitory effect of glycyrrhizin on NF-kappaB binding activity in CCl4- plus ethanol-induced liver cirrhosis in rats. *Liver*. 1998(a) Jun;18(3):180-5.

Wang L, Wang J, Wang BE, Xiao PG, Qiao YJ, Tan XH. Effects of herbal compound 861 on human hepatic stellate cell proliferation and activation. *World J Gastroenterol.* 2004 Oct 1;10(19):2831-5.

Wang SC, Ohata M, Schrum L, Rippe RA, Tsukamoto H. Expression of interleukin-10 by in vitro and in vivo activated hepatic stellate cells. *J Biol Chem.* 1998(b) Jan 2;273(1):302-8.

Wang ZE, Reiner SL, Zheng S, Dalton DK, Locksley RM. CD4⁺ effector cells default to the Th2 pathway in interferon gamma-deficient mice infected with *Leishmania major*. *J Exp Med.* 1994 Apr 1;179(4):1367-71.

Wanless IR, Nakashima E, Sherman M. Regression of human cirrhosis. Morphologic features and the genesis of incomplete septal cirrhosis. *Arch Pathol Lab Med.* 2000 Nov;124(11):1599-607.

Wehrle P, Stamm A. Statistical tools for process control and quality improvement in the pharmaceutical industry. *Drug Dev Ind Pharm.* 1994 Jan; 20(2):141-64.

Wehrle P, Nobelis P, Cuine A, Stamm A. Response surface methodology: an interesting statistical tool for process optimization and validation: example of wet granulation in a high shear mixer. *Drug Dev Ind Pharm.* 1993 Jan; 19(13):1637-53.

Westin J, Lagging LM, Wejstal R, Norkrans G, Dhillon AP. Interobserver study of liver histopathology using the Ishak score in patients with chronic hepatitis C virus infection. *Liver.* 1999 Jun;19(3):183-7.

Whalen R, Rockey DC, Friedman SL, Boyer TD. Activation of rat hepatic stellate cells leads to loss of glutathione S-transferases and their enzymatic activity against products of oxidative stress. *Hepatology.* 1999 Oct;30(4):927-33.

Winnock M, Garcia Barcina M, Lukomska B, Huet S, Saric J, Balabaud C, Bioulac-Sage P. Human liver-associated lymphocytes: an overview. *J Gastroenterol Hepatol.* 1995;10 Suppl 1:S43-6.

Winwood PJ, Schuppan D, Iredale JP, Kawser CA, Docherty AJ, Arthur MJ. Kupffer cell-derived 95-kd type IV collagenase/gelatinase B: characterization and expression in cultured cells. *Hepatology.* 1995 Jul;22(1):304-15.

Wisse E, De Zanger RB, Charels K, Van Der Smissen P, McCuskey RS. The liver sieve: considerations concerning the structure and function of endothelial fenestrae, the sinusoidal wall and the space of Disse. *Hepatology.* 1985 Jul-Aug;5(4):683-92.

Wong JB, Koff RS. Watchful waiting with periodic liver biopsy versus immediate empirical therapy for histologically mild chronic hepatitis C. A cost-effectiveness analysis. *Ann Intern Med.* 2000 Nov 7;133(9):665-75.

Wong VS, Wight DG, Palmer CR, Alexander GJ. Fibrosis and other histological features in chronic hepatitis C virus infection: a statistical model. *J Clin Pathol.* 1996 Jun;49(6):465-9.

Woo SW, Lee SH, Kang HC, Park EJ, Zhao YZ, Kim YC, Sohn DH. Butein suppresses myofibroblastic differentiation of rat hepatic stellate cells in primary culture. *J Pharm Pharmacol.* 2003 Mar;55(3):347-52.

Woo SW, Nan JX, Lee SH, Park EJ, Zhao YZ, Sohn DH. Aloe emodin suppresses myofibroblastic differentiation of rat hepatic stellate cells in primary culture. *Pharmacol Toxicol.* 2002 Apr;90(4):193-8.

Wright T, Rockey D. Liver disease: from bench to bedside. Report of the postgraduate course by the American Association for the Study of Liver Diseases. 2004 29-30 oct.

Yagura M, Murai S, Kojima H, Tokita H, Kamitsukasa H, Harada H. Changes of liver fibrosis in chronic hepatitis C patients with no response to interferon-alpha therapy: including quantitative assessment by a morphometric method. *J Gastroenterol.* 2000;35(2):105-11.

Yan X, Kuipers F, Havekes LM, Havinga R, Dontje B, Poelstra K, Scherphof GL, Kamps JA. The role of apolipoprotein E in the elimination of liposomes from blood by hepatocytes in the mouse. *Biochem Biophys Res Commun.* 2005(a) Mar 4;328(1):57-62.

Yan X, Poelstra K, Scherphof GL, Kamps JA. A role for scavenger receptor B-I in selective transfer of rhodamine-PE from liposomes to cells. *Biochem Biophys Res Commun.* 2004 Dec 17;325(3):908-14.

Yan X, Scherphof GL, Kamps JA. Liposome opsonization. *J Liposome Res.* 2005(b);15(1-2):109-39.

Yang C, Zeisberg M, Mosterman B, Sudhakar A, Yerramalla U, Holthaus K, Xu L, Eng F, Afdhal N, Kalluri R. Liver fibrosis: insights into migration of hepatic stellate cells in response to extracellular matrix and growth factors. *Gastroenterology.* 2003(a) Jan;124(1):147-59.

Yang W, Chen H, Jiang Y. Inhibitive effect of curcumin and amiloride on the fibrosis of rat hepatic stellate cells induced by oxidative stress. *Zhong Yao Cai.* 2003(b) Nov;26(11):795-8.

Yin M, Talwalkar JA, Glaser KJ, Manduca A, Grimm RC, Rossman PJ, Fidler JL, Ehman RL. Assessment of hepatic fibrosis with magnetic resonance elastography. *Clin Gastroenterol Hepatol.* 2007 Oct;5(10):1207-1213.e2.

Yoshiji H, Kuriyama S, Fukui H. Angiotensin-I-converting enzyme inhibitors may be an alternative anti-angiogenic strategy in the treatment of liver fibrosis and hepatocellular carcinoma. Possible role of vascular endothelial growth factor. *Tumour Biol.* 2002 Nov-Dec;23(6):348-56.

Yoshiji H, Kuriyama S, Yoshii J, Ikenaka Y, Noguchi R, Hicklin DJ, Wu Y, Yanase K, Namisaki T, Yamazaki M, Tsujinoue H, Imazu H, Masaki T, Fukui H. Vascular endothelial growth factor and receptor interaction is a prerequisite for murine hepatic fibrogenesis. *Gut.* 2003 Sep;52(9):1347-54.

Yu Q, Stamenkovic I. Cell surface-localized matrix metalloproteinase-9 proteolytically activates TGF-beta and promotes tumor invasion and angiogenesis. *Genes Dev.* 2000 Jan 15;14(2):163-76.

Zhang BB, Cai WM, Weng HL, Hu ZR, Lu J, Zheng M, Liu RH. Diagnostic value of platelet derived growth factor-BB, transforming growth factor-beta1, matrix metalloproteinase-1, and tissue inhibitor of matrix metalloproteinase-1 in serum and

peripheral blood mononuclear cells for hepatic fibrosis. *World J Gastroenterol.* 2003(a) Nov;9(11):2490-6.

Zhang JX, Pegoli W Jr, Clemens MG. Endothelin-1 induces direct constriction of hepatic sinusoids. *Am J Physiol.* 1994 Apr;266(4 Pt 1):G624-32.

Zhang LJ, Chen YX, Chen ZX, Huang YH, Yu JP, Wang XZ. Effect of interleukin-10 and platelet-derived growth factor on expressions of matrix metalloproteinases-2 and tissue inhibitor of metalloproteinases-1 in rat fibrotic liver and cultured hepatic stellate cells. *World J Gastroenterol.* 2004 Sep 1;10(17):2574-9.

Zhang WS, Cheng ML, Lu YY. Effect of HanDanGanLe on the cytokines in fibrotic rats. *Zhonghua Gan Zang Bing Za Zhi.* 2003(b) May;11(5):285-7.

Zhang XL, Liu L, Jiang HQ. Salvia miltiorrhiza monomer IH764-3 induces hepatic stellate cell apoptosis via caspase-3 activation. *World J Gastroenterol.* 2002 Jun;8(3):515-9.

Zhao YZ, Kim JY, Park EJ, Lee SH, Woo SW, Ko G, Sohn DH. Tetrandrine induces apoptosis in hepatic stellate cells. *Phytother Res.* 2004 Apr;18(4):306-9.

Zheng S, Chen A. Activation of PPARgamma is required for curcumin to induce apoptosis and to inhibit the expression of extracellular matrix genes in hepatic stellate cells in vitro. *Biochem J.* 2004 Nov 15;384(Pt 1):149-57.

Ziol M, Handra-Luca A, Kettaneh A, Christidis C, Mal F, Kazemi F, de Ledinghen V, Marcellin P, Dhumeaux D, Trinchet JC, Beaugrand M. Noninvasive assessment of liver fibrosis by measurement of stiffness in patients with chronic hepatitis C. *Hepatology.* 2005 Jan;41(1):48-54.

CHAPTER 3

ANALYTICAL METHOD DEVELOPMENT



Analytical Methods

3.1 PREPARATION OF CALIBRATION PLOT OF RGZ IN METHANOL

3.1.1 Reagents

3.1.2 Method

3.2 PREPARATION OF CALIBRATION PLOT OF RGZ IN DIFFUSION

MEDIUM [50 mM HPBCD, 20 mM HEPES, pH 7.4]

3.2.1 Reagents

3.2.2 Method

3.3 PREPARATION OF CALIBRATION PLOT OF CDS IN METHANOL

3.3.1 Reagents

3.3.2 Method

3.4 PREPARATION OF CALIBRATION PLOT OF CDS IN DIFFUSION

MEDIUM (100 mM HPBCD, 20 mM HEPES, pH 7.4)

3.4.1 Reagents

3.4.2 Method

3.5 PREPARATION OF CALIBRATION PLOT OF RGZ IN PLASMA BY HPLC METHOD

3.5.1 Reagents

3.5.2 Preparation of standard solutions and calibration standards

3.5.3 Instrumentation

3.5.4 Extraction procedure

3.5.5 HPLC conditions

3.6 PREPARATION OF CALIBRATION PLOT OF CDS IN PLASMA BY HPLC METHOD

3.6.1 Reagents

3.6.2 Preparation of standard solutions and calibration standards

3.6.3 Instrumentation

3.6.4 Extraction procedure

3.6.5 HPLC conditions

3.7 DETERMINATION OF D-MANNOSE

3.7.1 Reagents

3.7.2 Procedure

3.8 DETERMINATION OF PHOSPHORUS.

3.8.1 Principle

3.8.2 Reagents

3.8.3 Procedure

3.9 DETERMINATION OF TOTAL PROTEINS

3.9.1 Principle

3.9.2 Reagents

3.9.3 Procedure

3.9.4 Calculation

3.10 DETERMINATION OF ALBUMIN IN SERUM

3.10.1 Principle

3.10.2 Reagents

3.10.3 Procedure

3.10.4 Calculation

3.11 DETERMINATION OF GLOBULIN IN SERUM

3.12 DETERMINATION OF ASPARTATE AMINOTRANSFERASE (AST) IN SERUM

3.12.1 Principle

3.12.2 Reagents

3.12.3 Procedure

3.12.4 Calculation

3.13 DETERMINATION OF ALANINE AMINOTRANSFERASE (ALT) IN SERUM

3.13.1 Principle

3.13.2 Reagents

3.13.3 Procedure

3.13.4 Calculation

3.14 DETERMINATION OF HYDROXYPROLINE IN TISSUE

3.14.1 Reagents:

3.14.2 Procedure

3.14.2.1 Tissue hydrolysis

3.14.2.2 Hydroxyproline determination

3.14.2.3 Special considerations

3.15 DETERMINATION OF HYALURONIC ACID IN SERUM

3.15.1 Background

3.15.2 Reagent Preparation

3.15.3 Assay Procedure

3.15.4 Reference Values

3.16 DETERMINATION OF TOTAL BILIRUBIN IN SERUM

3.16.1 Principle

3.16.2 Reagents

3.16.3 Procedure

3.16.4 Calculation

3.17 CONCLUSIONS

3.18 REFERENCES

In this investigation, lyophilized formulation comprising functionalized liposomes of RGZ and CDS were prepared for the treatment of liver fibrosis. The chemical characterization of liposomes and developed formulation were carried out to determine the percentage drug entrapment and percentage drug retention. The stability studies were conducted to determine percentage drug retained in liposomes over stage of six months period. In vitro drug diffusion studies followed by in vivo pharmacokinetic studies were also carried out. The analytical methods employed in these investigations are discussed below.

3.1 PREPARATION OF CALIBRATION PLOT OF RGZ IN METHANOL

The spectroscopic determination of RGZ is based on the zero order UV spectra of RGZ giving maxima at 311.8 nm in methanol (The Merck Index, 2001; Martindale, 1996; Goyal and Singhvi, 2007; Jagathi et al., 2010).

3.1.1 Reagents

- (i) Methanol for spectroscopy Uvasol®.
- (ii) Stock solution of RGZ: 1 mg/mL solution of RGZ was prepared in methanol.

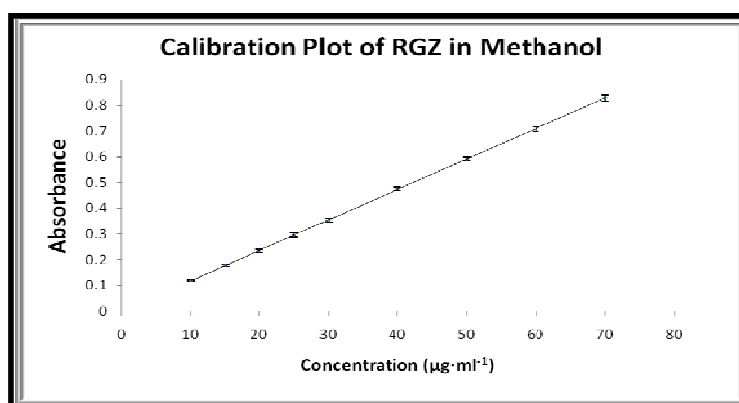
3.1.2 Method

Appropriate aliquots of the stock solution of RGZ were transferred to 10 mL volumetric flasks and were diluted up to the mark with methanol. The absorption maxima (λ_{max}) was determined by scanning 10 $\mu\text{g/mL}$ solution against reagent blank on UV-Visible Spectrophotometer (UV-1700, Shimadzu). The absorption of all the prepared solutions was then measured at the absorbance maxima, 311.8 nm against the reagent blank. The readings were recorded in triplicate. Mean value ($n=3$) along with the standard error of mean (SEM) are recorded in Table 3.1. The regressed values of absorption were plotted graphically against the concentrations, as shown in Figure 3.1.

Stability of the solutions of RGZ in methanol used for preparing the calibration plot was ascertained by observing the changes in the absorbance of the solution at the analytical wavelength, over a period of 48 hr at room temperature.

Table 3.1 Calibration plot of RGZ in methanol for the estimation of RGZ in liposomes (n=3)

Conc.($\mu\text{g/mL}$)	Absorbance ($\pm\text{SEM}$)
10	0.1197 ± 0.0040
15	0.1790 ± 0.0040
20	0.2357 ± 0.0065
25	0.2970 ± 0.0080
30	0.3537 ± 0.0095
40	0.4763 ± 0.0075
50	0.5917 ± 0.0105
60	0.7083 ± 0.0101
70	0.8283 ± 0.0115

Figure 3.1 Calibration plot of RGZ in methanol**Table 3.2 Optical characteristics of RGZ in methanol**

Characteristic	Value
λ_{max}	311.8 nm
Solvent	Methanol
Range	10-70 $\mu\text{g/mL}$
Regression equation	$y = 0.0118x + 0.0012$
Regression Coefficient (R^2)	1.0000

Table 3.3 Accuracy and precision of RGZ estimation by UV- spectroscopic method in methanol (n=6)

Conc.($\mu\text{g}/\text{mL}$)	Obtained Conc. ($\mu\text{g}/\text{mL}$) ($\pm\text{SEM}$)	% Recovery	% RSD
10	10.026 \pm 0.082	100.244	1.370
20	20.067 \pm 0.115	100.335	0.995
40	40.104 \pm 0.237	100.261	1.022
70	69.752 \pm 0.398	99.645	0.988

Accuracy is reflected from % Recovery and precision from % RSD

3.2 PREPARATION OF CALIBRATION PLOT OF RGZ IN DIFFUSION

MEDIUM [50 mM HPBCD, 20 mM HEPES, pH 7.4]

The spectroscopic determination of RGZ is based on the zero order UV spectra of RGZ giving maxima at 313.8 nm in diffusion medium (50 mM HPBCD, 20 mM HEPES, pH 7.4) (The Merck Index, 2001; Martindale, 1996; Goyal and Singhvi, 2007; Jagathi et al., 2010).

3.2.1 Reagents

- (i) Freshly prepared diffusion medium (50 mM HPBCD, 20 mM HEPES, pH 7.4).
- (ii) Stock solution of RGZ: 0.5 mg/mL solution of RGZ was prepared in diffusion medium (50 mM HPBCD, 20 mM HEPES, pH 7.4).

3.2.2 Method

Appropriate aliquots of the stock solution of RGZ were transferred to 10mL volumetric flasks and were diluted up to the mark with diffusion medium (50 mM HPBCD, 20 mM HEPES, pH 7.4). The absorption maxima (λ_{max}) was determined by scanning 10 $\mu\text{g}/\text{mL}$ solution against reagent blank on UV-Visible Spectrophotometer (UV-1700, Shimadzu). The absorption of all the prepared solutions was then measured at the absorbance maxima, 313.8 nm against the reagent blank. The readings were recorded in triplicate. Mean value (n=3) along with the standard error of mean (SEM) are recorded in Table 3.4. The regressed values of absorption were plotted graphically against the concentrations, as shown in Figure 3.2.

Stability of the solutions of RGZ in diffusion medium (50 mM HPBCD, 20 mM HEPES, pH 7.4) used for preparing the calibration plot, was ascertained by observing

the changes in the absorbance of the solution at the analytical wavelength, over a period of 48 hr at room temperature.

Table 3.4 Calibration plot of RGZ in diffusion medium (50 mM HPBCD, 20 mM HEPES, pH 7.4) for the estimation of RGZ during diffusion (n=3)

Conc.($\mu\text{g/mL}$)	Absorbance ($\pm\text{SEM}$)
10	0.1163 ± 0.0035
15	0.1747 ± 0.0043
20	0.2293 ± 0.0060
25	0.2892 ± 0.0075
30	0.3470 ± 0.0101
40	0.4650 ± 0.0085
50	0.5887 ± 0.0106
60	0.7087 ± 0.0075
70	0.8070 ± 0.0110

Figure 3.2 Calibration plot of RGZ in diffusion medium (50 mM HPBCD, 20 mM HEPES, pH 7.4)

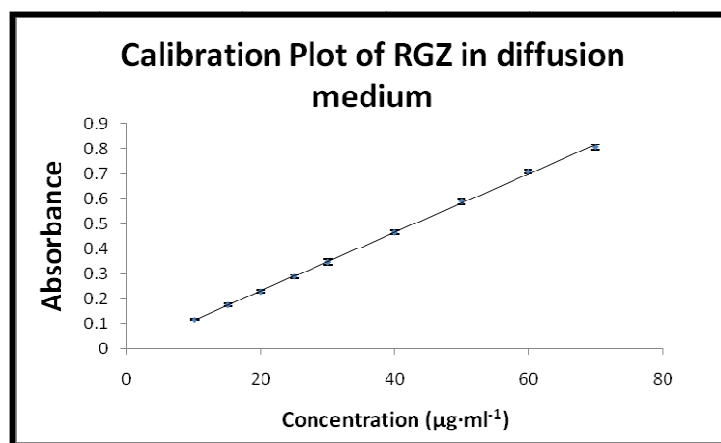


Table 3.5 Optical characteristics of RGZ in diffusion medium (50 mM HPBCD, 20 mM HEPES, pH 7.4)

Characteristic	Value
λ_{\max}	313.8 nm
Solvent	50 mM HPBCD, 20 mM HEPES, pH 7.4
Range	10-70 $\mu\text{g/mL}$
Regression equation	$y = 0.0117x - 0.0015$
Regression Coefficient (R^2)	0.9995

Table 3.6 Accuracy and precision of RGZ estimation by UV method in diffusion medium (n=6)

Conc. ($\mu\text{g/mL}$)	Obtained Conc. ($\mu\text{g/mL}$) ($\pm\text{SEM}$)	% Recovery	% RSD
10	9.986 ± 0.088	99.858	1.525
20	20.053 ± 0.163	100.267	1.410
40	40.112 ± 0.205	100.280	0.884
70	70.237 ± 0.419	100.339	1.033

Accuracy is reflected from % Recovery and precision from % RSD

3.3 PREPARATION OF CALIBRATION PLOT OF CDS IN METHANOL

The spectroscopic determination of CDS is based on the zero order UV spectra of CDS giving maxima at 304.8 nm in methanol (The Merck Index, 2006; Martindale, 2002; Patil et al., 2011).

3.3.1 Reagents

- (i) Methanol for spectroscopy Uvasol®.
- (ii) Stock solution of CDS: 1 mg/mL solution of CDS was prepared in methanol.

3.3.2 Method

Appropriate aliquots of the stock solution of CDS were transferred to 10 mL volumetric flasks and were diluted up to the mark with methanol. The absorption maxima (λ_{\max}) was determined by scanning 10 $\mu\text{g/mL}$ solution against reagent blank on UV-Visible Spectrophotometer (UV-1700, Shimadzu). The absorption of all the prepared solutions was then measured at the absorbance maxima, 304.8 nm against

the reagent blank. The readings were recorded in triplicate. Mean value (n=3) along with the standard error of mean (SEM) are recorded in Table 3.7. The regressed values of absorption were plotted graphically against the concentrations, as shown in Figure 3.3.

Stability of the solutions of CDS in methanol used for preparing the calibration Plot was ascertained by observing the changes in the absorbance of the solution at the analytical wavelength, over a period of 48 hr at room temperature.

Table 3.7 Calibration Plot of CDS in methanol for the estimation of CDS in liposomes (n=3)

Conc.($\mu\text{g/mL}$)	Absorbance ($\pm\text{SEM}$)
5	0.0467 \pm 0.0015
10	0.0933 \pm 0.0040
15	0.1437 \pm 0.0051
20	0.1983 \pm 0.0067
25	0.2393 \pm 0.0086
30	0.2890 \pm 0.0105
35	0.3313 \pm 0.0116
40	0.3807 \pm 0.0097
50	0.4803 \pm 0.0120
60	0.5677 \pm 0.0111
70	0.6723 \pm 0.0115
80	0.7663 \pm 0.0120

Figure 3.3 Calibration plot of CDS in methanol

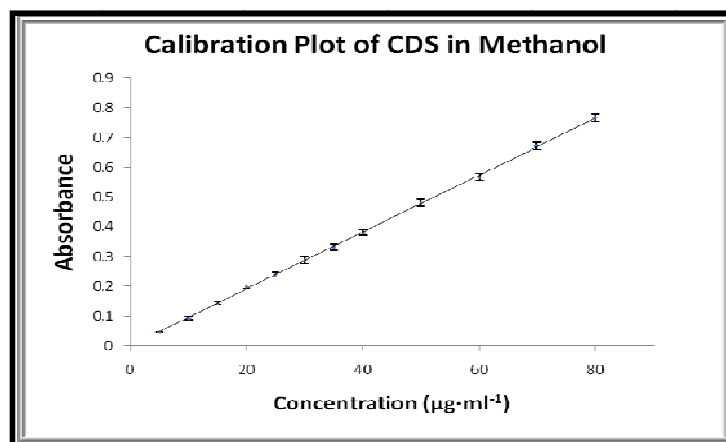


Table 3.8 Optical characteristics of CDS in methanol

Characteristic	Value
λ_{\max}	304.8 nm
Solvent	Methanol
Range	5-80 $\mu\text{g/mL}$
Regression equation	$y = 0.0096x + 0.0001$
Regression Coefficient (R^2)	0.9998

Table 3.9 Accuracy and precision of CDS estimation by UV- spectroscopic method in methanol (n=6)

Conc.($\mu\text{g/mL}$)	Obtained Conc. ($\mu\text{g/mL}$) ($\pm\text{SEM}$)	% Recovery	% RSD
10	10.026 ± 0.091	100.261	1.578
20	19.954 ± 0.123	99.771	1.070
40	39.897 ± 0.199	99.734	0.863
70	70.227 ± 0.368	100.324	0.906

Accuracy is reflected from % Recovery and precision from % RSD

3.4 PREPARATION OF CALIBRATION PLOT OF CDS IN DIFFUSION

MEDIUM (100 mM HPBCD, 20 mM HEPES, pH 7.4)

The spectroscopic determination of CDS is based on the zero order UV spectra of CDS giving maxima at 306.2 nm in diffusion medium (100 mM HPBCD, 20 mM HEPES, pH 7.4) (The Merck Index, 2006; Martindale, 2002; Patil et al., 2011).

3.4.1 Reagents

- (i) Freshly prepared diffusion medium (100 mM HPBCD, 20 mM HEPES, pH 7.4).
- (ii) Stock solution of CDS: 0.5 mg/mL solution of CDS was prepared in diffusion medium (100 mM HPBCD, 20 mM HEPES, pH 7.4).

3.4.2 Method

Appropriate aliquots of the stock solution of CDS were transferred to 10 mL volumetric flasks and were diluted up to the mark with diffusion medium (100 mM HPBCD, 20 mM HEPES, pH 7.4). The absorption maxima (λ_{\max}) was determined by scanning 10 $\mu\text{g/mL}$ solution against reagent blank on UV-Visible Spectrophotometer

(UV-1700, Shimadzu). The absorption of all the prepared solutions was then measured at the absorbance maxima, 306.2 nm against the reagent blank. The readings were recorded in triplicate. Mean value (n=3) along with the standard error of mean (SEM) are recorded in Table 3.10. The regressed values of absorption were plotted graphically against the concentrations, as shown in Figure 3.4.

Stability of the solutions of CDS in diffusion medium (100 mM HPBCD, 20 mM HEPES, pH 7.4) used for preparing the calibration plot, was ascertained by observing the changes in the absorbance of the solution at the analytical wavelength, over a period of 48 hr at room temperature.

Table 3.10 Calibration plot of CDS in diffusion medium (100 mM HPBCD, 20 mM HEPES, pH 7.4) for the estimation of CDS during diffusion (n=3)

Conc. ($\mu\text{g/mL}$)	Absorbance ($\pm\text{SEM}$)
5	0.0493 \pm 0.0035
10	0.0977 \pm 0.0047
15	0.1523 \pm 0.0057
20	0.2117 \pm 0.0075
25	0.2557 \pm 0.0095
30	0.3090 \pm 0.0125
35	0.3527 \pm 0.0111
40	0.4050 \pm 0.0092
50	0.5107 \pm 0.0115
60	0.6040 \pm 0.0105
70	0.7080 \pm 0.0122
80	0.8247 \pm 0.0106

Figure 3.4 Calibration plot of CDS in diffusion medium (100 mM HPBCD, 20 mM HEPES, pH 7.4)

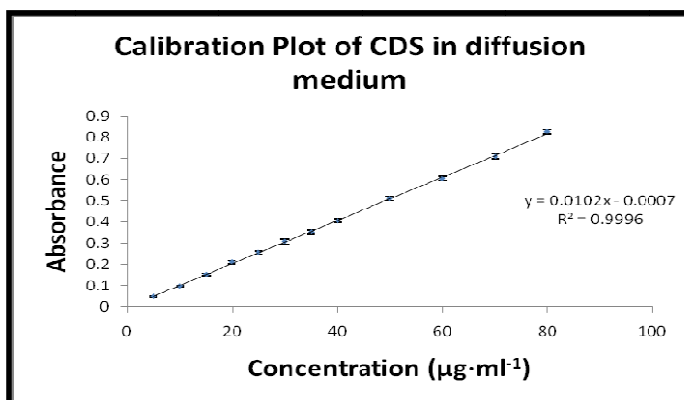


Table 3.11 Optical characteristics of CDS in diffusion medium (100 mM HPBCD, 20 mM HEPES, pH 7.4)

Characteristic	Value
λ_{\max}	306.2 nm
Solvent	100 mM HPBCD, 20 mM HEPES, pH 7.4
Range	5-80 $\mu\text{g/mL}$
Regression equation	$y = 0.0102x - 0.0007$
Regression Coefficient (R^2)	0.9996

Table 3.12 Accuracy and precision of CDS estimation by UV- spectroscopic method in diffusion medium (n=6)

Conc.($\mu\text{g/mL}$)	Obtained Conc. ($\mu\text{g/mL}$) ($\pm\text{SEM}$)	% Recovery	% RSD
10	9.973 ± 0.094	99.728	1.627
20	19.950 ± 0.194	99.749	1.686
40	40.993 ± 0.248	102.482	1.048
70	69.782 ± 0.427	99.689	1.061

Accuracy is reflected from % Recovery and precision from % RSD

3.5 PREPARATION OF CALIBRATION PLOT OF RGZ IN PLASMA BY HPLC METHOD

The chromatographic determination of RGZ in plasma is based on reversed-phase HPLC method with UV detection (Radhakrishna et al., 2002; Lin et al., 2004; Kang et al., 2009; Mamidi et al., 2003; Kim and Park, 2004; Muxlow, 2001; Kolte et al., 2003; Pedersen et al., 2005; Hruska and Frye, 2004).

3.5.1 Reagents

- (i) Sodium acetate solution 10 mM (pH 5) (0.8203 g of monobasic potassium phosphate in 800 mL of water and adjusting to pH 5 with 0.5 N HCl or 0.5 N NaOH and diluting to 1000 mL with water).
- (ii) Methanol for liquid chromatography LiChrosolv®
- (iii) Acetonitrile for liquid chromatography LiChrosolv®

(iv) Freshly prepared mobile phase (10mM sodium acetate pH 5: acetonitrile: methanol (40 : 40 : 20, v/v/v))

(v) Stock solution of RGZ: 1 mg/mL solution of RGZ was prepared in mobile phase.

3.5.2 Preparation of standard solutions and calibration standards

Stock solutions were prepared by dissolving RGZ in mobile phase to yield primary solutions with a concentration of 1 mg/mL of RGZ. Calibration standards were prepared by spiking working standard solutions into drug-free plasma to yield concentrations of 0.05 µg/mL – 10 µg/mL of RGZ. Triplicate calibration plots were analyzed daily for 3 days.

3.5.3 Instrumentation

The HPLC system Prominence LC-20AT (Shimadzu, Kyoto, Japan) consisted of a LC-20AT pump with a manual injector 20 µL fixed loop, equipped with a UV-VIS detector set at 245.0 nm, with Spinchrom CFR software version 2.4.1.93.

3.5.4 Extraction procedure

RGZ solutions (50 µL) were added and the tube was vortexed for 1 min, was added to plasma samples (200 µL) in microcentrifuge tubes and vortexed briefly. ACN (600 µL) was then added to each sample, vortexed for 2 min, and centrifuged at 3500 g for 10 min. Supernatant was evaporated using nitrogen gas at 45 °C. Dried samples were reconstituted with 200 µL of mobile phase and were ready for analysis by HPLC.

3.5.5 HPLC conditions

The chromatographic analysis was carried out on a GRACE Brava™ BDS C18 (5 µm, 25 cm × 4.6 mm) column maintained at 30 ± 0.5°C. RGZ was eluted using a mobile phase composition of 10mM sodium acetate (pH 5): acetonitrile: methanol (40:40:20, v/v/v) at a flow rate 1.0 mL·min⁻¹. The mobile phase was premixed, filtered through a 0.45 mm Nylon 66 membrane filter and degassed before use. RGZ was detected at 245.0 nm and was eluted in 6.7 min after injection.

The calibration plot was linear ($r^2 > 0.9996$) in the concentration range of 0.05-10 µg/mL, and the quantitation limit at 5:1 signal to noise ratio was 0.05 µg/mL.

Table 3.13 Calibration plot of RGZ in plasma by HPLC method (n=3)

Conc. ($\mu\text{g/mL}$)	Peak area ($\text{mV}\cdot\text{s}$) ($\pm\text{SEM}$)
0.05	1.854 ± 0.317
0.1	4.192 ± 0.485
0.2	7.014 ± 1.808
0.4	14.819 ± 2.059
0.8	26.828 ± 1.904
1	34.326 ± 2.151
2	68.254 ± 2.502
4	140.764 ± 3.513
5	177.454 ± 3.822
8	284.562 ± 3.541
10	364.511 ± 3.433

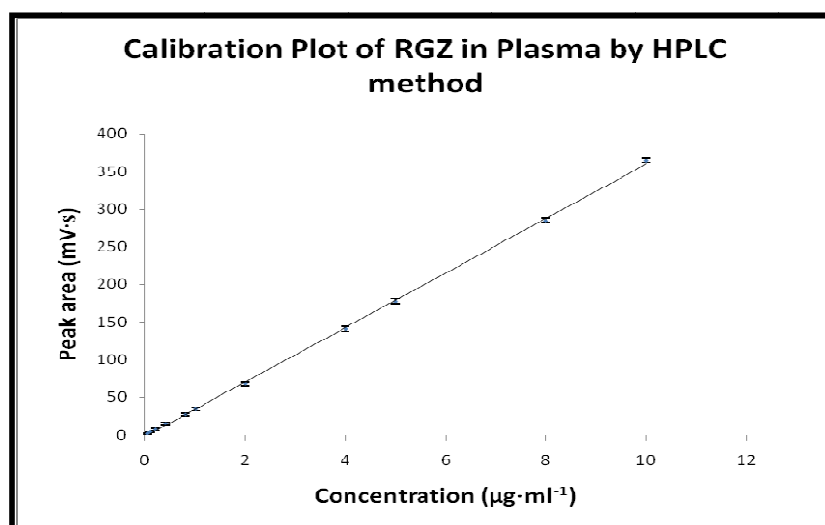
Figure 3.5 Calibration plot of RGZ in plasma by HPLC Method

Table 3.14 Chromatographic conditions

Characteristic	Condition
Column	GRACE Brava™ BDS C18 (5 µm, 25 cm × 4.6 mm)
Column temperature	30 ± 0.5°C
Mobile phase	10mM sodium acetate (pH 5): acetonitrile: methanol (40:40:20, v/v/v)
Flow rate	1.0 mL·min ⁻¹
Injection volume	20 µL
Detection wavelength	245.0
Range	0.05-10 µg/mL
Regression equation	y = 36.1473x - 1.5747
Regression Coefficient (R ²)	0.9996

Table 3.15 Accuracy and precision of RGZ estimation by HPLC method (n=6)

Conc.(µg/mL)	Obtained Conc. (µg/mL) (±SEM)	% Recovery	% RSD
0.8	0.802 ± 0.0073	100.276	1.576
2	1.992 ± 0.0173	99.585	1.506
4	3.916 ± 0.0219	97.910	0.970
8	8.029 ± 0.0399	100.357	0.861

Accuracy is reflected from % Recovery and precision from % RSD

3.6 PREPARATION OF CALIBRATION PLOT OF CDS IN PLASMA BY HPLC METHOD

The chromatographic determination of CDS in plasma is based on reversed-phase HPLC method with UV detection (Gonzalez et al., 2000; Daneshtalab et al., 2002; Qutab et al., 2007; Subba Rao et al., 2007; Stenhoff et al., 1999; Erk, 2003).

3.6.1 Reagents

- (i) Potassium dihydrogen phosphate 10 mM (1.3609 g of Potassium dihydrogen phosphate in 1000 mL of water).
- (ii) Methanol for liquid chromatography LiChrosolv®
- (iii) Acetonitrile for liquid chromatography LiChrosolv®
- (iv) Freshly prepared mobile phase (methanol: acetonitrile: 10mM sodium acetate pH 5 (74 : 16 : 10, v/v/v) pH 2.5 adjusted with 0.5 N HCl or 0.5 N NaOH)

(v) Stock solution of CDS: 1 mg/mL solution of CDS was prepared in mobile phase.

3.6.2 Preparation of standard solutions and calibration standards

Stock solutions were prepared by dissolving CDS in mobile phase to yield primary solutions with a concentration of 1 mg/mL of CDS. Calibration standards were prepared by spiking working standard solutions into drug-free plasma to yield concentrations of 0.05 µg/mL – 10 µg/mL of CDS. Triplicate calibration plots were analyzed daily for 3 days.

3.6.3 Instrumentation

The HPLC system Prominence LC-20AT (Shimadzu, Kyoto, Japan) consisted of a LC-20AT pump with a manual injector 20 µL fixed loop, equipped with a UV-VIS detector set at 260.0 nm, with Spinchrom CFR software version 2.4.1.93.

3.6.4 Extraction procedure

CDS solutions (50 µL) were added and the tube was vortexed for 1 min, was added to plasma samples (200 µL) in microcentrifuge tubes and vortexed briefly. ACN (600 µL) was then added to each sample, vortexed for 2 min, and centrifuged at 3500 g for 10 min. Supernatant was evaporated using nitrogen gas at 45 °C. Dried samples were reconstituted with 200 µL of mobile phase and were ready for analysis by HPLC.

3.6.5 HPLC conditions

The chromatographic analysis was carried out on a GRACE Brava™ BDS C18 (5 µm, 25 cm × 4.6 mm) column maintained at 30 ± 0.5°C. CDS was eluted using a mobile phase composition of methanol: acetonitrile: 10mM sodium acetate pH 5 (74 : 16 : 10, v/v/v) (pH 2.5) at a flow rate 1.0 mL·min⁻¹. The mobile phase was premixed, filtered through a 0.45 µm Nylon 66 membrane filter and degassed before use. CDS was detected at 260.0 nm and was eluted in 4.5 min after injection.

The calibration plot was linear ($r^2 > 0.9997$) in the concentration range of 0.05-10 µg/mL, and the quantitation limit at 5:1 signal to noise ratio was 0.05 µg/mL.

Table 3.16 Calibration plot of CDS in plasma by HPLC method (n=3)

Conc. ($\mu\text{g/mL}$)	Peak area ($\text{mV}\cdot\text{s}$) ($\pm\text{SEM}$)
0.05	1.247 ± 0.266
0.1	2.554 ± 0.433
0.2	4.645 ± 0.884
0.4	7.902 ± 1.083
0.8	14.958 ± 1.317
1	19.145 ± 1.857
2	36.057 ± 2.504
4	73.039 ± 2.837
5	92.977 ± 3.054
8	143.811 ± 3.268
10	184.242 ± 2.573

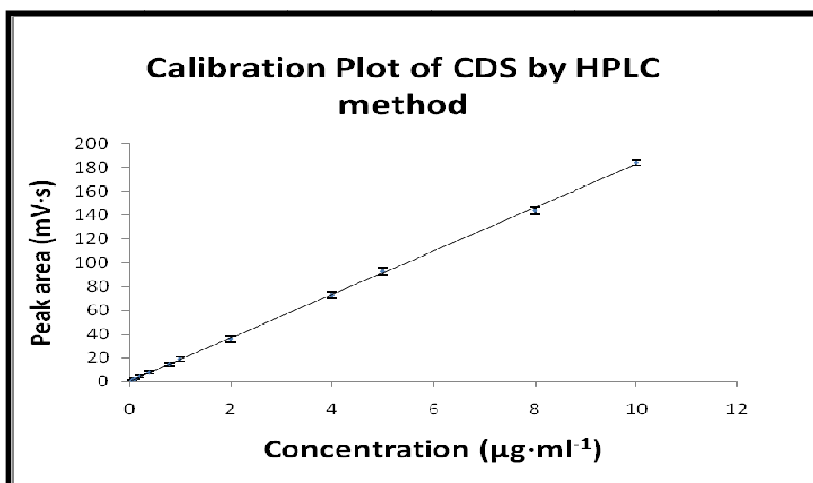
Figure 3.6 Calibration plot of CDS in plasma by HPLC

Table 3.17 Chromatographic conditions

Characteristic	Condition
Column	GRACE Brava™ BDS C18 (5 μ m, 25 cm \times 4.6 mm)
Column temperature	30 \pm 0.5°C
Mobile phase	Methanol: acetonitrile: 10mM sodium acetate pH 5 (74 : 16 : 10, v/v/v) (pH 2.5)
Flow rate	1.0 mL \cdot min ⁻¹
Injection volume	20 μ L
Detection wavelength	260.0
Range	0.05-10 μ g/mL
Regression equation	y = 18.2094x + 0.5733
Regression Coefficient (R ²)	0.9997

Table 3.18 Accuracy and precision of CDS estimation by HPLC method (n=6)

Conc.(μ g/mL)	Obtained Conc. (μ g/mL) (\pm SEM)	% Recovery	% RSD
0.8	0.799 \pm 0.0081	99.874	1.756
2	1.995 \pm 0.0152	99.749	1.320
4	4.100 \pm 0.0229	102.488	0.966
8	7.966 \pm 0.0319	99.571	0.694

Accuracy is reflected from % Recovery and precision from % RSD

3.7 DETERMINATION OF D-MANNOSE (Dubois et al., 1956)

3.7.1 Reagents

Reagent 1: Sulfuric acid

Reagent 2: Phenol (80% by weight in water)

3.7.2 Procedure

2 mL of sugar solution containing between 10-70 μ g of D-Mannose is pipette into a colorimetric tube, and 0.05 mL of 80% phenol is added. Then 5 mL of concentrated sulfuric acid is added rapidly, the stream of acid being directed against the liquid surface rather than against the side of the test tube in order to obtain good mixing. The tubes are allowed to stand for 10 minutes, and then they are shaken and placed for 10 to 20 minutes in a water bath at 25° to 30°C before readings are taken. The color is stable for several hours and readings may be made later if necessary. The absorbance

of the characteristic yellow-orange color is measured at 490 nm. Blank is prepared by substituting distilled water for sugar solution. All solutions were prepared in triplicate to minimize errors.

Table 3.19 Calibration plot of D-Mannose (n=3)

Conc. ($\mu\text{g/mL}$)	Absorbance ($\pm\text{SEM}$)
10	0.119 ± 0.013
20	0.237 ± 0.010
30	0.347 ± 0.012
40	0.438 ± 0.019
50	0.548 ± 0.019
60	0.677 ± 0.020
70	0.768 ± 0.015
80	0.893 ± 0.018

Figure 3.7 Calibration plot of D-Mannose

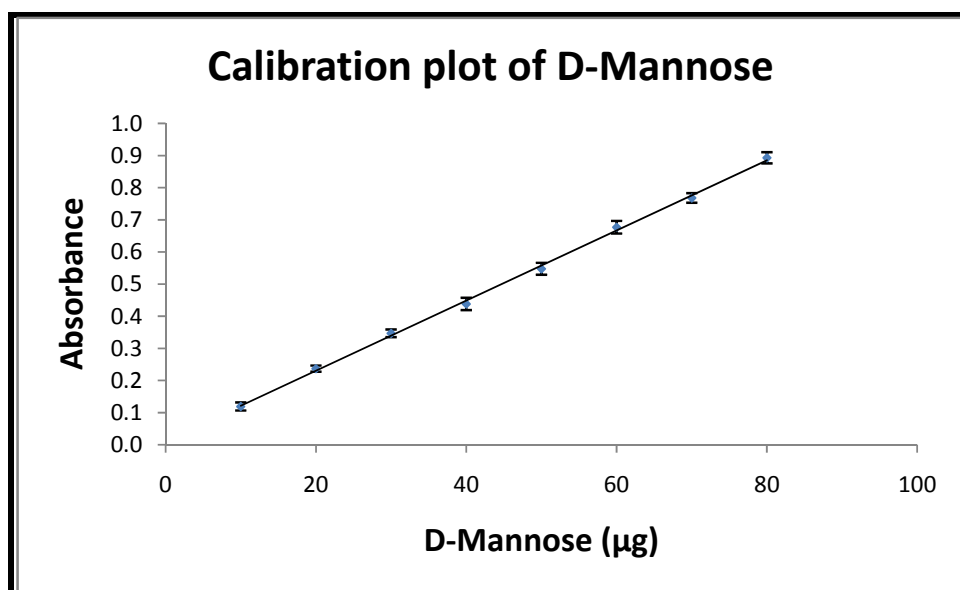


Table 3.20 Optical characteristics

Characteristic	Value
λ_{max}	490 nm
Range	10-80 μg
Regression equation	$y = 0.0109x - 0.0122$
Regression Coefficient (R^2)	0.9989

Table 3.21 Accuracy and precision of D-Mannose estimation by Colorimetric method (n=6)

Conc.($\mu\text{g}/\text{mL}$)	Obtained Conc. ($\mu\text{g}/\text{mL}$) ($\pm\text{SEM}$)	% Recovery	% RSD
10	10.030 \pm 0.157	100.299	2.597
20	19.936 \pm 0.305	99.682	2.646
40	39.883 \pm 0.464	99.706	2.014
70	69.787 \pm 0.870	99.695	2.160

Accuracy is reflected from % Recovery and precision from % RSD

3.8 DETERMINATION OF PHOSPHORUS.

3.8.1 Principle

In this method phosphorus in the sample is first acid hydrolyzed inorganic phosphate. This is converted to phosphor-molybdic acid by the addition of ammonium molybdate, and the pho-molybdic acid is quantitatively reduced to a blue colored compound by amino-naphthyl-sulfonic acid. The intensity of the blue color is measured spectroscopically, and is compared with calibration standards to give phosphorus content (Bottcher et al., 1961; Bartlett, 1959).

3.8.2 Reagents

1. Reagent 1: Sulfuric acid (5M) reagent
2. Reagent 2: Phosphate standard solutions: Dry a sample of solid anhydrous potassium dihydrogen phosphate at 105°C for 4 hours in a vacuum oven. Weigh out 43.55 mg of dried solid and transfer to a 100 mL volumetric flask. Dissolve in double distilled water, and make up to 100 mL. The final concentration should be 3.2 μmol phosphorus mL^{-1} . For working standard solutions transfer 0.5, 1.0, 1.5, 2.0, 2.5, 3.0, 3.5, 4.0, 4.5, 5.0 and 5.5 mL of stock phosphate solution into separate 100 mL volumetric flasks and make up to the mark with double distilled water to give solutions with concentration of 0.016, 0.032, 0.048, 0.064, 0.080, 0.096, 0.112, 0.128, 0.144, 0.160 and 0.176 μmol phosphorus mL^{-1} respectively (Equivalent to 0.5, 1.0, 1.5, 2.0, 2.5, 3.0, 3.5, 4.0, 4.5, 5.0, and 5.5 μg of phosphorus).
3. Reagent 3: Ammonium molybdate – sulfuric acid reagent: Add 5 mL of the sulfuric acid reagent to approximately 50 mL of distilled water and add 0.44 g

of ammonium molybdate. Mix well and make up to 200 mL with distilled water.

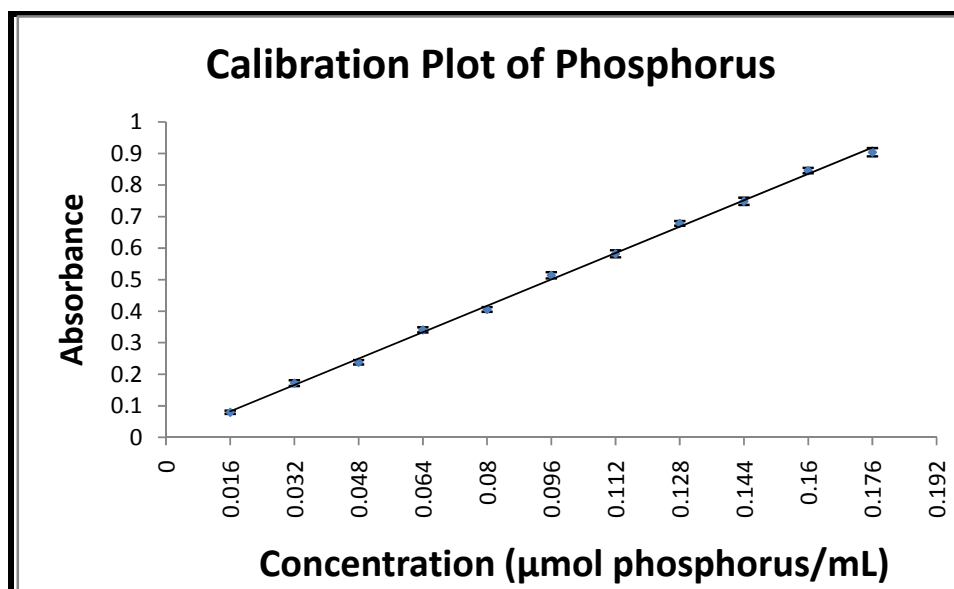
4. Reagent 4: 1-Amino 2-naphthyl 4-sulfonic acid reagent: Weigh out 0.8 g and dissolve in 5 mL of double distilled water. Prepare fresh on day of use.
5. Reagent 5: Hydrogen peroxide: Add 1 mL of 100 % hydrogen peroxide to 9 mL of distilled water and mix well. Prepare fresh immediately before use.

3.8.3 Procedure

1. Equilibrate heating block by pre-heating at 200°C for 30 min.
2. Set up calibration curve by pipetting, into separate 16 × 150 mm disposable borosilicate tubes, 0.5 mL of each working standard solution, together with a blank (0.5 mL of double distilled water).
3. Prepare sample tube in triplicate by adding 50 µL of the sample to each three empty tubes. Dry down and resuspend in 0.5 mL of distilled water.
4. Add 0.4 mL of sulfuric acid reagent to each tube, cover and incubate in a heating block in a fume hood at 180 – 200 °C for an hour.
5. Allow the tubes to cool by standing them at room temperature.
6. Prepare diluted hydrogen peroxide (10%) fresh.
7. To each tube add 0.1 mL of diluted hydrogen peroxide and incubate on the heating block at 180 – 200 for 30 min to achieve a clear solution. (If necessary, repeat addition and heating until solution is clear.)
8. Cool the tubes by standing them at room temperature.
9. Add 4.6 mL of acid – molybdate solution to each tube and mix thoroughly by vortexing.
10. Add 0.2 mL of reagent 4 to each tube and mix thoroughly by vortexing after addition.
11. Cover the tubes and place them in boiling water bath.
12. Leave the tubes in the bath for 7 min after boiling recommences.
13. Cool the tubes to room temperature.
14. Measure absorbance of all tubes against distilled water at 830 nm. The concentration in the starting sample is ten times that read off the graph of the standard curve.

Table 3.22 Calibration plot of Phosphorus (n=3)

Conc. (μmol phosphorus/mL) [μg of phosphorus]	Absorbance ($\pm\text{SEM}$)
0.016 [0.5]	0.079 \pm 0.0051
0.032 [1.0]	0.172 \pm 0.0090
0.048 [1.5]	0.238 \pm 0.0070
0.064 [2.0]	0.341 \pm 0.0080
0.080 [2.5]	0.406 \pm 0.0075
0.096 [3.0]	0.514 \pm 0.0099
0.112 [3.5]	0.582 \pm 0.0111
0.128 [4.0]	0.678 \pm 0.0074
0.144 [4.5]	0.749 \pm 0.0115
0.160 [5.0]	0.846 \pm 0.0086
0.176 [5.5]	0.904 \pm 0.0132

Figure 3.8 Calibration plot of Phosphorus**Table 3.23 Optical characteristics**

Characteristic	Value
λ_{max}	830 nm
Range	0.5-5.5 μg of phosphorus
Regression equation	$y = 5.2302x - 0.0014$
Regression Coefficient (R^2)	0.9987

Table 3.24 Accuracy and precision of Phosphorus by spectroscopic method (n=6)

Conc.($\mu\text{mol/mL}$)	Obtained Conc. ($\mu\text{mol/mL}$) ($\pm\text{SEM}$)	% Recovery	% RSD
0.032	0.0320 \pm 0.0008	100.125	4.207
0.064	0.0646 \pm 0.0014	100.953	3.753
0.128	0.1264 \pm 0.0022	98.719	3.016
0.176	0.1771 \pm 0.0026	100.648	2.542

Accuracy is reflected from % Recovery and precision from % RSD

3.9 DETERMINATION OF TOTAL PROTEINS

3.9.1 Principle

Proteins react with copper of Biuret reagent in alkaline medium to form a blue purple complex with absorption maximum at 550 nm (Gornall et al., 1949; Smith et al., 1985).

3.9.2 Reagents

Reagent 1: Biuret reagent

Reagent 2: Protein standard

3.9.3 Procedure

Table 3.25 Procedure for determination of total protein

	Blank (B)	Standard (S)	Test (T)
Sample	---	---	0.1 mL
Reagent 2: Protein standard	---	0.1 mL	---
Reagent 1: Biuret reagent	2.5 mL	2.5 mL	2.5 mL

Mix well. Allow tubes to stand at R.T. for 5 min. measure the O.D. of Standard(S) and Test(T) at 550 nm on spectrophotometer.

3.9.4 Calculation

$$\text{Total protein } \left(\frac{g}{100ml}\right) = \frac{O.D. \text{ Test}}{O.D. \text{ Std.}} \times \text{Conc. of total protein (Std.)}$$

3.10 DETERMINATION OF ALBUMIN IN SERUM

3.10.1 Principle

Determination of albumin in serum or plasma is based on the binding behavior of the protein with the dye bromocresol green. At pH 4.0, albumin acts as a cation and binds to the anionic dye, forming a green complex, the absorbance of which is measured at 630 nm against reagent blank(B) (Rodkey, 1965; McDonald and Gerarde, 1963; Varley, 1980; Corcoran and Durnan, 1977; Gustafsson, 1976).

3.10.2 Reagents

Reagent 1: Albumin reagent (Bromocresol green, Buffer pH 3.8, preservative, surfactant)

Reagent 2: Albumin standard 4.0 gm/dL (Bovine serum albumin, Buffer, Preservatives)

3.10.3 Procedure

Table 3.26 Basic parameters for determination of Albumin in serum

Parameter	Value
Detection wavelength	630 nm
Temperature	Room temperature
Blank	Reagent blank
Incubation time	1 min
Sample volume	10 μ L
Reagent volume	1000 μ L
Concentration of standard	4.0 gm/dL
Stability of color	2 hours
Unit	gm/dL

Table 3.27 Procedure for determination of Albumin in serum

	Blank (B)	Standard (S)	Test (T)
Sample	---	---	0.1 μ L
Reagent 2: Albumin standard	---	10 μ L	---
Reagent 1: Albumin reagent	1.0 mL	1.0 mL	1.0 mL

Mix well. Allow tubes to stand at R.T. for 1 min. measure the O.D. of Standard(S) and Test(T) at 630 nm on colorimeter against reagent blank(B).

3.10.4 Calculation

$$\text{Albumin} \left(\frac{g}{dl} \right) = \frac{\text{Absorbance of Test}}{\text{Absorbance of Std.}} \times 4.0$$

3.11 DETERMINATION OF GLOBULIN IN SERUM

Amount of globulin in serum was derived from the amount of total protein and albumin in serum according to following formula.

$$\text{Globulin} \left(\frac{g}{100 ml} \right) = \text{Serum total protein} \left(\frac{g}{100 ml} \right) - \text{Serum albumin} \left(\frac{g}{100 ml} \right)$$

3.12 DETERMINATION OF ASPARTATE AMINOTRANSFERASE (AST) IN SERUM

3.12.1 Principle

Aspartate aminotransferase (AST) catalyses the transamination of L- Aspartate and α -ketoglutarate (α -KG) to form Oxaloacetate and L- Glutamate. Oxaloacetate so formed is coupled with 2,4-Dinitrophenyl hydrazine (2,4-DNHP) to form a corresponding hydrazone, a brown colored complex in alkaline medium and this can be measured colorimetrically.



Reitman and Frankel method is an end point colorimetric method for the estimation of enzyme activity. To obtain accurate results, method has been standardized with kinetic method (standard karmen unit assay). The method used here is single point calibration version of original method for maximum ease of use and convenience (Henry et al., 1960; Karmen, 1955; Reitman and Frankel, 1957; Feri et al., 1995).

3.12.2 Reagents

Reagent 1: Buffered Aspartate - α -KG substrate, pH 7.4 (Phosphate buffer, L-Aspartic acid, α -KG, Stabilizer, Preservative)

Reagent 2: 2,4-DNHP color reagent (2,4-Dinitrophenyl hydrazine, Stabilizer, Preservative)

Reagent 3: Sodium hydroxide, 4N

Reagent 4: Working Pyruvate standard, 6 mM (114 IU/L) (Sodium pyruvate, Stabilizer, Preservative)

Solution I: Dilute 1 mL of reagent 3 to 10 mL with purified water.

3.12.3 Procedure

Table 3.28 Procedure for determination of AST

	Blank	Standard	Test	Control
	Volume in mL			
Reagent 1	0.25	0.25	0.25	0.25
Serum	--	--	0.05	--
Reagent 4	--	0.05	--	--
Mix well and incubate at 37°C for 60 minutes				
Reagent 2	0.25	0.25	0.25	0.25
Deionized water	0.05	--	--	--
Serum	--	--	--	0.05
Mix well and allow to stand at room temperature (15-30°C) for 20 minutes				
Solution I	2.5	2.5	2.5	2.5

Mix well and read the O.D. against purified water in a spectrophotometer at 505 nm, within 15 minutes.

3.12.4 Calculation

$$\begin{aligned}
 \text{AST (SGOT) activity } \left(\text{in } \frac{\text{IU}}{\text{L}} \right) &= \frac{\text{Absorbance of Test} - \text{Absorbance of control}}{\text{Absorbance of Standard} - \text{Absorbance of Blank}} \times \text{Conc. of Standard}
 \end{aligned}$$

3.13 DETERMINATION OF ALANINE AMINOTRANSFERASE (ALT) IN SERUM

3.13.1 Principle

Alanine aminotransferase (AST) catalyses the transamination of L- Alanine and α -ketoglutarate (α -KG) to form Pyruvate and L- Glutamate. Pyruvate so formed is coupled with 2,4-Dinitrophenyl hydrazine (2,4-DNHP) to form a corresponding hydrazone, a brown colored complex in alkaline medium and this can be measured colorimetrically.



Reitman and Frankel method is an end point colorimetric method for the estimation of enzyme activity. To obtain accurate results, method has been standardized with kinetic method (standard karmen unit assay). The method used here is single point calibration version of original method for maximum ease of use and convenience (Henry et al., 1960; Karmen, 1955; Reitman and Frankel, 1957; Feri et al., 1995).

3.13.2 Reagents

Reagent 1: Buffered Alanine - α -KG substrate, pH 7.4 (Phosphate buffer, L-Alanine, α -KG, Stabilizer, Preservative)

Reagent 2: 2,4-DNHP color reagent (2,4-Dinitrophenyl hydrazine, Stabilizer, Preservative)

Reagent 3: Sodium hydroxide, 4N

Reagent 4: Working Pyruvate standard, 8 mM (150 IU/L) (Sodium pyruvate, Stabilizer, Preservative)

Solution I: Dilute 1 mL of reagent 3 to 10 mL with purified water.

3.13.3 Procedure

Table 3.29 Procedure for determination of ALT

	Blank	Standard	Test	Control
	Volume in mL			
Reagent 1	0.25	0.25	0.25	0.25
Serum	--	--	0.05	--
Reagent 4	--	0.05	--	--
Mix well and incubate at 37°C for 60 minutes				
Reagent 2	0.25	0.25	0.25	0.25
Deionized water	0.05	--	--	--
Serum	--	--	--	0.05
Mix well and allow to stand at room temperature (15-30°C) for 20 minutes				
Solution I	2.5	2.5	2.5	2.5

Mix well and read the O.D. against purified water in a spectrophotometer at 505 nm, within 15 minutes.

3.13.4 Calculation

$$ALT (SGPT) activity \left(in \frac{IU}{L} \right) = \frac{Absorbance \ of \ Test - Absorbance \ of \ control}{Absorbance \ of \ Standard - Absorbance \ of \ Blank} \times Conc. \ of \ Standard$$

3.14 DETERMINATION OF HYDROXYPROLINE IN TISSUE (Switzer, 1991)

3.14.1 Reagents:

- I. **Hydroxyproline standard, 0.1 mg/mL.** Dissolve 250 mg of vacuum-dried L-hydroxyproline (Sigma, Cat. No. H-6002) in 25 mL 0.001 N HCl. One mL of this solution is diluted to 100 mL with 0.001 N HCl.
- II. **Hydroxyproline working standard, 10 µg/mL.** Dilute 10 mL 0.1 mg/mL hydroxyproline standard with deionized water to 100 mL.
- III. **Potassium borate buffer, pH 8.7.** Mix 61.84 g boric acid and 225 g KCl in about 800 mL deionized water. Adjust the pH to 8.7 with 10 N and 1 N KOH and make the final volume up to 1 liter. Prepare a 1:5 dilution of buffer as needed.
- IV. **Chloramine T solution.** Prepare fresh daily a solution of 536.4 mg of chloramine T (Sigma, Cat. No. C-9887) in 10 mL methyl cellosolve (ethylene glycol monomethyl ether, Fisher, Cat. No. E-182).
- V. **Sodium thiosulfate, 3.6 M.** Dissolve 893.4 g sodium thiosulfate in about 900 mL deionized water and bring the final volume to 1 liter. Store under toluene at room temperature for several weeks.
- VI. **Ehrlich's reagent.** Add 27.4 mL concentrated sulfuric acid to 200 mL absolute ethanol in a beaker and cool the mixture. In another beaker, place 120 g p-dimethylaminobenzaldehyde (Fisher, Cat. No. D7 I- 100) and 200 mL absolute ethanol and then add slowly with stirring the acid-ethanol mixture from the first beaker. The solution can be stored in the refrigerator for several weeks and the crystals that form can be redissolved by warming the solution.

VII. **Glass culture tubes, 150×16 mm, screw-capped with Teflon liners** (Fisher, Cat. No. 14-930-10E) are used both for hydrolysis and for hydroxyproline oxidation.

3.14.2 Procedure

3.14.2.1 Tissue hydrolysis

1. Place 25-350 mg wet weight of tissue in dry culture tube of known weight.
2. Dry the samples in an oven at 65 ° C for 18-24 hours and then allow the tubes to cool to room temperature in a desiccator.
3. Weigh the tubes.
4. Add 2.0 mL 6 N HCl, cap and hydrolyze the samples at 110 ° C for 24 hr.
5. Evaporate the samples to dryness with a stream of nitrogen.
6. Add 10.0 mL deionized water to each tube and mix well.

3.14.2.2 Hydroxyproline determination

1. Transfer 0.2 mL hydrolyzate to a clean, labeled culture tube followed by 1.6 mL deionized water.
2. Prepare a set of tubes containing known amounts of hydroxyproline (1.0-8.0 µg) and water as reagent blank.
3. Add 1.0 mL 1:5 diluted borate buffer to all tubes.
4. Add 0.3 mL chloramine T to each tube in a timed sequence to oxidize the hydroxyproline and mix well.
5. After 20 min, add 1.0 mL sodium thiosulfate and mix well.
6. Add about 1.5 g potassium chloride to saturate all tubes. If indole, dehydroproline, or similar compounds are anticipated in the samples, extract with 2.5 mL toluene and discard the toluene extract.
7. Cap and heat the tubes in boiling water for 20 min.
8. Cool tubes to room temperature, add 2.5 mL toluene, and cap all tubes tightly. Invert the tubes 100 times or shake them about 5 min.

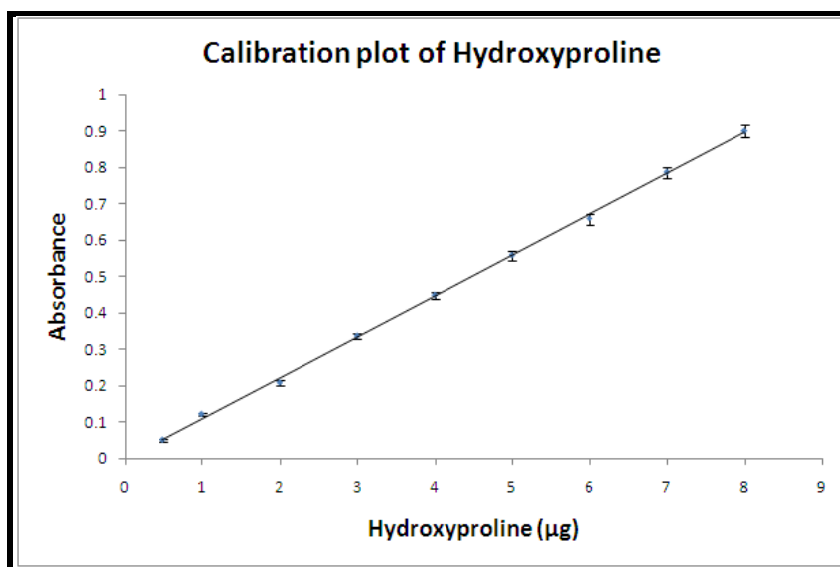
9. Centrifuge the tubes at low speed briefly and transfer 1.0 mL toluene extract to labeled 12 × 75 mm test tubes.
10. Add 0.4 mL Ehrlich's reagent and allow the color to develop by 30 min.
11. Read the absorbances at 565 nm against a reagent blank.
12. A linear regression of absorbance versus μg hydroxyproline standard can be used to calculate the hydroxyproline content of each unknown sample. Multiply the values by the dilution factor of 50 to determine the hydroxyproline content of the original hydrolyzate.

3.14.2.3 Special considerations

1. The toluene extract in step 6 of hydroxyproline determination can be used to determine the concentration of proline by a periodate oxidation method.
2. The potassium chloride can be added at any point before oxidation with chloramine T without any effect on the color yield.
3. Toluene may be added before heating the samples in order to save time in removing caps and recapping tubes in step 8. Any toluene lost appears to be proportional in all tubes, but the caps need to be checked for tightness since they frequently become loose on cooling after heating.
4. Centrifugation in step 9 may not be necessary if no emulsion is present in any of the samples.
5. Hydroxyproline can be determined in 48-60 samples in about 4 hours.

Table 3.30 Calibration plot of Hydroxyproline (n=3)

Conc. ($\mu\text{g/mL}$)	Absorbance ($\pm\text{SEM}$)
0.5	0.0499 \pm 0.0028
1	0.1209 \pm 0.0047
2	0.2078 \pm 0.0083
3	0.3361 \pm 0.0071
4	0.4483 \pm 0.0100
5	0.5579 \pm 0.0127
6	0.6587 \pm 0.0150
7	0.7867 \pm 0.0148
8	0.8997 \pm 0.0160

Figure 3.9 Calibration plot of Hydroxyproline**Table 3.31 Calibration parameters**

Characteristic	Value
λ	565 nm
Range	0.5-8 µg
Regression equation	$y = 0.1124x - 0.0040$
Regression Coefficient (R^2)	0.9993

Table 3.32 Accuracy and precision of Hydroxyproline by spectroscopic method (n=6)

Amount (µg)	Obtained Amount (µg) (\pm SEM)	% Recovery	% RSD
1	1.004 \pm 0.0256	100.435	4.290
2	2.007 \pm 0.0377	100.335	3.252
4	4.010 \pm 0.0668	100.261	2.886
8	7.972 \pm 0.1089	99.645	2.366

Accuracy is reflected from % Recovery and precision from % RSD

3.15 DETERMINATION OF HYALURONIC ACID IN SERUM

3.15.1 Background

Hyaluronan (HA) is a high molecular weight (1000-5000 kD) anionic polysaccharide composed of repeating disaccharides of glucuronate acetylglucosamine. The HA-

3.15.3 Assay Procedure

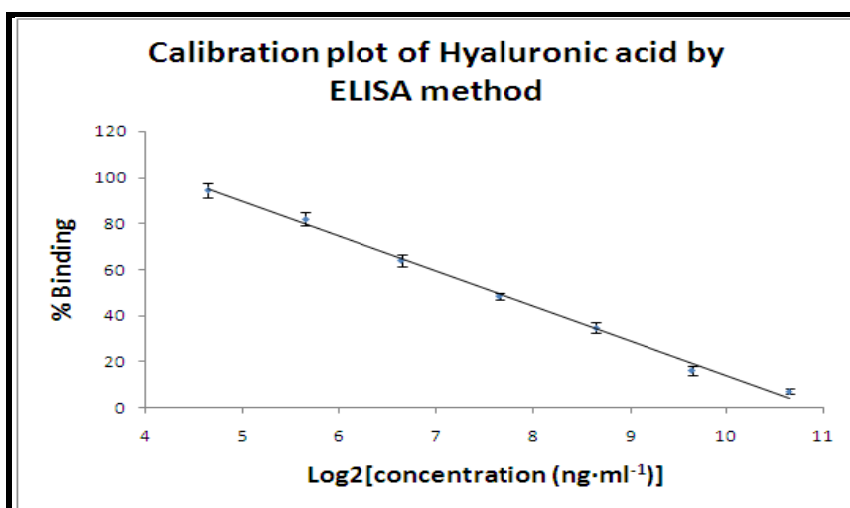
1. Set up the incubation plate as illustrated above. We suggest the HA Standard dilution series be run in triplicate for best results. Add 100 μL of Standards and samples into corresponding wells. Add 150 μL of Diluent to Blank Control and 100 μL of Diluent to Zero HA Control wells. Add 50 μL of Working Detector to all wells except the Blank. Mix well. Cover plate and incubate for one hour at 37°C.
2. Following the incubation, transfer 100 μL of controls and samples to the corresponding wells of the HA ELISA plate. Cover plate and incubate for 30 minutes at 4°C.
3. Discard the solution and wash the wells four times with 300 μL of 1X Wash Buffer.
4. Add 100 μL of Working Enzyme to each well. Cover plate and incubate at 37°C for 30 minutes.
5. Repeat wash step 3.
6. Add 100 μL Working Substrate Solution to each well. Incubate the plate in the dark at room temperature for 30-45 minutes
7. Measure the absorbance of each well at 405 nm. The Blank should have an absorbance of < 0.10 and the ratio of the Zero HA Control to the 1600 ng/mL HA Standard should be > 4.0. If the ratio is < 4.0, continue incubation and read plate every 15 minutes until ratio is reached.
8. Stop the reaction by adding 50 μL Stop Solution to each well.
9. Calculate the binding percentage for each sample using the formula:

$$\% \text{ Binding} = 100 \times \frac{[A_{405}(\text{Sample}) - A_{405}(\text{Blank})]}{[A_{405}(\text{Zero HA}) - A_{405}(\text{Blank})]}$$

Using linear or nonlinear regression, plot a standard plot of percent binding versus concentrations of HA standards. A Log2 plot with linear regression is shown as an example. Determine HA levels of unknowns by comparing their percentage of binding relative to the standard plot.

Table 3.33 Calibration plot of Hyaluronic acid by ELISA method (n=3)

Conc. (ng/mL)	% Binding (\pm SEM)
25	94.331 \pm 3.214
50	82.085 \pm 2.973
100	63.911 \pm 2.768
200	48.637 \pm 1.442
400	34.772 \pm 2.095
800	16.094 \pm 1.978
1600	7.003 \pm 1.283

Figure 3.10 Calibration plot of Hyaluronic acid by ELISA method

Table 3.34 ELISA parameters

Characteristic	Value
λ	405 nm
Range	25-1600 ng/mL
Regression equation	$y = -15.111x + 165.05$
Regression Coefficient (R^2)	0.9960

Table 3.35 Accuracy and precision of Hyaluronic acid estimation by ELISA assay (n=6)

Conc.(ng/mL)	Obtained Conc. (ng/mL) (\pm SEM)	% Recovery	% RSD
50	50.118 \pm 1.892	100.236	6.360
200	199.027 \pm 5.011	99.514	4.361
800	803.846 \pm 16.689	100.481	3.596
1600	1609.710 \pm 38.490	100.607	4.142

Accuracy is reflected from % Recovery and precision from % RSD

3.15.4 Reference Values

Normal HA levels in serum from healthy blood donors are less than 120 ng/mL. Serum HA levels are elevated in several disease states including hepatitis (greater than 160ng/mL) and cirrhosis (greater than 250ng/mL).

3.16 DETERMINATION OF TOTAL BILIRUBIN IN SERUM (Dangerfield, 1953)

3.16.1 Principle

In the method the serum is treated with diazo reagent- and a mixture of caffeine sodium benzoate and a phosphate buffer; the azobilirubin is formed rapidly and it is measured in a photo-electric colorimeter and compared with that of an azobilirubin standard previously prepared. A blank is used to compensate for any slight cloudiness or any color other than bilirubin, which may be present in the test serum.

3.16.2 Reagents

Reagent 1: Diazo Reagent

Diazo A:

Sulphanilic acid _____ 1 g.

Concentrated hydrochloric acid _____ 15 mL.

Distilled water to _____ 1000 mL.

Diazo B:

Sodium nitrite _____ 0.5 g.

Distilled water to _____ 100 mL.

For use 10 mL of diazo A is mixed with 0.3 mL. of diazo B.

Reagent 2: Diazo Blank

Concentrated hydrochloric acid _____ 15 mL.

Distilled water to _____ 1000 mL.

Reagent 3: Caffeine Buffer Mixture

Caffeine (25 g) and sodium benzoate (25 g) are dissolved in about 400 mL warm distilled water then cooled and potassium dihydrogen phosphate (4.1 g) and 1N sodium hydroxide (3.4 mL) are added. The mixture is diluted to 500 mL with water. The mixture, which should be filtered if not clear, will keep for at least a month.

Reagent 4: Bilirubin Solution

About 20 mg of pure bilirubin is weighed accurately and 0.2 mL wetting agent added (10% lissapol or 10% teepol). When wetting is complete 7 mL of 0.2N sodium hydroxide is added and the mixture is stirred until the bilirubin is completely dissolved. It is diluted with 0.1N sodium carbonate to a volume of 500 mL. It is important that this preparation should be carried out rapidly (within five minutes). Immediately after this solution has been made it should be used for the preparation of the standard azobilirubin and standard blank solution as below.

Reagent 5: Azobilirubin Standard

This standard solution should be prepared in duplicate. To 50 mL of caffeine buffer mixture 5 mL of diazo solution is added, followed by 10 mL of bilirubin solution, mixed, and allowed to stand for 10 minutes. Then its optical density (S) is measured using a green filter. If stored in the dark this solution can be used for checking the photometer in the subsequent serum determinations made during the following two weeks.

Reagent 6: Standard Blank Solution

This solution also should be prepared in duplicate. To 10 mL of caffeine buffer mixture, 1 mL water is added, followed by 2 mL of bilirubin solution. The solution is mixed and allowed to stand for 10 minutes, and then its optical density (SB) is measured using the same green filter as employed in measuring the density of the standard.

3.16.3 Procedure

Fresh serum (1 mL) is pipetted into each of two test tubes. To one tube (the test) 0.5 mL diazo reagent is added and to the other tube (the blank) 0.5 mL diazo blank. The tubes are shaken and stood for approximately one minute and it is noted if a red develops in the test solution indicating a positive direct van den Bergh reaction. To both tubes 5 mL of caffeine buffer mixture is added. The contents are mixed well and stood for 15 minutes to allow for full color development. The color is stable for at least one hour.

The optical densities of the test (T) and the blank (B) are measured in a photoelectric colorimeter using a green light filter or in a spectrophotometer at 525 nm, making the zero setting with water.

3.16.4 Calculation

$$\text{Concentration of bilirubin in serum (in } \frac{\text{mg}}{100 \text{ ml}}) = \frac{T - B}{S - SB} \times \frac{W}{5}$$

Where W= weight of bilirubin in mg. taken in preparing the bilirubin solution, and T, B, S, and SB, the optical densities of the solutions indicated above.

3.17 CONCLUSIONS

From above mentioned experimentation it was found that analytical methods for estimation of both RGZ and CDS in the dosage forms, in diffusion medium and in plasma as well as estimation of D-mannose, phosphorus, total protein, albumin, globulin, aspartate aminotransferase, alanine aminotransferase, hydroxyproline and hyaluronic acid showed good linearity, accuracy and precision. So these methods can be used for further study.

3.18 REFERENCES

- Bartlett GR.** Phosphorus assay in column chromatography. *J Biol Chem.* 1959 Mar;234(3):466-8.
- Bottcher CSF,** van Gent CM, Fries C. A rapid and sensitive sub-micro phosphorus determination. *Anal Chim Acta* 1961;24:203–4.
- Corcoran RM,** Durnan SM. Albumin determination by a modified bromocresol green method. *Clin Chem.* 1977;23(4):765-6.
- Daneshtalab N,** Lewanczuk RZ, Jamali F. High-performance liquid chromatographic analysis of angiotensin II receptor antagonist valsartan using a liquid extraction method. *J Chromatogr B Analyt Technol Biomed Life Sci.* 2002 Jan 25;766(2):345-9.
- Dangerfield WG,** Finlayson R. Estimation of bilirubin in serum. *J Clin Pathol.* 1953;6(3):173-7.
- Dubois M,** Gilles KA, Hamilton JK, Rebers PA, Smith F. Colorimetric method for determination of sugars and related substances. *Anal Chem.* 1956;28:350-6.
- Erk N.** Simultaneous analysis of candesartan cilexetil and hydrochlorothiazide in human plasma and dosage forms using HPLC with a photodiode array detector. *J Liq Chromatogr Relat Technol.* 2003;26(15):2581-91.
- Feri J,** Heuck CC, Riesen W, Lang H, Hill PG, EL-Nageh NM, Poller L. Production of basic diagnostic laboratory reagents, Eastern Mediterranean Series: 11 (WHO regional publication):1995:40-4.
- Gonzalez L,** Alonso RM, Jimenez RM. A high-performance liquid chromatographic method for screening angiotensin II receptor antagonists in human urine. *Chromatographia* 2000;52(11/12):735-40.
- Gornall AG,** Bardawill CJ, David MM. Determination of serum proteins by means of the biuret reaction. *J Biol Chem.* 1949 Feb;177(2):751-66.
- Goyal A,** Singhvi I. Simultaneous spectrophotometric estimation of rosiglitazone maleate and glimepiride in tablet dosage forms. *Indian J Pharm Sci.* 2007;69:780-3.
- Gustafsson JE.** Improved specificity of serum albumin determination and estimation of "acute phase reactants" by use of the bromocresol green reaction. *Clin Chem.* 1976 May;22(5):616-22.

Henry RJ, Chiamori N, Golub OJ, Berkman S. Revised spectrophotometric methods for the determination of glutamic-oxalacetic transaminase, glutamic-pyruvic transaminase, and lactic acid dehydrogenase. *Am J Clin Pathol*. 1960 Oct;34:381-98.

Hruska MW, Frye RF. Simplified method for determination of rosiglitazone in human plasma. *J Chromatogr B Analyt Technol Biomed Life Sci*. 2004 Apr 25;803(2):317-20.

Jagathi V, Devala Rao G, Sai Praveen P, Manohar Babu CH. Assay of rosiglitazone by visible spectrophotometry. *International Journal of Pharmacy and Technology*. 2010;2(3):757-61.

Kang X, Wang F, Xie Z, Li H. A high performance liquid chromatography method for simultaneous determination of rosiglitazone and gemfibrozil in human plasma. *J Chromatogr B Analyt Technol Biomed Life Sci*. 2009 Mar 1;877(7):645-8.

Karmen A. A note on the spectrometric assay of glutamic-oxalacetic transaminase in human blood serum. *J Clin Invest*. 1955 Jan;34(1):131-3.

Kim KA, Park JY. Simple and extractionless high-performance liquid chromatographic determination of rosiglitazone in human plasma and application to pharmacokinetics in humans. *Biomed Chromatogr*. 2004 Oct;18(8):613-5.

Kolte BL, Raut BB, Deo AA, Bagool MA, Shinde DB. Liquid chromatographic method for the determination of rosiglitazone in human plasma. *J Chromatogr B Analyt Technol Biomed Life Sci*. 2003 May 5;788(1):37-44.

Kongtawelert P, Ghosh P. An enzyme-linked immunosorbent-inhibition assay for quantitation of hyaluronan (hyaluronic acid) in biological fluids. *Anal Biochem*. 1989 May 1;178(2):367-72.

Lin ZJ, Desai-Krieger D, Shum L. Simultaneous determination of glipizide and rosiglitazone unbound drug concentrations in plasma by equilibrium dialysis and liquid chromatography-tandem mass spectrometry. *J Chromatogr B Analyt Technol Biomed Life Sci*. 2004 Mar 5;801(2):265-72.

Mamidi RN, Benjamin B, Ramesh M, Srinivas NR. Simple method for the determination of rosiglitazone in human plasma using a commercially available internal standard. *Biomed Chromatogr*. 2003 Sep;17(6):417-20.

Martindale, The Extra Pharmacopoeia, 31st ed., Reynolds, J. E. F., ed., Royal Pharmaceutical Society (London, UK: 1996), p. 1165.

Martindale, The Extra Pharmacopoeia, 33rd ed., Sweetman SC, ed., The pharmaceutical press, (London, UK: 2002), p. 907.

McDonald C, Gerarde HW. A spectrophotometric micromethod for the direct determination of serum albumin. *Microchem J.* 1963;7(1):57-62.

McHutchison JG, Blatt LM, de Medina M, Craig JR, Conrad A, Schiff ER, Tong MJ. Measurement of serum hyaluronic acid in patients with chronic hepatitis C and its relationship to liver histology. Consensus Interferon Study Group. *J Gastroenterol Hepatol.* 2000 Aug;15(8):945-51.

Muxlow AM, Fowles S, Russell P. Automated high-performance liquid chromatography method for the determination of rosiglitazone in human plasma. *J Chromatogr B Biomed Sci Appl.* 2001 Mar;752(1):77-84.

Patil BS, Rao RNG, Jadhav S, Kulkarni U, Gada MM. Estimation of candesartan cilexetil in bulk and tablet dosage form by UV spectrophotometric method. *International Journal of Research in Ayurveda and Pharmacy.* 2011;2(1):204-6.

Pedersen RS, Brosen K, Nielsen F. HPLC method for determination of rosiglitazone in plasma. *Chromatographia* 2005 Aug;62(3/4),197–201.

Plevris JN, Haydon GH, Simpson KJ, Dawkes R, Ludlum CA, Harrison DJ, Hayes PC. Serum hyaluronan--a non-invasive test for diagnosing liver cirrhosis. *Eur J Gastroenterol Hepatol.* 2000 Oct;12(10):1121-7.

Qutab SS, Razzaq SN, Ashfaq M, Shuja ZA, and Khan IU. Simple and sensitive LC–UV method for simultaneous analysis of hydrochlorothiazide and candesartan cilexetil in pharmaceutical formulations. *Acta Chromatogr.* 2007;19:119-29.

Radhakrishna T, Satyanarayana J, Satyanarayana A. LC determination of rosiglitazone in bulk and pharmaceutical formulation. *J Pharm Biomed Anal.* 2002 Jul 31;29(5):873-80.

Reitman S, Frankel S. A colorimetric method for the determination of serum glutamic oxalacetic and glutamic pyruvic transaminases. *Am J Clin Pathol.* 1957 Jul;28(1):56–63.

Rodkey FL. Direct spectrophotometric determination of albumin in human serum. Clin Chem. 1965 Apr;11:478-87.

Smith PK, Krohn RI, Hermanson GT, Mallia AK, Gartner FH, Provenzano MD, Fujimoto EK, Goeke NM, Olson BJ, Klenk DC. Measurement of protein using bicinchoninic acid. Anal Biochem. 1985;150(1):76-85.

Stenhoff H, Lagerstrom PO, Andersen C. Determination of candesartan cilexetil, candesartan and a metabolite in human plasma and urine by liquid chromatography and fluorometric detection. J Chromatogr B Biomed Sci Appl. 1999 Aug;731(2):411-7.

Subba Rao DV, Radhakrishnanand P, Suryanarayana MV, Himabindu V. A Stability-Indicating LC Method for Candesartan Cilexetil. Chromatographia 2007 Oct;66(7/8):499-507.

Switzer BR. Determination of hydroxyproline in tissue. J Nutr Biochem. 1991;2:229-31.

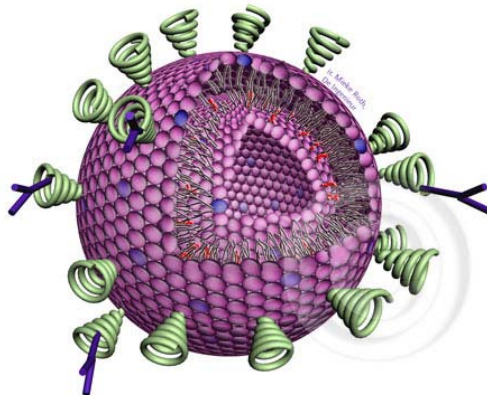
The Merck Index, 13th edition, Merck Research laboratories, White House station, NJ, 2001, pg.1041.

The Merck Index, 14th edition, Merck Research laboratories, White House station, NJ, 2006, pg.281.

Varley H. (1980). Practical Clinical Biochemistry, 5th edn. William Hienemann Medical Books Ltd., London, pp 550-5.

CHAPTER 4

FORMULATION OPTIMIZATION AND M6P-HSA CONJUGATION OF LIPOSOMES



Formulation Optimization and M6P-HSA Conjugation of Liposomes

4.1 INTRODUCTION

4.2 MATERIALS AND EQUIPMENTS

4.3 PREPARATION OF LIPOSOMES

4.3.1 Preparation of RGZ Liposomes by TFH Method

4.3.2 Formulation Optimization RGZ Loaded Liposomes Using Response Surface Methodology (RSM)

4.3.3 Preparation of CDS Liposomes by TFH Method

4.3.4 Formulation Optimization CDS Loaded Liposomes Using Response Surface Methodology (RSM)

4.4 PREPARATION OF M6P-HSA

4.5 CONJUGATION OF M6P-HSA TO LIPOSOMES

4.6 PARTICLE SIZE AND ZETA POTENTIAL OF UNCONJUGATED AND M6P- HSA CONJUGATED LIPOSOMES

4.7 TRANSMISSION ELECTRON MICROSCOPY (TEM)

4.8 LYOPHILIZATION OF LIPOSOMES AND OPTIMIZATION OF CRYOPROTECTANT CONCENTRATION

4.9 SOLID-STATE ANALYSIS

4.9.1 Differential Scanning Calorimetry (DSC):

4.9.2 X-ray Diffraction (XRD):

4.10 RESULTS AND DISCUSSION

4.10.1 Optimization of TFH Method Process Variables

4.10.2 Formulation Optimization RGZ Loaded Liposomes Using Response Surface Methodology (RSM)

4.10.2.1 Checkpoint Analysis

4.10.3 Formulation Optimization CDS Loaded Liposomes Using Response Surface Methodology (RSM)

4.10.3.1 Checkpoint Analysis

4.10.4 Preparation of M6P-HSA

4.10.5 Conjugation of M6P-HSA to Liposomes

4.10.6 Particle Size and Zeta Potential

4.10.7 Transmission Electron Microscopy (TEM)

4.10.8 Lyophilization of Liposomes and Optimization of Cryoprotectant
Concentration

4.10.9 Solid-state Analysis:

4.11 CONCLUSION

4.12 REFERENCES

4.1 INTRODUCTION

The liposomes are classified in to small unilamellar vesicles, large unilamellar vesicles, oligolamellar vesicles, and multi-lamellar vesicles. Various methods have been utilized for preparation of liposomes. There are at least fourteen major reported methods (Ostro, 1987; Martin et al., 1990(a)). The most commonly employed method are lipid film hydration also referred as thin film hydration method (TFH) (Bangham et al., 1965), reverse phase evaporation technique (REV) (Szoka and Papahadjopoulos, 1978; Sakai et al., 2008; Smirnov, 1984), rehydration-dehydration technique (Shew and Deamer, 1985; Seltzer et al., 1988; Kirby and Gregoriadis, 1984), ethanol injection method (Batzri and Korn, 1975; Jaafar-Maalej et al., 2010; Du and Deng, 2006; Maitani, 2010), ether infusion method (Deamer and Bangham, 1976; Cortesi et al., 1999), French press technique (Barenholz et al., 1979; Hamilton et al., 1980) and detergent dialysis technique (Matz and Jonas, 1982; Zumbuehl and Weder, 1981; Jiskoot et al., 1986; Ollivon et al., 2000). The difference lies between various methods of manufacture in the manner the membrane components are dispersed in aqueous media before being allowed to coalesce in the bilayer sheets form. In pharmaceutical point of view, the three most important aspects to be evaluated before selecting the method of preparation are the trapping efficiency, drug retention property and drug/lipid ratio (Betageri et al., 1993).

TFH method was selected for the preparation of liposomes in this investigation due to non-tediousness and feasible at lab scale compared to other techniques. Also, from the viewpoint of stability, the saturated phospholipid 1,2-Dilinoleoyl-sn-glycero-3-phosphocholine (DLPC), 1,2-diacyl-sn-glycero-3-phosphocholine (soy-hydrogenated) (HSPC), and 1,2-distearoyl-sn-glycero-3-phosphoethanolamine (DSPE) were used in this investigation. Trapping efficiency is one of the prime important factors in selection of method of liposome preparation. The trapping efficiency of 90% or more would be achieved with an optimum loading procedure. This necessitates the need for removal of untrapped drug because loading doses of 10% or less of free drug can usually be tolerated. Separation of untrapped or unincorporated drug (Betageri et al., 1993) from liposomes can be achieved either by 'gel filtration' (Sephadex mini-column centrifugation), ultra centrifugation, protamine aggregation, dialysis or controlled centrifugation at low speed. The free drug procedures, such as dialysis and

passage through exclusion columns, for removal of untrapped drug are often time-consuming, tedious, expensive, and makes recovery of untrapped drug difficult. Gel filtration was found to be very tenuous method with limited capacity and was not feasible for the entire formulation purification. Slight modification in the procedure was required for each specific liposome. Dialysis method was time consuming and was observed that drug leaks during the dialysis period. Protamine aggregation was destructive approach and its use is restricted for the determination of the drug entrapment and could not be used for the separation of the liposomal dispersion. Hence, controlled centrifugation at low speed was used in this investigation due to easy and faster method suitable for separation of untrapped drug.

Many lipid compositions can be employed for liposomal delivery systems; however, stability and cost are important determinants. Thus, acidic (negatively charged) lipids such as phosphatidyl serine, cardiolipin and phosphatidic acid are not preferred components as compared to phosphatidylcholine due to high costs and the often labile nature. Similarly, the use of unsaturated lipids, such as soya phosphatidylcholine or naturally occurring lipids, phosphatidylethanolamine and cardiolipin should be avoided due to its susceptibility towards oxidation. Thus, given similar loading and retention characteristics, liposomal systems composed of hydrogenated varieties of egg or soya phosphatidylcholine are pharmaceutically more preferred. Considering drug retention, it is unlikely that most drug-liposome formulations can exhibit sufficiently low leakage rates to allow retention times of one year or more (in dried or lyophilized form). However, if the trapping efficiencies are sufficiently high (e.g. 90% or more), removal of the untrapped drug may not be that necessary. No leakage of drug would then occur on extended storage due to absence of transmembrane drug concentration gradients. The optimum drug/lipid ratio of a liposomal formulation will likely be dictated by the biological efficacy and toxicity of the preparation and from a pharmaceutical point of view, high drug/lipid ratios are obviously more economical.

In summary, optimum liposomal formulations will exhibit drug trapping efficiencies of more than 90%, employ inexpensive and relatively saturated lipids and cholesterol and using highest possible drug/lipid ratio results in consistent and maintained efficacy of the preparation. Apart from these factors; other factors which need to be

considered in selection of the methods of preparation include selection of methods which would avoid the use of organic solvents and detergents which are difficult to remove, yield well-defined and reproducible liposomes and which are rapid and feasible for scale up procedures. Selection of the appropriate method is also dependent on applications of the liposomes. In the stabilization of liposomes using freeze or spray drying technique there is a basic necessity, that is sufficient rigidity in the liposomal membrane to withstand drying with minimum or least leakage of the entrapped drug.

Mannose 6-phosphate/ insulin like growth factor II (M6P/IGF II) receptor are over expressed on the surface of HSCs during liver fibrosis. Mannose 6-phosphate modified human serum albumin (M6P-HSA) is selective to M6P/IGF II receptor and thus accumulates in activated HSCs of fibrotic liver. M6P-HSA as such has been investigated as a carrier for a number of drugs, including pentoxifylline (Gonzalo et al., 2006), mycophenolic acid (Greupink et al., 2005), doxorubicine (Greupink et al., 2006) and gliotoxin (Hagens et al., 2006). M6P-HSA conjugated liposomes can be used as HSCs selective carrier of antifibrotic drugs to improve the efficacy of drugs at the same time to reduce their adverse effects. Liposomes with few parts of bioactive lipid dilinoleoylphosphatidylcholine (DLPC) into the membrane act as a bioactive drug carrier which can deliver drugs and simultaneously have beneficial antifibrotic effects (Beljaars et al., 1999; Beljaars et al., 2001; De Bleser et al., 1996; De Bleser et al., 1995; Adrian et al., 2006; Cao et al., 2002).

This chapter demonstrates the preparation of liposomes considering the above discussed factors. Liposomes of Rosiglitazone (RGZ), and Candesartan (CDS) were prepared using TFH technique with membrane composition consisting of lipids such as DLPC, HSPC, DSPE and cholesterol. Various formulation variables are optimized to achieve desired response variables using factorial design and response surface methodology (RSM). Prepared liposomes were characterized for size and size distribution, zeta potential, percent drug Entrapment (PDE) and percentage reduction (PR) in PDE after 10 days kept at refrigerated condition.

4.2 MATERIALS AND EQUIPMENTS

1,2-Dilinoleoyl-sn-glycero-3-phosphocholine (DLPC), 1,2-diacyl-sn-glycero-3-phosphocholine (soy-hydrogenated) (HSPC), and 1,2-distearoyl-sn-glycero-3-phosphoethanolamine (DSPE) were obtained as a gift sample from Genzyme Pharmaceuticals, Switzerland. RGZ as a PPAR γ ligand was obtained as a gift sample from Zydus Research Center, Ahmedabad, India. CDS was obtained as a gift sample from Alembic Research Center, Vadodara, India. Cholesterol (CH) ($\geq 99\%$) was purchased from Sigma-Aldrich Corporation, Bangalore, India. Cholesterol (CH) ($\geq 99\%$), human serum albumin ($\geq 96\%$, lyophilized powder, Mw 66478 Da), 4-Nitrophenyl α -Dmannopyranoside, sebacic acid, and dialysis tubing cellulose membrane (Mw cutoff 12400 Da) were purchased from Sigma-Aldrich Corporation, Bangalore, India. N,N-dicyclohexyl carbodiimide (DCCI) and 1-(3-dimethylamino propyl)-3-ethylcarbodiimide hydrochloride (EDCI) were purchased from Himedia Laboratories, Mumbai, India. Chloroform (LiChrosolv®) and methanol (LiChrosolv®) were purchased from Merck specialties limited, Mumbai, India. Mannitol, Sucrose, Lactose, Trehalose and Glycine were purchased from Himedia Laboratories, Mumbai, India. polycarbonate membrane filter (1 μ m, 0.4 μ m, 0.2 μ m and 0.1 μ m) were purchased from Whatman, Mumbai, India. All other reagents used were of analytical grade. Water used was distilled and prefiltered through 0.2 μ m filter.

The equipments such as rotary evaporator with vacuum pump and thermostatically controlled water bath and nitrogen purging facility (Superfit Equipments, India); Analytical balance (Precisa 205A SCS, Switzerland); high-pressure extruder (Avestin® EmulsiFlex- C5 with extruder, Avestin Inc., Ottawa, Canada); pH meter (Systronics 335, India); Cyclomixer, three blade stirrer (Remi Scientific Equipments, Mumbai); Cooling Centrifuge (Sigma Laboratory centrifuge, 3 K 30, Osterode, GmBH); Water bath, Magnetic stirrer and heating mantle (Remi, Mumbai); UV-Visible Spectrophotometer, (Shimadzu UV-1700, Japan); Vacuum Pump F16, (Bharat Vacuum pumps, Bangalore); Optical microscope with polarizer (BX 40, Olympus Optical Co. Ltd., Japan); Malvern Zetasizer analyzer (NanoZS, Malvern Instruments, UK), Karl fisher Auto-titrator [Toshiwal Instruments (Bombay) Pvt. Ltd., Nasik] FTIR spectrophotometer (BRUKER, α -Alpha T, Germany) were used.

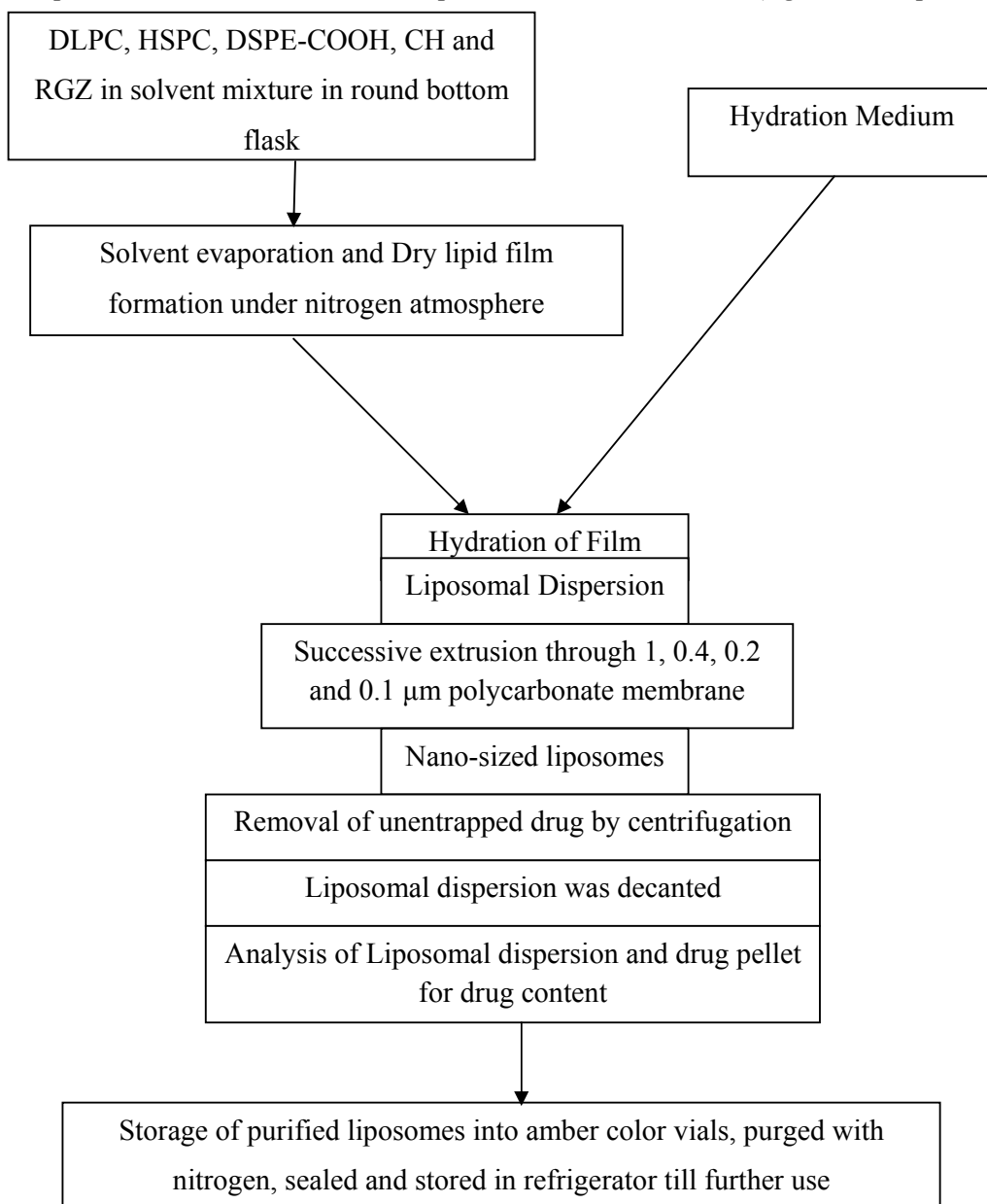
4.3 PREPARATION OF LIPOSOMES

4.3.1 Preparation of RGZ Liposomes by TFH Method

Liposomes of RGZ consisting of DLPC, HSPC, DSPE-COOH and CH were prepared by TFH technique (New, 1990). Briefly, the lipids and RGZ were dissolved in a mixture of chloroform and methanol (ratio 4:1 v/v) in a 250ml round bottom flask in different molar ratios. The solvent was evaporated in the rotary flash evaporator. The thin dry lipid film thus formed was hydrated using purified water at 65°C. The size of liposomes was reduced using successive extrusion through 1, 0.4, 0.2 and 0.1 µm polycarbonate membrane filter using Avestin high-pressure extruder. Untrapped free drug in the liposomal dispersion was separated by centrifuging (Sigma Laboratory centrifuge, 3 K 30, Osterode, GmBH) liposomal suspension at 7500 rpm (4779 g) for 2 minutes. Liposomal suspension was decanted and drug pellet was separated. Liposomal suspension was then characterized for vesicle size, size distribution (in term of poly dispersity index) and zeta potential using Malvern Zetasizer vesicle size. The encapsulation efficiency of RGZ liposomes was determined by dissolving known quantity of liposomes (after separation of free drug) in methanol and estimating drug content by UV/VIS spectrophotometric method (As discussed in chapter 3). Mass balance was evaluated by measuring untrapped drug in pellet. A flowchart depicting the process is shown in scheme 4.1. The liposomal compositions and process parameters were optimized to achieve maximum drug entrapment.

PDE was calculated using the formula:

$$\text{PDE} = \frac{\text{Amount of Drug Encapsulated in Liposomes}}{\text{Amount of Drug Used in Liposome Preparation}} \times 100$$



Scheme 4.1 TFH process stages in the preparation of RGZ liposomes

4.3.2 Formulation Optimization RGZ Loaded Liposomes Using Response Surface Methodology (RSM)

The RGZ loaded liposomal formulations were optimized using 3^3 full factorial design by varying drug: lipid molar ratio (1:15, 1:20 and 1:25), lipid: cholesterol molar ratio (9:1, 8:2 and 7:3), and total solid content: volume of hydration media ratio (1:10, 1:12.5 and 1:15) at 3 different levels as low (-1), medium (0) and high (1), by keeping all other process and formulation parameter invariant, to maximize PDE and to

minimize PR in PDE after 10 days kept at refrigerated condition (Cochran and Cox, 1992). The response variables considered for formulation optimization were PDE and PR in PDE (Fannin et al., 1981; Subramanian et al., 2004; Padamwar and Pokharkar, 2006; Loukas, 1997; Vali et al., 2008; Murthy and Umrethia, 2004; Seth and Misra, 2002; Gonzalez-Mira et al., 2011; Gonzalez-Rodriguez et al., 2007).

Table 4.1 Coded Values of the formulation parameters

Coded value	Actual value		
	X1	X2	X3
-1	1:15	9:1	1:10
0	1:20	8:2	1:12.5
1	1:25	7:3	1:15

X1 = Drug: Lipid molar ratio

X2 = Lipid: Cholesterol molar ratio

X3 = Total solid content: Volume of hydration media ratio

RSM was applied using comprehensive software, Design-Expert®8.0.4 (Stat-Ease Inc., MN) to fit second order polynomial equations, obtained by multiple linear regression analysis (MLRA) approach. A full and reduced model for both PDE and PR was established by putting the values of regression coefficients in polynomial equation. Statistical soundness of the polynomial equations was established on the basis of analysis of variance (ANOVA) statistics (Anthony Armstrong and James, 1996; Singh et al., 2005(c); Stensrud et al., 2000; Xiong et al., 2009; Singh et al., 2005(b); Singh et al., 2005(a); Naik et al., 2010; Ducat et al., 2010).

Two dimensional contour plots and three dimensional response surface plots (Box and Wilson, 1951; Box et al., 1978; Kenneth et al., 1995) were established by varying levels of two factors and keeping the third factor at fixed levels at a time. In this way, they are more helpful in understanding the actual interaction amongst the varying factors on the response parameter and are more meaningful. The 2-D contour plots and 3-D response surface graphs were constructed using the Design Expert software.

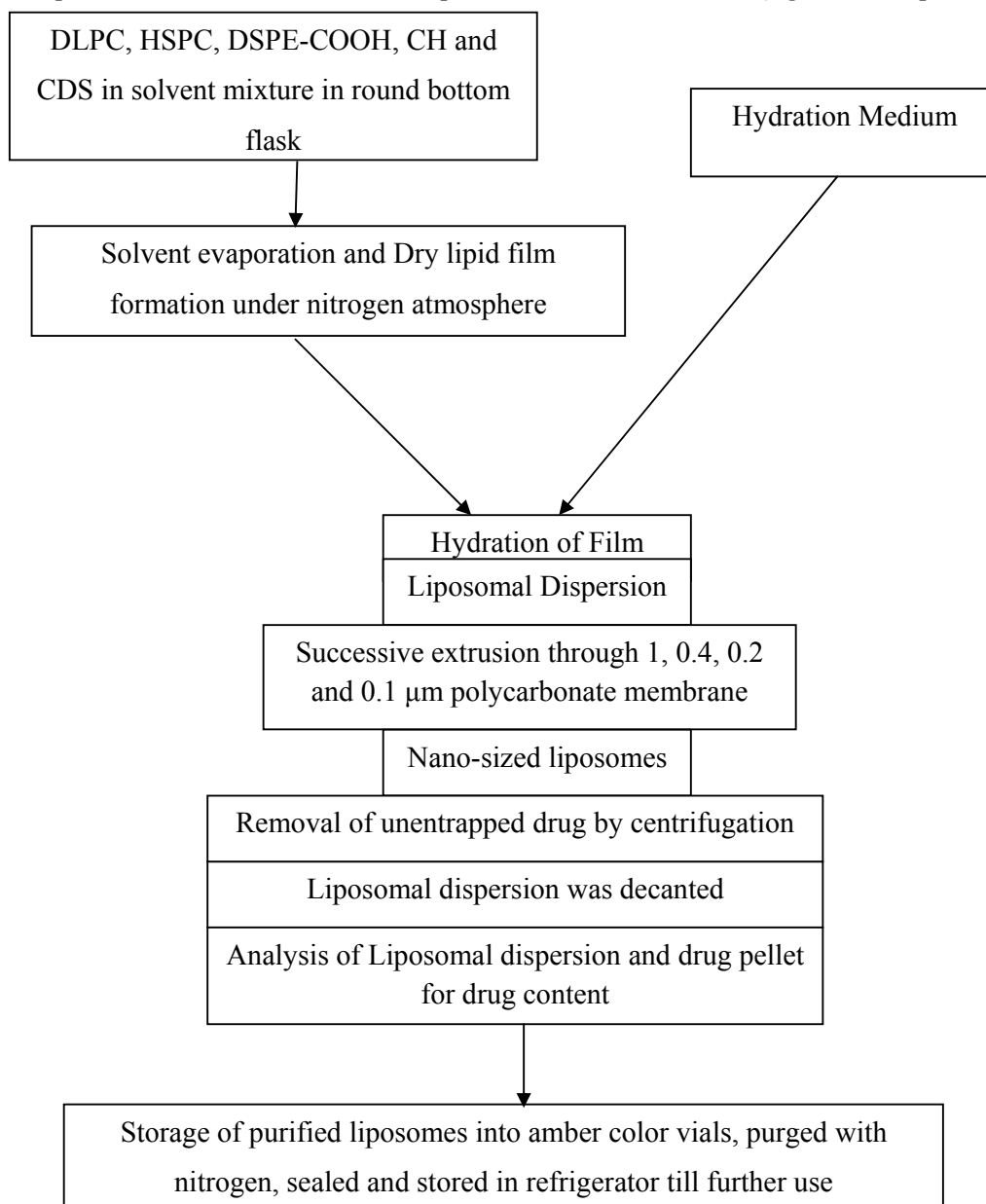
The experimental design and the derived polynomial equation for the optimization of liposomal formulation were validated for their utility by performing check point analysis. Eight optimum checkpoints were selected, prepared and evaluated for response parameters i.e. PDE and PR. Statistical comparison between the predicted

values and average of three experimental values of the response parameters was performed to derive percentage error and to evaluate significant difference between these values.

Optimized formulation was derived by specifying goal and importance to the formulation variables and response parameters. Results obtained from the software were further verified by actual preparation of the batches and comparing the predicted and actual results.

4.3.3 Preparation of CDS Liposomes by TFH Method

Liposomes of CDS consisting of DLPC, HSPC, DSPE-COOH and CH were prepared by TFH technique (New, 1990). Briefly, the lipids and CDS were dissolved in a mixture of chloroform and methanol (ratio 4:1 v/v) in a 250ml round bottom flask in different molar ratios. The solvent was evaporated in the rotary flash evaporator. The thin dry lipid film thus formed was hydrated using purified water at 65°C. The size of liposomes was reduced using successive extrusion through 1, 0.4, 0.2 and 0.1 µm polycarbonate membrane filter using Avestin high-pressure extruder. Untrapped free drug in the liposomal dispersion was separated by centrifuging (Sigma Laboratory centrifuge, 3 K 30, Osterode, GmbH) liposomal suspension at 7500 rpm (4779 g) for 2 minutes. Liposomal suspension was decanted and drug pellet was separated. Liposomal suspension was then characterized for vesicle size, size distribution (in term of poly dispersity index) and zeta potential using Malvern Zetasizer vesicle size. The encapsulation efficiency of RGZ liposomes was determined by dissolving known quantity of liposomes (after separation of free drug) in methanol and estimating drug content by UV/VIS spectrophotometric method (As discussed in chapter 3). Mass balance was evaluated by measuring untrapped drug in pellet. A flowchart depicting the process is shown in scheme 4.2. The liposomal compositions and process parameters were optimized to achieve maximum drug entrapment.



Scheme 4.2 TFH process stages in the preparation of CDS liposomes

4.3.4 Formulation Optimization CDS Loaded Liposomes Using Response Surface Methodology (RSM)

The liposomal formulations were optimized using 3^3 full factorial design by varying Drug: Lipid molar ratio (1:15, 1:20 and 1:25), Lipid: Cholesterol molar ratio (9:1, 8:2 and 7:3), and total solid content: volume of hydration media (1:10, 1:12.5 and 1:15) at 3 different levels as low (-1), medium (0) and high (1), by keeping all other process and formulation parameter invariant, to maximize PDE and to minimize percentage

reduction (PR) in PDE after 10 days kept at refrigerated condition (Cochran and Cox, 1992). The response variables considered for formulation optimization were PDE and PR in PDE. (Fannin et al., 1981; Subramanian et al., 2004; Padamwar and Pokharkar, 2006; Loukas, 1997; Vali et al., 2008; Murthy and Umrethia, 2004; Seth and Misra, 2002; Gonzalez-Mira et al., 2011; Gonzalez-Rodriguez et al., 2007)

Table 4.2 Coded Values of the formulation parameters

Coded value	Actual value		
	X1	X2	X3
-1	1:15	9:1	1:10
0	1:20	8:2	1:12.5
1	1:25	7:3	1:15

X1 = Drug: Lipid molar ratio

X2 = Lipid: Cholesterol molar ratio

X3 = Total solid content: Volume of hydration media

RSM was applied using comprehensive software, Design-Expert 8.0.4 (Stat-Ease Inc., MN) to fit second order polynomial equations, obtained by multiple linear regression analysis (MLRA) approach. A full and reduced model for both PDE and PR was established by putting the values of regression coefficients in polynomial equation. Statistical soundness of the polynomial equations was established on the basis of ANOVA statistics (Anthony Armstrong and James, 1996; Singh et al., 2005(c); Stensrud et al., 2000; Xiong et al., 2009; Singh et al., 2005(b); Singh et al., 2005(a); Naik et al., 2010; Ducat et al., 2010).

Two dimensional contour plots and three dimensional response surface plots (Box and Wilson, 1951; Box et al., 1978; Kenneth et al., 1995) were established by varying levels of two factors and keeping the third factor at fixed levels at a time. In this way they are more helpful in understanding the actual interaction amongst the varying factors on the response parameter and are more meaningful. The 2-D contour plots and 3-D response surface graphs were constructed using the Design Expert software.

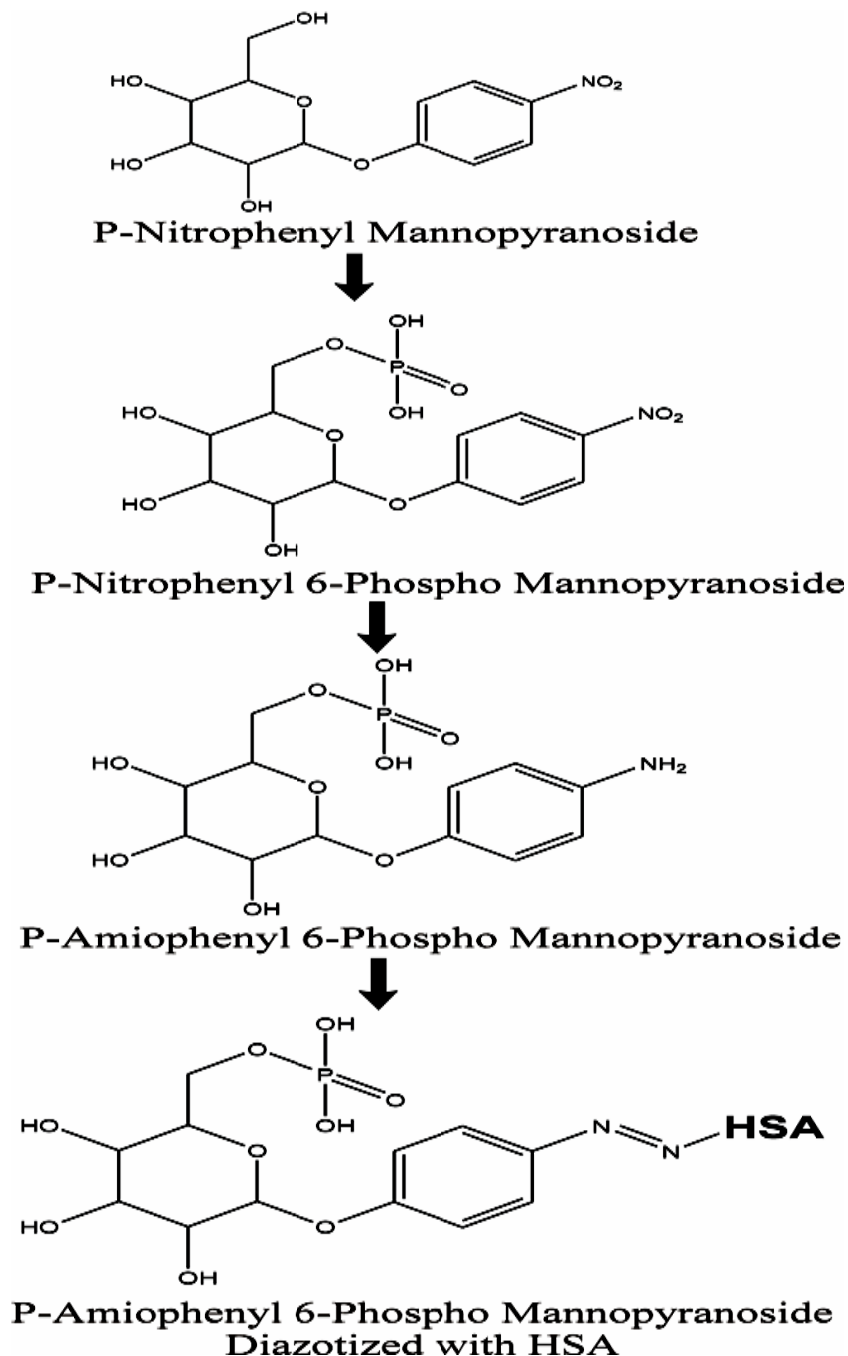
The experimental design and the derived polynomial equation for the optimization of liposomal formulation were validated for their utility by performing check point analysis. Eight optimum checkpoints were selected, prepared and evaluated for response parameters i.e. PDE and PR. Statistical comparison between the predicted

values and average of three experimental values of the response parameters was performed to derive percentage error and to evaluate significant difference between these values.

Optimized formulation was derived by specifying goal and importance to the formulation variables and response parameters. Results obtained from the software are further verified by actual preparation of the batches and comparing the predicted and actual results.

4.4 PREPARATION OF M6P-HSA

M6P-HSA was synthesized and characterized. Firstly, p-nitrophenyl- α -D-mannopyranoside was phosphorylated by reacting with phosphoryl chloride (Roche et al., 1985) to get p-nitrophenyl-6-phospho- α -D-mannopyranoside whose p-nitro group was further reduced with 10% palladium on active carbon under a hydrogen atmosphere of 1 atm (Monsigny et al., 1984) to obtain p-aminophenyl-6-phospho- α -D-mannopyranoside, which was then coupled to HSA by diazo bond formation (Kataoka and Tavassoli, 1984). Prepared M6P-HSA was purified, characterized for protein content (Colorimetric estimation at 550 nm after reacting with Biuret reagent in alkaline medium), number of M6P molecules (colorimetric estimation at 490 nm after reaction with phenol in presence of sulfuric acid) and number of phosphate groups coupled to each HSA molecules (Colorimetric estimation at 830 nm after reacting with ammonium molybdate – sulfuric acid reagent, 1-Amino 2-naphthyl 4-sulfonic acid reagent and hydrogen peroxide), lyophilized and stored at -20 °C till further use (Dubois et al., 1956; Bottcher et al., 1961)

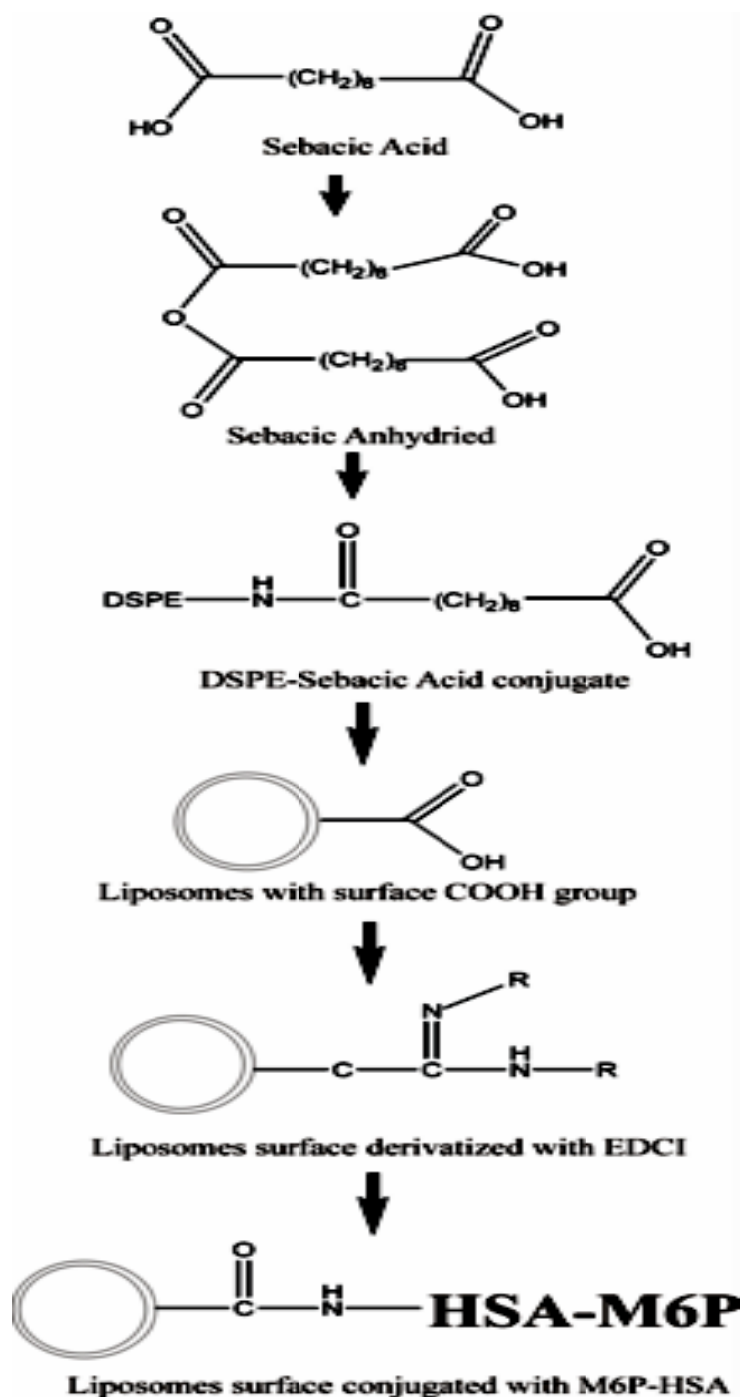


Scheme 4.3 Synthesis of M6P-HSA

4.5 CONJUGATION OF M6P-HSA TO LIPOSOMES

M6P-HSA was conjugated to liposomes containing DSPE-COOH by EDCI method as described by Martin et al., 1990(a). First of all, liposomal suspension was activated for an hour with EDCI (2.5mg/ml) in phosphate buffered saline pH 5. Add 50 μ l of M6P-HSA solution (10 mg/ml) to each milliliter of liposome suspension (DSPE-

COOH 0.05 $\mu\text{mol/ml}$). Ionic strength was increased by adding 50 μl of 1 M sodium chloride solution and adjusting the pH at pH 8. The reaction was carried out over night at 4 $^{\circ}\text{C}$. Particle size and zeta-potential of M6P-HSA liposomes were determined.



Scheme 4.4 M6P-HSA Conjugation to Liposomes

4.6 PARTICLE SIZE AND ZETA POTENTIAL OF UNCONJUGATED AND M6P-HSA CONJUGATED LIPOSOMES

The size of Liposomes was measured by dynamic light scattering with a Malvern Zetasizer. Diluted liposome suspension was added to the sample cuvette and then cuvette is place in zetasizer. Sample is stabilized for two minutes and reading was measured. The average particle size was measured after performing the experiment in triplicate. The zeta potential of developed liposomes was determined using Malvern Zetasizer. The zeta potential was calculated by Smoluchowski's equation from the electrophoretic mobility of liposomes at 25 °C (Mu and Feng, 2001).

4.7 TRANSMISSION ELECTRON MICROSCOPY (TEM)

The unconjugated and M6P-HSA conjugated liposomal vesicles were observed by TEM to illustrate their ultrastructure. A drop of liposome samples were applied to a carbon film-covered copper grid to form a thin film, which was then stained with 1% phosphotungstic acid. The samples were then observed with a Tecnai 20 transmission electron microscope (PHILIPS, Holland) (Zasadzinski, 1986).

4.8 LYOPHILIZATION OF LIPOSOMES AND OPTIMIZATION OF CRYOPROTECTANT CONCENTRATION

The liposomal suspensions have thermodynamic instability upon storage and lead to drug leakage and formation of aggregates. Freeze drying/ lyophilization is one of the known methods to recover the liposomes in the dried form and suitably redisperse the cake at time of administration. The liposomal suspension was stabilized by lyophilization. The dispersion was frozen at -70 °C and dried under negative displacement pressure (Heto Drywinner model DW1 0-60E, Denmark), for 24 h. Different cryoprotectants at various ratios and anti-adherent are evaluated. The lyophilized formulations were tested for particle size, zeta potential and percentage drug retention (PDR) (Ozer and Talsma, 1989; Hinrichs et al., 2006; Nounou et al., 2005; Crowe et al., 1985; Hernandez Caselles et al., 1990; Patel et al., 2009).

4.9 SOLID-STATE ANALYSIS

Differential Scanning Calorimetry (DSC) studies and X-ray Diffraction (XRD) studies were conducted for lyophilized batches of M6P-HSA conjugated liposomes.

The main objective of these studies was to determine possible changes in crystallinity of drug after incorporation into liposomes.

4.9.1 Differential Scanning Calorimetry (DSC)

DSC experiments were carried out using differential thermal analyzer (Mettler Toledo star® SW 7.01, USA) to evaluate thermal properties and to characterize the physical state of drugs in pure form and in liposomal formulations. Five to ten milligrams of pure drug and its liposomes were put separately in aluminum pan and hermetically sealed. The heating rate was adjusted at 10°C/min, nitrogen was used as purging gas and liquid nitrogen was employed to cool down the system (Yousefi et al., 2009; Atyabi et al., 2009; Crosasso et al., 2000; Van Winden et al., 1998).

4.9.2 X-ray Diffraction (XRD)

XRD was carried out with a BRUKER (D8 Advance, Germany) diffractometer. The diffraction patterns were recorded over 2 θ angular range of 3°-35° with a scan speed of 2°/min at room temperature (Cavalcanti et al., 2007; Patil and Gaikwad, 2009).

4.10 RESULTS AND DISCUSSION

Liposomal formulations of RGZ and CDS were prepared by the selected TFH method using DLPC, HSPC, DSPE-COOH and CH, were optimized to maximize PDE and minimize PR in PDE. Drugs entrapment in to liposomes involved co-evaporation of the lipid and drug from the solvent system in a round bottom flask. First of all, various process variables were optimized and then formulation variables were optimized using RSM. The results are summarized and discussed in the following sections.

4.10.1 Optimization of TFH Method Process Variables

Process variables, such as vacuum conditions for dry film formation, hydration time, and speed of rotation of flask were optimized for desired results. The effect of one variable was studied at a time keeping other variables constant. The results are recorded in Table 4.3 from which the following conclusions are drawn:

1. The vacuum required for solvent evaporation to form a uniform thin film was raised from 400 mm Hg to 650 mm Hg. The low vacuum (400 mm Hg) was found to be insufficient for the complete removal of the solvent mixture. The presence of residual solvent may lead to physical destabilization of liposomes

by interfering with the co-operative hydrophobic interactions among the phospholipid methylene groups that hold the structure together (Martin et al., 1990(a)). The vacuum of 600 mm of Hg for 60 minutes was found to be optimum for complete evaporation of solvent mixture and producing more translucent and thin lipid film. However, for complete solvent removal of residual solvent (post film formation) the flask was kept in a desiccator for 24 hrs containing activated silica. Higher vacuum (650 mm Hg) resulted in rapid evaporation of the solvent system leading to crystallization of the drug and hence resulted in poor percent drug entrapment in the liposomes. This is in agreement with the findings of Martin et al (1990) that differential solubilities of amphiphilic components of bilayer and drug in organic solvents are often encountered and must be taken into consideration in order to avoid crystallization of a single component during solvent-stripping operations.

2. Speed of rotation: The speed of rotation of flask was increased from 50 rpm to 150 rpm. Rotation of 50 rpm resulted in thick incompletely dried film and presence of residual solvents. While at 150-rpm speed, a dry film with varying thickness was produced with a thicker film at periphery and thinner film at the center. A speed of 100 rpm was found to be adequate to give thin, uniform and completely dry film. Hence, 100-rpm speed of rotation of flask was selected to be optimum for liposomal preparations.
3. Hydration time: The lipid film was hydrated from 30 minutes to 2 hours before size reduction. An optimal hydration time was required for complete conversion of planner bilayers to spherical liposomes. Lower hydration time led to a non-uniform shape and size of the liposomes and also the un-hydrated part posed difficulty in size reduction. The hydration time beyond 1 h resulted in no further improvement. Hence, 1 hr hydration time was found to be optimum for both RGZ and CDS liposome preparation.

Table 4.3 Selection of process parameters by TFH method for RGZ and CDS liposomes

	RGZ	CDS
COMPOSITION OF SOLVENT SYSTEM		
CHLOROFORM: METHANOL	Observation	
1:1	No proper film, not proper hydration	No proper film, not proper hydration
2:1	No proper film, not proper hydration	No proper film, not proper hydration
1:2	No proper film, not proper hydration	No proper film, not proper hydration
4:1	Suitable	Suitable
SOLVENT EVAPORATION TIME		
Time (minutes)	Observation	
45 minutes	Not proper hydration	Not proper hydration
60 minutes	Suitable (Solvent is completely removed)	Suitable (Solvent is completely removed)
90 minutes	No further improvement	No further improvement
SPEED OF ROTATION		
rpm	Observation	
50 rpm	Non Uniform distribution	Non Uniform distribution
100 rpm	Suitable	Suitable
150 rpm	Non Uniform distribution	Non Uniform distribution
HYDRATION TIME		
Time (min)	Observation	
30 minutes	Not properly hydrated	Not properly hydrated
60 minutes	Suitable hydration	Suitable hydration
90 minutes	No further improvement but decrease in PDE	No further improvement but decrease in PDE
VACUUM APPLIED		
vacuum (mm of Hg)	Observation	
400	Flecking during hydration	Flecking during hydration
500	Flecking during hydration	Flecking during hydration
600	Uniform film and uniform liposomal dispersion	Uniform film and uniform liposomal dispersion
650	Un-uniform film	Un-uniform film

4.10.2 Formulation Optimization RGZ Loaded Liposomes Using Response Surface Methodology (RSM)

All twenty seven batches of liposomes were prepared according to the formulation variables as shown in Table 4.4. All formulations were evaluated for PDE and PR and the results obtained are shown in Table 4.4.

Table 4.4 3³ Full factorial design outline with results for PDE and PR. The data represent the mean ± SEM (n = 3).

Batch No.	X1	X2	X3	X1 ²	X2 ²	X3 ²	X1X2	X2X3	X1X3	X1X2 X3	PDE (mean* ± SEM)	PR (mean* ± SEM)
1	0	0	-1	0	0	1	0	0	0	0	79.79 ± 1.272	2.99 ± 0.051
2	0	0	0	0	0	0	0	0	0	0	78.24 ± 0.944	2.63 ± 0.070
3	0	0	1	0	0	1	0	0	0	0	69.70 ± 0.962	2.84 ± 0.063
4	0	-1	-1	0	1	1	0	1	0	0	81.83 ± 0.916	4.55 ± 0.096
5	0	-1	0	0	1	0	0	0	0	0	80.63 ± 0.848	4.14 ± 0.091
6	0	-1	1	0	1	1	0	-1	0	0	75.84 ± 1.024	5.25 ± 0.116
7	0	1	-1	0	1	1	0	-1	0	0	75.13 ± 0.957	2.20 ± 0.067
8	0	1	0	0	1	0	0	0	0	0	73.23 ± 1.122	2.32 ± 0.074
9	0	1	1	0	1	1	0	1	0	0	61.23 ± 0.638	2.32 ± 0.069
10	-1	0	-1	1	0	1	0	0	1	0	60.34 ± 0.886	2.67 ± 0.084
11	-1	0	0	1	0	0	0	0	0	0	58.00 ± 0.769	3.84 ± 0.098
12	-1	0	1	1	0	1	0	0	-1	0	51.52 ± 0.950	3.16 ± 0.084
13	-1	-1	-1	1	1	1	1	1	1	-1	65.15 ± 0.770	6.05 ± 0.139
14	-1	-1	0	1	1	0	1	0	0	0	62.61 ± 0.734	5.59 ± 0.120
15	-1	-1	1	1	1	1	1	-1	-1	1	55.62 ± 0.824	5.16 ± 0.117
16	-1	1	-1	1	1	1	-1	-1	1	1	52.50 ± 0.722	2.32 ± 0.065
17	-1	1	0	1	1	0	-1	0	0	0	51.17 ± 0.758	2.72 ± 0.063
18	-1	1	1	1	1	1	-1	1	-1	-1	44.06 ± 0.696	2.77 ± 0.077
19	1	0	-1	1	0	1	0	0	-1	0	79.66 ± 0.935	2.81 ± 0.067
20	1	0	0	1	0	0	0	0	0	0	78.39 ± 0.988	2.62 ± 0.058
21	1	0	1	1	0	1	0	0	1	0	68.43 ± 0.837	3.01 ± 0.080
22	1	-1	-1	1	1	1	-1	1	-1	1	83.01 ± 1.119	5.29 ± 0.104
23	1	-1	0	1	1	0	-1	0	0	0	82.16 ± 1.050	6.16 ± 0.132
24	1	-1	1	1	1	1	-1	-1	1	-1	75.32 ± 1.141	5.46 ± 0.121
25	1	1	-1	1	1	1	1	-1	-1	-1	73.78 ± 0.984	2.09 ± 0.051
26	1	1	0	1	1	0	1	0	0	0	72.25 ± 0.852	2.12 ± 0.058
27	1	1	1	1	1	1	1	1	1	1	60.02 ± 0.746	2.22 ± 0.079

A full model for both PDE and PR was established by putting the values of intercepts and regression coefficients in polynomial equation.

PDE Full equation

$$Y_{\text{PDE}} = 78.14468 + 9.558367 X_1 - 5.48965 X_2 - 4.96913 X_3 - 9.84887 X_1^2 - 1.25302 X_2^2 - 3.35766 X_3^2 + 0.099888 X_1 X_2 - 1.07391 X_2 X_3 - 0.49006 X_1 X_3 - 0.8949 X_1 X_2 X_3$$

PR Full equation

$$Y_{\text{PR}} = 2.714256 - 0.13946 X_1 - 1.47617 X_2 + 0.068833 X_3 + 0.421645 X_1^2 + 0.866131 X_2^2 - 0.06424 X_3^2 - 0.12592 X_1 X_2 + 0.059925 X_2 X_3 + 0.037889 X_1 X_3 - 0.17164 X_1 X_2 X_3$$

The Model F-value of 284.38 and 24.47 respectively for PDE and PR implies the model is significant. For both PDE and PR, there is only a 0.01% chance that a

"Model F-Value" this large could occur due to noise. Values of "Probability value > F" less than 0.0500 indicate model terms are significant. In the case of PDE X_1 , X_2 , X_3 , X_2X_3 , X_1^2 , X_2^2 , X_3^2 and $X_1X_2X_3$ and in the case of PR X_2 , X_1^2 , X_2^2 are significant model terms. Values greater than 0.1000 indicate the model terms are not significant. If there are many insignificant model terms model reduction may improve the model.

PDE Reduced equation

$$Y_{\text{PDE}} = 78.14468 + 9.558367 X_1 - 5.48965 X_2 - 4.96913 X_3 - 9.84887 X_1^2 - 1.25302 X_2^2 - 3.35766 X_3^2 - 1.07391 X_2X_3 - 0.8949 X_1X_2X_3$$

PR Reduced equation

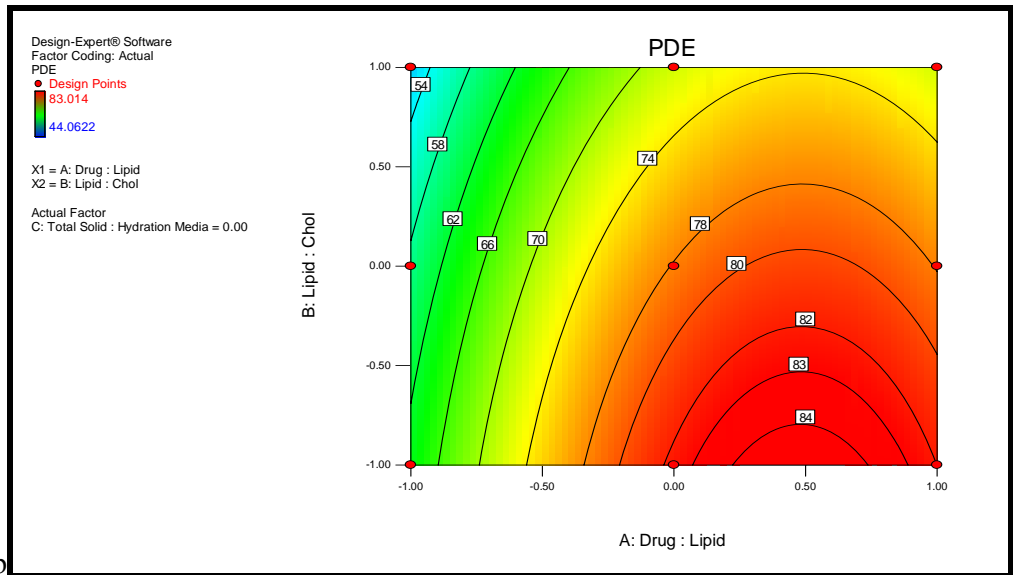
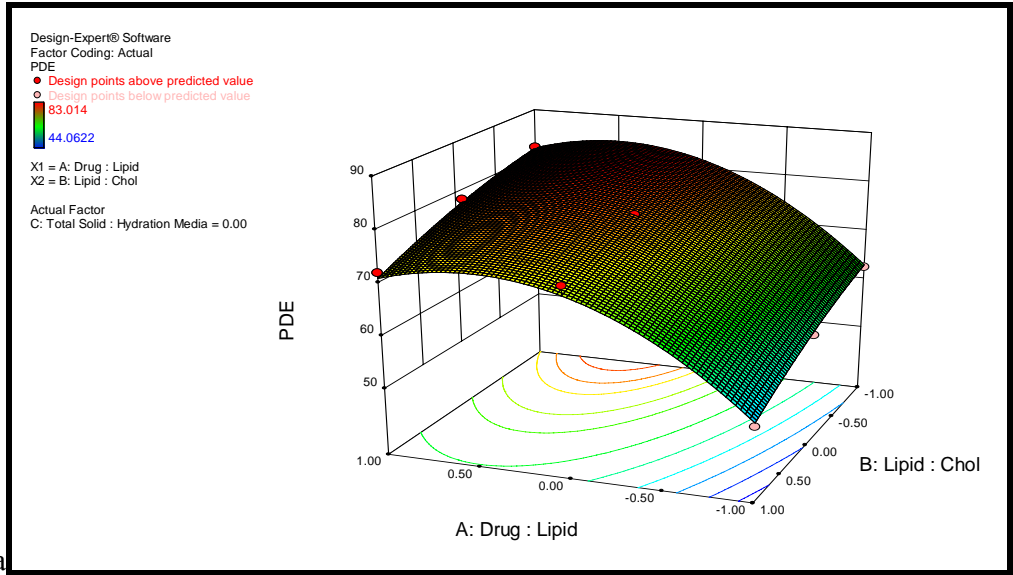
$$Y_{\text{PR}} = 2.671429 - 1.47617 X_2 + 0.421645 X_1^2 + 0.866131 X_2^2$$

The "Predicted R-Squared" of 0.9802 is in reasonable agreement with the "Adjusted R-Squared" of 0.9909 in case of PDE and the "Predicted R-Squared" of 0.8418 is in reasonable agreement with the "Adjusted R-Squared" of 0.9003 in the case of PE. "Adequate Precision" measures the signal to noise ratio. A ratio greater than 4 is desirable. The ratio of 56.661 for PDE and 13.470 for PR indicates an adequate signal. This model can be used to navigate the design space.

Comparison of full model (FM) and reduced model (RM) was done by ANOVA by applying the F-Statistic to check effect of omission of the statistically insignificant coefficients from the full model and the results are shown in Table 4.5.

Table 4.5 Analysis of Variance (ANOVA) of full and reduced models

Response	Model		df	SS	MS	F	Adjusted R ²	Predicted R ²	ANOVA comparison	
									F Calculated	F Tabulated
PDE	Regression	FM	10	3313.75	331.38	284.38	0.9909	0.9802	1.2880	3.63
		RM	8	3310.75	413.84	344.14				
	Residual (Error)	FM	16	18.64	1.17					
		RM	18	21.65	1.20					
PE	Regression	FM	10	45.74	4.57	24.47	0.9003	0.8418	0.7233	2.66
		RM	3	44.79	14.93	87.23				
	Residual (Error)	FM	16	2.99	0.19					
		RM	23	3.94	0.17					



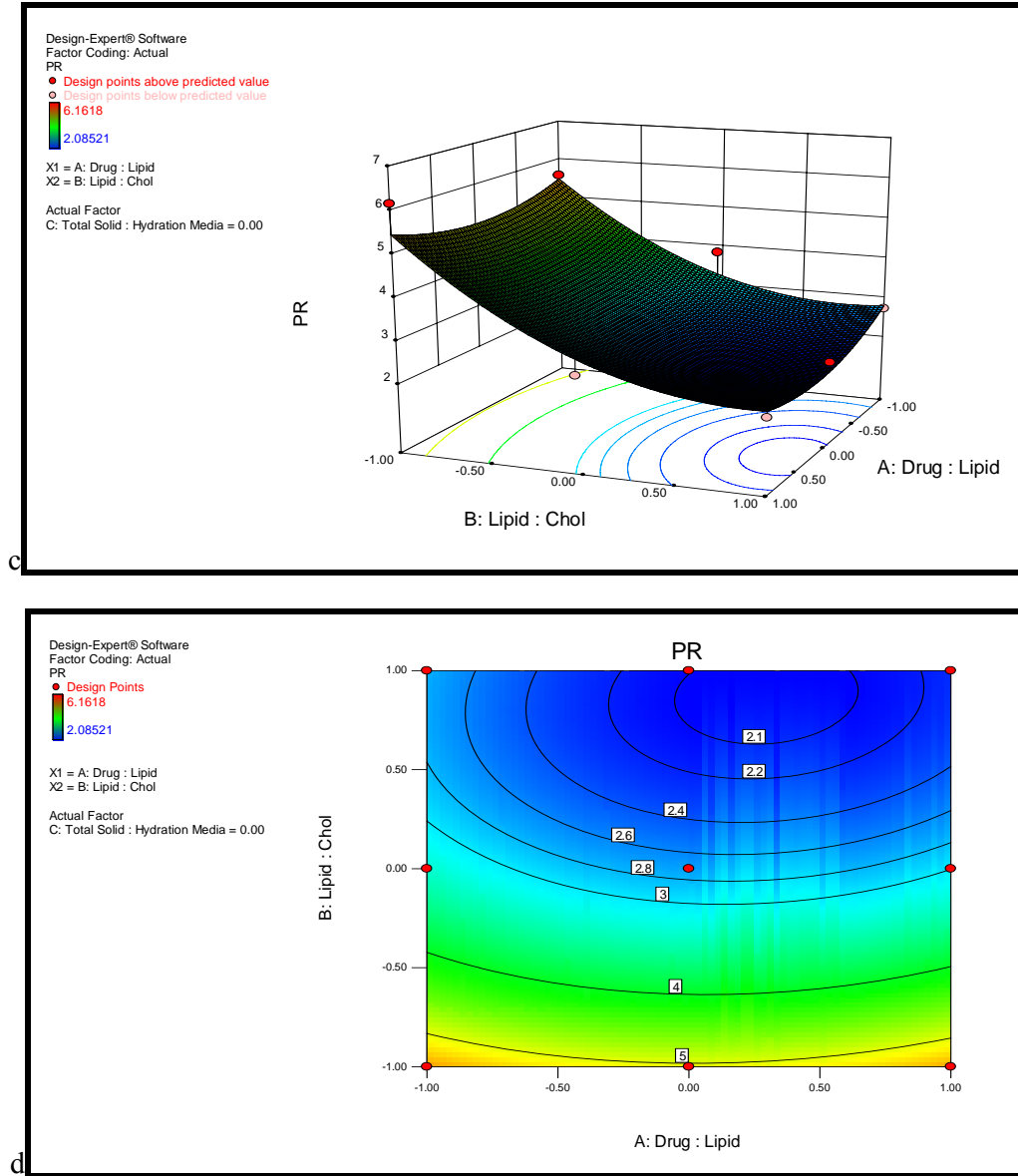
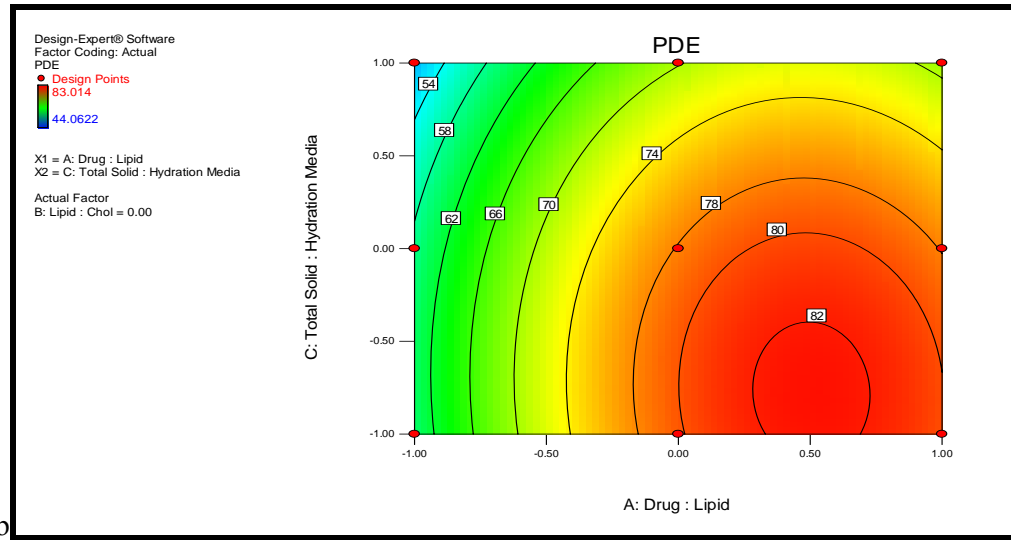
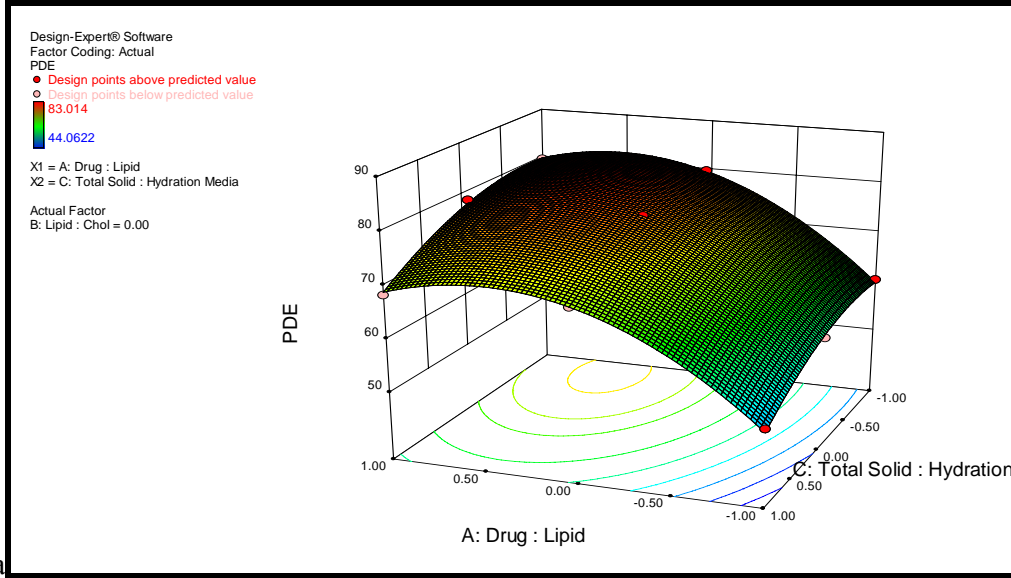


Figure 4.1 Response surface plot and corresponding contour plot showing the influence of Drug:Lipid and Lipid:Chol ratio on PDE (a & b) and PR (c & d) for **RGZ**



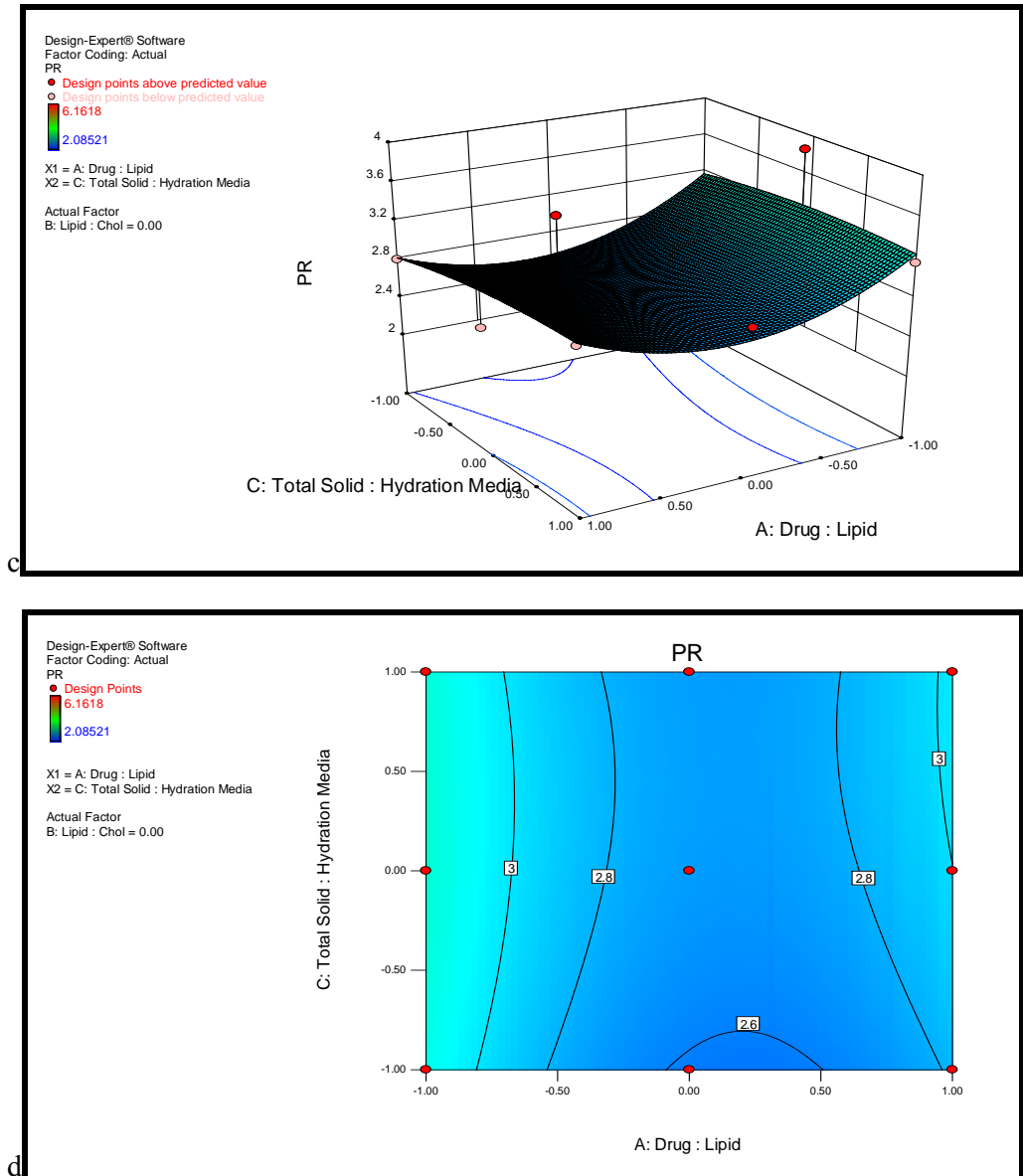
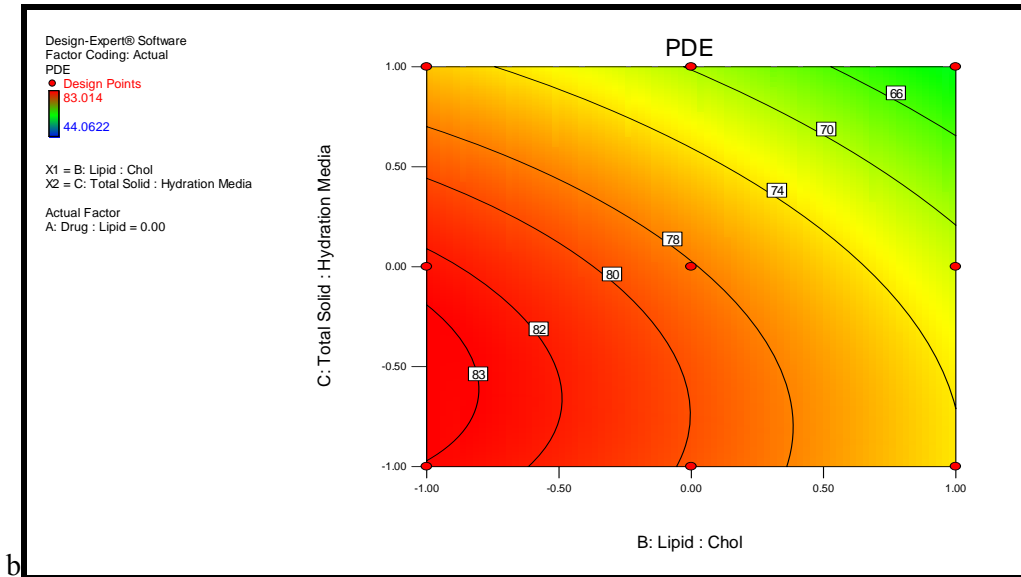
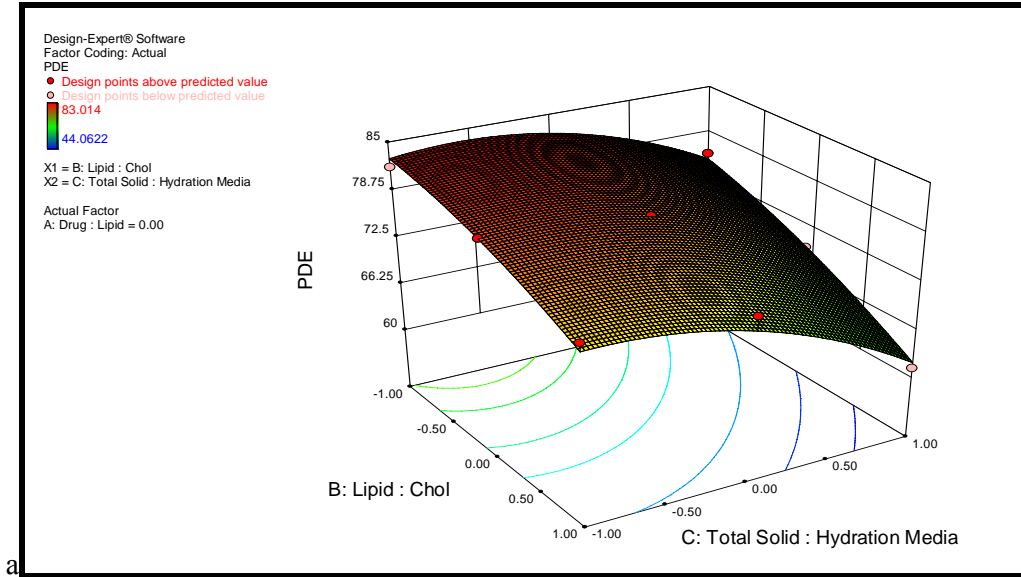


Figure 4.2 Response surface plot and corresponding contour plot showing the influence of Drug:Lipid and Total solid:Hydration medium ratio on PDE (a & b) and PR (c & d) for RGZ



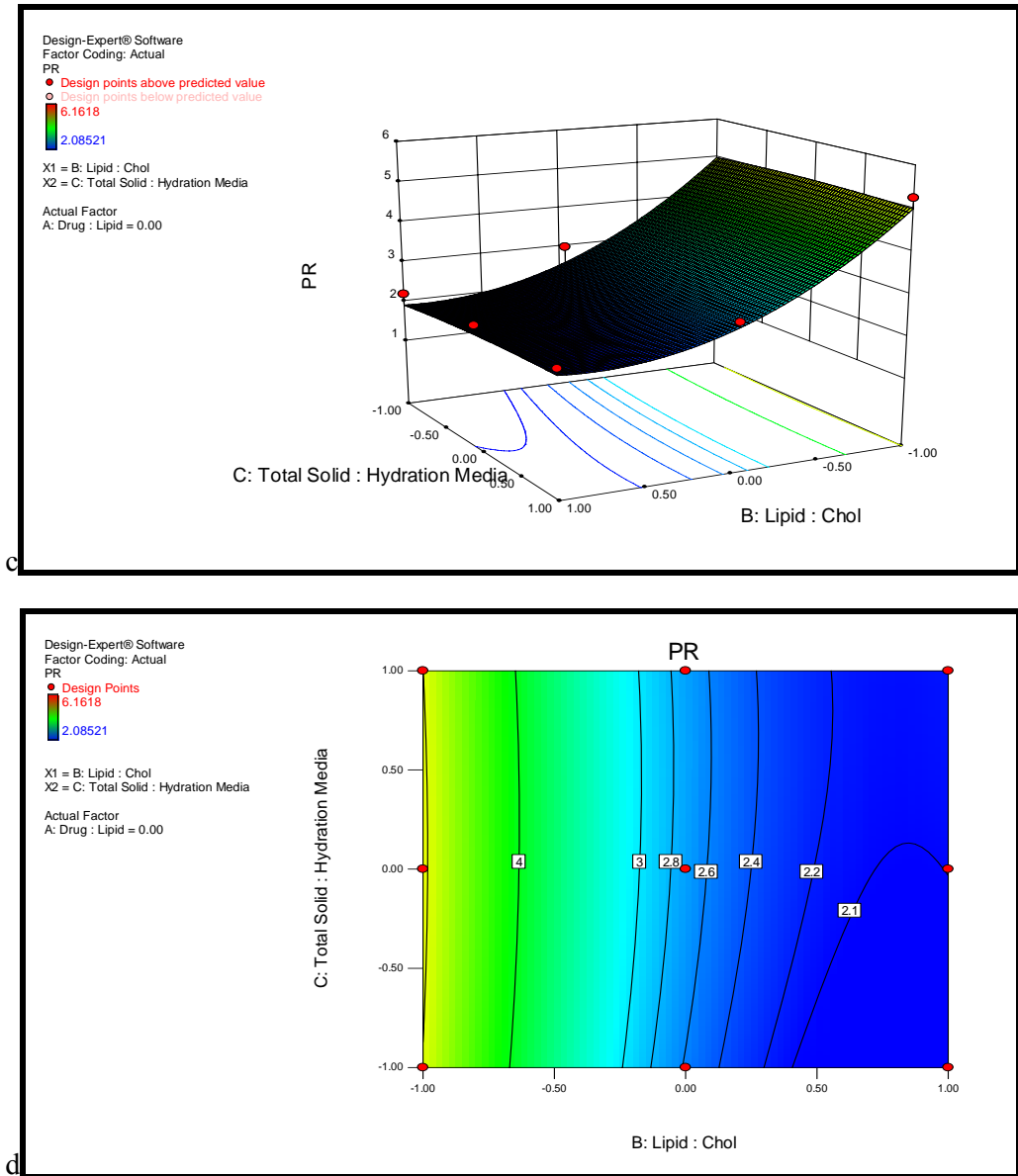


Figure 4.3 Response surface plot and corresponding contour plot showing the influence of Lipid:Chol and Total solid:Hydration medium ratio on PDE (a & b) and PR (c & d) for RGZ

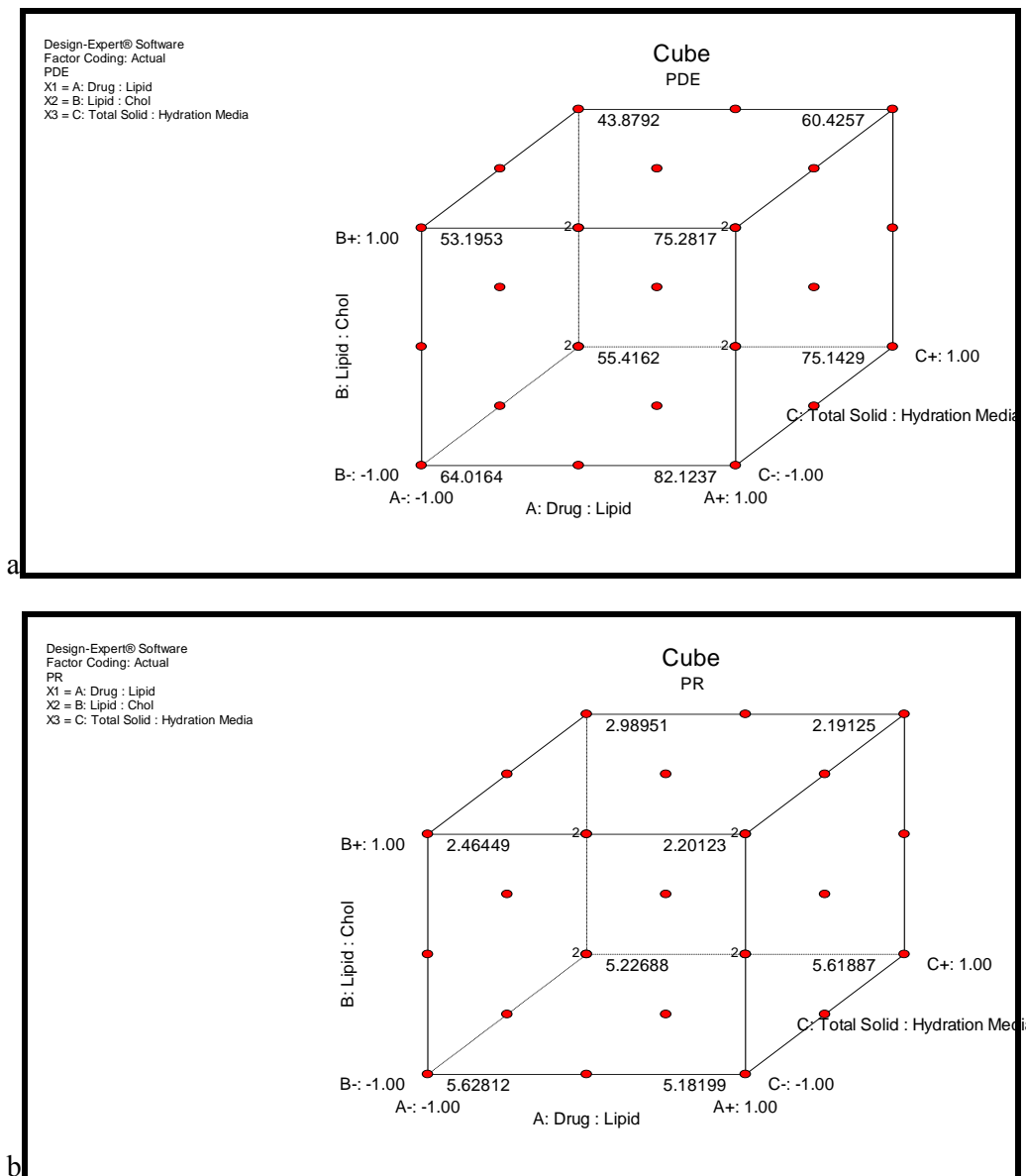


Figure 4.4 Cube plots for PDE (a) and PR (b) representing the effects of three factors at a time for RGZ

Figure 4.1a and 4.1c represent response surface plot and figure 4.1b and 4.1d correspond to contour plots showing the influence of drug:lipid and lipid:cholesterol ratio on PDE (figure 4.1a & 4.1b) and PR (figure 4.1c & 4.1d) by keeping the total solid:hydration medium ratio at 0.0. Rapid increase in PDE was observed with increase in drug:lipid ratio from -1.0 to 0.0, thereafter there was a bare minimum change in PDE and drug:lipid ratio had very little or no effect on PR. On the other

part, increase in lipid: cholesterol ratio was associated with rapid decrease in PR and had minimum effect on PDE.

Figure 4.2a and 4.2c represent response surface plot and figure 4.2b and 4.2d correspond to contour plots showing the influence of drug:lipid and total solid:hydration medium ratio on PDE (figure 4.2a & 4.2b) and PR (figure 4.2c & 4.2d) by keeping the lipid:cholesterol ratio at 0.0. Hasty increase in PDE was observed with raise in drug:lipid ratio from -1.0 to 0.0, thereafter there was a least change in PDE. Slight decrease in PR was seen with increase in drug:lipid ratio from -1.0 to 0.0 but from 0.0 to 1.0 there was a slight increase in PR. On the other side, total solid:hydration medium ratio had minimum effect on both PDE and PR.

Figure 4.3a and 4.3c represent response surface plot and figure 4.3b and 4.3d correspond to contour plots showing the influence of lipid:cholesterol and total solid:hydration medium on PDE (figure 4.3a & 4.3b) and PR (figure 4.3c & 4.3d) by keeping the drug:lipid ratio at 0.0. Slow decrease in PDE and rapid decrease in PR were observed with increase in lipid:cholesterol ratio from -1.0 to 0.0, thereafter i.e. from 0.0 to 1.0, the decrease in PDE was slightly faster and the decrease in PR was somewhat sluggish. On the other part, no change in PDE was observed with increase in total solid:hydration medium ratio from -1.0 to 0.0 thereafter, i.e. from 0.0 to 1.0, there was a decrease in PDE. Total solid:hydration medium ratio had minimum effect on PR.

Effect of all the three formulation variables on the response parameters at a time are represented in the form of cube plots in figure 4.4a (PDE) and figure 4.4b (PR).

4.10.2.1 Checkpoint Analysis

Eight checkpoint batches were prepared three times and evaluated for the results of response variables. Compositions of each checkpoint batch along with the predicted and experimental values, percentage error and p-value is listed in Table 4.6. Linear correlation plots between the observed and predicted response variables along with r^2 values are shown in figure 4.5a and 4.5b for PDE and PR respectively. P-value > 0.05 indicates the differences between predicted and experimental values are statistically insignificant. Higher r^2 values (0.9947 and 0.9995 for PDE and PR respectively) of

the linear correlation plots suggest excellent goodness of fit and high predictive capability of RSM.

Table 4.6 Checkpoint Analysis. The data represent the mean \pm SEM (n = 3).

S r. N o. ·	Formulation composition			Comparison							
	Drug:Lipid molar ratio	Lipid:Cholesterol molar ratio	Total solid content: Volume of hydration media	PDE				PR			
				Predicted Value	Experimental value (Mean* \pm SEM)	Percentage error	P value	Predicted Value	Experimental value (Mean* \pm SEM)	Percentage error	P value
1	-0.7 (1:16.5)	0.4 (7.6:2.4)	0.2 (13:1)	63.11	64.12 \pm 0.972	1.596	P > 0.05 Non significant	2.62	2.58 \pm 0.035	-1.400	P > 0.05 Non significant
2	-0.4 (1:18)	0.2 (7.8:2.2)	-0.3 (11.75:1)	72.76	71.64 \pm 1.006	-1.539		2.56	2.57 \pm 0.047	0.521	
3	0.9 (1:24.5)	-0.3 (8.3:1.7)	0.6 (14:1)	76.16	75.31 \pm 1.083	-1.116		3.54	3.49 \pm 0.052	-1.506	
4	0.7 (1:23.5)	-0.5 (8.5:1.5)	-0.5 (11.25:1)	83.8	82.56 \pm 1.038	-1.476		3.74	3.68 \pm 0.055	-1.604	
5	0.2 (1:21)	-0.8 (8.8:1.2)	0.5 (13.75:1)	80.36	79.15 \pm 1.040	-1.506		4.47	4.39 \pm 0.064	-1.715	
6	-0.3 (1:18.5)	0.8 (7.2:2.8)	-0.8 (10.5:1)	71.4	69.58 \pm 1.026	-2.545		2.04	2.00 \pm 0.038	-1.961	
7	-0.9 (1:15.5)	0.9 (7.1:2.9)	0.8 (14.5:1)	49.56	48.67 \pm 0.970	-1.796		2.8	2.74 \pm 0.041	-2.024	
8	-0.8 (1:16)	-0.7 (8.7:1.3)	-0.6 (11:1)	68.87	68.07 \pm 0.873	-1.157		4.52	4.45 \pm 0.064	-1.622	

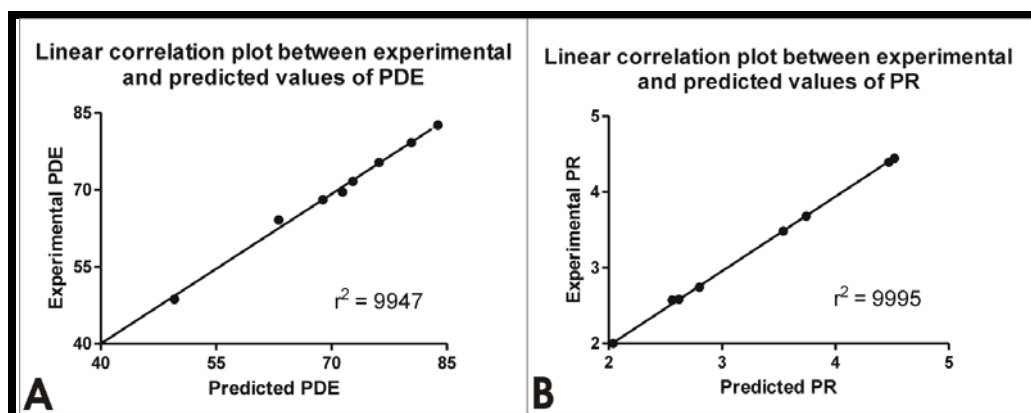


Figure 4.5 Linear correlation plots of the experimental response values versus the predicted response values for PDE (a) and PR (b) for RGZ

The optimum formulation was derived by deciding goals for each formulation variable and response parameter and allotting the importance to each of them. By fixing the goal and importance we derived an optimum formulation as described in Table 4.7. The optimized batch (Drug: Lipid molar ratio = -0.02; Lipid: Cholesterol molar ratio = 0.40; Total solid content: Volume of hydration media = 0.02) was actually prepared and the experimental results were compared with predicted values.

P-value > 0.05 indicates the differences between predicted and experimental values are statistically insignificant.

Table 4.7 Derivation of optimized formulation. The data represent the mean \pm SEM (n = 3).

Constrains			Lower Limit	Upper Limit	Predicted solution [A]	Actual results (Mean \pm SEM) [B]	Comparison of A and B (P value)
Name	Goal	Importance					
Drug:Lipid molar ratio	Minimize	5	-1	1	-0.20	-0.02	
Lipid:Cholesterol molar ratio	Maximize	2	-1	1	0.40	0.40	
Total solid content: Volume of hydration media	Minimize	2	-1	1	0.02	0.02	
PDE	Maximize	5	44.062	83.014	73.32	71.83 \pm 0.683	P > 0.05, Non significant
PR	Minimize	2	2.0852	6.1618	2.32	2.41 \pm 0.081	P > 0.05 Non significant

4.10.3 Formulation Optimization CDS Loaded Liposomes Using Response Surface Methodology (RSM)

All twenty seven batches of liposomes were prepared according to the formulation variables as shown in Table 4.8. All formulations were evaluated for PDE and PR and the results obtained are shown in Table 4.8.

Table 4.8 3³ Full factorial design outline with results for PDE and PR. The data represent the mean \pm SEM (n = 3).

Batch No.	X1	X2	X3	X1 ²	X2 ²	X3 ²	X1X2	X2X3	X1X3	X1X2 X3	PDE (mean* \pm SEM)	PR (mean* \pm SEM)
1	0	0	-1	0	0	1	0	0	0	0	71.53 \pm 0.994	3.06 \pm 0.063
2	0	0	0	0	0	0	0	0	0	0	70.28 \pm 1.021	3.00 \pm 0.074
3	0	0	1	0	0	1	0	0	0	0	61.64 \pm 0.857	3.77 \pm 0.068
4	0	-1	-1	0	1	1	0	1	0	0	74.17 \pm 1.113	4.95 \pm 0.089
5	0	-1	0	0	1	0	0	0	0	0	72.57 \pm 0.991	5.34 \pm 0.097
6	0	-1	1	0	1	1	0	-1	0	0	66.28 \pm 0.894	5.81 \pm 0.121
7	0	1	-1	0	1	1	0	-1	0	0	65.97 \pm 0.786	2.72 \pm 0.059
8	0	1	0	0	1	0	0	0	0	0	64.37 \pm 0.954	2.91 \pm 0.068
9	0	1	1	0	1	1	0	1	0	0	52.49 \pm 0.584	2.64 \pm 0.062
10	-1	0	-1	1	0	1	0	0	1	0	51.68 \pm 0.701	3.26 \pm 0.093
11	-1	0	0	1	0	0	0	0	0	0	49.96 \pm 0.723	3.65 \pm 0.105
12	-1	0	1	1	0	1	0	0	-1	0	43.94 \pm 0.631	3.76 \pm 0.091
13	-1	-1	-1	1	1	1	1	1	1	-1	56.58 \pm 0.711	5.82 \pm 0.118
14	-1	-1	0	1	1	0	1	0	0	0	54.85 \pm 0.672	5.94 \pm 0.133
15	-1	-1	1	1	1	1	1	-1	-1	1	45.48 \pm 0.559	5.92 \pm 0.108
16	-1	1	-1	1	1	1	-1	-1	1	1	42.82 \pm 0.598	2.69 \pm 0.073
17	-1	1	0	1	1	0	-1	0	0	0	40.52 \pm 0.635	3.17 \pm 0.072
18	-1	1	1	1	1	1	-1	1	-1	-1	36.41 \pm 0.526	3.26 \pm 0.081
19	1	0	-1	1	0	1	0	0	-1	0	71.20 \pm 0.739	3.00 \pm 0.066
20	1	0	0	1	0	0	0	0	0	0	69.65 \pm 0.971	3.02 \pm 0.068
21	1	0	1	1	0	1	0	0	1	0	61.10 \pm 0.877	3.45 \pm 0.075
22	1	-1	-1	1	1	1	-1	1	-1	1	73.93 \pm 0.955	5.78 \pm 0.119
23	1	-1	0	1	1	0	-1	0	0	0	72.42 \pm 0.911	5.90 \pm 0.120
24	1	-1	1	1	1	1	-1	-1	1	-1	66.56 \pm 0.858	5.75 \pm 0.114
25	1	1	-1	1	1	1	1	-1	-1	-1	65.82 \pm 1.042	2.04 \pm 0.059
26	1	1	0	1	1	0	1	0	0	0	63.19 \pm 0.793	2.11 \pm 0.054
27	1	1	1	1	1	1	1	1	1	1	51.79 \pm 0.667	2.32 \pm 0.066

A full model for both PDE and PR was established by putting the values of intercepts and regression coefficients in polynomial equation.

PDE Full equation

$$Y_{\text{PDE}} = 69.99638 + 9.633683 X_1 - 5.52636 X_2 - 4.88825 X_3 - 10.0405 X_1^2 - 1.98564 X_2^2 - 3.12295 X_3^2 + 0.420818 X_1 X_2 - 0.63064 X_2 X_3 - 0.52058 X_1 X_3 - 1.41881 X_1 X_2 X_3$$

PR Full equation

$$Y_{\text{PR}} = 3.24391 - 0.22759 X_1 - 1.51856 X_2 + 0.18723 X_3 + 0.13591 X_1^2 + 0.83919 X_2^2 - 0.00416 X_3^2 - 0.19882 X_1 X_2 - 0.01364 X_2 X_3 - 0.03916 X_1 X_3 - 0.01992 X_1 X_2 X_3$$

The Model F-value of 311.861 and 71.205 respectively for PDE and PR implies the model is significant. For both PDE and PR, there is only a 0.01% chance that a "Model F-Value" this large could occur due to noise. Values of "Probability value > F" less than 0.0500 indicate model terms are significant. In the case of PDE X_1 , X_2 ,

X_3 , X_1^2 , X_2^2 , X_3^2 and $X_1X_2X_3$ and in the case of PR X_1 , X_2 , X_3 , X_2^2 and X_1X_2 are significant model terms. Values greater than 0.1000 indicate the model terms are not significant. If there are many insignificant model terms model reduction may improve the model.

PDE Reduced equation

$$Y_{PDE} = 69.99638 + 9.633683 X_1 - 5.52636 X_2 - 4.88825 X_3 - 10.0405 X_1^2 - 1.98564 X_2^2 - 3.12295 X_3^2 - 1.41881 X_1X_2X_3$$

PR Reduced equation

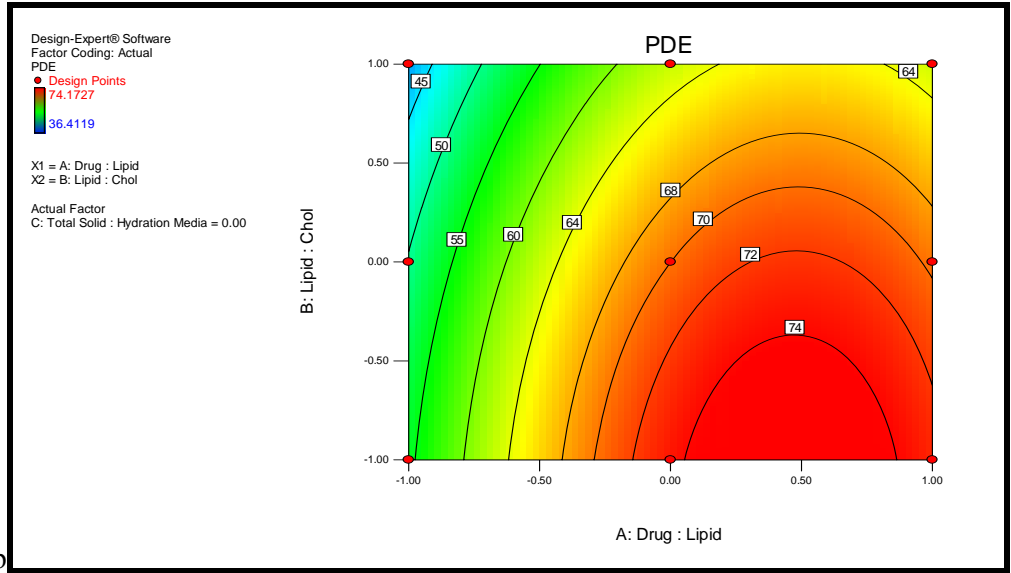
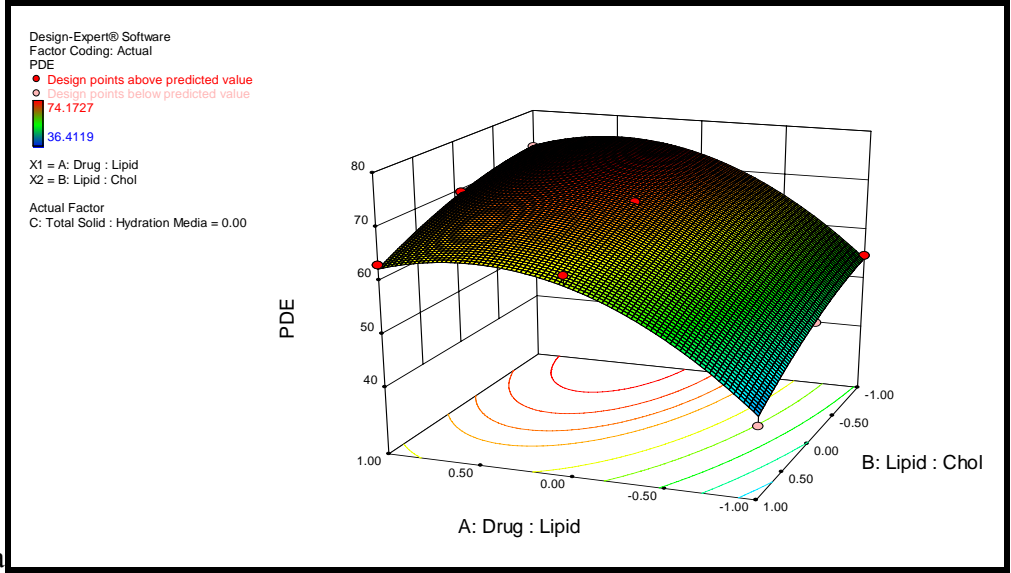
$$Y_{PR} = 3.33174 - 0.2276 X_1 - 1.51856 X_2 + 0.18723 X_3 + 0.83919 X_2^2 - 0.19882 X_1X_2$$

The "Predicted R-Squared" of 0.9843 is in reasonable agreement with the "Adjusted R-Squared" of 0.9917 in case of PDE and the "Predicted R-Squared" of 0.9286 is in reasonable agreement with the "Adjusted R-Squared" of 0.9643 in the case of PE. "Adequate Precision" measures the signal to noise ratio. A ratio greater than 4 is desirable. The ratio of 58.81 for PDE and 23.12 for PR indicates an adequate signal. This model can be used to navigate the design space.

Comparison of full model (FM) and reduced model (RM) was done by analysis of variance (ANOVA) by applying the F-Statistic to check effect of omission of the statistically insignificant coefficients from the full model and the results are shown in Table 4.9.

Table 4.9 Analysis of Variance (ANOVA) of full and reduced models

Response	Model		df	SS	MS	F	Adjusted R ²	Predicted R ²	ANOVA comparison	
									F Calculated	F Tabulated
PDE	Regression	FM	10	3363.677	336.368	311.861	0.9917	0.9843	3.1367	3.24
		RM	8	3353.527	479.075	332.122				
	Residual (Error)	FM	16	17.257	1.079					
		RM	18	27.407	1.443					
PE	Regression	FM	10	47.906	4.791	71.205	0.9643	0.9286	0.4005	2.85
		RM	3	43.182	10.796	40.947				
	Residual (Error)	FM	16	1.076	0.067					
		RM	23	5.800	0.264					



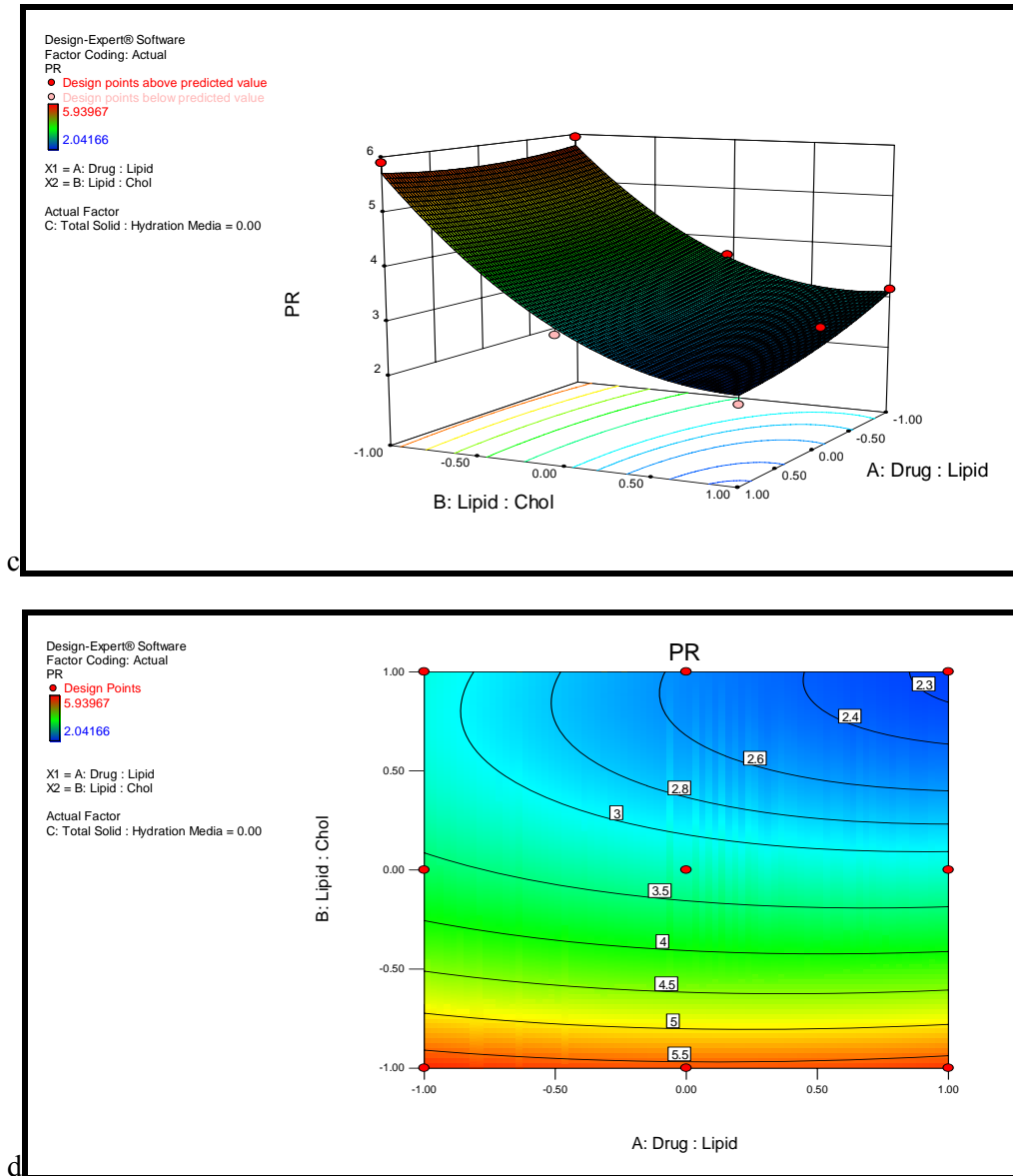
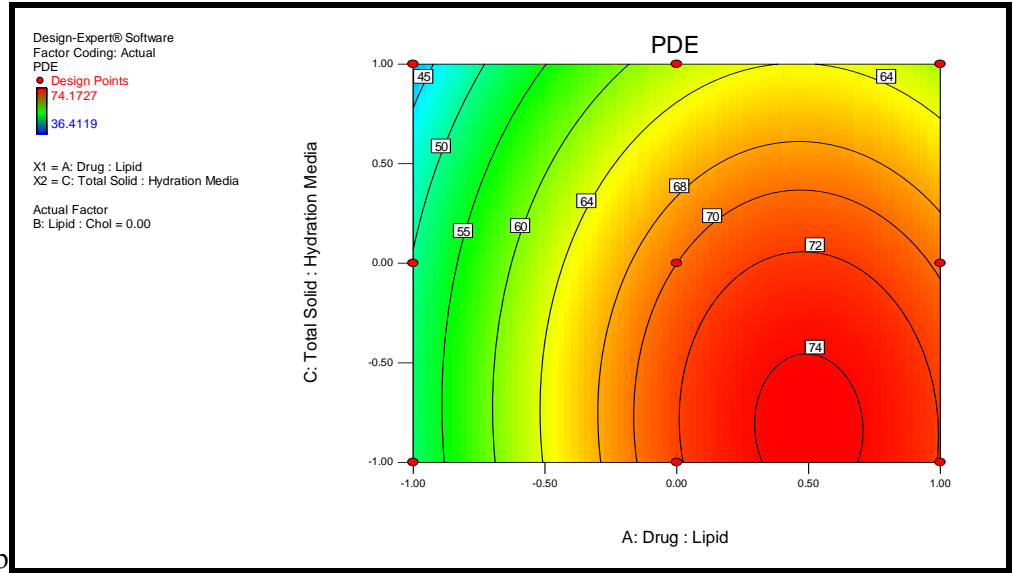
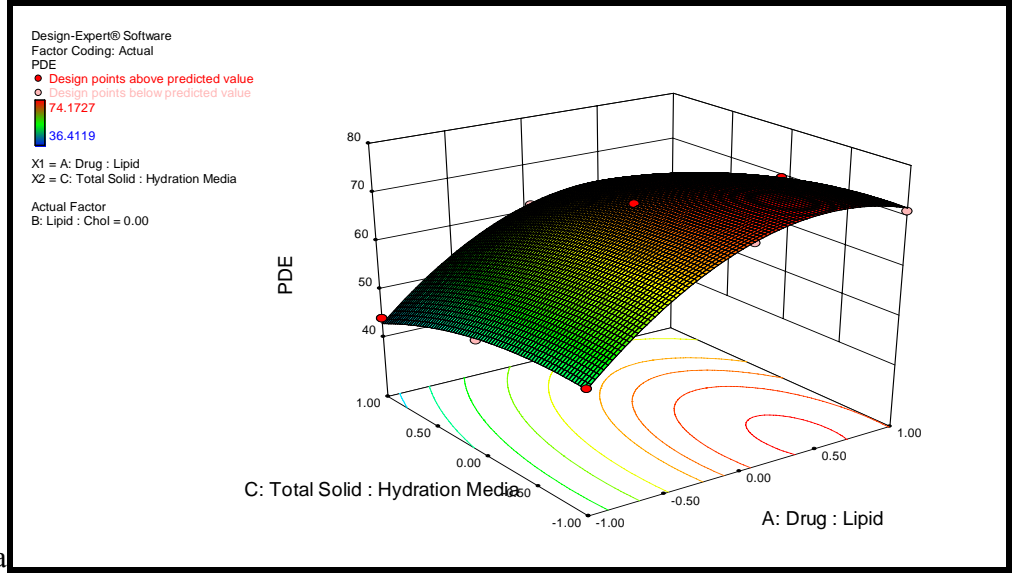


Figure 4.6 Response surface plot and corresponding contour plot showing the influence of Drug: Lipid and Lipid: Chol ratio on PDE (a & b) and PR (c & d) for CDS



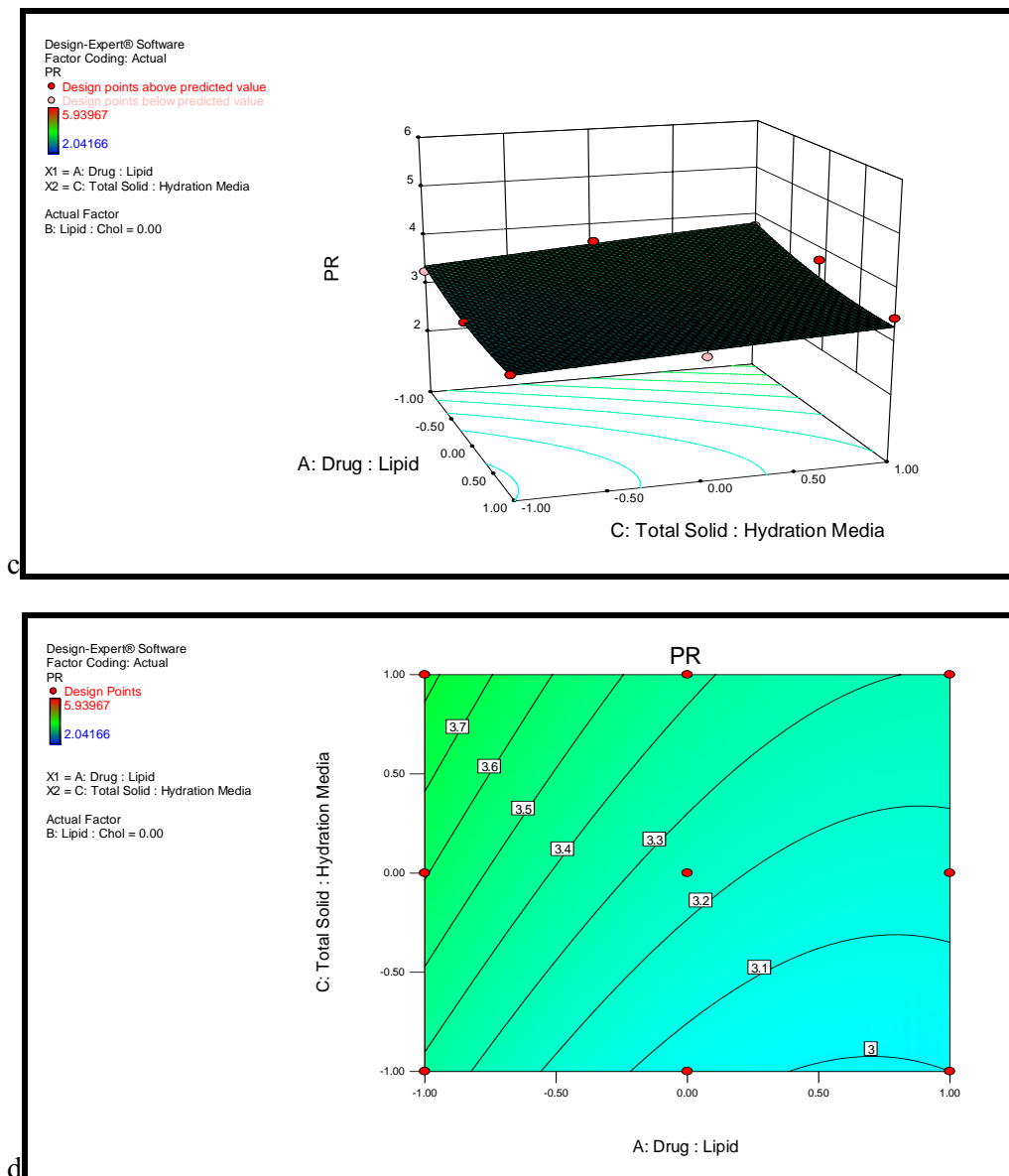
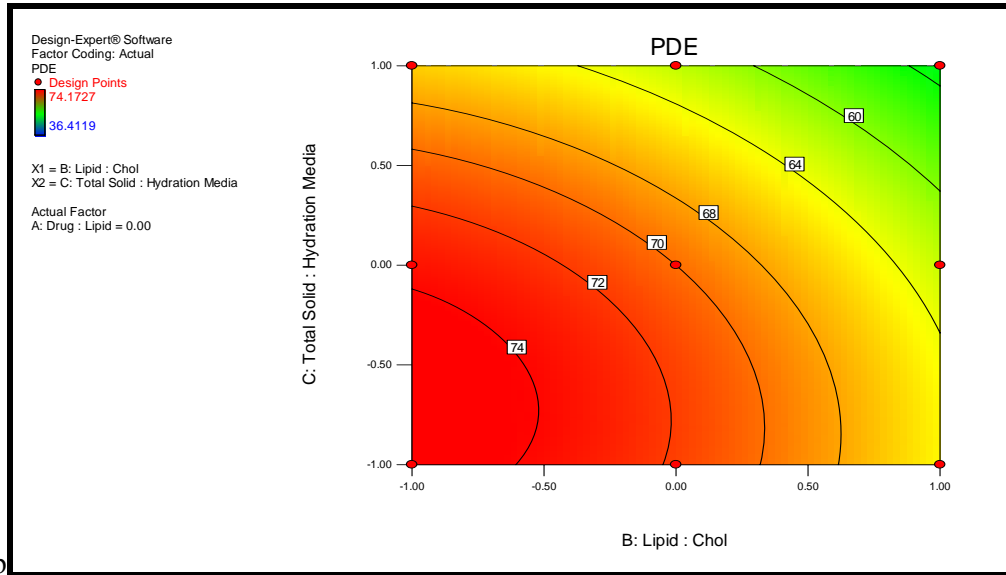
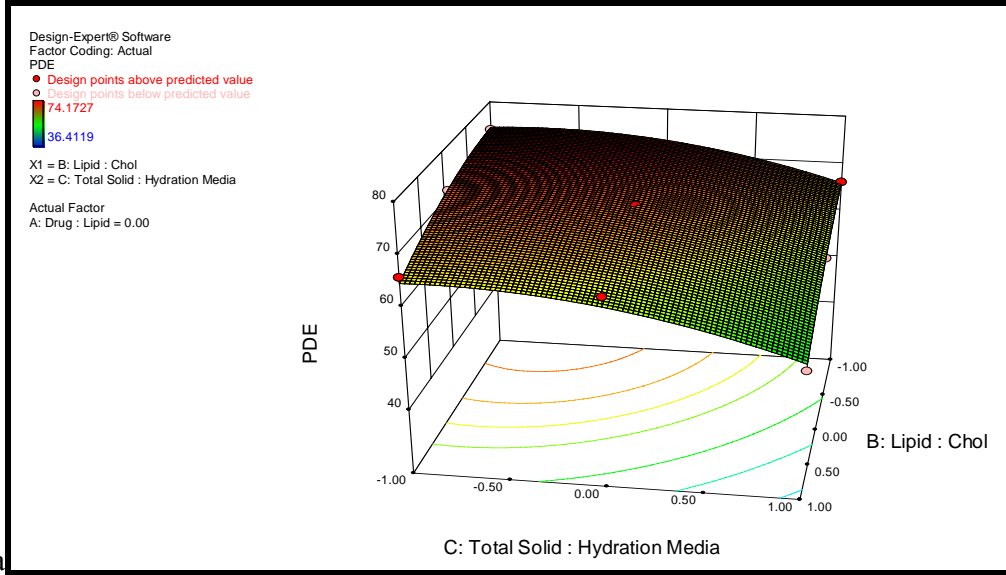


Figure 4.7 Response surface plot and corresponding contour plot showing the influence of Drug: Lipid and Total solid: Hydration medium ratio on PDE (a & b) and PR (c & d) for CDS



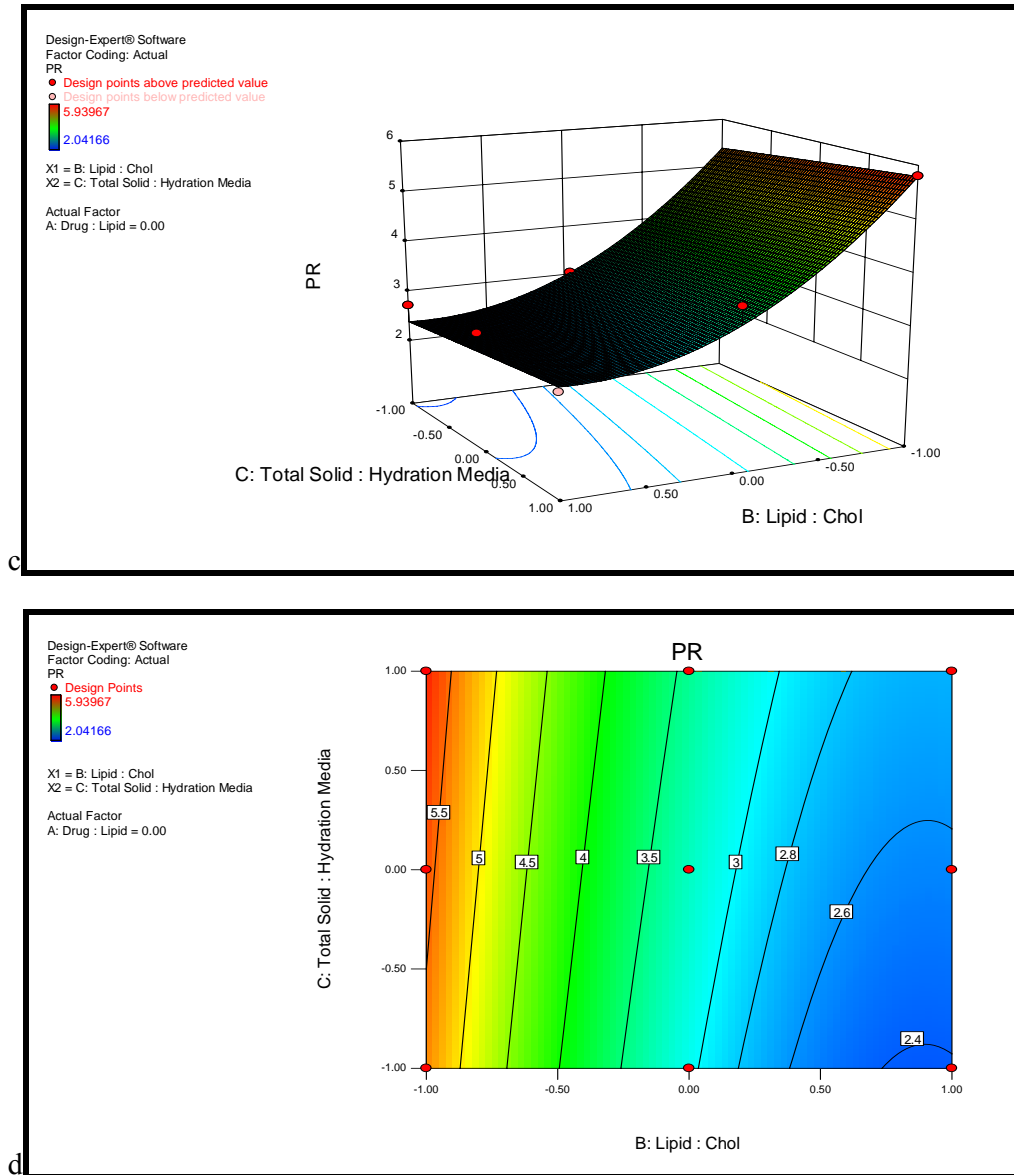


Figure 4.8 Response surface plot and corresponding contour plot showing the influence of Lipid: Chol and Total solid: Hydration medium ratio on PDE (a & b) and PR (c & d) for CDS

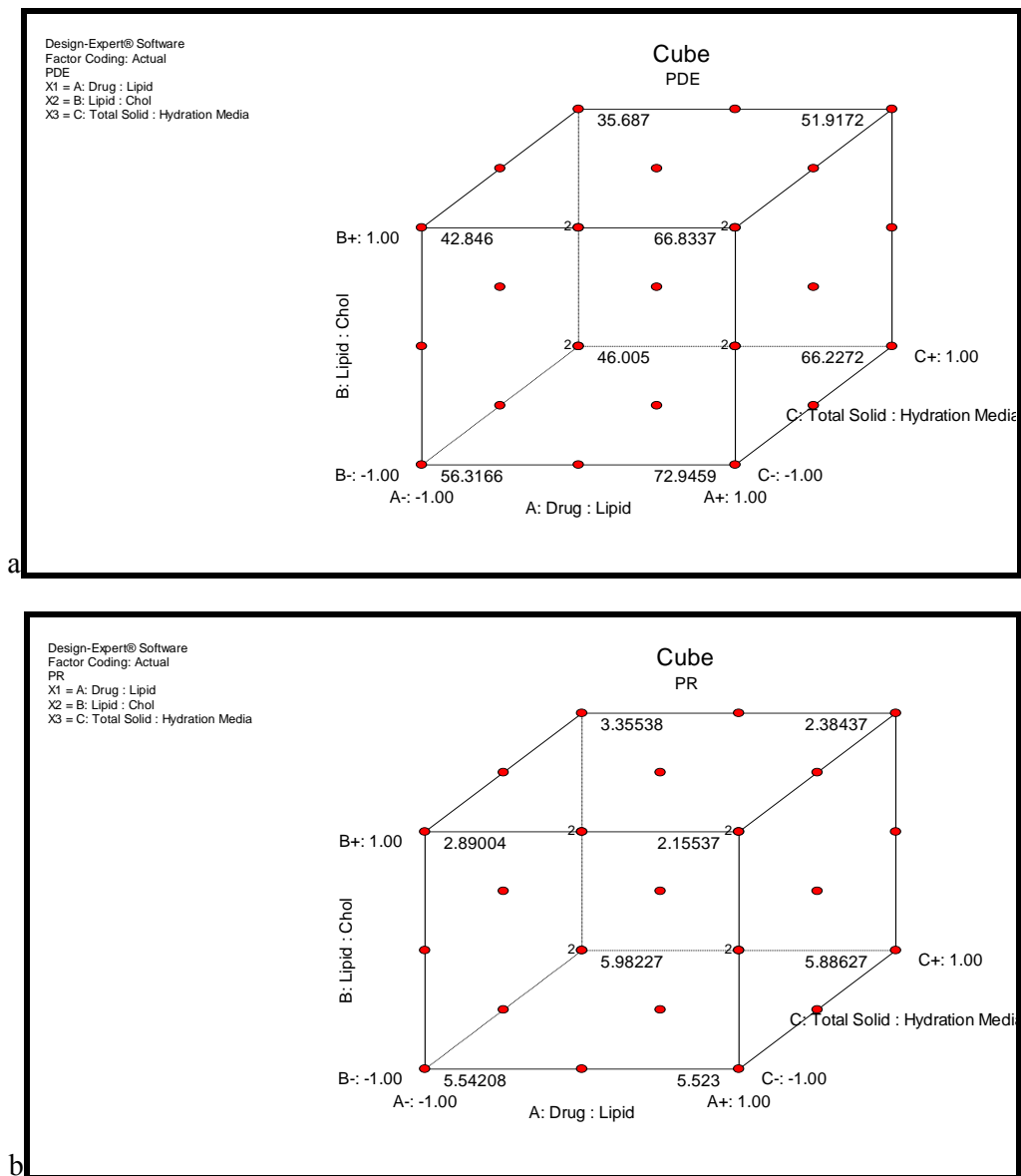


Figure 4.9 Cube plots for PDE (a) and PR (b) representing the effects of three factors at a time for CDS

Figure 4.6a and 4.6c represent response surface plot and figure 4.6b and 4.6d correspond to contour plots showing the influence of drug: lipid and lipid: cholesterol ratio on PDE (4.6a & 4.6b) and PR (4.6c & 4.6d) by keeping the total solid: hydration medium ratio at 0.0. Rapid increase in PDE was observed with increase in drug: lipid ratio from -1.0 to 0.0 then after there was a bare minimum change in PDE and drug: lipid ration had very little or no effect on PR. On the other part, increase in lipid:

cholesterol ratio was associated with rapid decrease in PR and had minimum effect on PDE.

Figure 4.7a and 4.7c represent response surface plot and figure 4.7b and 4.7d correspond to contour plots showing the influence of drug: lipid and total solid: hydration medium ratio on PDE (4.7a & 4.7b) and PR (4.7c & 4.7d) by keeping the lipid: cholesterol ratio at 0.0. Hasty increase in PDE was observed with raise in drug: lipid ratio from -1.0 to 0.0 then after there was a least change in PDE. Slight decrease in PR was seen with increase in drug: lipid ration from -1.0 to 1.0. On the other side, total solid: hydration medium ratio had minimum effect on PDE and very slight increase in PR is observed with increase in total solid: hydration medium ratio.

Figure 4.8a and 4.8c represent response surface plot and figure 4.8b and 4.8d correspond to contour plots showing the influence of lipid: cholesterol and total solid: hydration medium on PDE (4.8a & 4.8b) and PR (4.8c & 4.8d) by keeping the drug: lipid ratio at 0.0. Slow decrease in PDE and rapid decrease in PR were observed with increase in lipid: cholesterol ratio from -1.0 to 0.0 then after, i.e. from 0.0 to 1.0, the decrease in PDE was slightly faster and the decrease in PR was somewhat sluggish. On the other part, no change in PDE was observed with increase in total solid: hydration medium ratio from -1.0 to 0.0 then after, i.e. from 0.0 to 1.0, there was a decrease in PDE. Total solid: hydration medium ratio had minimum effect on PR.

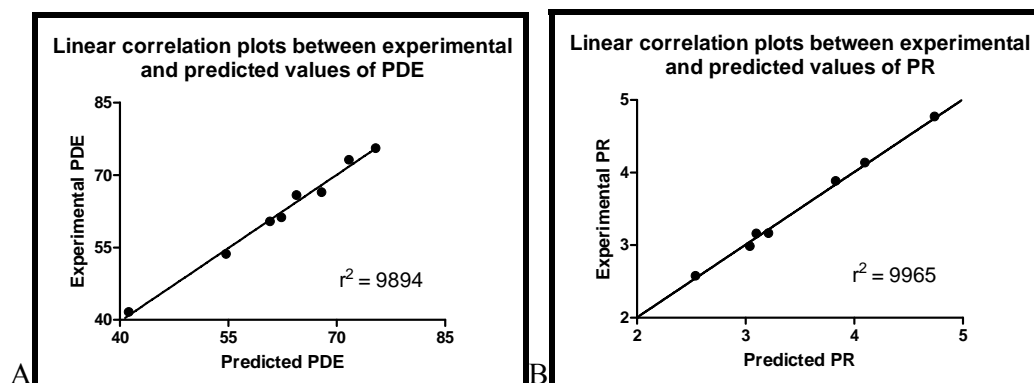
Effect of all the three formulation variables on the response parameters at a time are represented in the form of cube plots in figure 4.9a (PDE) and figure 4.9b (PR).

4.10.3.1 Checkpoint Analysis

Eight checkpoint batches were prepared three times and evaluated for the results of response variables. Compositions of each checkpoint batch along with the predicted and experimental values, percentage error and p-value is listed in Table 4.10. Linear correlation plots between the observed and predicted response variables along with r^2 values are shown in figure 4.10a and 4.10b for PDE and PR respectively. P-value > 0.05 indicates the differences between predicted and experimental values are statistically insignificant. Higher r^2 values (0.9894 and 0.9965 for PDE and PR respectively) of the linear correlation plots suggest excellent goodness of fit and high predictive capability of RSM.

Table 10 Checkpoint Analysis. The data represent the mean \pm SEM (n = 3).

S r. N o.	Formulation composition			Comparison							
	Drug: Lipid molar ratio	Lipid: Choleste rol molar ratio	Total solid content: Volume of hydratio n media	PDE			P value	PR			P value
				Predi cted Valu e	Experim ental value (Mean* \pm SEM)	Perce ntage error		Predi cted Valu e	Experim ental value (Mean* \pm SEM)	Perce ntage error	
1	-0.7 (1:16.5)	0.4 (7.6:2.4)	0.2 (13:1)	54.69	53.68 \pm 0.806	-1.847	P > 0.05 Non signif icant	3.10	3.16 \pm 0.057	1.936	P > 0.05 Non signif icant
2	-0.4 (1:18)	0.2 (7.8:2.2)	-0.3 (11.75:1)	64.45	65.87 \pm 0.593	2.203		3.04	2.99 \pm 0.058	-1.645	
3	0.9 (1:24.5)	-0.3 (8.3:1.7)	0.6 (14:1)	67.91	66.44 \pm 0.394	-2.165		3.83	3.89 \pm 0.055	1.567	
4	0.7 (1:23.5)	-0.5 (8.5:1.5)	-0.5 (11.25:1)	75.38	75.56 \pm 0.390	0.239		4.10	4.14 \pm 0.069	0.976	
5	0.2 (1:21)	-0.8 (8.3:1.2)	0.5 (13.75:1)	71.69	73.15 \pm 0.546	2.037		5.08	5.01 \pm 0.074	-1.378	
6	-0.3 (1:18.5)	0.8 (7.2:2.8)	-0.8 (10.5:1)	62.33	61.25 \pm 0.709	-1.733		2.54	2.58 \pm 0.055	1.575	
7	-0.9 (1:15.5)	0.9 (7.1:2.9)	0.8 (14.5:1)	41.20	41.67 \pm 0.711	1.141		3.21	3.17 \pm 0.062	-1.246	
8	-0.8 (1:16)	-0.7 (8.7:1.3)	-0.6 (11:1)	60.77	60.41 \pm 0.607	-0.592		4.74	4.77 \pm 0.059	0.633	

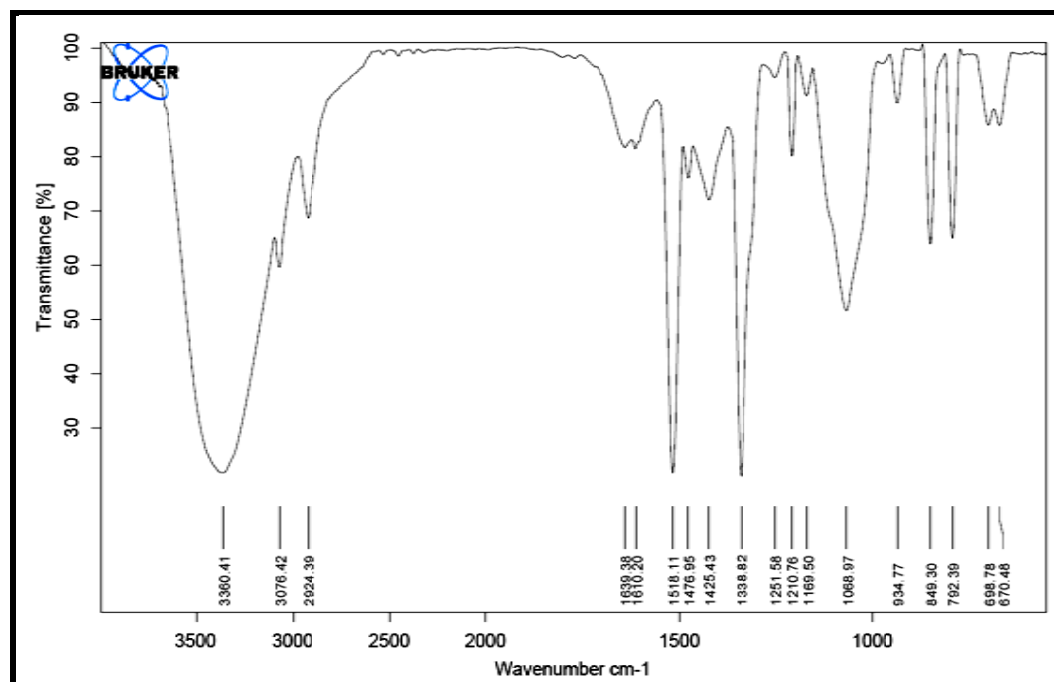

Figure 4.10 Linear correlation plots of the experimental response values versus the predicted response values for PDE (a) and PR (b) for CDS

The optimum formulation was derived by deciding goals for each formulation variable and response parameter and allotting the importance to each of them. By fixing the goal and importance we derived an optimum formulation as described in Table 4.11. The optimized batch (Drug: Lipid molar ratio = -0.35; Lipid: Cholesterol molar ratio = 0.60; Total solid content: Volume of hydration media = -1.00) was actually prepared and the experimental results were compared with predicted values. P-value > 0.05 indicates the differences between predicted and experimental values are statistically insignificant.

Table 4.11 Derivation of optimized formulation. The data represent the mean \pm SEM (n = 3).

Constrains			Lower Limit	Upper Limit	Predicted solution [A]	Actual results (Mean \pm SEM) [B]	Comparison of A and B (P value)
Name	Goal	Importance					
Drug: Lipid molar ratio	Minimize	5	-1	1	-0.35	-0.35	
Lipid: Cholesterol molar ratio	Maximize	2	-1	1	0.60	0.60	
Total solid content: Volume of hydration media	Minimize	2	-1	1	-1.00	-1.00	
PDE	Maximize	5	36.412	74.173	62.879	64.01 \pm 0.772	P > 0.05, Non significant
PR	Minimize	2	2.042	5.940	2.570	2.481 \pm 0.076	P > 0.05 Non significant

4.10.4 Preparation of M6P-HSA

**Figure 4.11 IR spectra of p-nitrophenyl- α -D-mannopyranoside**

In FTIR spectroscopy (BRUKER, α -Alpha T, Germany) presence of strong peaks at 2345.56 and 941.88 and a broad peak at 1708.14 confirms presence of (O=P-OH) group and strong peak at 2850.47 confirms presence of (P-O-H) group (figure 4.12).

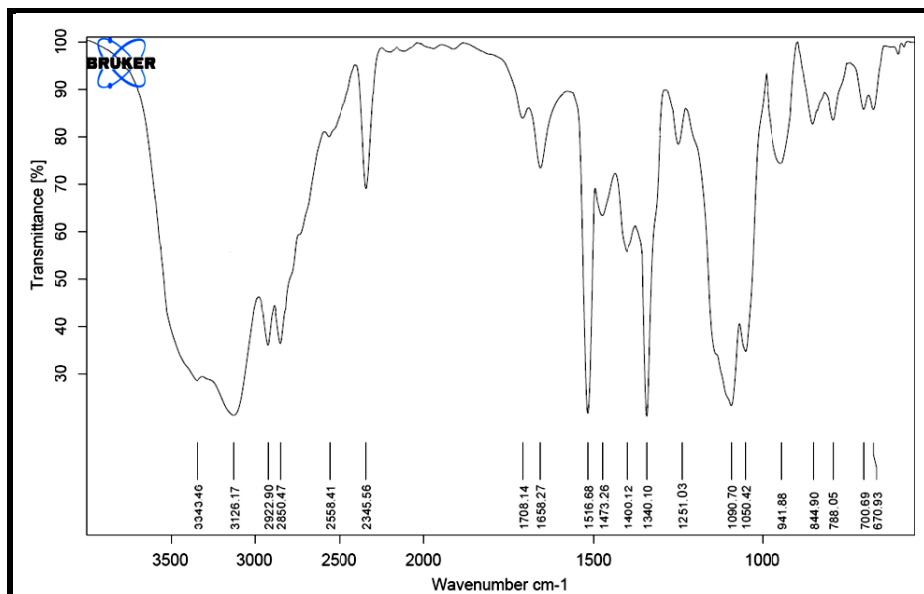


Figure 4.12 IR spectra of p-nitrophenyl-6-phospho-a-D-mannopyranoside

Presence of weak peaks at 3510.31 and 3420.28 and a medium peak at 1616.28 confirms presence of (N-H) group. Absence of peaks at 1516.68 and 1340.10 confirms conversion of (NO₂) group to (NH₂) group (figure 4.13).

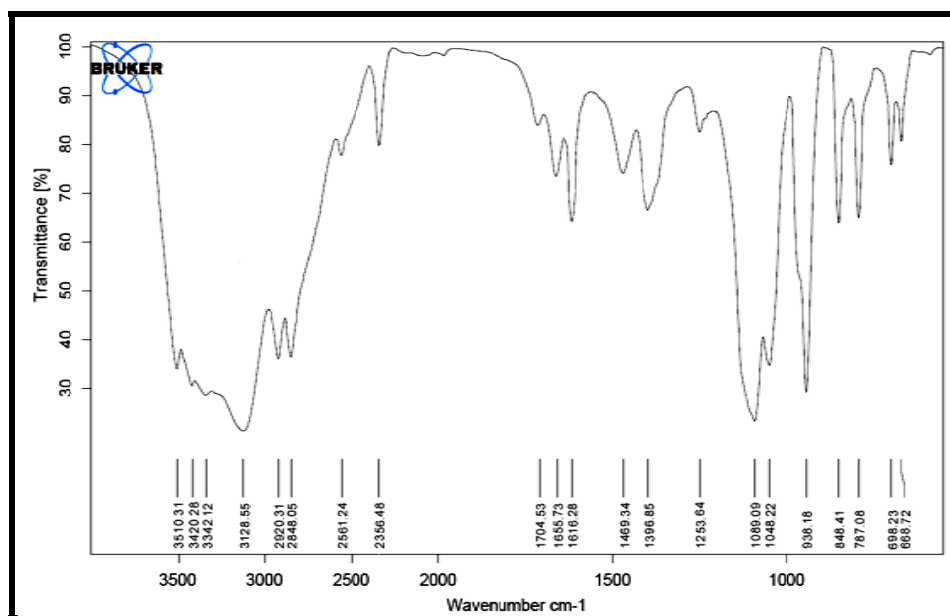


Figure 4.13 IR spectra of p-aminophenyl-6-phospho-a-D-mannopyranoside

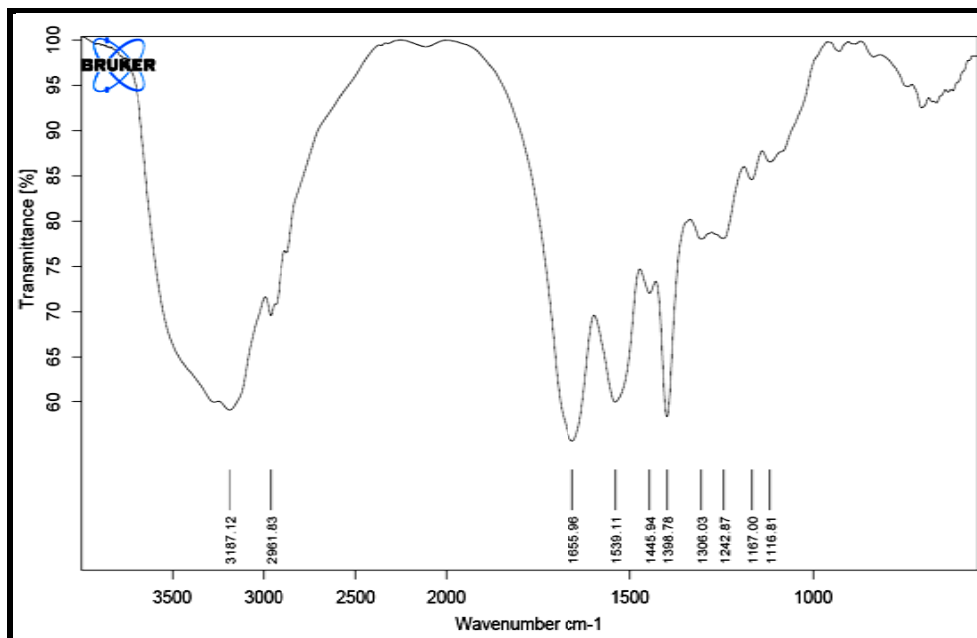


Figure 4.14 IR spectra of HSA

Presence of peak at 1575.32 confirms presence of (-N=N-) group (figure 4.15).

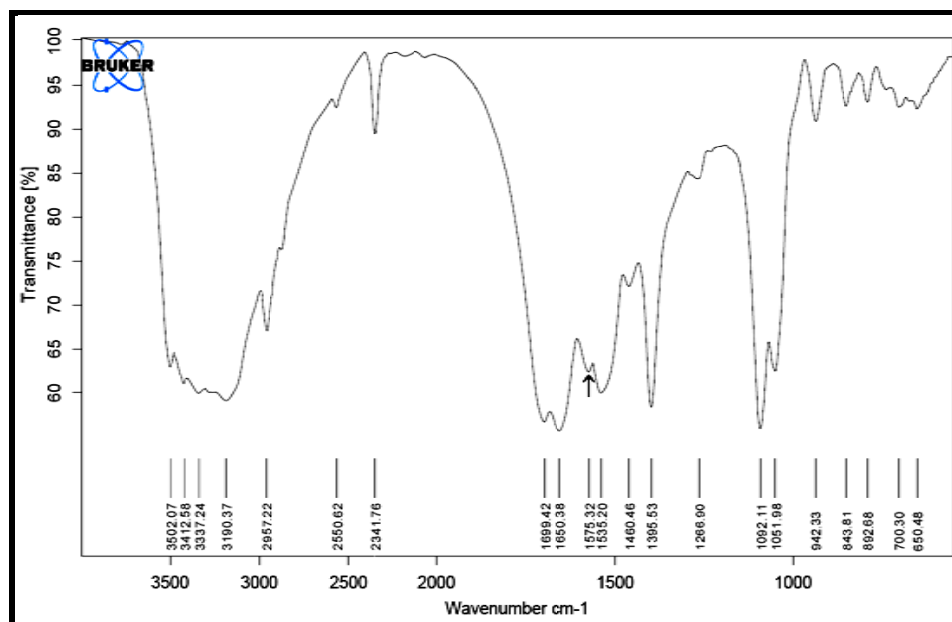


Figure 4.15 IR spectra of M6P-HSA

Prepared M6P-HSA was purified, characterized for protein content, number of M6P molecules and number of phosphate groups coupled to each HSA molecules. The prepared neoglycoprotein had $95.22 \pm 1.74\%$ of protein, 29.73 ± 1.21 numbers of

M6P molecules and 31.28 ± 2.01 numbers of phosphate groups coupled to each HSA molecule.

4.10.5 Conjugation of M6P-HSA to Liposomes

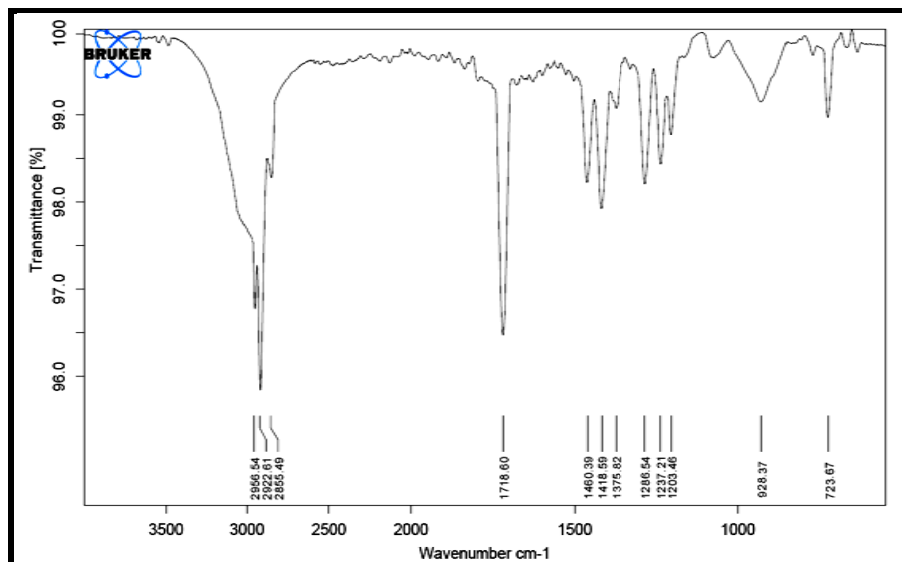


Figure 4.16 IR spectra of Sebacic acid

Presence of weak peaks at 1819.77 and 1751.16 confirms presence of (C=O) group coupled stretching. Three peaks at 1000.74, 1043.02 and 1103.61 confirms presence of (C-CO-O-CO-C) group (figure 4.17).

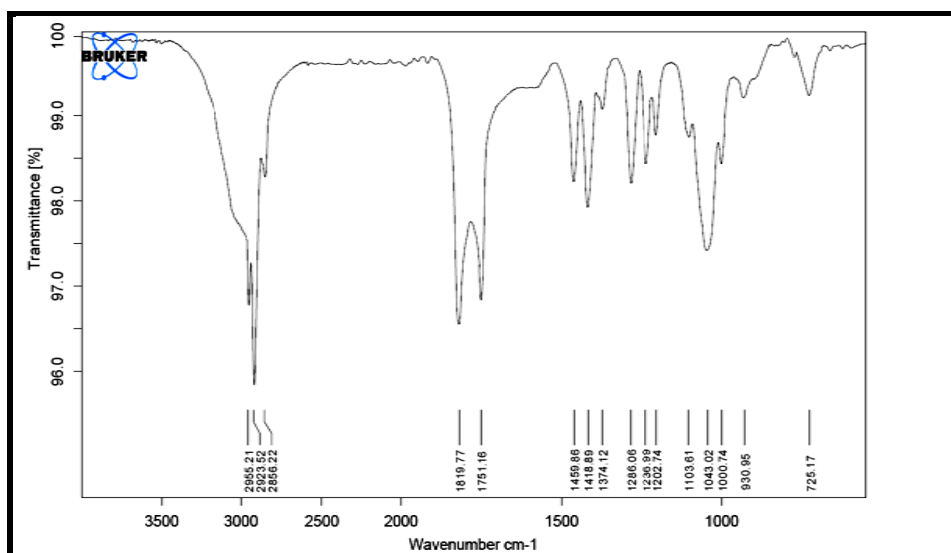


Figure 4.17 IR spectra of Sebacic anhydride

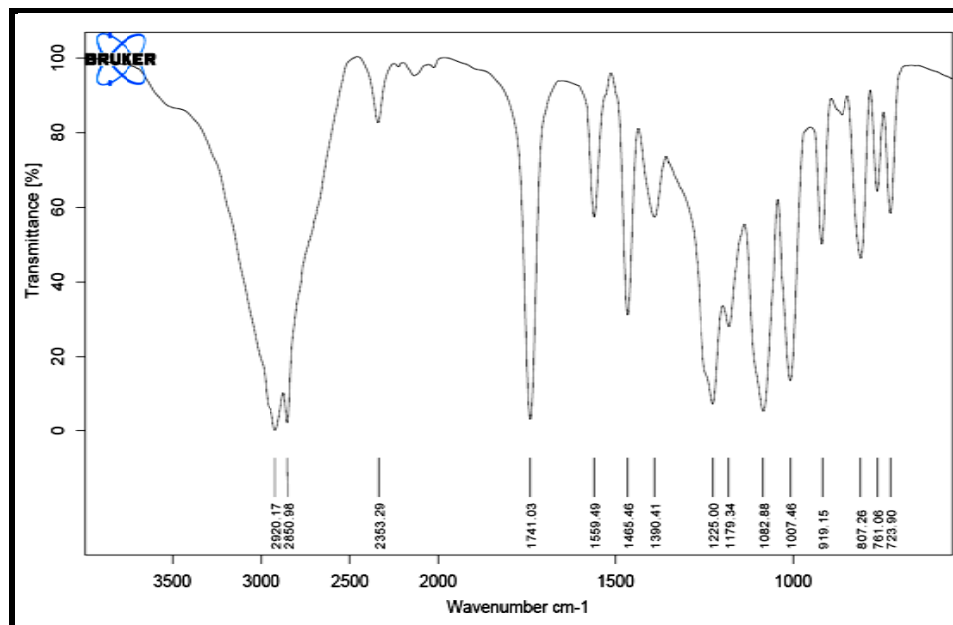


Figure 4.18 IR spectra of DSPE

Presence of a peak at 1637.48 confirms presence of (O=C-NH) group (figure 4.19).

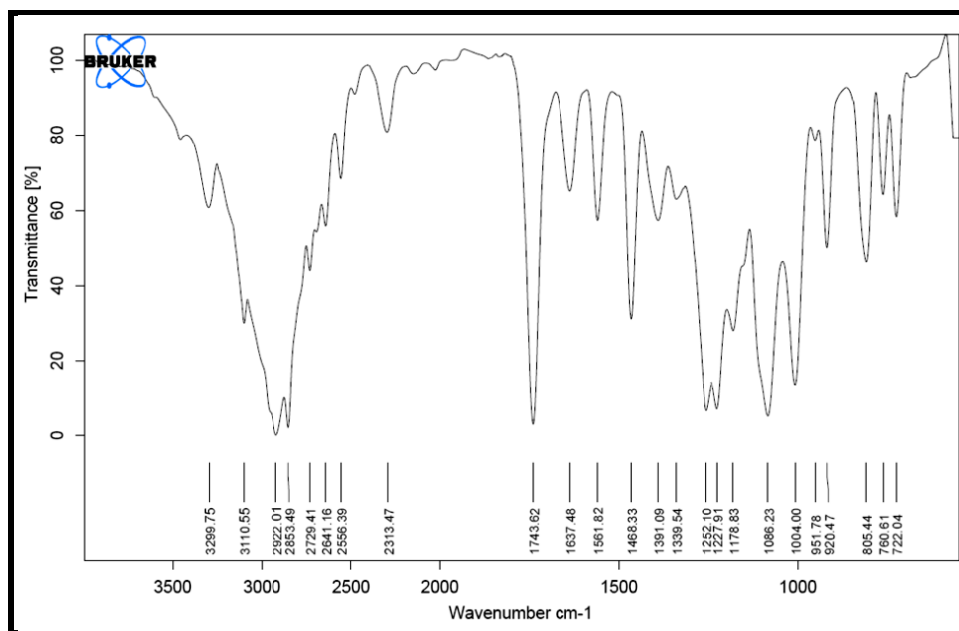


Figure 4.19 IR spectra of DSPE-Sebacic acid conjugate

4.10.6 Particle Size and Zeta Potential

The size of Liposomes was measured by dynamic light scattering with a Malvern Zetasizer. Increased particle size and zeta potential of liposomes substantiate conjugation of M6P-HSA to liposomes.

Table 4.12 Size and Zeta Potential of RGZ and CDS Liposomal Formulations

Batch	Particle size		Zeta potential (mV)
	Z-Average (d.nm)	Poly dispersity index (PDI)	
Unconjugated RGZ Liposomes	92.37 ± 3.28	0.064 ± 0.0075	-19.7 ± 1.72
M6P-HSA conjugated RGZ Liposomes	135.1 ± 3.74	0.079 ± 0.004	-30.5 ± 2.64
Unconjugated CDS Liposomes	96.45 ± 3.71	0.059 ± 0.0067	-24.4 ± 1.49
M6P-HSA conjugated CDS Liposomes	139.5 ± 3.98	0.082 ± 0.0079	-40.7 ± 1.99

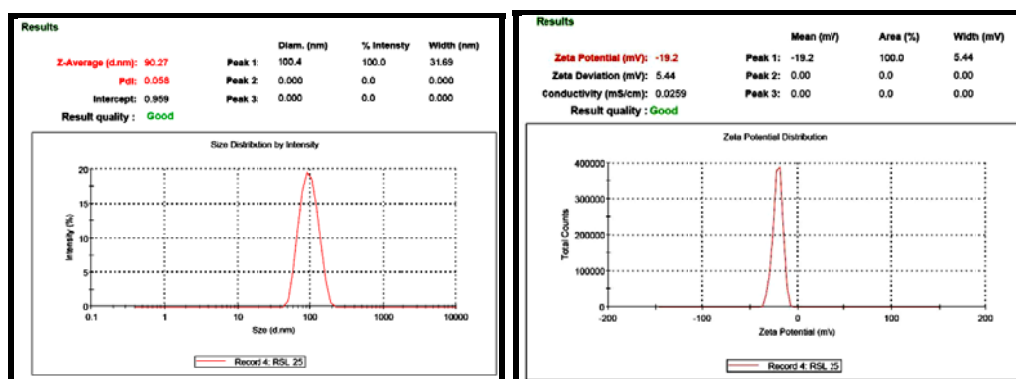


Figure 4.20 Particle size and Zeta potential of unconjugated RGZ liposomes

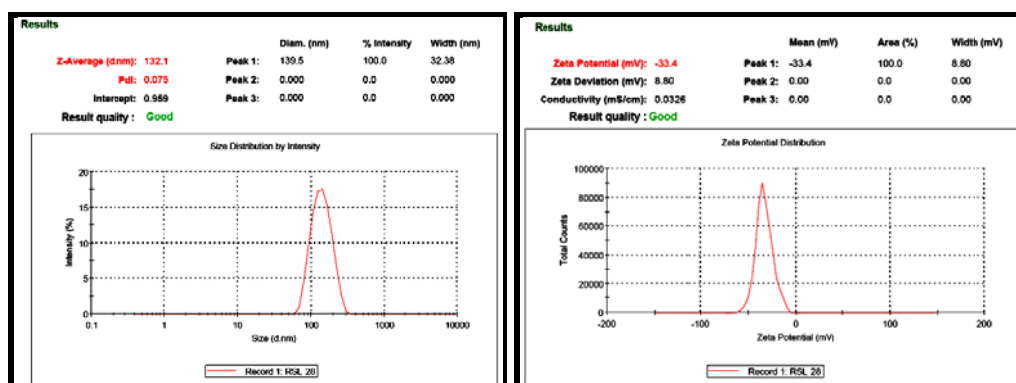


Figure 4.21 Particle size and Zeta potential of M6P-HSA conjugated RGZ liposomes

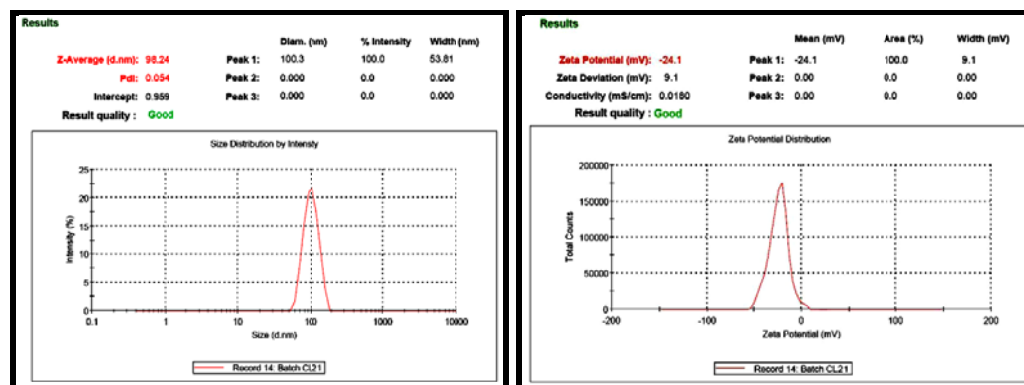


Figure 4.22 Particle size and Zeta potential of unconjugated CDS liposomes

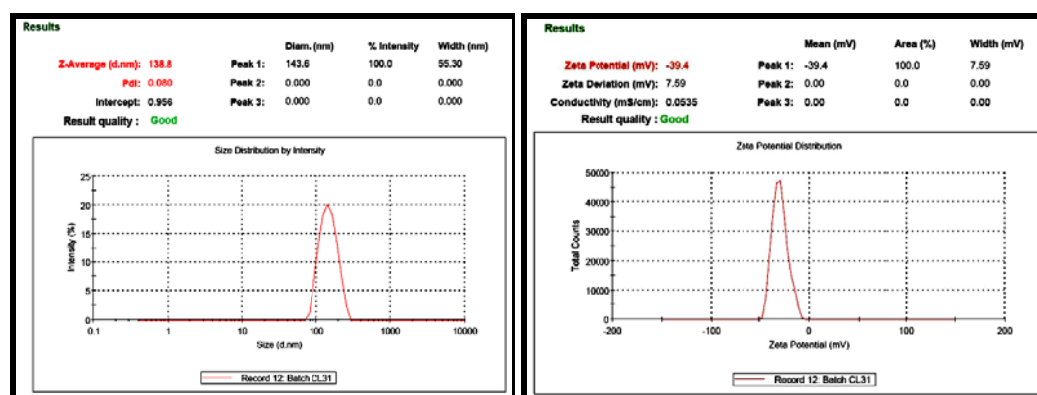


Figure 4.23 Particle size and Zeta potential of M6P-HSA conjugated CDS liposomes

4.10.7 Transmission Electron Microscopy (TEM)

The structure of liposomes was examined by TEM before and after conjugation of M6P-HSA. Liposomes had spherical shape and unilamellar structure. The liposome membranes were clearly observable because the inner aqueous compartments were slightly darker than the surrounding perimeters. The size of liposomes varied from 70 nm to 130 nm with an average diameter of 92.37 ± 3.28 nm for RGZ unconjugated liposomes (figure 4.24a) and 96.45 ± 3.71 for CDS unconjugated liposomes (figure 4.25a). The size of liposomes varied from 120 nm to 160 nm with an average diameter of 135.1 ± 3.74 nm for RGZ M6P-HSA conjugated liposomes (figure 4.24b), and 139.5 ± 3.98 for CDS M6P-HSA conjugated liposomes (figure 4.25b) measured by laser diffraction using Malvern Zetasizer. Results obtained from both TEM study and laser diffraction are parallel to each other.

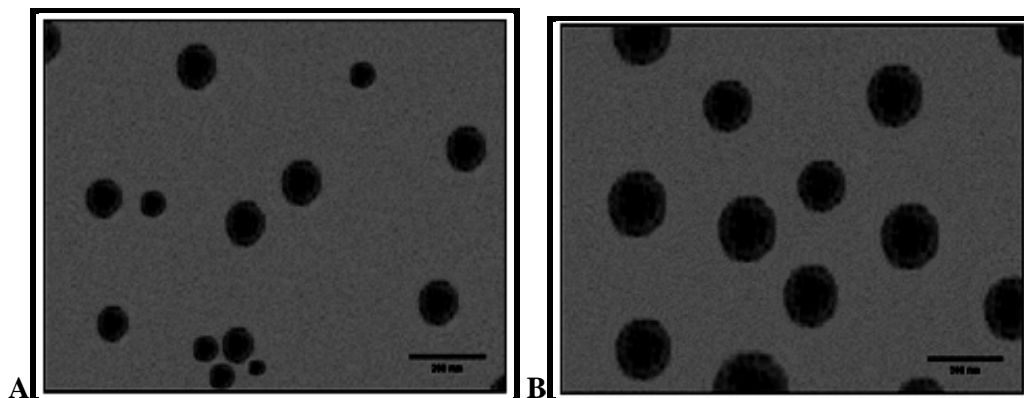


Figure 4.24 TEM images of RGZ unconjugated (A) and RGZ M6P-HSA conjugated (B) liposomes

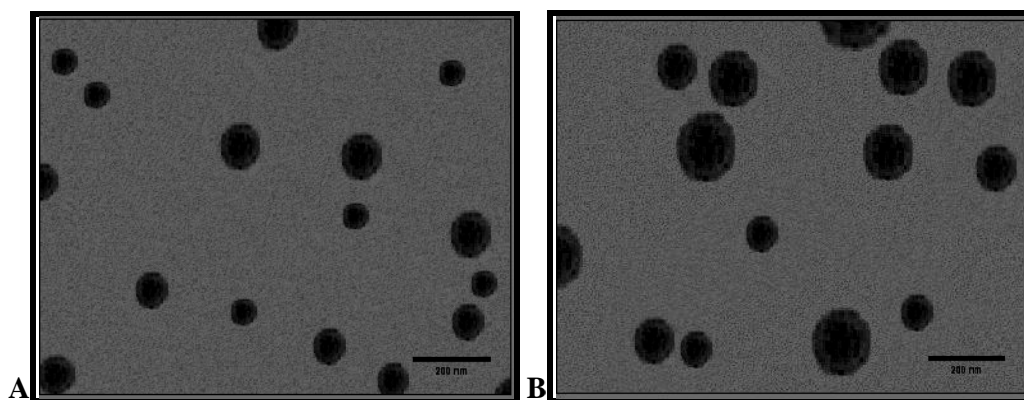


Figure 4.25 TEM images of CDS unconjugated (A) and CDS M6P-HSA conjugated (B) liposomes

4.10.8 Lyophilization of Liposomes and Optimization of Cryoprotectant Concentration

The liposomal suspensions were stabilized by lyophilization. Different cryoprotectants at various ratios and anti-adherent were evaluated. The lyophilized formulations were tested for particle size, zeta potential and percentage drug retention (PDR).

With use of sucrose as a cryoprotectant, the cake formed after lyophilization was condensed and had collapsed structure. The redispersibility of liposomes with sucrose was poor and was only possible after sonication. Particle size of liposomes was increased significantly and zeta-potential was decreased significantly after lyophilization (Table 4.13 and 4.14). The increase in the particle size could have been

due to the cohesive nature of the sucrose. Further, it was observed that the lyophilized liposomes with sucrose had tendency to absorb moisture quickly.

With mannitol and lactose, the lyophilized liposome product formed was fluffy and snow like voluminous cake. The liposomal formulation showed free flowing ability, however the redispersion was difficult and possible only after vigorous shaking. Particle size of liposomes was increased significantly and zeta-potential was decreased significantly after lyophilization (Table 4.13 and 4.14). This may be due to the low solubility of mannitol and lactose in water.

With trehalose also, the lyophilized liposomes formed fluffy and snow like voluminous cake. With trehalose as cryoprotectant, the lyophilized liposomes were redispersed easily and the increase in particle size and decrease in zeta-potential were not significant as recorded in Table 4.13 and 4.14. The redispersion of liposomes depends on the hydrophilicity of the surface. The easy redispersibility is probably due to the higher solubility of trehalose in water i.e. 0.7 parts in 1 part of water. The cryoprotective effect may be attributed to the ability of trehalose to form a glassy amorphous matrix around the liposomes, preventing the particles from sticking together during removal of water (Konan et al., 2002). Also the very property of the Tindal effect observed with liposomes was retained after redispersion of the liposomes lyophilized using trehalose. Furthermore, trehalose, a non-reducing disaccharide of glucose, has previously exhibited satisfactory cryoprotective effect for pharmaceutical and biological materials (De Jaeghere et al., 1999).

Therefore, trehalose at a ratio of 1:5 was used (as no further improvement was observed at 1:10) as a cryoprotectant and 10 % (of total solid) of glycine as antiadherent for lyophilization of optimized batches of liposomes for further studies.

Table 4.13 Lyophilization of RGZ liposomes. The data represent the mean \pm SEM (n = 3).

Different Cryoprotectants	Total solid:cryoprotectant ratio	Initial			After lyophilization								
		PDE	particle size [Z-Average (d.nm)]	Zeta potential (mV)	Percentage drug retention (PDR)	Particle size [Z-Average (d.nm)]	Zeta potential (mV)						
Lactose	1:2	71.83 \pm 0.683	135.1 \pm 3.74	-30.5 \pm 3.64	93.25 \pm 1.02	602.1 \pm 10.11	-7.7 \pm 1.10						
Sucrose					94.53 \pm 1.15	731.5 \pm 13.35	-4.6 \pm 0.92						
Mannitol					95.72 \pm 0.97	420.1 \pm 8.04	-13.2 \pm 1.23						
Trehalose					96.10 \pm 1.11	241.3 \pm 3.47	-19.2 \pm 1.78						
Lactose	1:5				71.83 \pm 0.683	135.1 \pm 3.74	-30.5 \pm 3.64	96.72 \pm 0.88	511.3 \pm 9.22	-8.3 \pm 1.01			
Sucrose								95.18 \pm 0.99	650.8 \pm 11.31	-7.0 \pm 0.98			
Mannitol								97.11 \pm 1.03	287.6 \pm 7.52	-15.8 \pm 1.21			
Trehalose								97.88 \pm 0.92	180.1 \pm 2.93	-21.9 \pm 1.33			
Lactose	1:10							71.83 \pm 0.683	135.1 \pm 3.74	-30.5 \pm 3.64	97.01 \pm 0.91	487.2 \pm 9.09	-9.0 \pm 1.13
Sucrose											95.96 \pm 1.12	632.1 \pm 10.62	-7.7 \pm 1.01
Mannitol											97.82 \pm 1.31	271.0 \pm 7.11	-16.3 \pm 1.19
Trehalose											98.12 \pm 1.22	174.3 \pm 2.62	-22.4 \pm 1.28

Table 4.14 Lyophilization of CDS liposomes. The data represent the mean \pm SEM (n = 3).

Different Cryoprotectants	Total solid : cryoprotectant ratio	Initial			After lyophilization								
		PDE	particle size [Z-Average (d.nm)]	Zeta potential (mV)	Percentage drug retention (PDR)	Particle size [Z-Average (d.nm)]	Zeta potential (mV)						
Lactose	1:2	64.01 \pm 0.772	139.5 \pm 3.98	-40.7 \pm 1.99	92.51 \pm 0.93	622.7 \pm 9.73	-10.2 \pm 0.93						
Sucrose					91.26 \pm 0.87	753.3 \pm 10.19	-6.0 \pm 0.84						
Mannitol					94.48 \pm 0.76	432.8 \pm 6.98	-17.1 \pm 1.08						
Trehalose					95.07 \pm 0.95	251.2 \pm 4.12	-25.3 \pm 1.39						
Lactose	1:5				64.01 \pm 0.772	139.5 \pm 3.98	-40.7 \pm 1.99	96.29 \pm 0.84	527.0 \pm 8.61	-11.4 \pm 0.89			
Sucrose								94.09 \pm 0.91	674.0 \pm 9.06	-9.1 \pm 0.77			
Mannitol								97.27 \pm 0.79	299.3 \pm 5.17	-21.7 \pm 1.10			
Trehalose								97.96 \pm 1.02	184.6 \pm 3.01	-29.3 \pm 1.41			
Lactose	1:10							64.01 \pm 0.772	139.5 \pm 3.98	-40.7 \pm 1.99	97.12 \pm 0.86	502.1 \pm 8.28	-12.7 \pm 0.98
Sucrose											94.74 \pm 0.72	651.7 \pm 8.89	-10.5 \pm 1.04
Mannitol											97.79 \pm 1.10	277.8 \pm 3.96	-21.9 \pm 1.09
Trehalose											98.19 \pm 0.97	180.0 \pm 2.73	-29.8 \pm 1.34

4.10.9 Solid-state Analysis

DSC curves of plain drugs and liposomal formulations are contained in figure 4.26 and 4.27. DSC curves suggest loss of drug crystallinity when drugs were loaded into the liposomes.

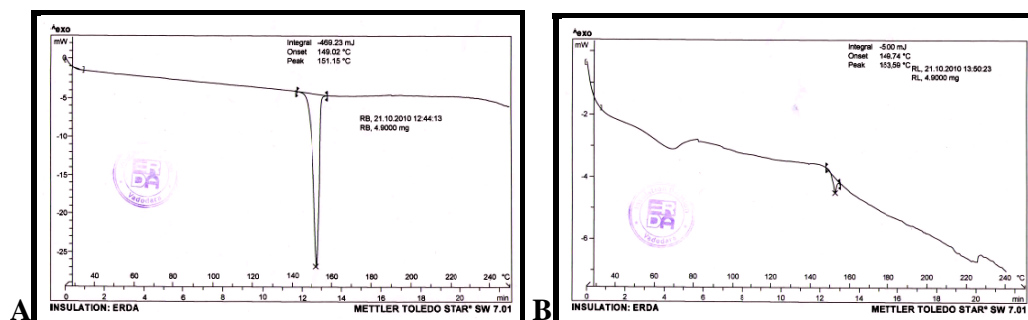


Figure 4.26 DSC curve of RGZ plain drug (A) RGZ liposomes (B)

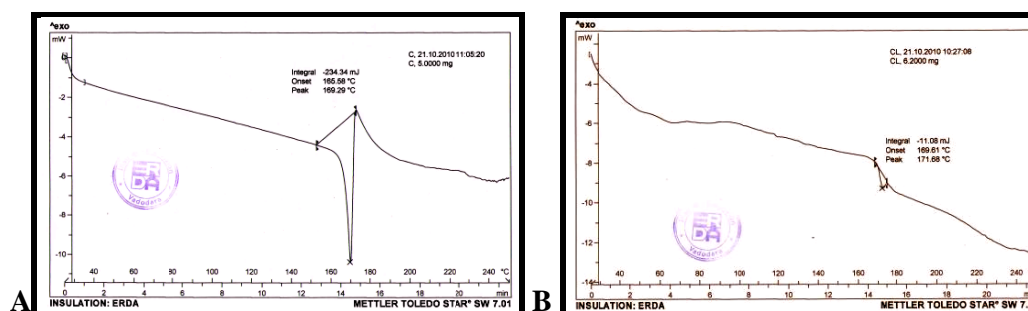


Figure 4.27 DSC curve of CDS plain drug (A) CDS liposomes (B)

X-ray diffractograms of plain drugs and liposomal formulation are demonstrated in figure 4.28 and 4.29. X-ray diffractograms showed less intensity of peaks corresponding to liposomal formulation than plain drug suggesting loss of drug crystallinity when drug was loaded into the liposomes.

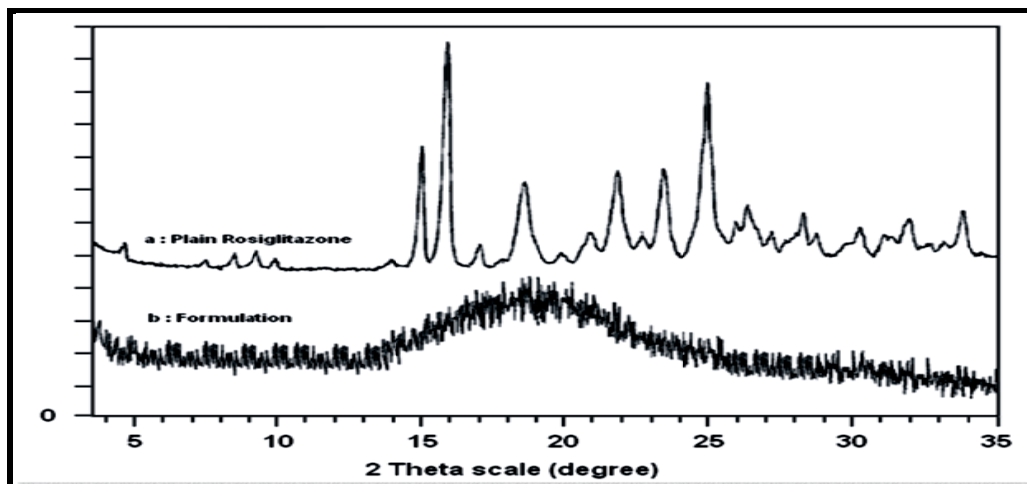


Figure 4.28 X-ray diffractograms of RGZ plain drug and liposomal formulation

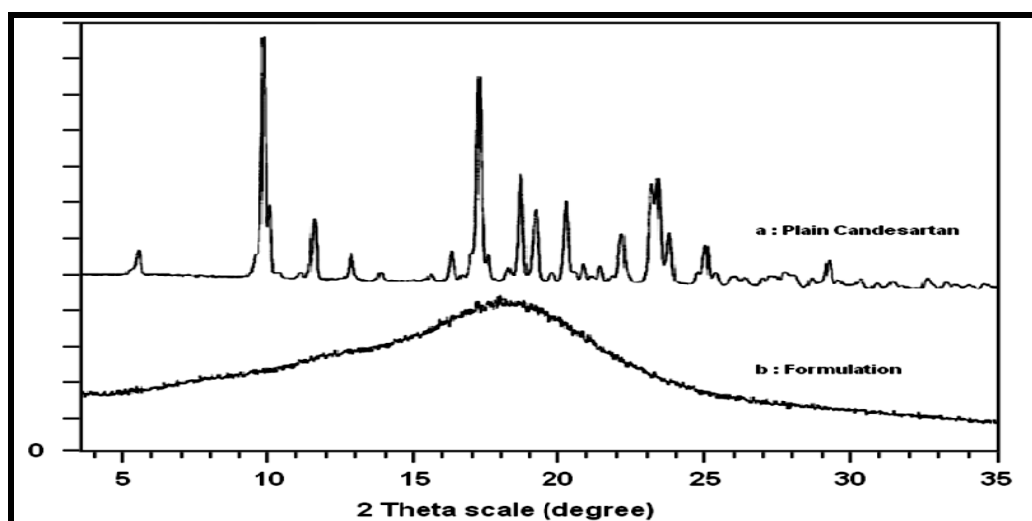


Figure 4.29 X-ray diffractograms of CDS plain drug and liposomal formulation

4.11 CONCLUSION

Liposomes of rosiglitazone and candesartan were successfully prepared by thin film hydration method. Liposomal formulations were optimized for various process and formulation variables to maximize percentage drug entrapment (PDE) and minimize percentage reduction in PDE. The liposomes were surface conjugated with M6P-HSA for potential hepatic stellate cell targeting. The optimized surface conjugated liposomal suspensions were stabilized by lyophilization.

4.12 REFERENCES

Adrian JE, Poelstra K, Scherphof GL, Molema G, Meijer DK, Reker-Smit C, Morselt HW, Kamps JA. Interaction of targeted liposomes with primary cultured hepatic stellate cells: Involvement of multiple receptor systems. *J Hepatol.* 2006 Mar;44(3):560-7.

Anthony Armstrong N, James KC. *Pharmaceutical experimental design and interpretation.* Taylor and Francis Publishers, Bristol, PA, USA, 1996;131-92.

Atyabi F, Farkhondehfai A, Esmaeili F, Dinarvand R. Preparation of pegylated nano-liposomal formulation containing SN-38: In vitro characterization and in vivo biodistribution in mice. *Acta Pharm.* 2009 Jun;59(2):133-44.

Bangham AD, Standish MM, Watkins JC. Diffusion of univalent ions across the lamellae of swollen phospholipids. *J Mol Biol.* 1965 Aug;13(1):238-52.

Barenholz Y, Amselem S, Lichtenberg D. A new method for preparation of phospholipid vesicles (liposomes) - French press. *FEBS Lett.* 1979 Mar 1;99(1):210-4.

Batzri S, Korn ED. Interaction of phospholipid vesicles with cells. Endocytosis and fusion as alternate mechanisms for the uptake of lipid-soluble and water-soluble molecules. *J Cell Biol.* 1975 Sep;66(3):621-34.

Beljaars L, Molema G, Weert B, Bonnema H, Olinga P, Groothuis GM, Meijer DK, Poelstra K. Albumin modified with mannose 6-phosphate: A potential carrier for selective delivery of antifibrotic drugs to rat and human hepatic stellate cells. *Hepatology.* 1999 May;29(5):1486-93.

Beljaars L, Olinga P, Molema G, de Bleser P, Geerts A, Groothuis GM, Meijer DK, Poelstra K. Characteristics of the hepatic stellate cell-selective carrier mannose 6-phosphate modified albumin (M6P(28)-HSA). *Liver.* 2001 Oct;21(5):320-8.

Betageri GV, Jenkins SA, Parsons DL. *Liposome Drug Delivery Systems.* PA, USA: Technomic Publishing company Inc, 1993; 16-7.

Bottcher CJF, van Gent CM, Fries C. A rapid and sensitive sub-micro phosphorous determination. *Anal Chim Acta* 1961; 24, 203-4.

Box GEP, Wilson KB. On the experimental attainment of optimum conditions. *J. Roy. Statist. Soc. Ser. B Metho.* 1951;13:1-45.

Box GEP, Hunter WG, Hunter JS. *Statistics for experiments.* John Wiley and Sons, New York, 1978;291-334.

Cao Q, Mak KM, Lieber CS. Dilinoleoylphosphatidylcholine prevents transforming growth factor-beta1-mediated collagen accumulation in cultured rat hepatic stellate cells. *J Lab Clin Med.* 2002 Apr;139(4):202-10.

Cavalcanti LP, Konovalov O, Haas H. X-ray diffraction from paclitaxel-loaded zwitterionic and cationic model membranes. *Chem Phys Lipids.* 2007 Nov;150(1):58-65.

Cochran WG, Cox GM. *Experimental designs.* 2nd ed; John Wiley and Sons, New York, 1992;335-75.

Cortesi R, Esposito E, Gambarin S, Telloli P, Menegatti E, Nastruzzi C. Preparation of liposomes by reverse-phase evaporation using alternative organic solvents. *J Microencapsul.* 1999 Mar-Apr;16(2):251-6.

Crosasso P, Ceruti M, Brusa P, Arpicco S, Dosio F, Cattel L. Preparation, characterization and properties of sterically stabilized paclitaxel-containing liposomes. *J Control Release.* 2000 Jan 3;63(1-2):19-30.

Crowe LM, Crowe JH, Rudolph A, Womersley C, Appel L. Preservation of freeze-dried liposomes by trehalose. *Arch Biochem Biophys.* 1985 Oct;242(1):240-7.

De Bleser PJ, Jannes P, van Buul-Offers SC, Hoogerbrugge CM, van Schravendijk CF, Niki T, Rogiers V, van den Brande JL, Wisse E, Geerts A. Insulinlike growth factor-II/mannose 6-phosphate receptor is expressed on CCl4-exposed rat fat-storing cells and facilitates activation of latent transforming growth factor-beta in cocultures with sinusoidal endothelial cells. *Hepatology.* 1995 May;21(5):1429-37.

De Bleser PJ, Scott CD, Niki T, Xu G, Wisse E, Geerts A. Insulin-like growth factor II/mannose 6-phosphate-receptor expression in liver and serum during acute CCl4 intoxication in the rat. *Hepatology.* 1996 Jun;23(6):1530-7.

De Jaeghere F, Allemann E, Leroux JC, Stevels W, Feijen J, Doelker E, Gurny R. Formulation and lyoprotection of poly(lactic acid-co-ethylene oxide) nanoparticles:

influence on physical stability and in vitro cell uptake. *Pharm Res.* 1999 Jun;16(6):859-66.

Deamer D, Bangham AD. Large volume liposomes by an ether vaporization method. *Biochim Biophys Acta.* 1976 Sep 7;443(3):629-34.

Du S, Deng Y. Studies on the encapsulation of oxymatrine into liposomes by ethanol injection and pH gradient method. *Drug Dev Ind Pharm.* 2006 Aug;32(7):791-7.

Dubois M, Gilles KA, Hamilton JK, Rebers PA, Smith F. Colorimetric method for determination of sugars and related substances. *Anal Chem.* 1956;28:350-6.

Ducat E, Brion M, Lecomte F, Evrard B, Piel G. The experimental design as practical approach to develop and optimize a formulation of peptide-loaded liposomes. *AAPS PharmSciTech.* 2010 Jun;11(2):966-75.

Fannin TE, Marcus MD, Anderson DA, Bergman HL. Use of a fractional factorial design to evaluate interactions of environmental factors affecting biodegradation rates. *Appl Environ Microbiol.* 1981 Dec;42(6):936-43.

Gonzalez-Mira E, Egea MA, Souto EB, Calpena AC, Garcia ML. Optimizing flurbiprofen-loaded NLC by central composite factorial design for ocular delivery. *Nanotechnology.* 2011 Jan 28;22(4):045101.

Gonzalez-Rodriguez ML, Barros LB, Palma J, Gonzalez-Rodriguez PL, Rabasco AM. Application of statistical experimental design to study the formulation variables influencing the coating process of lidocaine liposomes. *Int J Pharm.* 2007 Jun 7;337(1-2):336-45.

Gonzalo T, Talman EG, van de Ven A, Temming K, Greupink R, Beljaars L, Reker-Smit C, Meijer DK, Molema G, Poelstra K, Kok RJ. Selective targeting of pentoxifylline to hepatic stellate cells using a novel platinum-based linker technology. *J Control Release.* 2006 Mar 10;111(1-2):193-203.

Greupink R, Bakker HI, Bouma W, Reker-Smit C, Meijer DK, Beljaars L, Poelstra K. The antiproliferative drug doxorubicin inhibits liver fibrosis in bile duct-ligated rats and can be selectively delivered to hepatic stellate cells in vivo. *J Pharmacol Exp Ther.* 2006 May;317(2):514-21.

Greupink R, Bakker HI, Reker-Smit C, van Loenen-Weemaes AM, Kok RJ, Meijer DK, Beljaars L, Poelstra K. Studies on the targeted delivery of the antifibrogenic compound mycophenolic acid to the hepatic stellate cell. *J Hepatol.* 2005 Nov;43(5):884-92.

Hagens WI, Olinga P, Meijer DK, Groothuis GM, Beljaars L, Poelstra K. Gliotoxin non-selectively induces apoptosis in fibrotic and normal livers. *Liver Int.* 2006 Mar;26(2):232-9.

Hamilton RL Jr, Goerke J, Guo LS, Williams MC, Havel RJ. Unilamellar liposomes made with the French pressure cell: a simple preparative and semiquantitative technique. *J Lipid Res.* 1980;21(8):981-92.

Hernandez Caselles T, Villalain J, Gomez Fernandez JC. Stability of liposomes on long term storage. *J Pharm Pharmacol.* 1990;42(6):397-400.

Hinrichs WL, Mancenido FA, Sanders NN, Braeckmans K, De Smedt SC, Demeester J, Frijlink HW. The choice of a suitable oligosaccharide to prevent aggregation of PEGylated nanoparticles during freeze thawing and freeze drying. *Int J Pharm.* 2006 Mar 27;311(1-2):237-44.

Jaafar-Maalej C, Diab R, Andrieu V, Elaissari A, Fessi H. Ethanol injection method for hydrophilic and lipophilic drug-loaded liposome preparation. *J Liposome Res.* 2010;20(3):228-43.

Jiskoot W, Teerlink T, Beuvery EC, Crommelin DJ. Preparation of liposomes via detergent removal from mixed micelles by dilution. The effect of bilayer composition and process parameters on liposome characteristics. *Pharm Weekbl Sci.* 1986;8(5):259-65.

Kataoka M, Tavassoli M. Synthetic neoglycoproteins: a class of reagents for detection of sugar-recognizing substances. *J. Histochem. Cytochem.* 1984; 32(10): 1091-8.

Kenneth WY, Mark Miranda GS, Yap Wah Koon T. Formulation and optimization of two culture media for the production of tumor necrosis factor- β in *Escherichia coli*. *J Chem Technol Biotechnol.* 1995 Mar;62(3):289-94.

Kirby C, Gregoriadis G. Dehydration-Rehydration Vesicles: A Simple Method for High Yield Drug Entrapment in Liposomes. *Nat Biotechnol.* 1984;2:979-84.

Konan YN, Gurny R, Allemann E. Preparation and characterization of sterile and freeze-dried sub-200 nm nanoparticles. *Int J Pharm.* 2002;233(1-2):239-52.

Loukas YL. 2(k-p) fractional factorial design via fold over: application to optimization of novel multicomponent vesicular systems. *Analyst.* 1997;122(10):1023-7.

Maitani Y. Lipoplex formation using liposomes prepared by ethanol injection. *Methods Mol Biol.* 2010;605:393-403.

Martin FJ, Heath TD, New RRC. Chapter 4: Covalent attachment of proteins to liposomes. In: New RRC, ed. *Liposomes-A Practical Approach.* Oxford, England: IRL Press, Oxford University Press, 1990(a):163-82.

Martin FJ. Pharmaceutical manufacturing of liposomes, In: Praveen Tyle (Ed) *Specialized drug delivery systems: manufacturing and production technology.* Marcel Dekker, Inc., New York, NY, 1990(b):267-316.

Matz CE, Jonas A. Micellar complexes of human apolipoprotein A-I with phosphatidylcholines and cholesterol prepared from cholate-lipid dispersions. *J Biol Chem.* 1982 Apr 25;257(8):4535-40.

Monsigny M, Roche AC, Midoux P. Uptake of neoglycoproteins via membrane lectin(s) of L1210 cells evidenced by quantitative flow cytometry and drug targeting. *Biol. Cell.* 1984; 51(2): 187-96.

Mu L, Feng SS. Fabrication, characterization and in vitro release of paclitaxel (Taxol) loaded poly (lactic-co-glycolic acid) microspheres prepared by spray drying technique with lipid/cholesterol emulsifiers. *J Control Release.* 2001 Oct 19;76(3):239-54.

Murthy RS, Umrethia ML. Optimization of formulation parameters for the preparation of flutamide liposomes by 3(3) factorial 26-term logit model. *Pharm Dev Technol.* 2004 Nov;9(4):369-77.

Naik S, Patel D, Surti N, Misra A. Preparation of PEGylated liposomes of docetaxel using supercritical fluid technology. *J Supercrit Fluids.* 2010;54:110-9.

New RRC. "Preparation of Liposomes" in *Liposomes: A Practical Approach*, New RRC (ed.) Oxford University Press, Oxford, 1990; 33-104.

Nounou MM, El-Khordagui L, Khallafallah N, Khalil S. Influence of different sugar cryoprotectants on the stability and physico-chemical characteristics of freeze-dried 5-fluorouracil plurilamellar vesicles. *DARU*, 2005,13(4),133-42.

Ollivon M, Lesieur S, Grabielle-Madelmont C, Paternostre M. Vesicle reconstitution from lipid-detergent mixed micelles. *Biochim Biophys Acta*. 2000 Nov 23;1508(1-2):34-50.

Ostro MJ. Liposomes. *Sci Am*. 1987 Jan;256(1):102-11.

Ozer AY, Talsma H. Preparation and stability of liposomes containing 5-fluorouracil. *Int J Pharm*. 1989 Oct 15;55(2-3):185-91.

Padamwar MN, Pokharkar VB. Development of vitamin loaded topical liposomal formulation using factorial design approach: drug deposition and stability. *Int J Pharm*. 2006 Aug 31;320(1-2):37-44.

Patel G, Chougule M, Singh M, Misra A. Chapter 9 - Nanoliposomal dry powder formulations. *Methods Enzymol*. 2009;464:167-91.

Patil MP, Gaikwad NJ. Preparation and characterization of gliclazide-polyethylene glycol 4000 solid dispersions. *Acta Pharm*. 2009 Mar;59(1):57-65.

Roche AC, Midoux P, Bouchard P, Monsigny M. Membrane lectins on human monocytes. Maturation-dependent modulation of 6-phosphomannose and mannose receptors. *FEBS Lett*. 1985 Nov 25;193(1):63-8.

Sakai H, Gotoh T, Imura T, Sakai K, Otake K, Abe M. Preparation and properties of liposomes composed of various phospholipids with different hydrophobic chains using a supercritical reverse phase evaporation method. *J Oleo Sci*. 2008;57(11):613-21.

Seltzer SE, Gregoriadis G, Dick R. Evaluation of the dehydration-rehydration method for production of contrast-carrying liposomes. *Invest Radiol*. 1988 Feb;23(2):131-8.

Seth AK, Misra A. Mathematical modelling of preparation of acyclovir liposomes: reverse phase evaporation method. *J Pharm Pharm Sci*. 2002 Sep-Dec;5(3):285-91.

Shew RL, Deamer DW. A novel method for encapsulation of macromolecules in liposomes. *Biochim Biophys Acta*. 1985 Jun 11;816(1):1-8.

Singh B, Dahiya M, Saharan V, Ahuja N. Optimizing drug delivery systems using systematic "design of experiments." Part II: retrospect and prospects. *Crit Rev Ther Drug Carrier Syst.* 2005(a);22(3):215-94.

Singh B, Kumar R, Ahuja N. Optimizing drug delivery systems using systematic "design of experiments." Part I: fundamental aspects. *Crit Rev Ther Drug Carrier Syst.* 2005(b);22(1):27-105.

Singh B, Mehta G, Kumar R, Bhatia A, Ahuja N, Katare OP. Design, development and optimization of nimesulide-loaded liposomal systems for topical application. *Curr Drug Deliv.* 2005(c) Apr;2(2):143-53.

Smirnov AA. Preparation of liposomes by reverse-phase evaporation and by freezing and thawing. *Bull Exp Biol Med.* 1984 Aug;98(2):1146-1149.

Stensrud G, Sande SA, Kristensen S, Smistad G. Formulation and characterisation of primaquine loaded liposomes prepared by a pH gradient using experimental design. *Int J Pharm.* 2000 Apr 5;198(2):213-28.

Subramanian N, Yajnik A, Murthy RS. Artificial neural network as an alternative to multiple regression analysis in optimizing formulation parameters of cytarabine liposomes. *AAPS PharmSciTech.* 2004 Feb 2;5(1):E4.

Szoka F Jr, Papahadjopoulos D. Procedure for preparation of liposomes with large internal aqueous space and high capture by reverse-phase evaporation. *Proc Natl Acad Sci U S A.* 1978 Sep;75(9):4194-8.

Vali AM, Toliyat T, Shafaghi B, Dadashzadeh S. Preparation, optimization, and characterization of topotecan loaded PEGylated liposomes using factorial design. *Drug Dev Ind Pharm.* 2008 Jan;34(1):10-23.

Van Winden EC, Talsma H, Crommelin DJ. Thermal analysis of freeze-dried liposome-carbohydrate mixtures with modulated temperature differential scanning calorimetry. *J Pharm Sci.* 1998 Feb;87(2):231-7.

Xiong Y, Guo D, Wang L, Zheng X, Zhang Y, Chen J. Development of nobiliside A loaded liposomal formulation using response surface methodology. *Int J Pharm.* 2009 Apr 17;371(1-2):197-203.

Yousefi A, Esmaeili F, Rahimian S, Atyabi F, Dinarvand R. Preparation and In Vitro Evaluation of a Pegylated Nano-Liposomal Formulation Containing Docetaxel. *Sci Pharm*. 2009 Mar 19;77:453-64.

Zasadzinski JA. Transmission electron microscopy observations of sonication-induced changes in liposome structure. *Biophys J*. 1986 Jun;49(6):1119-30.

Zumbuehl O, Weder HG. Liposomes of controllable size in the range of 40 to 180 nm by defined dialysis of lipid/detergent mixed micelles. *Biochim Biophys Acta*. 1981 Jan 8;640(1):252-62.

CHAPTER 5

IN-VITRO DRUG DIFFUSION STUDY



In-vitro Drug Diffusion Study

5.1 INTRODUCTION

5.2 EXPERIMENTAL SETUP

5.2.1 Artificial Membrane

5.2.2 Activation of Dialysis Membrane

5.2.3 Selection of Diffusion Medium

5.3 METHOD

5.4 DATA AND STATISTICAL ANALYSIS

5.5 RESULTS AND DISCUSSIONS

5.6 CONCLUSION

5.7 REFERENCES

5.1 INTRODUCTION

The encapsulated drug releases from liposomal systems are useful to establish relevance to the *in-vivo* as well as to the non *in-vivo* arenas (Margalit and Yerushalmi, 1996).

The drug release studies are expected to yield data and gives understanding for prediction of liposomal behavior in the *in-vivo* arena:

- a) Minimizing the loss of encapsulated drug on route from the site of administration to the site of drug action i.e. bioavailability.
- b) The ability to match the release rate (once the liposomes arrive at the target) to the requirements of the therapy.

The objectives of *in-vitro* drug release studies that concern the non *in-vivo* arena are

- a) Physicochemical characterizations of the systems, including liposomes lyophilized to form dried powders.
- b) Various aspects of system optimization such as the selection of liposome type, lipid composition and parameters of shelf life.
- c) Criteria for quality assurance.

In order to derive relevant data from such experiments, the experimental conditions should be set to fit the specific objectives especially with respect to the extent of liposomes and drug (each, separately) dilutions that the system is anticipated to undergo.

The prime factor for successful development of a promising drug delivery system and assessments of the drug release profile of drugs from the delivery system is the proper design and selection of an *in-vitro* drug release system that permits accurate evaluation and mechanistic analysis of the drug release profiles. Physiological availability of the drug depends on the rate of release from the liposomes and permeability through alveolar surface into the lungs. The *in-vitro* methods are valuable and important screening procedures for understanding physico-chemical parameters such as fluxes, partition coefficients and diffusion coefficients etc. Though according to Gemmell and Morison (Gemmell and Morrison, 1957), *in-vitro* methods may be of limited predictive value but they are the means of assessing the ability of a vehicle or base to release drug under experimental conditions. The constraint of such

a technique is that the method does not exactly simulate the *in situ* behavior, especially with respect to unpredictable blood supply and metabolism. However, since performing bio-studies on every manufactured batch is impractical and costlier affair, formulators must rely on *in-vitro* testing to ensure batch-to-batch uniformity and consistency in bioavailability among developed formulations (Mojaverian et al., 1997).

In present scenario, *in-vitro* test systems have not been developed which can accurately predict the rate of drug release from liposomal formulations *in-vivo* (Fielding and Abra, 1992). Therefore an *in-vitro* release technique is proposed, validated and utilized for drug release studies from optimized liposomal formulations.

5.2 EXPERIMENTAL SETUP

5.2.1 Artificial Membrane

Dialysis membrane (250-9U, molecular weight cut off: 12400 Dalton; Sigma, Bangalore, India), 200 μm in thickness, pH 5.8 to 8, breaking strength 2.75 kg f/cm and porosity 0.45 μm was used as a artificial membrane for preliminary *In-vitro* studies because of simplicity, homogeneity and uniformity.

5.2.2 Activation of Dialysis Membrane

The dialysis membrane tubings were washed in running water for 3-4 hours to remove glycerol followed by treatment of tubing with sodium sulfide solution (0.3% w/v) at 80°C for 1 minute to remove sulfur compounds. Wash with hot water (60°C) for 2 minutes, followed by acidification with a 0.2% (v/v) solution of sulfuric acid, then rinse with hot water to remove the acid. Then the dialysis membranes were dipped overnight in the diffusion medium before dialysis for thorough wetting of the tubings.

5.2.3 Selection of Diffusion Medium

Receptor compartment containing 50 ml of diffusion medium (50 mM Hydroxypropyl-beta-cyclodextrin, 20 mM HEPES, pH 7.4) for RGZ and 50 ml of diffusion medium (100 mM Hydroxypropyl-beta-cyclodextrin, 20 mM HEPES, pH 7.4) for CDS, with constant stirring kept at $37^\circ \pm 0.5^\circ\text{C}$. This diffusion medium is selected to maintain sink condition (Saarinen-Savolainen et al., 1997).

5.3 METHOD

Diffusion studies were carried out for plain drugs (RGZ, CDS), developed unconjugated liposomal formulations and conjugated liposomal formulations. Known quantity of the plain drug and equivalent amount of the drug-loaded unconjugated and conjugated liposomes were dispersed in 2 ml diffusion medium and were taken into the dialysis bags respectively. Then bags were transferred into 50 ml diffusion medium kept at $37^{\circ} \pm 0.5^{\circ}\text{C}$. The dispersion in the dialysis bag was stirred with a magnetic stirrer and the solution outside the bag with an electric stirrer. At fixed time intervals 200 μl samples were withdrawn from outer medium of the bag and replaced with equal volumes of fresh diffusion medium and analyzed by UV spectrophotometric method, as described in chapter no 3, after suitable dilutions with methanol. All diffusion studies and sample analysis were carried out three times and mean values along with standard error of mean are recorded (Nounou et al., 2006; Henriksen et al., 1995).

5.4 DATA AND STATISTICAL ANALYSIS

1) Percentage drug diffused: (Shah et al., 1991; Shah et al., 1993)

$$\text{Percentage Drug Diffused} = \left(\frac{C_r \times V_r}{A} \right) \times 100$$

Where, C_r = conc. of drug in receptor compartment,

V_r = volume of the receptor compartment,

A = amount of drug in donor compartment at zero time.

2) Kinetics of release: The order of drug release was determined by fitting the data in various models utilizing drug release data modeling software DD Solver 1.0 of Microsoft. Percentage drug release was calculated and plotted against the time to accomplish drug release profile (figure 5.1 and 5.2). The *in-vitro* release data obtained were fitted into equations for the zero-order, first-order and Higuchi release models. Correlation coefficient values resulting from linear regression were used to interpret the data (Dash et al., 2010; Enden and Schroeder, 2009; Chien, 1992; Higuchi, 1962; Higuchi, 1961; Koizumi et al., 1975).

3) Steady state flux:

$$\text{Steady state flux (J)} = V_r \times \left(\frac{dc}{dt}\right)$$

Where, V_r = volume of receptor compartment and

(dc/dt) = rate of change of concentration,

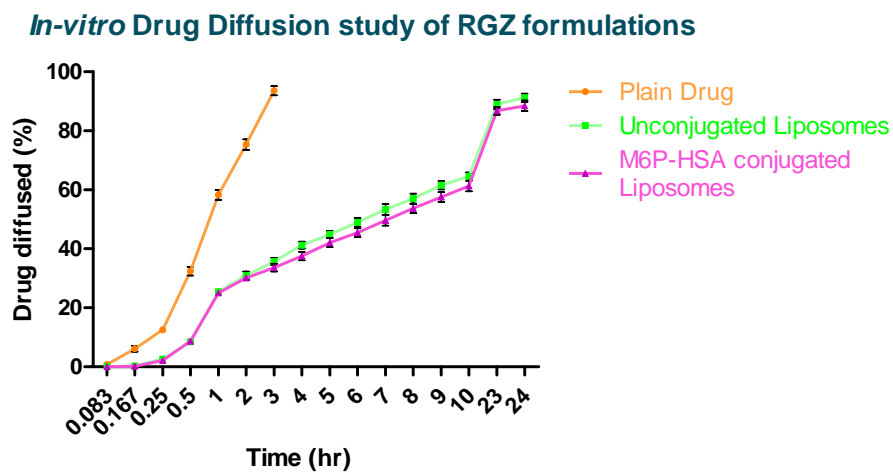
5.5 RESULTS AND DISCUSSIONS

Comparative diffusion studies were carried out of plain drugs, unconjugated and M6P-HSA conjugated liposomal formulations using diffusion membrane for a period of 24 hours. The results of these studies are recorded in Table 5.1, 5.2 and 5.3.

Table 5.1 Comparative *in-vitro* drug diffusion of plain RGZ and RGZ liposomal formulations

Time (hrs.)	Mean Cumulative Percent Drug Diffused across the membrane (mean \pm SEM)*		
	RGZ formulations		
	Plain RGZ	Unconjugated Liposomes	M6P-HAS conjugated Liposomes
0.083	0.79 \pm 0.031	0.03 \pm 0.003	0.02 \pm 0.003
0.167	6.10 \pm 1.016	0.28 \pm 0.018	0.23 \pm 0.010
0.25	12.57 \pm 0.604	2.65 \pm 0.211	2.11 \pm 0.199
0.5	32.44 \pm 1.445	8.43 \pm 0.652	8.70 \pm 0.545
1	58.30 \pm 1.735	25.48 \pm 0.655	25.05 \pm 0.750
2	75.36 \pm 1.788	30.88 \pm 1.430	30.10 \pm 0.862
3	93.59 \pm 1.576	35.70 \pm 1.259	33.60 \pm 1.320
4	--	41.24 \pm 1.180	37.55 \pm 1.402
5	--	44.89 \pm 1.162	42.08 \pm 1.532
6	--	48.95 \pm 1.480	45.45 \pm 1.526
7	--	53.37 \pm 1.809	49.67 \pm 1.758
8	--	57.017 \pm 1.663	53.67 \pm 1.540
9	--	61.53 \pm 1.435	57.57 \pm 1.678
10	--	64.50 \pm 1.366	61.30 \pm 1.846
23	--	88.96 \pm 1.589	86.75 \pm 1.286
24	--	91.22 \pm 1.439	88.48 \pm 1.793

* n=3

Figure 5.1 Comparative *in-vitro* drug diffusion profiles of plain RGZ and RGZ liposomal formulations

n = 3 (\pm SEM)

P < 0.001: (Plain drug and unconjugated liposomes; plain drug and conjugated liposomes)

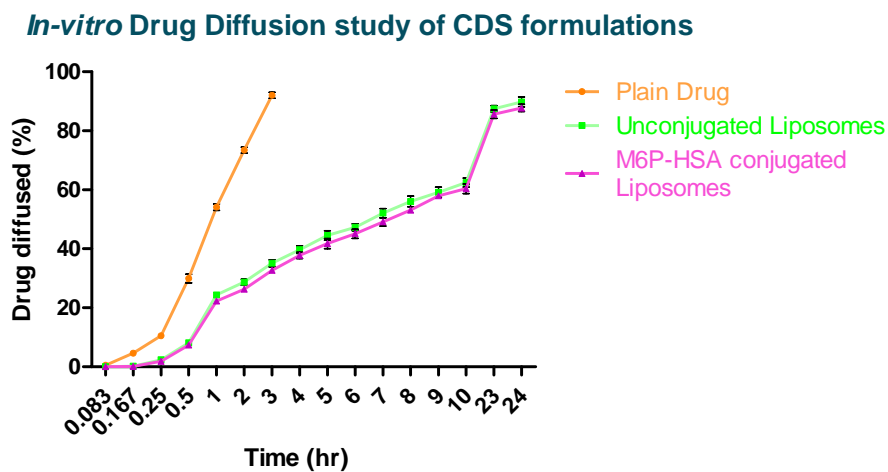
P > 0.05: (Unconjugated liposomes and conjugated liposomes)

Table 5.2 Comparative *in-vitro* drug diffusion of plain CDS and CDS liposomal formulations

Time (hrs.)	Mean Cumulative Percent Drug Diffused across the membrane (mean \pm SEM)*		
	CDS formulations		
	Plain CDS	Unconjugated Liposomes	M6P-HAS conjugated Liposomes
0.083	0.52 \pm 0.020	0.02 \pm 0.003	0.02 \pm 0.003
0.167	4.62 \pm 0.477	0.17 \pm 0.009	0.14 \pm 0.009
0.25	10.56 \pm 0.383	2.36 \pm 0.264	1.91 \pm 0.149
0.5	29.92 \pm 1.455	8.10 \pm 0.532	7.37 \pm 0.551
1	54.16 \pm 1.091	24.38 \pm 0.753	22.29 \pm 0.866
2	73.43 \pm 0.993	28.69 \pm 1.037	26.29 \pm 0.788
3	92.04 \pm 1.019	35.09 \pm 1.229	32.69 \pm 0.909
4	--	39.75 \pm 1.305	37.75 \pm 1.009
5	--	44.55 \pm 1.558	41.75 \pm 1.671
6	--	47.28 \pm 1.140	45.09 \pm 1.515
7	--	52.09 \pm 1.547	49.14 \pm 1.393
8	--	56.06 \pm 1.788	53.14 \pm 0.607
9	--	59.16 \pm 1.692	57.96 \pm 0.841
10	--	62.44 \pm 1.512	60.35 \pm 1.601
23	--	87.43 \pm 1.086	85.62 \pm 1.406
24	--	89.82 \pm 1.675	87.72 \pm 1.210

n=3

Figure 5.2 Comparative *in-vitro* drug diffusion profiles of plain CDS and CDS liposomal formulations



n = 3 (\pm SEM)

P < 0.001: (Plain drug and unconjugated liposomes; plain drug and conjugated liposomes)

P > 0.05: (Unconjugated liposomes and conjugated liposomes)

Table 5.3 Drug diffusion model, Regression coefficient (r^2) and mean steady state flux of different formulations

	Name of the formulation	Drug diffusion model	Regression coefficient (r^2)	Mean steady state flux
RGZ and liposomal formulations	Plain RGZ	First order model	0.9833	37.78
	Unconjugated Liposomes	Higuchi model	0.9768	6.89
	M6P-HAS conjugated Liposomes	Higuchi model	0.9796	6.48
CDS and liposomal formulations	Plain CDS	First order model	0.9827	30.66
	Unconjugated Liposomes	Higuchi model	0.9789	6.58
	M6P-HAS conjugated Liposomes	Higuchi model	0.9818	6.08

The order of drug release was determined by fitting the data in various models utilizing drug release data modeling software DD Solver 1.0 of Microsoft. Percentage drug diffused was calculated and plotted against the time to accomplish drug release profile. Cumulative percent drug diffusion was plotted against time (t) and shown in Figure 5.1 and 5.2. The *in-vitro* release data obtained were fitted into equations for the zero-order, first-order and Higuchi release models. Correlation coefficient values, resulting from linear regression, were used to interpret the data. The non-linearity of the graph for unconjugated and conjugated liposomal formulations suggests that the diffusion pattern does not follow zero order kinetics of release. Highest regression coefficient value for the first order model was found for plain drugs [RGZ (0.9833); CDS (0.9827)] and for the Higuchi model for both the unconjugated [RGZ (0.9768); CDS (0.9789)] and M6P-HSA conjugated liposomes [RGZ (0.9796); CDS (0.9818)], indicating diffusion to be the predominant mechanism of drug release in both the cases of liposomes. In case of RGZ, Mean steady state flux were 37.78, 6.89 and 6.48 for plain drug, unconjugated liposomes and M6P-HSA conjugated liposomes respectively. In case of CDS, mean steady state flux were 30.66, 6.58 and 6.08 for plain drug, unconjugated liposomes and M6P-HSA conjugated liposomes respectively.

There are two rate-controlling barriers influencing the drug diffusion to the receptor compartment, one is the liposomal membrane and the other is the artificial membrane. The percentage drug diffusion of liposomal drugs is found to be dependent upon the composition of formulation. Hence, we can conclude that the liposomal membrane controls the drug diffusion and not the artificial membrane. The artificial membrane acts only as physical barrier preventing the liposomes to diffuse into the donor compartment and not regulating the drug diffusion to the receptor compartment.

5.6 CONCLUSION

Hence, liposomal encapsulation, composition of liposomal membrane and charge are expected to help in retaining the drug within the liposomes. All these observations lead us to the conclusion that liposomal drug delivery has a greater potential for sustained diffusion of drug. Drug diffusion from liposomal formulations obeys Higuchi's diffusion controlled model and the diffusion rate is close to first order kinetics. The diffusion rate depends upon the physicochemical property, concentration of drug within the liposomes and the composition of the liposomal membrane. Hence

by altering the composition of the liposomal membrane, different loading dose followed by maintenance dose can be achieved. This model of diffusion study may be used to assess the desired diffusion pattern by modulating the composition of the bilayer membrane and *in-vitro* evaluation of the formulations before going for *in-vivo* studies.

5.7 REFERENCES

Chien YW. Novel drug delivery systems, *Drugs and the Pharmaceutical Sciences*, Vol.50, Marcel Dekker, New York, NY;1992;797.

Dash S, Murthy PN, Nath L, Chowdhury P. Kinetic modeling on drug release from controlled drug delivery systems. *Acta Pol Pharm.* 2010 May-Jun;67(3):217-23.

Enden G, Schroeder A. A mathematical model of drug release from liposomes by low frequency ultrasound. *Ann Biomed Eng.* 2009 Dec;37(12):2640-5.

Fielding RM, Abra RM. Factors affecting the release rate of terbutaline from liposome formulations after intratracheal instillation in the guinea pig. *Pharm Res.* 1992 Feb;9(2):220-3.

Gemmell DH, Morrison JC. The release of medicinal substances from topical applications and their passage through the skin. *J Pharm Pharmacol.* 1957 Oct;9(10):641-56.

Henriksen I, Sande SA, Smistad G, Agren T, Karlsen J. In vitro evaluation of drug release kinetics from liposomes by fractional dialysis. *Int. J. Pharm.* 1995;119(2):231-8.

Higuchi T. Rate of release of medicaments from ointment bases containing drugs in suspension. *J Pharm Sci.* 1961 Oct;50:874-5.

Higuchi WI. Analysis of data on the medicament release from ointments. *J Pharm Sci.* 1962 Aug;51:802-4.

Koizumi T, Ueda M, Kakemi M, Kameda H. Rate of release of medicaments from ointment bases containing drugs in suspension. *Chem Pharm Bull (Tokyo).* 1975 Dec;23(12):3288-92.

Margalit R, Yerushalmi N. Pharmaceutical aspects of liposomes: "Perspectives in, and integration of, academic and industrial research and development" In: Benita s.

(ed.), *Microencapsulation: Methods and Industrial Applications*. Marcel Dekker Inc., New York, 1996; 259-95.

Mojaverian P, Rosen J, Vadino WA, Liebowitz S, Radwanski E. In-vivo/in-vitro correlation of four extended release formulations of pseudoephedrine sulfate. *J Pharm Biomed Anal.* 1997 Jan;15(4):439-45.

Nounou MM, El-Khordagui LK, Khalafallah NA, Khalil SA. In vitro release of hydrophilic and hydrophobic drugs from liposomal dispersions and gels. *Acta Pharm.* 2006 Sep;56(3):311-24.

Saarinen-Savolainen P, Jarvinen T, Taipale H, Urtti A. Method for evaluating drug release from liposomes in sink conditions. *Int. J. Pharm.* 1997;159(1):27-33.

Shah VP, Elkins J, Hanus J, Noorizadeh C, Skelly JP. In vitro release of hydrocortisone from topical preparations and automated procedure. *Pharm Res.* 1991 Jan;8(1):55-9.

Shah VP, Elkins JS, Williams RL. In vitro drug release measurement of topical glucocorticoid creams. *Pharmacoepial Forum.* 1993;19:5048-59.

CHAPTER 6

STABILITY STUDIES



Stability Studies

6.1 INTRODUCTION

6.2 METHOD

6.3 RESULTS AND DISCUSSION

6.3.1 Stability testing of RGZ liposomal formulation

6.3.1 Stability testing of CDS liposomal formulation

6.4 CONCLUSION

6.5 REFERENCES

6.1 INTRODUCTION

For liposomal products an attention has been focused on two processes affecting the quality and therefore acceptability of liposomes (Talsma and Crommelin, 1992). Especially, with liposomal product to see the market it should stable during the shelf life (storage or transport). In general, a shelf life of at least one year is a minimum prerequisite criterion for a commercial product First leakage of drug from the vesicles may take place into the extra liposomal compartment. Secondly, there is a possibility of liposomal aggregation and/or fusion, which leads to formation of larger particles (Slabbert et al., 2011; Fang et al., 1997; Cliff et al., 1992; Grit and Crommelin, 1992). These parameters will alter the *in vivo* fate, affecting therapeutic index of the drug. Hydrolysis of phospholipids is one of the parameters like to cause the formation of fatty acids and lysophospholipids (Grit and Crommelin, 1993; Mowri et al., 1984). Although under dehydrated storage, there is least possibility of the formulation to encounter hydrolytic degradation. Another aspect to be considered is liposome oxidation (Frokjaer et al., 1984). Stability is considered as chemical stability of drug substance in a dosage form. However, the performance of liposomal formulation is not only dependent upon the content of the drug substance, but also dependent on reproducible *in vivo* performance of the formulations. Formulations under stability studies were considered chemically stable by evaluating the drug leakage from liposomes. The stability protocol was designed as per ICH guidelines (Singh, 1999) for countries falling under zone III (hot, dry) and zone IV (very hot, humid) (US FDA, 2002).

6.2 METHOD

Comparative stability studies were carried out of the potential liposomal formulations at accelerated condition ($25^{\circ}\text{C} \pm 2^{\circ}\text{C}$, 60% RH \pm 5% RH) for six months and at long-term conditions ($5^{\circ}\text{C} \pm 3^{\circ}\text{C}$) up to twelve months. Lyophilized liposomal formulations containing 0.2 mg RGZ and 0.2 mg CDS were filled into amber color glass vials, purged with nitrogen, sealed and stored at the above mentioned condition. At each sampling time different vial is used for the stability testing (Bhalerao and Raje, 2003; Manosroi et al., 2004; Manosroi et al., 2002; Yang et al., 2007; Anderson and Omri, 2004; Changsan et al., 2009; Winterhalter and Lasic, 1993; Ugwu et al., 2005).

The liposomal formulations were examined visually for the evidence of discoloration. The content of the vial are tested for percentage drug retention (PDR), particle size, zeta-potential, assay and water content. The stability results are summarized in Tables 6.1 (RGZ) and Table 6.2 (CDS).

6.3 RESULTS AND DISCUSSION

The physical stability of liposomes is one of the biggest obstacles in formulation commercially viable product (Fildes, 1981). Liposomes should be stable for 1-2 years preferably at room temperature to be pharmaceutically acceptable with high drug retention within liposome and the particle size should be maintained during storage time, hence the drug leakage, particle size growth, change in zeta-potential and the chemical stability of drugs were studied at accelerated condition ($25^{\circ}\text{C} \pm 2^{\circ}\text{C}$, 60% RH \pm 5% RH) for six months and at long-term conditions ($5^{\circ}\text{C} \pm 3^{\circ}\text{C}$) up to twelve months. No significant differences were found in all above mentioned parameters at both conditions.

6.3.1 Stability testing of RGZ liposomal formulation

The stability testing of prepared RGZ liposomal formulation was performed at accelerated condition ($25^{\circ}\text{C} \pm 2^{\circ}\text{C}$, $60\% \text{ RH} \pm 5\% \text{ RH}$) for six months and at long-term conditions ($5^{\circ}\text{C} \pm 3^{\circ}\text{C}$) up to twelve months and the effect on various parameters was studied and reported below.

Table 6.1 Stability testing data of RGZ liposomal formulation

Sampling time (Month)	Description	Assay (%)	Percent drug retained	Water content (%)	Particle size [Z-Average (d.nm)]	Zeta potential (mV)
Initial	White powder	101.16 \pm 2.27	101.55 \pm 3.21	3.1 \pm 0.21	180.1 \pm 2.93	-21.9 \pm 1.33
Accelerated condition ($25^{\circ}\text{C} \pm 2^{\circ}\text{C}$, $60\% \text{ RH} \pm 5\% \text{ RH}$)						
1	White powder	101.08 \pm 2.45	100.46 \pm 3.47	3.2 \pm 0.18	183.4 \pm 2.74	-21.6 \pm 1.27
2	White powder	101.32 \pm 1.98	99.19 \pm 2.87	3.2 \pm 0.19	186.2 \pm 2.22	-20.8 \pm 1.43
3	White powder	100.73 \pm 3.03	98.77 \pm 2.63	3.3 \pm 0.21	188.7 \pm 3.19	-20.9 \pm 1.51
6	White powder	99.79 \pm 3.28	97.66 \pm 3.07	3.4 \pm 0.24	194.3 \pm 3.35	-19.7 \pm 1.20
Long-term conditions ($5^{\circ}\text{C} \pm 3^{\circ}\text{C}$)						
1	White powder	101.77 \pm 2.83	101.81 \pm 2.26	3.1 \pm 0.19	180.4 \pm 3.02	-22.1 \pm 1.21
2	White powder	101.43 \pm 2.42	101.07 \pm 3.09	3.1 \pm 0.22	179.2 \pm 3.11	-21.8 \pm 1.49
3	White powder	101.09 \pm 3.11	101.24 \pm 3.13	3.1 \pm 0.22	183.3 \pm 2.95	-21.3 \pm 1.46
6	White powder	101.82 \pm 2.07	100.92 \pm 3.42	3.2 \pm 0.28	182.4 \pm 2.84	-21.1 \pm 1.13
9	White powder	100.68 \pm 1.84	100.76 \pm 2.86	3.2 \pm 0.29	184.6 \pm 2.50	-21.3 \pm 1.59
12	White powder	100.31 \pm 3.21	100.01 \pm 2.29	3.2 \pm 0.24	186.2 \pm 3.14	-20.7 \pm 1.09

6.3.2 Stability testing of CDS liposomal formulation

The stability testing of prepared CDS liposomal formulation was performed at accelerated condition ($25^{\circ}\text{C} \pm 2^{\circ}\text{C}$, $60\% \text{ RH} \pm 5\% \text{ RH}$) for six months and at long-term conditions ($5^{\circ}\text{C} \pm 3^{\circ}\text{C}$) up to twelve months and the effect on various parameters was studied and reported below.

Table 6.2 Stability testing data of CDS liposomal formulation

Sampling time (Month)	Description	Assay (%)	Percent drug retained	Water content (%)	Particle size [Z-Average (d.nm)]	Zeta potential (mV)
Initial	White powder	99.82 ± 2.53	98.93 ± 3.38	2.7 ± 0.19	184.6 ± 3.01	-29.3 ± 1.41
Accelerated condition ($25^{\circ}\text{C} \pm 2^{\circ}\text{C}$, $60\% \text{ RH} \pm 5\% \text{ RH}$)						
1	White powder	99.98 ± 2.21	98.12 ± 3.19	2.7 ± 0.23	185.1 ± 2.69	-28.5 ± 1.38
2	White powder	99.76 ± 2.33	96.74 ± 3.26	2.7 ± 0.23	188.4 ± 2.09	-27.6 ± 1.26
3	White powder	99.41 ± 2.72	96.39 ± 2.87	2.8 ± 0.19	190.3 ± 2.84	-27.3 ± 2.01
6	White powder	98.63 ± 1.97	95.28 ± 2.82	2.9 ± 0.20	196.8 ± 3.09	-26.2 ± 1.42
Long-term conditions ($5^{\circ}\text{C} \pm 3^{\circ}\text{C}$)						
1	White powder	99.54 ± 3.02	98.47 ± 2.71	2.7 ± 0.18	183.9 ± 3.25	-29.2 ± 1.19
2	White powder	99.61 ± 2.21	98.59 ± 3.31	2.7 ± 0.25	184.7 ± 2.88	-29.6 ± 1.44
3	White powder	99.71 ± 2.95	98.38 ± 3.47	2.7 ± 0.23	185.5 ± 2.61	-28.1 ± 1.37
6	White powder	99.34 ± 3.16	98.16 ± 2.56	2.7 ± 0.31	187.2 ± 3.37	-27.6 ± 1.33
9	White powder	99.28 ± 2.78	97.87 ± 2.72	2.7 ± 0.25	189.9 ± 3.00	-27.4 ± 1.72
12	White powder	98.94 ± 2.45	97.12 ± 3.01	2.8 ± 0.27	193.1 ± 2.98	-26.9 ± 1.21

6.4 CONCLUSION

The decrease in drug assay, percentage drug retained, and zeta-potential and increase in water content, particle size were observed at accelerated condition ($25^{\circ}\text{C} \pm 2^{\circ}\text{C}$, $60\% \text{ RH} \pm 5\% \text{ RH}$) for six months and at long-term conditions ($5^{\circ}\text{C} \pm 3^{\circ}\text{C}$) up to twelve months for both RGZ and CDS liposomal formulation but the changes were statistically insignificant. Hence, both the formulations were considered as stable and were selected for further studies.

6.5 REFERENCES

Anderson M, Omri A. The effect of different lipid components on the in vitro stability and release kinetics of liposome formulations. *Drug Deliv.* 2004 Jan-Feb;11(1):33-9.

Bhalerao SS, Raje Harshal A. Preparation, optimization, characterization, and stability studies of salicylic acid liposomes. *Drug Dev Ind Pharm.* 2003 Apr;29(4):451-67.

Changsan N, Chan HK, Separovic F, Srichana T. Physicochemical characterization and stability of rifampicin liposome dry powder formulations for inhalation. *J Pharm Sci.* 2009 Feb;98(2):628-39.

Cliff RO, Ligler F, Goins B, Hoffmann PM, Spielberg H, Rudolph AS. Liposome encapsulated hemoglobin: long-term storage stability and in vivo characterization. *Biomater Artif Cells Immobilization Biotechnol.* 1992;20(2-4):619-26.

Fang JY, Lin HH, Hsu LR, Tsai YH. Characterization and stability of various liposome-encapsulated enoxacin formulations. *Chem Pharm Bull (Tokyo).* 1997 Sep;45(9):1504-9.

Fildes FJT (1981) Liposomes: The Industrial view point. In: *Liposomes from Physical Structure to Therapeutic Applications*, Knight CG (Ed), Elsevier Biomedical Press, New York, 465-483.

Frokjaer S, Hjorth EL, Worts O. (1984) Stability testing of liposomes during storage. In: *Liposome Technology: Preparation of liposomes*, Gregoriadis G (Ed), CRC Press, Boca Raton, Florida, 235-245.

Grit M, Crommelin DJ. The effect of aging on the physical stability of liposome dispersions. *Chem Phys Lipids.* 1992 Sep;62(2):113-22.

Grit M, Zuidam NJ, Underberg WJ, Crommelin DJ. Hydrolysis of partially saturated egg phosphatidylcholine in aqueous liposome dispersions and the effect of cholesterol incorporation on hydrolysis kinetics. *J Pharm Pharmacol.* 1993 Jun;45(6):490-5.

Manosroi A, Kongkaneramt L, Manosroi J. Characterization of amphotericin B liposome formulations. *Drug Dev Ind Pharm.* 2004 May;30(5):535-43.

Manosroi A, Podjanasoonthon K, Manosroi J. Stability and release of topical tranexamic acid liposome formulations. *J Cosmet Sci.* 2002 Nov-Dec;53(6):375-86.

Mowri H, Nojima S, Inoue K. Effect of lipid composition of liposomes on their sensitivity to peroxidation. *J Biochem.* 1984 Feb;95(2):551-8.

Singh S. Drug stability testing and shelf-life determination according to international guidelines. *Pharm. Technol.* 1999;23:68-88.

Slabbert C, Plessis LH, Kotze AF. Evaluation of the physical properties and stability of two lipid drug delivery systems containing mefloquine. *Int J Pharm.* 2011 May 16;409(1-2):209-15.

Talsma H, Crommelin DJA. Liposomes as Drug Delivery Systems, Part III: Stabilization. *Pharm. Technol.* 1992;17:48-59.

Ugwu S, Zhang A, Parmar M, Miller B, Sardone T, Peikov V, Ahmad I. Preparation, characterization, and stability of liposome-based formulations of mitoxantrone. *Drug Dev Ind Pharm.* 2005 Jan;31(2):223-9.

US FDA (CDER), (2002), Draft Guidance for Industry Liposome Drug Products. CMC Documentation.

Winterhalter M, Lasic DD. Liposome stability and formation: experimental parameters and theories on the size distribution. *Chem Phys Lipids.* 1993 Sep;64(1-3):35-43.

Yang T, Cui FD, Choi MK, Lin H, Chung SJ, Shim CK, Kim DD. Liposome formulation of paclitaxel with enhanced solubility and stability. *Drug Deliv.* 2007 Jul;14(5):301-8.

CHAPTER 7

IN-VIVO STUDIES



In-vivo Studies

7.1 INTRODUCTION

7.2 ANIMALS

7.3 CAUTION

7.4 CCL4-INDUCED LIVER FIBROSIS MODEL AND EXPERIMENTAL DESIGN

7.5 BIOCHEMICAL ESTIMATION

7.6 HYDROXYPROLINE CONTENT OF LIVER TISSUE

7.7 HISTOPATHOLOGY

7.7.1 Hematoxylin and Eosin Staining

7.7.2 Masson's Trichrome Staining

7.7.3 Sirius Red Staining

7.7.4 α -SMA Staining

7.8 PHARMACOKINETIC AND BIODISTRIBUTION

7.9 RESULTS

7.9.1 Biochemical Estimation and Histopathological Examination

7.9.2 Pharmacokinetic and Biodistribution

7.10 CONCLUSION

7.11 REFERENCES

7.1 INTRODUCTION

Animal models of liver fibrosis remain a vital experimental tool. Animal models are essential to the investigation of liver fibrosis and other fibrotic diseases because they provide the only model in which the serial sampling of tissue, which facilitates the dissection of the cell and molecular processes that underlie fibrosis, can be made. The importance of studying human models of disease cannot be overemphasized. Nevertheless, at best they can only provide a snapshot of a disease process which may develop over weeks or months. In addition, the morbidity, potential mortality, and ethical issues associated with liver biopsy in humans, significantly limits the use of biopsy material for research. Finally, it is, of course, ethically impossible to manipulate the pathogenic process of liver fibrosis experimentally *in vivo* in human beings. For these reasons, animal models of liver fibrosis remain a vital experimental tool.

Many experimental models of hepatic fibrosis have been described. These include those associated with toxic damage [e.g., carbon tetrachloride, diamethylnitrosamine, thioacetamide (Ala-Kokko et al., 1989; Cameron and Karunaratne, 1936; Igarashi et al., 1986; Madden et al., 1970; Morrione, 1949; Martinez-Hernandez, 1985; Nakamura et al., 1975; Rojkind and Dunn, 1979; Rubin et al., 1963; Zimmerman, 1976)], immunological damage [e.g., that mediated by heterologous serum and experimental schistosomiasis (Ballardini et al., 1983; Yokoi et al., 1988)], biliary fibrosis [e.g., common bile duct ligation (Issa et al., 2001; Tams, 1957)], and alcoholic liver disease [e.g., the baboon ethanol diet or the Tsukamoto/French model in rats (Tsukamoto et al., 1990)].

Carbon tetrachloride-induced fibrosis and cirrhosis is one of the oldest and probably the most widely used toxin-based experimental model for the induction of fibrosis. It has the advantages that it has been clearly characterized and in many respects mirrors the pattern of disease seen in human fibrosis and cirrhosis associated with toxic damage (Tsukamoto et al., 1990; Perez Tamayo, 1983). In addition, there is extensive experience with this model with respect to the characterization of histological and biochemical changes and changes associated with injury, inflammation, and fibrosis (Perez Tamayo, 1983; Maher and McGuire, 1990). Most specifically, the cellular sources of key matrix components, including collagen-1 in addition to the matrix

degrading metalloproteinases (matrix metalloproteinases [MMPs]) and their inhibitors (tissue inhibitors of metalloproteinases [TIMPs]), have been determined (Maher and McGuire, 1990; Iredale et al., 1996; Iredale et al., 1998). Finally, in experienced hands, and even with outbred rats or mice, this model elicits a reproducible and predictable fibrotic response, making it a valuable basis for study. For these reasons, there is a relatively extensive experience and growing literature in which CCl₄-induced fibrosis is used as a basis for mechanistic study, either through the use of genetically modified mice (Issa et al., 2003) or the manipulation of the process via a drug or other mediator (Ala-Kokko et al., 1989; Nakamura et al., 1975; Yokoi et al., 1988; Wright et al., 2001).

Of course, the CCl₄ model has disadvantages. In comparison, as a model, it has no direct human disease counterpart (Perez Tamayo, 1983). Additionally, unlike human liver fibrosis, there is more pronounced cholangiolar cell hyperplasia in advanced CCl₄ fibrosis and, in rats, in the presence of CCl₄-induced cirrhosis, and there is failure to progress to the development of hepatocellular carcinoma (this has been reported in mice subjected to CCl₄ injury, however) (Perez Tamayo, 1983). A final consideration is that, in comparison with studies of human tissue and murine tissue, the availability of protein-based reagents such as antibodies, which work effectively in rat models, is relatively limited. These comments notwithstanding, this article will describe the methods for using CCl₄ as an *in vivo* model of fibrosis in rats.

Carbon tetrachloride, like other halokanes, is activated by oxidases to yield a trichloromethyl radical. This free radical initiates lipid peroxidation and can react with the sulphhydryl group of proteins. CCl₄ has been administered to rodents by inhalation, gastric gavage, and by subcutaneous and intraperitoneal injections. Because of the necessity for bioactivation, the severity of CCl₄ injury will be strongly influenced by the type of diet and the presence of other xenobiotics. Specifically, microsomal cytochrome p450 induction significantly enhances CCl₄-mediated damage (Tsukamoto et al., 1990; Perez Tamayo, 1983). Thus, diet or drugs that activate cytochrome p450 enhance CCl₄ toxicity and the speed of development of fibrosis. This evidence has been used to increase the speed of development of fibrosis via the addition of barbiturates to drinking water in conjunction with CCl₄ intoxication (Tsukamoto et al., 1990). Conversely, of course, p450 inhibitors will reduce the toxicity and fibrosis induced by CCl₄ intoxication.

In vitro diffusion studies are dependent on the instrument's hydrodynamic condition and the diffusion medium. The in vivo parameters that help in assessing the rate and extent of absorption, AUC, C_{max} and T_{max} may not be sufficient to evaluate the pharmacokinetic performance, particularly the diffusion rate of controlled release liposomal formulations. However, when in vivo and in vitro data are combined it would add another useful dimension for the evaluation of a product's performance (Mojaverian et al., 1997).

Researchers have used CCl₄ experiments in a series of experimental models of liver injury and fibrosis. These include using CCl₄: to induce acute injury characterized by self-limiting hepatic stellate cell (HSC) activation and hepatocellular regeneration (Oakley et al., 2003), to develop early and established fibrosis [4–6 wk of CCl₄, administered as described later (Iredale et al., 1996; Iredale et al., 1998)], to develop early reversible cirrhosis (8 wk of CCl₄ intoxication), and to develop cirrhosis that demonstrates only partial reversibility (12 wk CCl₄ intoxication). In the current in vivo studies, using CCl₄ induced model of liver fibrosis, we determined the pharmacokinetic properties and the biodistribution of M6P-HSA conjugated liposomes in diseased animals.

7.2 ANIMALS

Specified pathogen free male Sprague-Dawley rats of 180 to 220 g were obtained from Torrent Research Centre (TRC), Gandhinagar, India. All experiments and protocols described in present study were approved by the Institutional Animal Ethics Committee (IAEC) of Pharmacy Department, The M.S. University of Baroda and with permission from Committee for the Purpose of Control and Supervision of Experiments on Animals (CPCSEA), Ministry of Social Justice and Empowerment, Government of India. All animals were housed in-group of 3 animals and maintained under standardized conditions (12-h light/dark cycle, 24 ± 2 °C, 35 to 60% humidity) and provided free access to pelleted CHAKKAN diet (Nav Maharashtra Oil Mills Pvt. Ltd., Pune) and purified drinking water ad libitum.

7.3 CAUTION

Carbon tetrachloride is toxic to humans by inhalation and ingestion. Preparation of carbon tetrachloride should take place in a fume hood. Injection of animals should take place, where possible, in a fume hood; although for experienced users, if a sealed

stock solution of CCl₄ is being used and only opened for filling syringes, then use in a well-ventilated room is probably acceptable. All unused solutions containing CCl₄ should be disposed of in accordance with local regulations.

7.4 CCl₄-INDUCED LIVER FIBROSIS MODEL AND EXPERIMENTAL DESIGN

Experimental liver fibrosis was developed, using an established protocol (Constandinou et al., 2005) with slight modification, that involved: intraperitoneal (i.p.) injections of 0.2 mL/100 g of the CCl₄:olive oil mixture (equal parts of CCl₄ and olive oil i.e. 1:1), twice weekly at equal intervals, for 2 week followed by 0.1 mL of the 1:1 ratio CCl₄:olive oil mixture for 8 weeks (i.e., rats received 0.1 mL/100 g of CCl₄ for 2 week followed by 0.05 mL CCl₄/100 g for rest of the duration). After 4 weeks from the first injection of CCl₄, the rats were randomly divided into 9 subgroups (n=8):

Group 1 (control): Animals received standard laboratory diet and drinking water ad libitum and served as a control group.

Group 2 (CCl₄): Animals received only CCl₄ as per the standard protocol.

Group 3 (Plain M6P-HSA conjugated liposomes + CCl₄): Animals received plain M6P-HSA conjugated liposomes (equivalent to amount of liposomes required in group 5, intravenous) along with CCl₄.

Group 4 (RGZ + CCl₄): Animals received RGZ (1 mg/kg/day, intravenous) along with CCl₄.

Group 5 (RGZ loaded unconjugated liposomes + CCl₄): Animals received RGZ loaded unconjugated liposomes (equivalent to RGZ 1 mg/kg/day, intravenous) along with CCl₄.

Group 6 (RGZ loaded M6P-HSA conjugated liposomes + CCl₄): Animals received RGZ loaded M6P-HSA conjugated liposomes (equivalent to RGZ 1 mg/kg/day, intravenous) along with CCl₄.

Group 7 (CDS + CCl₄): Animals received CDS (3 mg/kg/day, intravenous) along with CCl₄.

Group 8 (CDS loaded unconjugated liposomes + CCl₄): Animals received CDS loaded unconjugated liposomes (equivalent to CDS 3 mg/kg/day, intravenous) along with CCl₄.

Group 9 (CDS loaded M6P-HSA conjugated liposomes + CCl₄): Animals received CDS loaded M6P-HSA conjugated liposomes (equivalent to CDS 3 mg/kg/day, intravenous) along with CCl₄.

All formulations were administered via the tail-vein injection.

7.5 BIOCHEMICAL ESTIMATION

After 8 weeks from the first injection of CCl₄, animals were sacrificed and blood samples were collected and serum separated from each sample and used for the biochemical analysis. Serum albumin (ALB), globulin (GLB), total protein, alanine amino-transferase (ALT), glutamate-pyruvate transaminase (AST) and blood glucose were measured by routine biochemical methods utilizing kits according to the manufacturer's instructions (described in chapter 3). Serum levels of hyaluronic acid were measured by ELISA kits according to the manufacturer's instructions (described in chapter 3). Immediately after sacrifice, liver was isolated in ice cold condition. They were blotted free of blood and tissue fluids. Then were weighed and stored at -80 °C till further use for the further analysis (CryoScientific, India). Liver weight to body weight ratio (liver coefficient) was calculated by dividing liver weight (g) by body weight (g) and multiplying it with 100 (Ye and Liu, 1985).

7.6 HYDROXYPROLINE CONTENT OF LIVER TISSUE

Hydroxyproline content of the liver tissue was determined according to Boyd R. Switzer's method as previously reported (described in chapter 3) (Switzer, 1991). The data was expressed as hydroxyproline (µg)/wet liver weight (g).

7.7 HISTOPATHOLOGY

After sacrificing the animals, liver was immediately removed and washed with saline and fixed in 10% buffered formalin. The fixed tissues were embedded in paraffin, five µm thick serial sections were cut and then processed for hematoxylin and eosin (H&E), masson's trichrome, picro-sirius red and α-SMA staining according to standard procedures (Constandinou et al., 2005).

7.7.1 Hematoxylin and Eosin Staining

Hematoxylin and eosin staining provides a specimen in which the overall architecture, degree of inflammation, necrosis, cellular apoptosis, and cellular mitosis can be assessed. For paraffin-embedded tissue sections:

1. Dip tissue sections in filtered Mayer's Haemalum for approx 30 s to 1 min.
2. Thoroughly wash tissue sections in tap water until the water is clear.
3. Blue tissue sections in Scott's tap water for 1 min.
4. Thoroughly wash tissue sections in tap water.
5. Dip tissue sections in eosin for 30 s.
6. Thoroughly wash tissue sections in tap water until the water is clear.
7. Dehydrate tissue sections through IMS twice, followed by xylene twice, each time for 5 min.
8. Sections were mounted using cover slips with distrene, plasticizer, xylene (DPX) medium.

7.7.2 Masson's Trichrome Staining

Description: This method is used for the detection of collagen fibers in tissue specimens on formalin-fixed, paraffin-embedded sections, and may be used for frozen sections as well. The collagen fibers will be stained blue and the nuclei will be stained black and the background is stained red.

Fixation: 10% formalin or Bouin's solution

Solutions and Reagents:

Bouin's Solution:

Picric acid (saturated) ----- 75 ml

Formaldehyde (37-40%) ----- 25 ml

Glacial acetic acid ----- 5 ml

Mix well. This solution will improve Masson Trichrome staining quality.

Weigert's Iron Hematoxylin Solution:

Stock Solution A:

Hematoxylin ----- 1 g

95% Alcohol ----- 100 ml

Stock Solution B:

29% Ferric chloride in water ----- 4 ml

Distilled water ----- 95 ml

Hydrochloric acid, concentrated ---- 1ml

Weigert's Iron Hematoxylin Working Solution:

Mix equal parts of stock solution A and B. This working solution is stable for 3 months (no good after 4 months)

Biebrich Scarlet-Acid Fuchsin Solution:

Biebrich scarlet, 1% aqueous ----- 90 ml

Acid fuchsin, 1% aqueous -----10 ml

Acetic acid, glacial ----- 1 ml

Phosphomolybdic-Phosphotungstic Acid Solution:

5% Phosphomolybdic acid ----- 25 ml

5% Phosphotungstic acid ----- 25 ml

Aniline Blue Solution:

Aniline blue ----- 2.5 g

Acetic acid, glacial ----- 2 ml

Distilled water ----- 100 ml

1% Acetic Acid Solution:

Acetic acid, glacial ----- 1 ml

Distilled water ----- 99 ml

Procedure:

1. Deparaffinize and rehydrate through 100% alcohol, 95% alcohol 70% alcohol.
2. Wash in distilled water.
3. For Formalin fixed tissue, re-fix in Bouin's solution for 1 hour at 56 C to improve staining quality although this step is not absolutely necessary.
4. Rinse running tap water for 5-10 minutes to remove the yellow color.
5. Stain in Weigert's iron hematoxylin working solution for 10 minutes.
6. Rinse in running warm tap water for 10 minutes.
7. Wash in distilled water.
8. Stain in Biebrich scarlet-acid fuchsin solution for 10-15 minutes. Solution can be saved for future use.
9. Wash in distilled water.
10. Differentiate in phosphomolybdic-phosphotungstic acid solution for 10-15 minutes or until collagen is not red.
11. Transfer sections directly (without rinse) to aniline blue solution and stain for 5-10 minutes. Rinse briefly in distilled water and differentiate in 1% acetic acid solution for 2-5 minutes.
12. Wash in distilled water.
13. Dehydrate very quickly through 95% ethyl alcohol, absolute ethyl alcohol (these step will wipe off Biebrich scarlet-acid fuchsin staining) and clear in xylene.
14. Mount tissue sections using cover slips with DPX.

7.7.3 Sirius Red Staining

Sirius Red staining identifies the collagens in a section and provides an excellent visual index of the extent and distribution of fibrosis. The following protocol is for paraffin-embedded tissue sections.

1. Thoroughly wash all tissue sections in distilled water.
2. Place tissue sections into 0.2% phosphomolybdic acid at room temperature for 5 min.
3. Transfer tissue sections into picro-Sirius Red solution (0.1 g Sirius Red F3B in 100 mL saturated aqueous picric acid for 2 h).

4. With the exception of the GMA tissue samples, briefly wash tissue sections in 0.01% hydrochloric acid.
5. Thoroughly wash ALL tissue sections in tap water.
6. Counter stain tissue sections in filtered Mayer's Hemalum for approx 30 s to 1 min.
7. Thoroughly wash tissue sections in tap water until the water is clear.
8. Blue tissue sections in Scott's tap water for 1 min.
9. Thoroughly wash tissue sections in tap water.
10. Dehydrate tissue sections through IMS twice, followed by xylene twice, each time for 5 min.
11. Mount tissue sections using cover slips with DPX.

The sections were examined under the light microscope (Olympus BX10, Tokyo, Japan) for histopathological changes and photomicrographs (Olympus DP12 camera, Japan) were taken.

Histopathological grading was blindly executed by an independent pathologist according to the Ishak Knodell score (Goodman, 2007), which allows quantifying hepatic fibrosis in grades [0 = No fibrosis, 1 = Fibrous expansion of some portal areas, with or without short fibrous septa, 2 = Fibrous expansion of most portal areas, with or without short fibrous septa, 3 = Fibrous expansion of most portal areas with occasional portal to portal bridging, 4 = Fibrous expansion of portal areas with marked bridging (portal to portal as well as portal to central), 5 = Marked bridging (portal-portal and/or portal-central) with occasional nodules (incomplete cirrhosis) and 6 = Cirrhosis, probable or definite]

The activation of liver stellate cells indicated by the staining of α -SMA filaments is also considered as a marker for the degree of hepatic fibrosis. Paraffin-embedded serial liver sections were stained for α -SMA, using α -SMA monoclonal antibodies according to the Constandinou, Henderson, and Iredale method as previously reported (Constandinou et al., 2005).

7.7.4 α -SMA Staining

α -SMA staining will identify activated HSCs and other tissue myofibroblasts in liver sections. It provides an excellent visual index of the extent and distribution of activated HSCs in areas of liver injury and fibrosis. For paraffin-embedded tissue sections:

1. Wash all tissue section in 1X D-PBS for 5 min at room temperature.
2. Retrieval of antigens masked by crosslinkages occurring during the tissue fixation process can be accomplished by placing tissue sections in preheated 0.1% trypsin in 1X D-PBS and incubating at 37°C for 20 min.
3. Thoroughly wash all tissue sections in 1X D-PBS.
4. Endogenous peroxidase activity can be blocked by placing tissue sections into 0.6% hydrogen peroxide in methanol solution for 15 min at room temperature.
5. Thoroughly wash all tissue sections in 1X D-PBS.
6. To reduce background secondary staining, add 100 μ L of normal horse blocking serum (from the VECTASTAIN Universal Quick kit) diluted 1:40 in 1X D-PBS to the tissue section and incubate at room temperature for 10 min.
7. Remove excess serum and add 100 μ L of α -sma diluted 1:40 in 1X D-PBS. Incubate the tissue sections in a humidity chamber at 4°C overnight. No primary antibody and/or equivalent concentrations of mouse IgG2a can be added to tissue sections to act as negative controls. Vascular structures in the liver tissue sections or muscle tissue can act as positive controls.
8. Wash tissue sections in 1X D-PBS for 5 min.
9. Add 100 μ L of biotinylated universal secondary antibody (from the VECTASTAIN Universal Quick kit) diluted 1:20 in 1X D-PBS with blocking serum diluted 1:10. Incubate the tissue sections at room temperature for 15 min.
10. Wash tissue sections in 1X D-PBS for 5 min.
11. Add 100 μ L of streptavidin/peroxidase preformed complex antibody (from the VECTASTAIN Universal Quick kit) diluted 1:40 in 1X D-PBS. Incubate the tissue sections at room temperature for 10 min.
12. Wash tissue sections in 1X D-PBS for 5 min.
13. Antigen visualization can be performed adding 100 μ L of DAB (from the DAB substrate kit, to 5 mL distilled water add two drops of buffer, pH 7.5; four drops of DAB; and two drops of H₂O₂). α -sma antigen bound substrate is converted to an insoluble brown product.
14. Wash tissue sections thoroughly in tap water.
15. Dip tissue sections in filtered Mayer's Hemalum for approx 30 s to 1 min.
16. Thoroughly wash tissue sections in tap water until the water is clear.

17. Blue tissue sections in Scott's tap water for 1 min. Thoroughly wash tissue sections in tap water.
18. Dehydrate tissue sections through IMS twice, followed by xylene twice, each time for 5 min.
19. Mount tissue sections using cover slips with DPX.

7.8 PHARMACOKINETIC AND BIODISTRIBUTION

After 8 weeks of first injection of CCl₄, rats were injected with drug loaded M6P-HSA conjugated liposomes [(equivalent to RGZ 1 mg/kg, intravenous) or (equivalent to CDS 3 mg/kg, intravenous)], drug loaded unconjugated liposomes [(equivalent to RGZ 1 mg/kg, intravenous) or (equivalent to CDS 3 mg/kg, intravenous)] and plain drug (RGZ: 1 mg/kg or CDS: 1 mg/kg). Blood samples were collected at different time intervals of 5, 10, 20, 30 min and 1 h after injection. Total amount of the drug present in serum at each time point was measured by HPLC method (described in chapter 3). Similar experiments were performed for conjugated liposomes in rats pre-injected with M6P-HSA or HSA at the dose of 13 mg/kg of body weight (intravenous) 5 min before the injection of drug loaded M6P-HSA conjugated liposomes [(equivalent to RGZ 1 mg/kg, intravenous) or (equivalent to CDS 3 mg/kg, intravenous)]. From the obtained serum concentration data, the pharmacokinetic parameters were derived for each group using the Thermo Kinetica program. (Version 5.0, Thermo Fisher Scientific).

After one hour of injection, liver, spleen, kidneys, lungs and heart were excised, made free from any adhering tissues, weighed and drug content was measured in each organ by HPLC method after extraction (described in chapter 3).

7.9 RESULTS AND DISCUSSION

7.9.1 Biochemical Estimation and Histopathological Examination

The physical parameters such as liver fibrosis grade and liver:body weight ratio (i.e. liver coefficient) were significantly increased in the CCl₄ induced liver fibrosis group rats compared to control group. Biochemical parameters such as serum AST, ALT, total bilirubin, hyaluronic acid and liver hydroxyproline were significantly increased and serum albumin/globulin ratio was significantly reduced in fibrotic rats. Plain RGZ, plain CDS, RGZ as well as CDS loaded unconjugated liposome treated groups

demonstrated very modest improvement in the physical and biochemical parameters. Blank conjugated liposomes displayed slight improvement due to presence of bioactive lipid DLPC and targeting ability. Most improvement, i.e. 13 to 70% in physical and biological parameters, had been observed in RGZ loaded conjugated liposome and CDS loaded conjugated liposome treated animal groups. Fibrosis grade, liver coefficient, serum AST, ALT, total bilirubin, hyaluronic acid and liver hydroxyproline content were significantly reduced and serum albumin/globulin ratio was increased as compared to CCl₄ induced liver fibrosis model group rats as given in the table 7.1 and 7.2. Significant reduction in serum glucose level was observed for plain RGZ and RGZ loaded unconjugated liposomes but no significant change was observed for RGZ loaded M6P-HSA conjugated liposomes suggesting very minimal or no systemic side effects of RGZ when given in conjugated liposomes.

The sections were stained with hematoxylin and eosin (H&E), mason's trichrome, picro-Sirius red and for α -SMA and then examined under the light microscope for histopathological changes and photomicrographs were taken (figure 7.1). Sections taken from rats of the control group showed normal architecture and have very less collagen and α -SMA deposition. The tissue architecture was very much disordered in the sections from fibrosis model group. Collagen and α -SMA depositions were also much more extensive. Here also the improvement was in order of RGZ loaded conjugated liposome = CDS loaded conjugated liposome > blank conjugated liposomes > RGZ loaded unconjugated liposomes = CDS loaded unconjugated liposomes > plain RGZ = plain CDS.

Figure 7.1 Representative histopathological images (I: hematoxylin and eosin, II: mason's trichrome, III: Picro-Sirius red and IV: α -smooth muscle actin staining) of liver tissues of A: Control, B: CCl₄ treated, C: Plain M6P-HSA conjugated liposomes plus CCl₄, D: Plain RGZ plus CCl₄, E: RGZ loaded unconjugated liposomes plus CCl₄, F: RGZ loaded M6P-HSA conjugated liposomes plus CCl₄, G: Plain CDS plus CCl₄, H: CDS loaded unconjugated liposomes plus CCl₄, I: CDS loaded M6P-HSA conjugated liposomes plus CCl₄. (formulations equivalent to RGZ 1 mg/kg/day or CDS 3 mg/kg/day, intravenous)

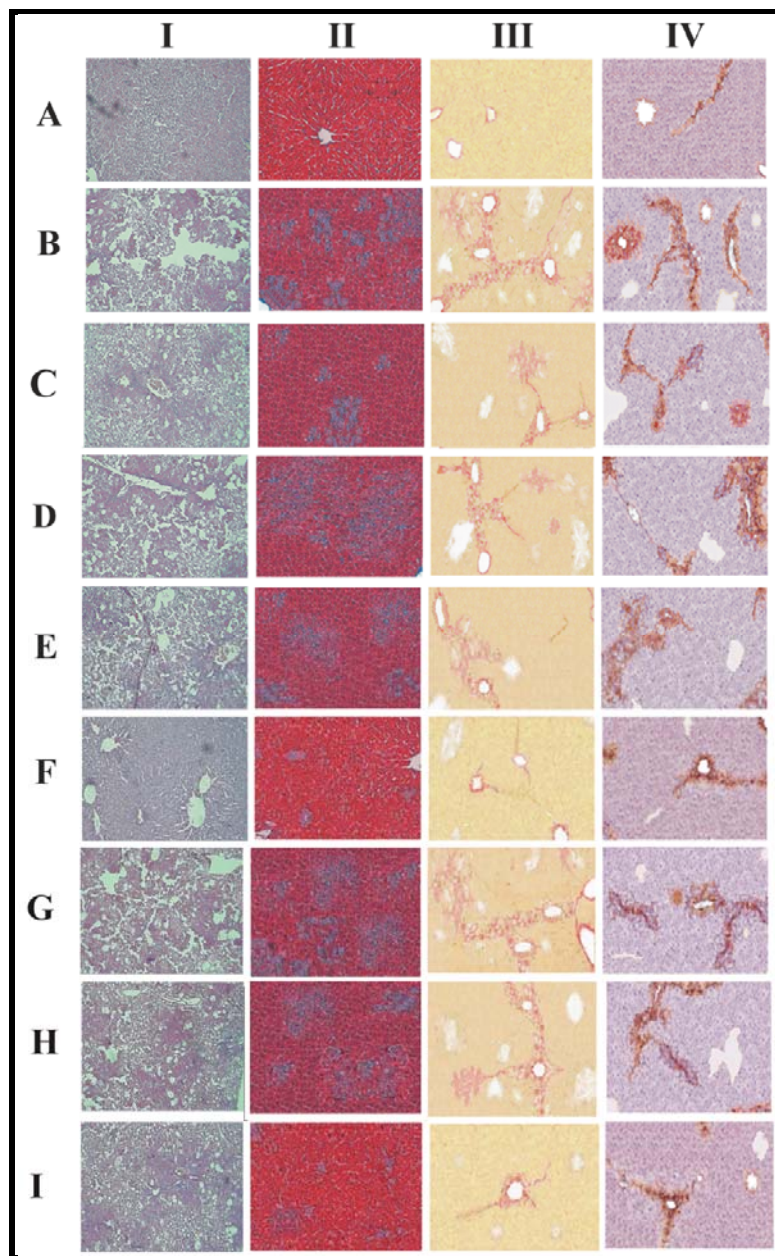


Table 7.1 The effect of various treatments on body weight, liver weight, liver coefficient and fibrosis grade

Formulation	Body weight (g)	Liver Weight (g)	Liver Coefficient	Fibrosis grade
Control	401.57 ± 19.29	14.53 ± 1.071	3.61 ± 0.101	--
CCl ₄	307.67 ± 15.52	15.80 ± 1.185	5.12 ± 0.129	4.33 ± 0.110
CCl ₄ + Plain M6P-HSA conjugated liposomes	318.43 ± 11.33	14.90 ± 0.954	4.67 ± 0.135*	3.88 ± 0.072**

CCl₄ + RGZ	317.00 ± 13.11	15.83 ± 1.041	4.99 ± 0.131	4.21 ± 0.042
CCl₄ + RGZ loaded unconjugated liposomes	320.20 ± 17.07	15.47 ± 1.186	4.82 ± 0.115	4.04 ± 0.083
CCl₄ + RGZ loaded M6P-HSA conjugated liposomes	328.73 ± 14.34	14.33 ± 0.984	4.35 ± 0.111***	3.17 ± 0.110***
CCl₄ + CDS	312.37 ± 13.11	15.91 ± 1.182	5.09 ± 0.107	4.27 ± 0.030
CCl₄ + CDS loaded unconjugated liposomes	316.81 ± 12.98	15.66 ± 0.956	4.94 ± 0.128	4.08 ± 0.042
CCl₄ + CDS loaded M6P-HSA conjugated liposomes	325.19 ± 16.21	14.51 ± 1.110	4.46 ± 0.124***	3.25 ± 0.072***

n = 10 (± SEM)

* p < 0.05, ** p < 0.01, *** p < 0.001 vs. the CCl₄ treated group. Significance was determined by one way analysis of AVONA followed by Tukey's multiple comparison test.

Table 7.2 The effect of various treatments on serum AST, ALT, A/G ratio, total bilirubin, hyaluronic acid, glucose and liver hydroxyproline content

Formulation	ALT (IU/L)	AST (IU/L)	Serum Albumin/Globulin ratio	Total Bilirubin (mg/dl)	Serum Hyaluronic acid (ng/ml)	Liver Hydroxyproline (µg/g)	Serum Glucose (mg/dl)
Control	31.48 ± 4.379	91.21 ± 4.859	1.89 ± 0.056	0.44 ± 0.035	46.79 ± 4.851	295.15 ± 7.695	97.31 ± 1.390
CCl₄	88.85 ± 5.544	212.60 ± 5.088	0.99 ± 0.055	2.11 ± 0.046	198.95 ± 4.016	1881.96 ± 8.704	96.18 ± 1.005

CCl₄ + Plain M6P-HSA conjugated liposomes	71.00 ± 4.254 **	182.89 ± 4.853 ***	1.29 ± 0.049***	1.79 ± 0.049 ***	145.25 ± 5.722***	1730.68 ± 7.796 ***	97.24 ± 1.210
CCl₄ + RGZ	81.86 ± 4.464	203.55 ± 5.115	1.06 ± 0.035	2.02 ± 0.041	187.75 ± 3.958	1855.00 ± 4.731	81.96 ± 1.200 ***
CCl₄ + RGZ loaded unconjugated liposomes	78.11 ± 4.106	194.92 ± 4.462 **	1.17 ± 0.043**	1.88 ± 0.047 ***	172.78 ± 4.945***	1843.03 ± 6.078**	85.02 ± 1.258 ***
CCl₄ + RGZ loaded M6P-HSA conjugated liposomes	46.69 ± 5.433 ***	128.24 ± 4.568 ***	1.69 ± 0.042***	1.18 ± 0.041 ***	88.61 ± 4.945***	1310.31 ± 5.710 ***	92.18 ± 1.156
CCl₄ + CDS	85.12 ± 5.208	206.04 ± 5.115	1.07 ± 0.051	2.06 ± 0.037	188.21 ± 4.156	1867.74 ± 8.664	--
CCl₄ + CDS loaded unconjugated liposomes	80.01 ± 4.663	198.23 ± 4.462*	1.13 ± 0.036	1.94 ± 0.043*	177.93 ± 3.763**	1840.63 ± 7.917**	--
CCl₄ + CDS loaded M6P-HSA conjugated liposomes	56.27 ± 3.994 ***	140.07 ± 4.568 ***	1.53 ± 0.038***	1.34 ± 0.045 ***	95.53 ± 3.442***	1363.55 ± 6.638 ***	--

n = 10 (± SEM)

* p < 0.05, ** p < 0.01, *** p < 0.001 vs. the CCl₄ treated group (For all except Serum glucose).

* p < 0.05, ** p < 0.01, *** p < 0.001 vs. the control group (For serum glucose).

Significance was determined by one way analysis of AVONA followed by Tukey's multiple comparison test.

7.9.2 Pharmacokinetic and Biodistribution

After 8 weeks of first injection of CCl₄, blood clearance of plain drug, unconjugated liposomes and conjugated liposomes were compared (figure 7.2 and 7.3). After 10 min of injection, almost 87.91% of the injected dose for RGZ loaded conjugated liposomes cleared from the blood circulation, which was 2.61 folds higher than RGZ unconjugated liposomes and 4.93 folds higher than plain RGZ. After one hour, only 3.12% of the injected dose was present in the blood for RGZ loaded conjugated

liposomes, which were 11.03 and 24.27 folds lower than RGZ loaded unconjugated liposomes and plain RGZ respectively.

After 10 min of injection, almost 88.27% of the injected dose for CDS loaded conjugated liposomes cleared from the blood circulation, which was 2.57 folds higher than CDS unconjugated liposomes and 5.23 folds higher than plain CDS. After one hour, only 3.53% of the injected dose was present in the blood for CDS loaded conjugated liposomes, which were 10.49 and 21.35 folds lower than CDS loaded unconjugated liposomes and plain CDS respectively.

Prior injection of M6P-HSA significantly reduced the blood clearance and increased half life of RGZ loaded and CDS loaded conjugated liposomes (table 7.3).

Figure 7.2 Pharmacokinetic profiles of RGZ (different formulations) after single intravenous bolus injection in fibrotic rats. The data represent the mean \pm SEM (n = 6)

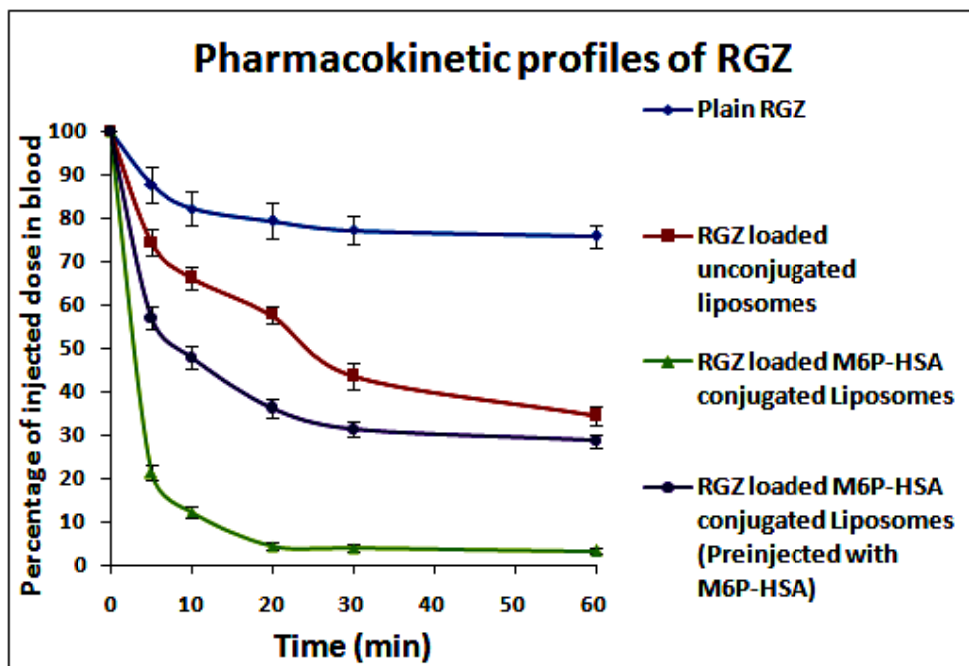


Figure 7.3 Pharmacokinetic profiles of CDS (different formulations) after single intravenous bolus injection in fibrotic rats. The data represent the mean \pm SEM (n = 6)

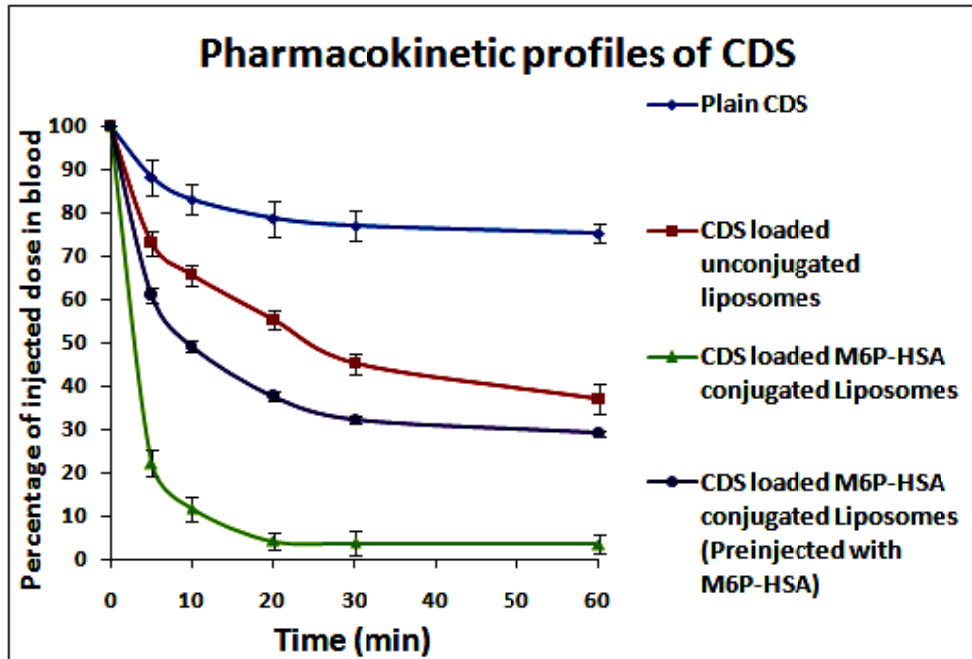


Table 7.3 The pharmacokinetic parameters for different formulations in fibrotic rats after single intravenous bolus injection. The data represent the mean \pm SEM (n = 6)

Formulation	AUC ($\mu\text{g}\cdot\text{min}/\text{ml}$)	MRT (min)	$T_{1/2}$ (min)	K_{el} (min^{-1})	V (ml)	CL (ml/min)
Plain RGZ	3653.1 4 \pm 28.73	281.48 \pm 5.11	195.11 \pm 6.61	0.0036 \pm 0.0003	23.66 \pm 1.63	0.084 \pm 0.004
RGZ loaded unconjugated liposomes	724.72 \pm 10.91	60.98 \pm 3.27	42.27 \pm 4.56	0.0164 \pm 0.0013	25.83 \pm 2.05	0.424 \pm 0.032
RGZ loaded M6P-HSA conjugated liposomes	51.66 \pm 3.39	27.62 \pm 2.93	19.15 \pm 1.28	0.0362 \pm 0.0025	164.13 \pm 8.83	5.942 \pm 0.921
RGZ loaded M6P-HSA conjugated liposomes (Pre-injected with M6P-HSA)	522.74 \pm 7.84	60.54 \pm 4.17	41.96 \pm 3.89	0.0165 \pm 0.0016	35.56 \pm 2.76	0.587 \pm 0.044
Plain CDS	3193.4 7 \pm 24.58	302.27 \pm 4.72	201.34 \pm 4.63	0.0039 \pm 0.0002	24.75 \pm 1.49	0.087 \pm 0.006
CDS loaded unconjugated liposomes	633.53 \pm 11.08	62.12 \pm 2.18	43.71 \pm 2.24	0.0168 \pm 0.0011	26.97 \pm 1.83	0.438 \pm 0.028
CDS loaded M6P-HSA conjugated liposomes	45.16 \pm 2.52	25.86 \pm 2.73	18.21 \pm 1.77	0.0348 \pm 0.0031	168.46 \pm 6.18	5.876 \pm 1.035
CDS loaded M6P-HSA conjugated liposomes (Pre-injected with M6P-HSA)	456.96 \pm 5.94	58.91 \pm 3.19	41.18 \pm 2.58	0.0164 \pm 0.0013	34.19 \pm 1.97	0.528 \pm 0.036

After one hour of injection, liver, spleen, kidneys, lungs and heart were excised and the distribution of various formulations was determined (figure 7.4 and 7.5). Almost $74.23 \pm 1.55\%$ of the injected dose had been taken up by the liver for the RGZ loaded conjugated liposomes which was 1.94 and 12.60 folds higher than RGZ loaded unconjugated liposomes and plain RGZ respectively. Very minuscule that is $4.82 \pm 0.69\%$, $1.94 \pm 0.47\%$, $3.61 \pm 0.61\%$ and $0.94 \pm 0.2\%$ of the injected dose had been taken up by the spleen, kidneys, lungs and heart respectively for the RGZ loaded conjugated liposomes. Amount taken up by the spleen, kidneys, lungs and heart was 2.08, 1.46, 1.08 and 1.18 folds more for RGZ loaded unconjugated liposomes and 1.10, 1.55, 0.56 and 1.43 folds more for plain drug than RGZ loaded conjugated liposomes.

Almost $73.97 \pm 1.67\%$ of the injected dose had been taken up by the liver for the CDS loaded conjugated liposomes which was 2.05 and 12.23 folds higher than CDS loaded unconjugated liposomes and plain CDS respectively. Very minuscule that is $4.94 \pm 0.71\%$, $1.76 \pm 0.43\%$, $3.57 \pm 0.60\%$ and $0.91 \pm 0.19\%$ of the injected dose had been taken up by the spleen, kidneys, lungs and heart respectively for the CDS loaded

conjugated liposomes. Amount taken up by the spleen, kidneys, lungs and heart was 2.00, 1.44, 1.11 and 1.29 folds more for CDS loaded unconjugated liposomes and 1.07, 1.84, 0.61 and 1.34 folds more for plain drug than CDS loaded conjugated liposomes.

Prior injection of M6P-HSA significantly reduced accumulation of RGZ and CDS in liver that is 1.60 and 1.61 folds lower than RGZ loaded conjugated liposomes and CDS loaded conjugated liposomes respectively.

Figure 7.4 Complete tissue distribution of RGZ formulations after single intravenous bolus injection. Each point represents the mean \pm SEM (n=6)

Organ Distribution of RGZ formulations

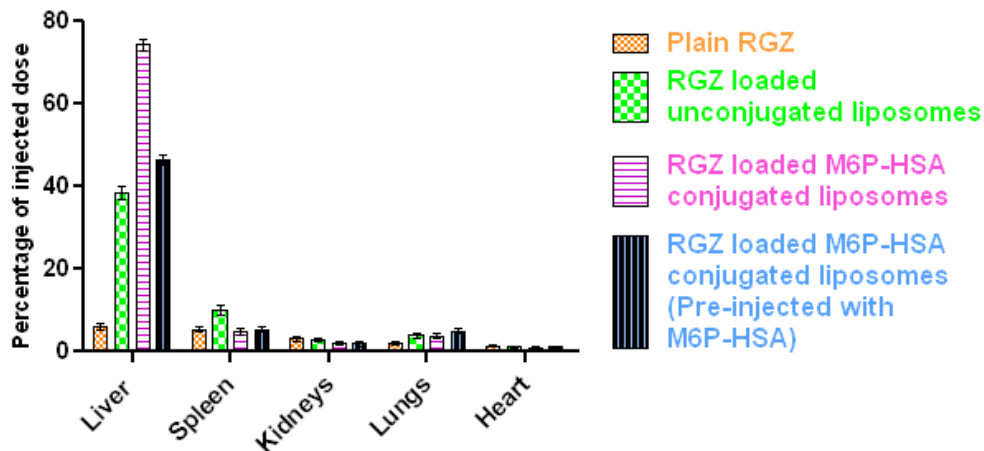
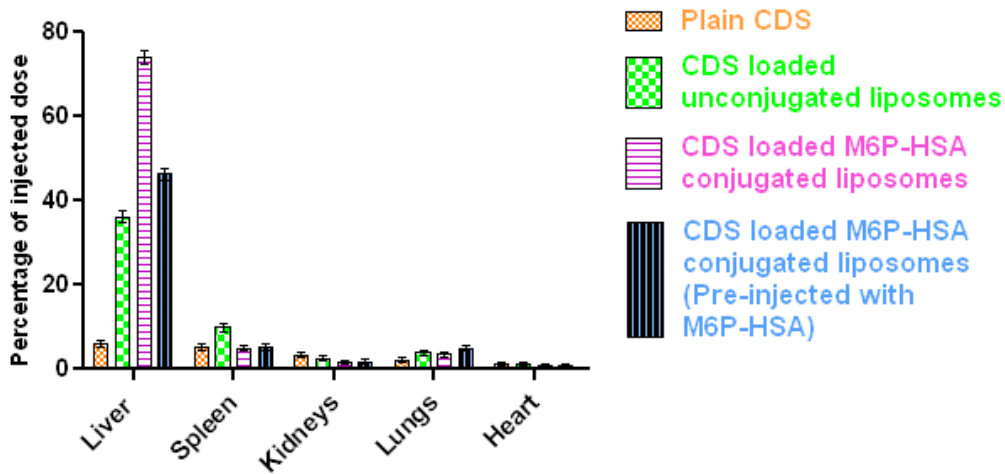


Figure 7.5 Complete tissue distribution of CDS formulations after single intravenous bolus injection. Each point represents the mean \pm SEM (n=6)

Organ Distribution of CDS formulations



7.10 CONCLUSION

Due to lack of targeting knack plain drug and drug loaded unconjugated liposome treated groups demonstrated very modest improvement in the physical and biochemical parameters. Blank conjugated liposomes displayed slight improvement due to presence of bioactive lipid DLPC and targeting ability. Most improvement had been observed in RGZ loaded conjugated liposome and CDS loaded conjugated liposome treated animal groups. Serum glucose level estimation studied suggests very minimal or no systemic side effects of RGZ when given in conjugated liposomes.

The histopathological studies suggests that improvement was in order of RGZ loaded conjugated liposome = CDS loaded conjugated liposome > blank conjugated liposomes > RGZ loaded unconjugated liposomes = CDS loaded unconjugated liposomes > plain RGZ = plain CDS.

M6P-HSA conjugated liposomes were rapidly taken up by the target cells as compared to unconjugated liposomes and plain drug. Prior injection of M6P-HSA significantly reduced the blood clearance and increased half life of RGZ loaded and CDS loaded conjugated liposomes, which confirms target specificity of M6P-HSA conjugated liposomes.

After one hour of injection, in case of M6P-HSA conjugated liposomes, much higher percentage of injected dose had been taken up by liver as compared to unconjugated liposomes and plain drug. In comparison to unconjugated liposomes and plain drug, very minuscule percentage of the injected dose had been taken up by the spleen, kidneys, lungs and heart for the RGZ loaded conjugated liposomes. Prior injection of M6P-HSA significantly reduced accumulation of RGZ and CDS in liver which confirms target specificity of M6P-HSA conjugated liposomes.

7.11 REFERENCES

Ala-Kokko L, Stenbäck F, Ryhanen L. Preventive effect of malotilate on dimethylnitrosamine-induced liver fibrosis in the rat. *J Lab Clin Med.* 1989 Feb;113(2):177-83.

Ballardini G, Degli Esposti S, Bianchi FB, de Giorgi LB, Faccani A, Biolchini L, Busachi CA, Pisi E. Correlation between Ito cells and fibrogenesis in an experimental model of hepatic fibrosis. A sequential stereological study. *Liver.* 1983 Feb;3(1):58-63.

Cameron GR, Karunaratne WAE. Carbon tetrachloride cirrhosis in relation to liver regeneration. *The Journal of Pathology and Bacteriology.* 1936;42(1):1-21.

Constandinou C, Henderson N, Iredale JP. Modeling liver fibrosis in rodents. *Methods Mol Med.* 2005;117:237-50.

Goodman ZD. Grading and staging systems for inflammation and fibrosis in chronic liver diseases. *J Hepatol.* 2007 Oct;47(4):598-607.

Igarashi S, Hatahara T, Nagai Y, Hori H, Sakakibara K, Katoh M, Sakai A, Sugimoto T. Anti-fibrotic effect of malotilate on liver fibrosis induced by carbon tetrachloride in rats. *Jpn J Exp Med.* 1986 Oct;56(5):235-45.

Iredale JP, Benyon RC, Arthur MJ, Ferris WF, Alcolado R, Winwood PJ, Clark N, Murphy G. Tissue inhibitor of metalloproteinase-1 messenger RNA expression is enhanced relative to interstitial collagenase messenger RNA in experimental liver injury and fibrosis. *Hepatology.* 1996 Jul;24(1):176-84.

Iredale JP, Benyon RC, Pickering J, McCullen M, Northrop M, Pawley S, Hovell C, Arthur MJ. Mechanisms of spontaneous resolution of rat liver fibrosis. Hepatic stellate cell apoptosis and reduced hepatic expression of metalloproteinase inhibitors. *J Clin Invest.* 1998 Aug 1;102(3):538-49.

Issa R, Williams E, Trim N, Kendall T, Arthur MJ, Reichen J, Benyon RC, Iredale JP. Apoptosis of hepatic stellate cells: involvement in resolution of biliary fibrosis and regulation by soluble growth factors. *Gut.* 2001 Apr;48(4):548-57.

Issa R, Zhou X, Trim N, Millward-Sadler H, Krane S, Benyon C, Iredale J. Mutation in collagen-1 that confers resistance to the action of collagenase results in failure of recovery from CCl₄-induced liver fibrosis, persistence of activated hepatic stellate cells, and diminished hepatocyte regeneration. *FASEB J.* 2003 Jan;17(1):47-9.

Madden JW, Gertman PM, Peacock EE Jr. Dimethylnitrosamine-induced hepatic cirrhosis: a new canine model of an ancient human disease. *Surgery*. 1970 Jul;68(1):260-7; discussion 267-8.

Maher JJ, McGuire RF. Extracellular matrix gene expression increases preferentially in rat lipocytes and sinusoidal endothelial cells during hepatic fibrosis in vivo. *J Clin Invest*. 1990 Nov;86(5):1641-8.

Martinez-Hernandez A. The hepatic extracellular matrix. II. Electron immunohistochemical studies in rats with CCl₄-induced cirrhosis. *Lab Invest*. 1985 Aug;53(2):166-86.

Mojaverian P, Rosen J, Vadino WA, Liebowitz S, Radwanski E. In-vivo/in-vitro correlation of four extended release formulations of pseudoephedrine sulfate. *J Pharm Biomed Anal*. 1997 Jan;15(4):439-45.

Morrione TG. Factors influencing collagen content in experimental cirrhosis. *Am J Pathol*. 1949 Mar;25(2):273-85.

Nakamura N, Fusamoto H, Koizumi T. The effects of aminoacetonitrile and its derivative on components of hepatic connective tissue in rats with chronic hepatic injury. *Acta Hepatogastroenterol (Stuttg)*. 1975 Apr;22(2):78-84.

Oakley F, Trim N, Constandinou CM, Ye W, Gray AM, Frantz G, Hillan K, Kendall T, Benyon RC, Mann DA, Iredale JP. Hepatocytes express nerve growth factor during liver injury: evidence for paracrine regulation of hepatic stellate cell apoptosis. *Am J Pathol*. 2003 Nov;163(5):1849-58.

Perez Tamayo R. Is cirrhosis of the liver experimentally produced by CCl₄ and adequate model of human cirrhosis? *Hepatology*. 1983 Jan-Feb;3(1):112-20.

Rojkind M, Dunn MA. Hepatic fibrosis. *Gastroenterology*. 1979 Apr;76(4):849-63.

Rubin E, Hutterer F, Popper H. Cell proliferation and fiber formation in chronic carbon tetrachloride intoxication. A morphologic and chemical study. *Am J Pathol*. 1963 Jun;42:715-28.

Switzer BR. Determination of hydroxyproline in tissue. *J. Nutr. Biochem*. 1991;2:229-31.

Symeonidis A, Trams EG. Morphologic and functional changes in the livers of rats after ligation or excision of the common bile duct. *Am J Pathol.* 1957 Jan-Feb;33(1):13-27.

Tams EG. Morphological and functional changes in the livers of rats after ligation and excision of the common bile duct. *Am J Pathol.* 1957;33:13-27.

Tsukamoto H, Matsuoka M, French SW. Experimental models of hepatic fibrosis: a review. *Semin Liver Dis.* 1990 Feb;10(1):56-65.

Wright MC, Issa R, Smart DE, Trim N, Murray GI, Primrose JN, Arthur MJ, Iredale JP, Mann DA. Gliotoxin stimulates the apoptosis of human and rat hepatic stellate cells and enhances the resolution of liver fibrosis in rats. *Gastroenterology.* 2001 Sep;121(3):685-98.

Ye ZJ, Liu YG. Effects of tetrachlorvinphos on hepatic microsomal enzymes in the rat. *Acta Acad Med Wuhan.* 1985;5(3):173-7.

Yokoi Y, Namihisa T, Matsuzaki K, Miyazaki A, Yamaguchi Y. Distribution of Ito cells in experimental hepatic fibrosis. *Liver.* 1988 Feb;8(1):48-52.

Zimmerman, H. (1976) Experimental hepatotoxicity, in *Experimental Production of Disease, Part 5: Liver.* (Eiciler, O., ed.), Springer-Verlag, Berlin: pp. 1–120.

CHAPTER 8

SUMMARY AND CONCLUSION



Liver fibrosis is the reversible wound healing response to a variety of chronic injurious events to the liver, induced by chronic viral hepatitis, iron or copper overload disease, certain autoimmune diseases, toxicity by certain drugs or chronic alcohol abuse and metabolic disorders, such as the metabolic syndrome. The disease is characterized by the deposition of excessive amounts of extracellular matrix (ECM) or "scar" tissues in the liver, which disturbs liver structure and functioning. In an advanced stage, the fibrotic process acquires a self-perpetuating character, and fibrosis will gradually progress into its end-stage called cirrhosis even when the injurious stimulus is removed. Finally, healthy liver cells are largely replaced by connective tissue. This remodeling of the liver parenchyma also results in impaired blood flow through the liver, which subsequently leads to portal hypertension and many secondary problems. In contrast to the early stages of the disease, when loss of functional liver parenchyma can still be compensated for by virtue of a functional over-capacity of the liver, liver function becomes de-compensated in the cirrhotic end-stage of the disease, ultimately leading to death. Liver transplantation is the ultimate treatment of advanced fibrosis but because of lack of liver donors, high costs and complexity of this therapy, there is a strong urge to establish alternative treatments.

The overall prevalence of cirrhosis in the United States is estimated at 360 per 100,000 population, or 900,000 total patients, the large majority of who have chronic viral hepatitis or alcoholic liver disease. Cirrhosis affects hundreds of millions of patients worldwide. In the US, it is the most common non-neoplastic cause of death among hepatobiliary and digestive diseases, accounting for approximately 30,000 deaths per year. In addition 10,000 deaths occur due to liver cancer, the majority of which arise in cirrhotic livers, with the mortality rate steadily rising.

Hepatic fibrosis has evolved in the past 20 years from a pure laboratory discipline to an area of great bedside relevance to practicing hepatologists. This evolution reflects growing awareness not only of the molecular underpinnings of fibrosis, but also of its natural history and methods of detection in chronic liver disease. These advances have culminated in clear evidence that cirrhosis can be reversible, and in realistic expectations that effective antifibrotic therapy will significantly alter the management and prognosis of patients with liver disease.

Within the fibrotic liver, activated hepatic stellate cells (HSC) produce excessive amounts of extracellular matrix proteins, which are the building blocks of the connective tissue. Under the influence of fibrogenic stimuli derived from damaged hepatocytes, activated Kupffer cells and liver endothelial cells, HSC transdifferentiate from a quiescent cell type into a cell with a myofibroblast-like phenotype. During fibrosis, the number of active fibrogenic cells in the liver also dramatically increases, mainly as a result of an increased local proliferation of HSC and is typically preceded by an influx of inflammatory cells and associated with subsequent ECM accumulation. Because the proliferation process plays an important role in the progression of the disease, inhibiting HSC proliferation could be a relevant strategy to inhibit liver fibrosis in a pharmacological manner.

The best anti-fibrogenic treatment would be represented by any strategy able to eliminate the primary cause of parenchymal damage, metabolic overload or excessive oxidative stress. Once this primary requirement is fulfilled, the association with an anti-fibrogenic drug would be relevant for stabilizing the cure and favor optimal remodeling. Since the fibrogenic process is in its essence a compensatory phenomenon aimed at maintaining sufficient tissue continuity and cohesion in the presence of continuous microscopic parenchymal collapse, it would be erroneous to attempt to cure fibrogenic chronic liver diseases (CLDs) only with anti-fibrogenic drugs once some effective compounds will become available for clinical use.

So far no effective treatment has been established other than removal of primary cause of the disease and liver transplantation for severe fibrosis. Therefore, research is being carried out on therapeutic agents who inhibit activation and proliferation of HSC, reduce ECM production by HSC, neutralize HSC contractile responses or stimulate HSC apoptosis.

Expression of PPAR- γ by Rosiglitazone (RGZ) inhibited PDGF-induced proliferation and migration of vascular smooth muscle cells. The level of PPAR- γ and its trans-activating activity were diminished during HSC activation in vitro, whereas NF- κ B and activator protein-1 (AP-1) activities were increased. PPAR- γ ligands (RGZ) inhibited cell proliferation and collagen- α 1(I) expression in primary HSC (3–4 days). The dramatic reduction in the abundance of PPAR- γ results in a significant decline in response to exogenous PPAR- γ ligands in activated HSC. These are suggestive of a

potential therapeutic value of PPAR- γ ligands in treatment of liver fibrosis if the expression of PPAR- γ can be induced in activated HSC.

The rennin-angiotensin system (RAS) plays an important role in the pathogenesis of organ fibrosis. Blockade of the RAS by angiotensin converting enzyme (ACE) inhibitors or by AT1 antagonists [Candesartan (CDS)] has been shown to improve the progression of organ fibrosis. Ang II induces proliferation and contraction of human HSCs, and TGF- β expression in rat HSCs, which are mainly mediated by AT1 receptors, and that ACE inhibitors or AT1 antagonists (CDS) attenuate the progression of liver fibrosis in vivo. These are suggestive that Ang II and RAS might play an important role in the pathogenesis of liver fibrosis.

One of the perceived benefits of liposomes as a drug carrier is based on their ability to alter favorably the pharmacokinetic profile of the encapsulated species and thus provide selective and prolonged pharmacological effects at these sites of administration. The resulting decrease in the frequency of drug dosing will significantly improve the quality of life for patients and at the same time reduce healthcare cost. Liposomes have tremendous potential as a carrier because they are nontoxic, non-immunogenic, and biodegradable and have a high loading capacity for a variety of therapeutic agents and have been investigated for long period of time.

Conventional liposomes are often less effective due to lack of the target specificity. In addition, rapid elimination and widespread distribution into targeted organs and tissues requires the administration of a drug in large quantities, which is not economical and often results in undesirable toxicity. Thus, drug targeting has evolved as the most desirable but elusive goal in drug delivery science. It can potentially increase efficacy and reduce toxicity of new and pre-existing drugs by altering their pharmacokinetics and biodistribution and restricting the action of drugs to the treated tissue. Hence, the major challenge is to design drug delivery strategies that deliver the therapeutic agents to the desired intracellular targets based on ability to understand, utilize, modify and exploit membrane trafficking pathways. Conjugating cell specific ligands to liposomes makes them target specific delivery system.

Mannose 6-phosphate receptor are over expressed on the surface of HSCs during liver fibrosis. Mannose 6-phosphate modified human serum albumin (M6P-HSA) is selective to M6P/IGF II receptor and thus accumulates in activated HSCs of fibrotic

liver. M6P-HSA conjugated liposomes can be used as HSCs selective carrier of antifibrotic drugs to improve the efficacy of drugs at the same time to reduce their adverse effects. Liposomes with bioactive lipid dilinoleoylphosphatidylcholine (DLPC) into the membrane as a major constituent act as a bioactive drug carrier which can deliver drugs and simultaneously have beneficial antifibrotic effects.

The objectives of this investigation were to develop liposomal formulation by thin film hydration method and optimized for drug: total lipid ratio, Phospholipid: cholesterol ratio and total solid: hydration medium ratio to maximize the percentage drug entrapment (PDE) and to minimize percentage reduction (PR) in PDE after 10 days by 3^3 full factorial design, to synthesize and characterize M6P-HSA and surface conjugation of optimized liposomal formulations. It was also an objective to assess release kinetics of developed formulations by performing *in vitro* drug diffusion studies and also to evaluate *in-vivo* pharmacokinetic and pharmacodynamic properties of prepared formulation in carbon tetrachloride (CCL_4) induced rat liver fibrosis model for exploitation of the findings of the studies in developing relevant product for effective treatment of liver fibrosis.

The developed spectroscopic determination methods of RGZ were based on the zero order UV spectra giving maxima at 311.8 nm in methanol (for estimation of RGZ in formulation) and at 313.8 nm in diffusion medium and found to be linear in the range of 10-70 $\mu\text{g/mL}$ having r^2 value of 1.0000 and 0.9995 respectively and had high accuracy and precision.

The developed spectroscopic determination methods of CDS were based on the zero order UV spectra giving maxima at 304.8 nm in methanol (for estimation of CDS in formulation) and at 306.2 nm in diffusion medium and found to be linear in the range of 5-80 $\mu\text{g/mL}$ having r^2 value of 0.9998 and 0.9996 respectively and had high accuracy and precision.

The developed chromatographic method of RGZ in plasma was based on reversed-phase HPLC method with UV detection having mobile phase composition of 10mM sodium acetate (pH 5): acetonitrile: methanol (40:40:20, v/v/v) at a flow rate 1.0 $\text{mL}\cdot\text{min}^{-1}$. RGZ was detected at 245.0 nm and calibration plot was linear ($r^2 > 0.9996$) in the concentration range of 0.05-10 $\mu\text{g/mL}$ and had high accuracy and precision.

The developed chromatographic method of CDS in plasma was based on reversed-phase HPLC method with UV detection having mobile phase composition of methanol: acetonitrile: 10mM sodium acetate pH 5 (74 : 16 : 10, v/v/v) (pH 2.5) at a flow rate 1.0 mL·min⁻¹. CDS was detected at 260.0 nm and calibration plot was linear ($r^2 > 0.9997$) in the concentration range of 0.05-10 µg/mL and had high accuracy and precision.

The developed analytical methods for estimation of mannose (colorimetric), phosphorus (colorimetric), total protein (colorimetric), albumin in serum (colorimetric), globulin in serum (colorimetric), aspartate aminotransferase (AST) in serum (colorimetric), alanine aminotransferase (AST) in serum (colorimetric), hydroxyproline in tissue (colorimetric), hyaluronic acid in serum (ELISA), total bilirubin in serum (colorimetric) were found to be linear in analytical ranges and had higher accuracy and precision.

Liposomes containing RGZ and CDS were prepared by TFH technique using DLPC, HSPC, DSPE-COOH and CH. Process parameters such as organic solvent composition, solvent evaporation time, speed of rotation, hydration time and vacuum applied were optimized to obtain desired formulation characteristics. The size of liposomes was reduced using successive extrusion through 1, 0.4, 0.2 and 0.1 µm polycarbonate membrane filter. Liposomal suspensions were then characterized for vesicle size, size distribution, zeta potential and encapsulation efficiency. The RGZ loaded and CDS loaded liposomal formulations were optimized using 3³ factorial design by varying drug: lipid molar ratio (1:15, 1:20 and 1:25), lipid: cholesterol molar ratio (9:1, 8:2 and 7:3), and total solid content: volume of hydration media ratio (1:10, 1:12.5 and 1:15) at 3 different levels as low (-1), medium (0) and high (1), by keeping all other process and formulation parameter invariant, to maximize PDE and to minimize PR in PDE after 10 days kept at refrigerated condition.

RSM was applied to fit second order polynomial equations, obtained by multiple linear regression analysis (MLRA) approach. Statistical soundness of the full and reduced polynomial equations was established on the basis of ANOVA statistics.

Two dimensional contour plots and three dimensional response surface plots were established by varying levels of two factors and keeping the third factor at fixed levels

at a time. Optimized formulation was derived by specifying goal and importance to the formulation variables and response parameters.

For RGZ liposomes, the optimized batch (Drug: Lipid molar ratio = -0.02; Lipid: Cholesterol molar ratio = 0.40; Total solid content: Volume of hydration media = 0.02) showed PDE of 71.83 ± 0.683 and PR in PDE of 2.41 ± 0.081 . P-value > 0.05 indicates the differences between predicted and experimental values are statistically insignificant. In checkpoint analysis higher r^2 values (0.9947 and 0.9995 for PDE and PR respectively) of the linear correlation plots suggest excellent goodness of fit and high predictive capability of RSM.

For CDS liposomes, the optimized batch (Drug: Lipid molar ratio = -0.35; Lipid: Cholesterol molar ratio = 0.60; Total solid content: Volume of hydration media = -1.00) showed PDE of 64.01 ± 0.772 and PR in PDE of 2.481 ± 0.076 . P-value > 0.05 indicates the differences between predicted and experimental values are statistically insignificant. In checkpoint analysis higher r^2 values (0.9894 and 0.9965 for PDE and PR respectively) of the linear correlation plots suggest excellent goodness of fit and high predictive capability of RSM.

M6P-HSA was successfully synthesized, purified, characterized for protein content, number of M6P molecules and number of phosphate groups coupled to each HSA molecules. The prepared neoglycoprotein had $95.22 \pm 1.74\%$ of protein, 29.73 ± 1.21 numbers of M6P molecules and 31.28 ± 2.01 numbers of phosphate groups coupled to each HSA molecule. Prepared M6P-HSA was then successfully conjugated to optimized liposomes and successful conjugation was confirmed by FTIR spectroscopy, particle size and zeta-potential analysis.

The size of Liposomes was measured by dynamic light scattering with a Malvern Zetasizer. Increased particle size and zeta potential of liposomes substantiate conjugation of M6P-HSA to liposomes.

The structure of liposomes was examined by TEM before and after conjugation of M6P-HSA. Liposomes had spherical shape and unilamellar structure. The liposome membranes were clearly observable because the inner aqueous compartments were slightly darker than the surrounding perimeters. The size of liposomes varied from 70 nm to 130 nm with an average diameter of 92.37 ± 3.28 nm for RGZ unconjugated liposomes (figure 4.24a) and 96.45 ± 3.71 for CDS unconjugated liposomes (figure

4.25a). The size of liposomes varied from 120 nm to 160 nm with an average diameter of 135.1 ± 3.74 nm for RGZ M6P-HSA conjugated liposomes (figure 4.24b), and 139.5 ± 3.98 for CDS M6P-HSA conjugated liposomes (figure 4.25b) measured by laser diffraction using Malvern Zetasizer. Results obtained from both TEM study and laser diffraction are parallel to each other.

The liposomal suspensions were stabilized by lyophilization. Different cryoprotectants at various ratios and anti-adherent were evaluated. The lyophilized formulations were tested for particle size, zeta potential and percentage drug retention (PDR). With use of sucrose, lactose and mannitol as cryoprotectant particle size of liposomes was increased and zeta-potential was decreased significantly after lyophilization. With trehalose, the lyophilized liposomes formed fluffy and snow like voluminous cake. With trehalose as cryoprotectant, the lyophilized liposomes were redispersed easily and the increase in particle size and decrease in zeta-potential were not significant. Trehalose at a ratio of 1:5 was used (as no further improvement was observed at 1:10) as a cryoprotectant and 10 % (of total solid) of glycine as antiadherent for lyophilization of optimized batches of liposomes.

Differential Scanning Calorimetry (DSC) studies and X-ray Diffraction (XRD) studies were conducted for lyophilized batches of M6P-HSA conjugated liposomes. DSC curves of plain drugs and liposomal formulations suggest loss of drug crystallinity when drugs were loaded into the liposomes. X-ray diffractograms showed less intensity of peaks corresponding to liposomal formulation than plain drug suggesting loss of drug crystallinity when drug was loaded into the liposomes.

To maintain sink condition, 50 ml of diffusion medium (50 mM Hydroxypropyl-beta-cyclodextrin, 20 mM HEPES, pH 7.4) for RGZ and 50 ml of diffusion medium (100 mM Hydroxypropyl-beta-cyclodextrin, 20 mM HEPES, pH 7.4) for CDS were selected and kept in receptor compartment with constant stirring at $37^\circ \pm 0.5^\circ\text{C}$.

Cumulative percent drug diffusion was plotted against time (t). The *in-vitro* release data obtained were fitted into equations for the zero-order, first-order and Higuchi release models. The non-linearity of the graph for unconjugated and conjugated liposomal formulations suggests that the diffusion pattern does not follow zero order kinetics of release. Highest regression coefficient value for the first order model was found for plain drugs [RGZ (0.9833); CDS (0.9827)] and for the Higuchi model for

both the unconjugated [RGZ (0.9768); CDS (0.9789)] and M6P-HSA conjugated liposomes [RGZ (0.9796); CDS (0.9818)], indicating diffusion to be the predominant mechanism of drug release in both the cases of liposomes. In case of RGZ, Mean steady state flux were 37.78, 6.89 and 6.48 for plain drug, unconjugated liposomes and M6P-HSA conjugated liposomes respectively. In case of CDS, mean steady state flux were 30.66, 6.58 and 6.08 for plain drug, unconjugated liposomes and M6P-HSA conjugated liposomes respectively.

Comparative stability studies were carried out of the potential liposomal formulations at accelerated condition ($25^{\circ}\text{C} \pm 2^{\circ}\text{C}$, $60\% \text{ RH} \pm 5\% \text{ RH}$) for six months and at long-term conditions ($5^{\circ}\text{C} \pm 3^{\circ}\text{C}$) up to twelve months. The liposomal formulations were examined visually for the evidence of discoloration. The content of the vial are tested for percentage drug retention (PDR), particle size, zeta-potential, assay and water content. No significant differences were found in all above mentioned parameters at both conditions.

Experimental liver fibrosis was developed, using an established protocol with slight modification, that involved intraperitoneal (i.p.) injections CCl_4 premixed with olive oil. After 8 weeks from the first injection of CCl_4 , animals were sacrificed and parameters such as serum albumin (ALB), serum globulin (GLB), total protein, serum alanine amino-transferase (ALT), serum glutamate-pyruvate transaminase (AST), blood glucose, serum levels of hyaluronic acid, liver coefficient, liver fibrosis grade, hydroxyproline content of the liver tissue were measured. After sacrificing the animals, liver was immediately removed and washed with saline and fixed in 10% buffered formalin. The fixed tissues were embedded in paraffin, five μm thick serial sections were cut and then processed for hematoxylin and eosin (H&E), masson's trichrome, picro-sirius red and α -SMA staining according to standard procedures.

The physical parameters such as liver fibrosis grade and liver coefficient were significantly increased in the CCl_4 induced liver fibrosis group rats compared to control group. Biochemical parameters such as serum AST, ALT, total bilirubin, hyaluronic acid and liver hydroxyproline were significantly increased and serum albumin/globulin ratio was significantly reduced in fibrotic rats. Plain RGZ, plain CDS, RGZ as well as CDS loaded unconjugated liposome treated groups demonstrated very modest improvement in the physical and biochemical parameters.

Blank conjugated liposomes displayed slight improvement due to presence of bioactive lipid DLPC and targeting ability. Most improvement, i.e. 13 to 70% in physical and biological parameters, had been observed in RGZ loaded conjugated liposome and CDS loaded conjugated liposome treated animal groups. Fibrosis grade, liver coefficient, serum AST, ALT, total bilirubin, hyaluronic acid and liver hydroxyproline content were significantly reduced and serum albumin/globulin ratio was increased as compared to CCl₄ induced liver fibrosis model group rats as given in the table 7.1 and 7.2. Significant reduction in serum glucose level was observed for plain RGZ and RGZ loaded unconjugated liposomes but no significant change was observed for RGZ loaded M6P-HSA conjugated liposomes suggesting very minimal or no systemic side effects of RGZ when given in conjugated liposomes.

Sections taken from rats of the control group showed normal architecture and have very less collagen and α -SMA deposition. The tissue architecture was very much disordered in the sections from fibrosis model group. Collagen and α -SMA depositions were also much more extensive. Here also the improvement was in order of RGZ loaded conjugated liposome = CDS loaded conjugated liposome > blank conjugated liposomes > RGZ loaded unconjugated liposomes = CDS loaded unconjugated liposomes > plain RGZ = plain CDS.

After 8 weeks of first injection of CCl₄, rats were injected with drug loaded M6P-HSA conjugated liposomes, drug loaded unconjugated liposomes and plain drug. Blood samples were collected at different time intervals of 5, 10, 20, 30 min and 1 h after injection. Total amount of the drug present in serum at each time point was measured by HPLC method. Similar experiments were performed for conjugated liposomes in rats pre-injected with M6P-HSA or HSA at the dose of 13 mg/kg of body weight (intravenous) 5 min before the injection of drug loaded M6P-HSA conjugated liposomes. From the obtained serum concentration data, the pharmacokinetic parameters were derived for each group.

After 10 min of injection, almost 87.91% of the injected dose for RGZ loaded conjugated liposomes cleared from the blood circulation, which was 2.61 folds higher than RGZ unconjugated liposomes and 4.93 folds higher than plain RGZ. After one hour, only 3.12% of the injected dose was present in the blood for RGZ loaded

conjugated liposomes, which were 11.03 and 24.27 folds lower than RGZ loaded unconjugated liposomes and plain RGZ respectively.

After 10 min of injection, almost 88.27% of the injected dose for CDS loaded conjugated liposomes cleared from the blood circulation, which was 2.57 folds higher than CDS unconjugated liposomes and 5.23 folds higher than plain CDS. After one hour, only 3.53% of the injected dose was present in the blood for CDS loaded conjugated liposomes, which were 10.49 and 21.35 folds lower than CDS loaded unconjugated liposomes and plain CDS respectively. Prior injection of M6P-HSA significantly reduced the blood clearance and increased half life of RGZ loaded and CDS loaded conjugated liposomes.

After one hour of injection, liver, spleen, kidneys, lungs and heart were excised, made free from any adhering tissues, weighed and drug content was measured in each organ by HPLC method after extraction. Almost $74.23 \pm 1.55\%$ of the injected dose had been taken up by the liver for the RGZ loaded conjugated liposomes which was 1.94 and 12.60 folds higher than RGZ loaded unconjugated liposomes and plain RGZ respectively. Very minuscule that is $4.82 \pm 0.69\%$, $1.94 \pm 0.47\%$, $3.61 \pm 0.61\%$ and $0.94 \pm 0.2\%$ of the injected dose had been taken up by the spleen, kidneys, lungs and heart respectively for the RGZ loaded conjugated liposomes. Amount taken up by the spleen, kidneys, lungs and heart was 2.08, 1.46, 1.08 and 1.18 folds more for RGZ loaded unconjugated liposomes and 1.10, 1.55, 0.56 and 1.43 folds more for plain drug than RGZ loaded conjugated liposomes.

Almost $73.97 \pm 1.67\%$ of the injected dose had been taken up by the liver for the CDS loaded conjugated liposomes which was 2.05 and 12.23 folds higher than CDS loaded unconjugated liposomes and plain CDS respectively. Very minuscule that is $4.94 \pm 0.71\%$, $1.76 \pm 0.43\%$, $3.57 \pm 0.60\%$ and $0.91 \pm 0.19\%$ of the injected dose had been taken up by the spleen, kidneys, lungs and heart respectively for the CDS loaded conjugated liposomes. Amount taken up by the spleen, kidneys, lungs and heart was 2.00, 1.44, 1.11 and 1.29 folds more for CDS loaded unconjugated liposomes and 1.07, 1.84, 0.61 and 1.34 folds more for plain drug than CDS loaded conjugated liposomes. Prior injection of M6P-HSA significantly reduced accumulation of RGZ and CDS in liver that is 1.60 and 1.61 folds lower than RGZ loaded conjugated liposomes and CDS loaded conjugated liposomes respectively.

Under this investigation, rosiglitazone and candesartan encapsulated liposomes were successfully prepared using thin film hydration technique. Particle size of the drug loaded liposomes was reduced by successive extrusion. Liposomal formulations were optimized using 3^3 full factorial design to maximize drug entrapment and to minimize percentage reduction in drug entrapment after 10 days kept at refrigerated condition. The experimental design and the derived polynomial equation for the optimization of liposomal formulation were validated for their utility by performing check point analysis. Optimized formulation was derived by specifying goal and importance to the formulation variables and response parameters. M6P-HSA was fruitfully synthesized and characterized. Prepared M6P-HSA was conjugated to optimized liposomes to impart ability to target hepatic stellate cells mainly responsible for liver fibrosis.

The characterization of conjugated liposomes demonstrated spherical shape, unilamellar structure and small particle size ($< 200\text{nm}$, even after lyophilization using trehalose as cryoprotectant) suitable for intravenous administration. Both drugs lost their crystallinity when loaded into the liposomes.

All these observations lead us to the conclusion that liposomal drug delivery has a greater potential for sustained diffusion of drug. Drug diffusion from liposomal formulations obeys Higuchi's diffusion controlled model and the diffusion rate is close to first order kinetics. The diffusion rate depends upon the physicochemical property, concentration of drug within the liposomes and the composition of the liposomal membrane. Hence by altering the composition of the liposomal membrane, different loading dose followed by maintenance dose can be achieved. Moreover the drug release been slower, it provides prolonged therapeutic response and also helps in prevention of development of drug resistance.

The decrease in drug assay, percentage drug retained, and zeta-potential and increase in water content, particle size were observed at accelerated condition ($25^\circ\text{C} \pm 2^\circ\text{C}$, $60\% \text{RH} \pm 5\% \text{RH}$) for six months and at long-term conditions ($5^\circ\text{C} \pm 3^\circ\text{C}$) up to twelve months for both RGZ and CDS liposomal formulation but the changes were statistically insignificant. Hence, both the formulations were considered as stable.

Due to lack of targeting knack plain RGZ, plain CDS, RGZ as well as CDS loaded unconjugated liposome treated groups demonstrated very modest improvement in the physical and biochemical parameters. Blank conjugated liposomes displayed slight

improvement due to presence of bioactive lipid DLPC and targeting ability. Most improvement had been observed in RGZ loaded conjugated liposome and CDS loaded conjugated liposome treated animal groups. Serum glucose level estimation studied suggests very minimal or no systemic side effects of RGZ when given in conjugated liposomes.

The histopathological studies suggests that improvement was in order of RGZ loaded conjugated liposome = CDS loaded conjugated liposome > blank conjugated liposomes > RGZ loaded unconjugated liposomes = CDS loaded unconjugated liposomes > plain RGZ = plain CDS.

M6P-HSA conjugated liposomes were rapidly taken up by the target cells as compared to unconjugated liposomes and plain drug. Prior injection of M6P-HSA significantly reduced the blood clearance and increased half life of RGZ loaded and CDS loaded conjugated liposomes, which confirms target specificity of M6P-HSA conjugated liposomes.

After one hour of injection, in case of M6P-HSA conjugated liposomes, much higher percentage of injected dose had been taken up by liver as compared to unconjugated liposomes and plain drug. In comparison to unconjugated liposomes and plain drug, very minuscule percentage of the injected dose had been taken up by the spleen, kidneys, lungs and heart for the RGZ loaded conjugated liposomes. Prior injection of M6P-HSA significantly reduced accumulation of RGZ and CDS in liver which confirms target specificity of M6P-HSA conjugated liposomes.

To conclude, M6P-HSA functionalized liposome based drug delivery systems of different class of drugs, such as PPAR gamma agonist (rosiglitazone) and angiotensin II receptor antagonist (candesartan), were successfully prepared, optimized and assessed pharmacokinetically and pharmacodynamically in suitable animal model. Drugs were selected on the basis of their possible potential efficacy in treatment of liver fibrosis but are not in use due to associated side effects. Pharmacokinetic data of the conjugated liposomes support effective liver targeting after intravenous administration. Pharmacodynamic studies, conducted in terms of biochemical and histopathological assessment, suggest potential application of drug loaded M6P-HSA conjugated liposomes in treating liver fibrosis which otherwise do not have any treatment except liver transplant, antioxidant therapy and vitamin supplements. The

studies of these investigations, support target specific exposure of drugs for prolonged period and reversal of liver fibrosis in experimental animal model. However, more extensive animal experimentation, on at least two more animal species, in terms of therapeutic efficacy and side effects are necessary to take up findings to clinical evaluation and use. This study provides a thinking which may result in development of product which can provide cure or at least prevention to this progressive disease necessitating liver transplant.